Design and Commissioning of Test Rigs for Erosion and Heat Transfer Testing of Dense Fluidized Beds

by Philipp Mayer

A thesis for the degree of
Master of Science (MSc or Dipl.-Ing. or DI)

In the
Master program Mechanical Engineering

At the
Faculty of Mechanical Engineering and Management, TU Wien

Supervised by
Univ.Prof. Dipl.-Ing. Dr.techn. Markus Haider

Univ.Ass. Dipl.-Ing. Stefan Thanheiser BSc.

Author
Philipp Mayer
Matr. Nr.: 01609399
philipp.mayer96@gmx.at

Supervisor
Univ.Prof. Dipl.-Ing. Dr.techn. Markus Haider
TU Wien
Institute for Energy Systems and Thermodynamics
Getreidemarkt 9, A-1060 Wien

Supervisor
Univ.Ass. Dipl.-Ing. Stefan Thanheiser BSc.
TU Wien
Institute for Energy Systems and Thermodynamics
Getreidemarkt 9, A-1060 Wien

Affidavit

I declare in lieu of oath, that I wrote this thesis and performed the associated research myself, using only literature cited in this volume. If text passages from sources are used literally, they are marked as such. I confirm that this work is original and has not been submitted elsewhere for any examination, nor is it currently under consideration for a thesis elsewhere.

I acknowledge that the submitted work will be checked electronically-technically using suitable and state-of-the-art means (plagiarism detection software). On the one hand, this ensures that the submitted work adheres to the high-quality standards of the current rules for ensuring good scientific practice "Code of Conduct" at the Vienna University of Technology. On the other hand, a comparison with other students' theses avoids violations of my copyright.

Vienna, December 5, 2022

Philipp Mayer

Abstract

This work includes the development and realization of test rigs for various experimental investigations of a storage system developed at the Institute for Energy Technology and Thermodynamics at the Vienna University of Technology. The associated research project SandTES - particle-basen high-temperature heat storage systems (TES - Thermal Energy Storage) deals with the storage of thermal energy in the industrial sector.

The first goal of this thesis was the experimental investigation of the erosion behavior of internals in fluidized beds using a specially developed test rig. The core task was to prove the low rate of erosion on internals, such as heat exchanger tubes. Until now this case was assumed without experimental confirmation. The results obtained should also make it possible to estimate the expected erosion rate over the lifetime of a component. The actual erosion was determined on one hand via the loss of mass and on the other hand via geometric changes. Metal sheets were mainly used as inspection elements, which are installed at different angles in the fluidized bed. This is necessary in order to be able to determine the dependency on the angle of attack. The difficulties for this test rig were the larger particle diameter and high flow velocities and pressures. These boundary conditions influenced both the basic concept of the test stand and the measuring devices for monitoring and setting the operating condition. In principle, the results are very satisfactory because the erosion rates are very low. Likewise, there have also been some new information that can be examined more closely.

The second goal was the development and implementation of another test rig for the experimental investigation of heat transfer in fluidized beds at high temperatures. With this test rig it will be possible to determine heat transfer coefficients in fluidized beds experimentally. The challenge in the construction and design of the test rig was the intended high medium temperature of up to 700 °C. At these temperatures, both the commonly used steel and the standard measuring equipment are unusable. The unique selling point of this test rig is the stationary circulation of the fluidized bed between the heating side and the cooling side without additional conveying equipment.

Kurzfassung

Diese Arbeit umfasst die Entwicklung und die Realisierung von Prüfständen für unterschiedliche experimentelle Untersuchungen einer am Institut für Energietechnik und Thermodynamik der TU Wien entwickelten Speichertechnologie. Das damit verbundene Forschungsprojekt SandTES - Partikelbasierte Hochtemperatur Wärmespeichersysteme (TES - Thermal Energy Storage) beschäftigt sich mit der Speicherung von thermischer Energie im industriellen Bereich.

Das erste Ziel dieser wissenschaftlichen Arbeit war die experimentelle Untersuchung von Erosionsverhalten an Einbauten in Wirbelschichten mit Hilfe eines eigens dafür entwickelten Prüfstandes. Die Kernaufgabe bestand darin die bis dato meist angenommene geringe Erosion an Einbauteilen, wie z.B. Wärmetauscherrohre, auch praktisch nachzuweisen. Ebenfalls soll es durch die gewonnenen Ergebnisse auch möglich sein die zu erwartende Erosionsrate über die Lebenszeit eines Bauteils abschätzen zu können. Die Ermittlung der tatsächlichen Erosion erfolgte zum einen über den Masseverlust und zum anderen über geometrische Änderungen. Als Erosionskörper wurden vorwiegend Bleche verwendet, welche unter verschieden Winkeln in der Wirbelschicht eingebaut wurden, um so auch die Abhängigkeit des Anströmwinkels beurteilen zu können. Die Schwierigkeit bei der Konstruktion und Inbetriebnahme des Prüfstandes bestand darin, dass für größere Partikeldurchmesser folglich auch größeren Strömungsgeschwindigkeiten und Drücke hervorgerufen werden. Diese Randbedingung beeinflussten sowohl das Grundkonzept des Prüfstandes als auch die Messeinrichtungen für die Überwachung und Einstellung des Betriebszustandes. Grundsätzlich sind die Ergebnisse sehr zufriedenstellend da die Erosionsraten so wie erhofft sehr gering sind, jedoch haben sich auch einige neue Erkenntnisse ergeben, die noch genauer untersucht werden können.

Das zweite Ziel dieser Arbeit war die Entwicklung und Implementierung eines weiteren Prüfstandes für die experimentelle Untersuchung des Wärmüberübergangs in Wirbelschichten bei hohen Temperaturen. Mit Hilfe dieses Prüfstandes wird es nun möglich sein Wärmeübergangskoeffizienten experimentell zu bestimmen. Die Herausforderung bei der Konstruktion und Auslegung des Prüfstandes waren die angestrebten hohen Mediumstemperaturen von bis zu 700 °C. Bei diesen Temperaturen können sowohl die normalerweise eingesetzten Stähle als auch standardmäßig erhältlichen Messmittel nicht mehr verwendet werden. Das Alleinstellungsmerkmal dieses Prüfstandes ist der stationäre Umlauf der Wirbelschicht zwischen der Heizseite und der Kühlseite ohne zusätzliche Fördereinrichtung.

Acknowledgments

At this point I would like to thank all those who supported me in the context of this master's thesis, but also on the way to it.

I would like to thank my thesis supervisor Dipl.-Ing. Stefan Thanheiser for his guidance, help and interest into my work. I would especially like to thank him for the professional input, the organizational support and the willingness to help in all matters.
I would like to thank my thesis supervisor Univ.Prof. Dipl.-Ing. Dr.techn. Markus Haider for the opportunity to write my thesis under his supervision. The high expectations made me grow, which i am very thankful for.
My thanks also go to the laboratory and workshop team, who have always given me excellent support in various practical work.

I also want to say thank you to my friends and fellow students Stefan, Thomas and Rupert who have always supported me during my studies and also privately. Especially Stefan who has accompanied me since my school days and has also given me professional support in writing this thesis.

I would like to express my sincerest gratitude to my parents. Without their unconditional support, always motivating words and an open ear at all times i would have lost sight of my goals. At last a very special thanks goes to my brother who took the time to proofread this work

"I know the price of success: dedication, hard work, and an unremitting devotion to the things you want to see happen."
-Frank Lloyd Wright

Contents

1. Introduction 1

2. Theoretical Background 3
- 2.1. Fluidized beds . . . 3
  - 2.1.1. Definitions and range of existence of fluidized beds . . . 3
  - 2.1.2. Characterization of particles and bulk goods . . . 4
  - 2.1.3. Characterization of fluidized beds . . . 10
  - 2.1.4. Fundamentals of fluid mechanics in fluidized beds . . . 11
  - 2.1.5. Gas distributor trays . . . 15
  - 2.1.6. Bubbling and mixing of solids . . . 16
- 2.2. Erosion in fluidized beds . . . 18
  - 2.2.1. Influencing parameters . . . 18
- 2.3. Heat transfer in fluidized beds . . . 21
  - 2.3.1. Definition of the heat transfer coefficient . . . 21
  - 2.3.2. Typical heat transfer coefficients . . . 21
  - 2.3.3. Parameters influencing the heat transfer coefficient . . . 22

3. Requirements and design considerations for the erosion test rig 25
- 3.1. Structure and basic function . . . 25
- 3.2. Measuring principle . . . 25
  - 3.2.1. Measuring arrangement . . . 26
  - 3.2.2. Recording of the pressure loss profile . . . 26
  - 3.2.3. Long-term test under specific operating conditions . . . 27
  - 3.2.4. Measurement of the inspection elements . . . 27
- 3.3. Design of the erosion experiments . . . 29
  - 3.3.1. Test duration . . . 29
  - 3.3.2. Planned Experiments . . . 32

4. Requirements and design considerations for the heat transfer test rig 34
- 4.1. Structure and basic function . . . 34
- 4.2. Measuring principle . . . 35
  - 4.2.1. Measuring arrangement . . . 36
  - 4.2.2. Recording of the pressure loss profile . . . 36
  - 4.2.3. High temperature heat transfer tests . . . 38

5. Design and Implementation of the erosion test rig 40
- 5.1. Calculations . . . 40
  - 5.1.1. Minimal fluidization velocity . . . 40

5.1.2. Sintered plate . . . 40
5.2. Construction . . . 42
5.2.1. Basic structure . . . 42
5.2.2. Integration of the sintered plate . . . 45
5.2.3. Incorporation and attachment of the inspection elements . . . 46
5.2.4. Filter system . . . 47
5.3. Manufacture and assembly . . . 49
5.3.1. Air supply . . . 49
5.3.2. Mechanical components . . . 49
5.3.3. Pneumatic and electrical components . . . 50
5.3.4. Air extraction . . . 51
5.4. Measurement setup and sensors . . . 53
5.5. Challenges and solution approaches . . . 54
5.5.1. Bypass valve . . . 54
5.5.2. Air supply line . . . 54
5.5.3. Transport disengagement height . . . 54
5.5.4. Impermissible over-pressure in the fluidized bed chamber . . . 55
5.5.5. scratch protection film . . . 56
5.5.6. Static charge . . . 56

6. Design and Implementation of the heat transfer test rig 57
6.1. Calculations . . . 57
6.1.1. Sintered plate . . . 57
6.1.2. Design of the heating elements . . . 57
6.2. Construction . . . 58
6.2.1. Basic structure . . . 58
6.2.2. Integration of the sintered plate . . . 61
6.2.3. Incorporation and attachment of the heating elements . . . 62
6.2.4. Design of the cooling lines . . . 65
6.3. Manufacturing and assembling . . . 67
6.3.1. Air supply . . . 67
6.3.2. Mechanical components . . . 67
6.3.3. Air extraction . . . 67
6.4. Measurement setup and sensors . . . 69

7. Results and Discussion 70
7.1. Erosion test rig . . . 70
7.1.1. Recording of the pressure loss profile . . . 70
7.1.2. Calculation of the minimal fluidization velocity . . . 70
7.1.3. Mass loss evaluation of the inspection elements . . . 72
7.1.4. Geometry change evaluation of the inspection elements . . . 74
7.1.5. Wear and tear of the resource sand . . . 76
7.2. Heat transfer test rig . . . 77

8. Conclusion and Outlook **78**

Bibliography **81**

A. Erosion test rig **83**

B. Heat transfer test rig **144**

Nomenclature

Greek symbols

α	Heat transfer coefficient	$\mathrm{W/m^2K}$
Δp	Pressure loss	Pa
ϵ	Porosity	
η	Dynamic viscosity	$\frac{\mathrm{kg\,s}}{\mathrm{m}}$
ϕ	Form factor	
ρ	Density	$\mathrm{kg/m^3}$

Subscripts

0	Superficial gas
B	Bed
C	cavity
f	fluidization
g	Gas
m	minimal
mf	minimal fluidization
O	Surface of the internals
opt	optimal
P	Particle
S	Surface
SV	Surface/Volume
l	transport
V	Volume

Roman symbols

A	Area	m^2
Ar	Archimedes-number	
BV	Bypass valve	
d	Diameter	m
FBC	Fluidized Bed Chamber	
FG	Degree of fluidization	
g	Gravitation constant	m/s^2
L	Length	m
M	Mass	kg
N	Number of particles	
$\dot{Q}$	Heat flow	W
Re	Reynolds number	
T	Temperature	°C
TDH	Transport disengagement height	
u	Velocity	$\frac{m}{s}$
V	Volume	m^3

List of Figures

1. Basic layout sandTES-technology [2] 2

2. Manifestations of fluidized beds [6] 4
3. Particle with open and closed pores [7] 7
4. Classification diagram according to Geldart[9] 8
5. Porosity in the fixed bed[7]. 9
6. a)Homogeneous fluidized bed, b)Heterogeneous (bubbling) fluidized bed, c)Thrusting fluidized bed[5] 11
7. a)Circulating fluidized bed, b)Channel forming in fluidized beds[5] . 12
8. Pressure loss profile of a homogeneously fluidized bed [5] 13
9. Determination of the point of minimal fluidization 14
10. gas distributor trays[6] 15
11. Relative flow in a) slow-bubbles and b) fast-bubbles[5] 17
12. Mechanism of mixing in solids in bubbling fluidized beds[6]. 17
13. Dependence of the erosion of a tube on the angle of incidence for different bed pressures[17]. 20
14. Heat transfer coefficient between immersed surface and fluidized bed of 400 µm glass spheres versus gas velocity [10] 22
15. Maximum heat transfer coefficient map dependent on particle diameter and porosity, at variable FG [10]. 23
16. Maximum heat transfer coefficient dependent on the particle diameter, at variable FG [10] 23

17. Structure erosion test rig. 26
18. Plexiglas insert for front and back wall for the erosion test rig. . . . 27
19. Measuring arrangement erosion test rig 29
20. Measurement points metal sheets. 30
21. Measurement points tube. 31

22. Structure of the heat transfer test rig. 35
23. Measuring arrangement for heat transfer test rig. 39

24. Basic structure of the erosion test rig. 44
25. Integration of the sintered plate erosion test rig. 45
26. Incorporation of the inspection element. 46
27. Sectional view of the attachment of the inspection element. 47
28. Filter system. 48
29. Bypass valve in air supply line. 50

30. Pneumatic and electrical components of the filter system. 51
31. Erosion test rig with air extraction. 52
32. Built-in volume flow sensor IL30.020. 53
33. Mechanism of ejection of solids from a fluidized bed into the freeboard [20]. 55

34. Basic structure of the heat transfer test rig. 58
35. Integration of the sintered plate heat transfer test rig. 61
36. Atachment of the heating element. 62
37. Attachment rear side. 63
38. Attachment front side. 64
39. Structure of the cooling lines. 65
40. Integration of the cooling lines. 66
41. Air extraction cooling tower. 68

42. Pressure loss profile for falling volume flow rate.n 70
43. Determination of the minimal fluidization volume flow rate 71
44. Mass loss over installation angle (0°-vertical / 90°-horizontal) of the metal sheets 74
45. Heatmap of geometric material loss of metal sheet 1. 75
46. Sieve analysis of the used sand. 77

47. Calculation of the minimal fluidization volume flow rate for the different test configurations. 129

List of Tables

1. Geometrical equivalent diameters 5
2. Form factor of technical interesting materials [6]. 6
3. Gas/solid flow conditions[6]. 12

4. Description of the pressure sensors in the erosion test rig. 28
5. Characteristics inspection elements 30
6. Design table for erosion rate. 33

7. Description of the temperature sensors for the heat transfer test rig. 36
8. Description of the pressure sensors heat transfer test rig. 37

9. Measuring range pressure sensors erosion test rig 54

10. Measuring range pressure sensors heat transfer test rig 69

11. Calculation of the minimal fluidization volume flow rate 72
12. Mass loss evaluation of the inspection elements 73
13. Geometry change of the metal sheet inspection elements 75
14. Geometry change of the tube inspection element 76

15. Geometric measurement data metal sheet inspection elements 130
16. Geometric measurement data tube inspection element 131

1. Introduction

Due to the increasing effects of climate change a turning point has been initiated in the energy sector in recent years. However, the path away from greenhouse gas-producing fossil fuels towards renewable energies involves a number of hurdles. The energy production with wind or photovoltaic has the main problem that these resources are time dependent. To ensure a constant power supply it is necessary to provide energy at any time and with strongly changing performance levels. This leads to the demand of energy storage systems. Primary produced energy is stored in different ways, like thermal, chemical, electrical or combinations of it, which is not used for the time in order to use it later when there is a demand for it [1].

The area of the thermal energy storage is the starting point for this scientific work. The Institute for Energy Technology and Thermodynamics at the Vienna University of Technology developed an energy storage technology which was published under the name SandTES - particle-based high-temperature heat storage systems (TES - Thermal Energy Storage). In the course of the research project, the need for further research arose. In this thesis special cases of this technology are examined in order to obtain a better planning basis for future large-scale plants [1].

The sandTES-project´s aim was to find a thermal energy storage for a high storage demand and high temperature. The used bulk materials, such as bauxite, corundum or quartz sand have no temperature limitations for industrial applications. In contrast to commonly used liquid storage materials, such as salts or thermal oil. The basic layout of the sandTES-technology is shown in Fig.1. The main components of the sandTES-technology are two bulk storage tanks, a hot and a cold one, and a particle heat exchanger between them. The particles are fluidized in the heat exchanger and flow through the system as a particle suspension. Bulk conveyors must be used for transport between the individual main components. In general, sandTES can be described as a storage technology for high temperatures with low-cost powders [2].

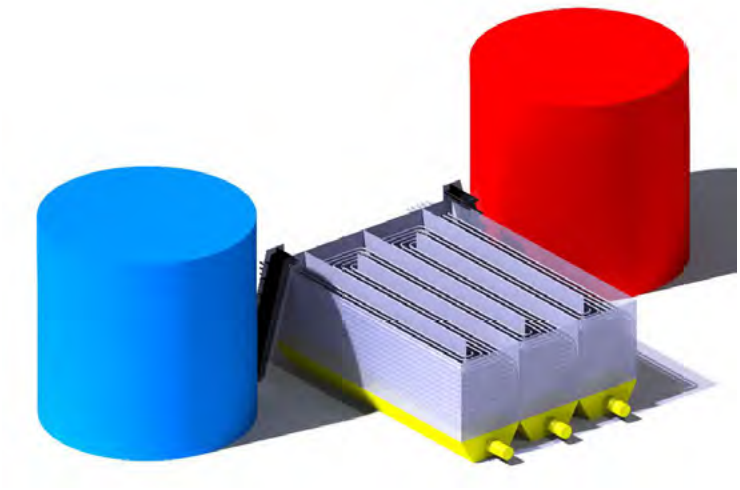

Figure 1.: *Basic layout sandTES-technology [2]*

Since erosion inevitably occurs between moving particles and fixtures, this must also be taken into account in designs. For fluidized beds of fine particles it was assumed, that little erosion occurs but almost no definite values exist. This uncertainty and the risk of system failures were the background for the erosion test rig, which is designed for erosion tests for special inspection elements. The inspection elements can be varied without much effort due to the construction of the test stand. The main measuring parameter of erosion are the mass loss and the geometry change of the inspection elements over the test period. The tasks of the master thesis for the erosion test rig included the development, construction, production and assembly planning, commissioning and the implementation and evaluation of long-term tests.

The efficiency and effectiveness of SandTES-technology also depends on the heat transfer in the fluidized bed. The values of the heat transfer coefficient are normally quite good. However, it is necessary to to know the exact values of the heat transfer coefficient for different configurations in order to achieve both better controllability and higher efficiency. This resulted in the development, construction, production and assembly planning of a heat transfer test rig.

2. Theoretical Background

2.1. Fluidized beds

Fluidized beds are widely used in combustion and chemical industries to convert solids with gases, liquids or others and bring them into close contact [3].
Fluidization is the operation in which solid particles are transferred from a static solid-like state to a dynamic fluid-like state, by forcing a fluid up through the particle bed [4].
Fluidized beds are mainly used because of the following characteristics [4]:

- The strong mixing within a fluidized bed results in large interfaces between the fluid-solid phases
- Excellent heat transfer between the fluidized bed and heat exchangers immersed in the bed
- Fluidized particles can be easily transported between different reactors

2.1.1. Definitions and range of existence of fluidized beds

When a fluid (liquid or gas) flows through a bulk layer with low velocity particles stay in position relative to each other (fixed bed). This can be seen in Fig.2(a). After the velocity reaches the minimal fluidization velocity u_{mf} the fixed bed loosens up, the particles gain some mobility and the bed height increases from the minimum or fixed bed heigt L_m to the minimal fluidization height L_{mf}, see Fig.2(b). If the velocity is increased the fluidization height L_f also increases and the particles can move even more, see Fig.2(c-g). If the velocity reaches the transport velocity u_t a pneumatic transport condition is established, see Fig.2(h) [5].

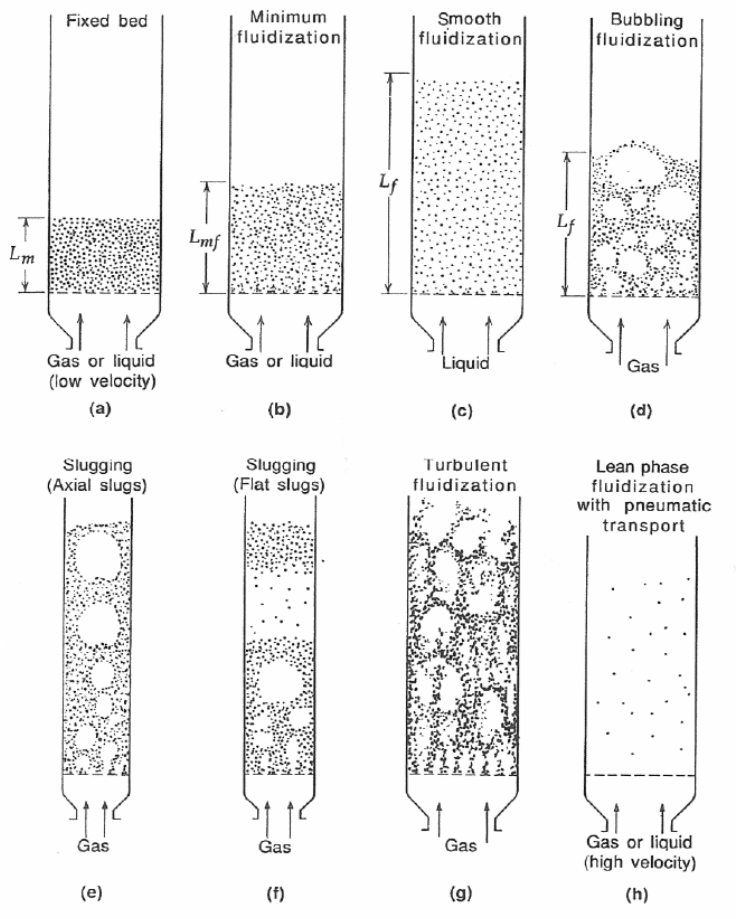

Figure 2.: *Manifestations of fluidized beds [6]*

2.1.2. Characterization of particles and bulk goods

The description and characterization of individual particles for fluidized beds is made using the following parameters [6].

- Particle size
- Particle shape
- Particle density

Since the particles in fluidized beds are not considered individually and are therefore bulk materials, the following parameters are used [6].

- Particle size distribution
- Porosity
- Bulk density

Particle size

The particle size is described by the diameter d. For the used technical relevant solids the shape of the particles deviates more or less from a sphere. Therefore the equivalent diameter is used, which is the diameter of a sphere with the same geometrical (volume, surface, etc.) or physical properties (rate of descent, etc.) [6][7]. The various different definitions of the equivalent diameter can be seen in Tab.1

Table 1.: *Geometrical equivalent diameters*

Symbol	Description	Explanation
d_P	screen diameter	Side length of the square through which the particle goes through
d_V	volume related diameter	Diameter of the sphere with the same volume as the particle
d_S	surface related diameter	Diameter of the sphere with the same surface like the particle
d_{SV}	surface/volume related diameter	Diameter of the sphere with the same surface/volume ratio as the particle

Particle shape

In bulk solids, each individual particle has a different shape, making it difficult to determine a meaningful parameter for description. In many industrial cases the designations *spherical, round, cubic, angular, platy, fibrous, etc.* are used. However, since it is not possible to continue working with this large number of designations for calculations, the form factor ϕ was introduced. The form factor describes the shape of a particle using two independent parameters. Wadell(1932) defines the form factor as the ratio of two surfaces which is also known as sphericity (see Eqn.(1)) [7].

$$\phi_{Wa} = \frac{Surface\ of\ a\ volume\ equation\ sphere}{Surface\ of\ the\ particle} = \left(\frac{d_V}{d_S}\right)^2 \tag{1}$$

For a sphere the form factor has a value of 1. For every other particle form it is between $0 < \phi < 1$. Tab.2 shows a collection of the form factors of various materials of technical importance [6].

Table 2.: *Form factor of technical interesting materials [6].*

Material	**Form factor** ϕ
crushed sand	0.70 to 0.85
rounded sand	0.90 to 0.95
technical glas spheres	0.98 to 1.00
normal salt	0.80 to 0.85

The connection between some geometrical equivalent diameters can be described with the form factor[6].

(a) for particles, which do not deviate significantly from the spherical shape:

$$d_{SV} \approx \phi \cdot d_P \tag{2}$$

(b) for particles, with one dimension significant bigger than the others, but not more than 2:1:

$$d_{SV} \approx d_P \tag{3}$$

(c) for particles, with one dimension significant smaller than the others, but not less than 1:2:

$$d_{SV} \approx \phi^2 \cdot d_P \tag{4}$$

Particle density

Particles can include pores, which can have an open or closed structure. This can be seen in Fig.3.
The difference between the material or absolute density $\rho_{P,abs}$ and the hydrodynamic density ρ_P of a particle lies in the consideration of these pores. The definition of the hydrodynamic density, see Eqn.5, uses the full volume of the particle including the volume of all pores. In contrast, for the absolute density the pore volume is subtracted, as can be seen in Eqn.6 [6].

$$\rho_P = \frac{M_P}{V_P} \tag{5}$$

$$\rho_{P,abs} = \frac{M_P}{V_P - V_{pores}} \tag{6}$$

In the previous equations(5)(5), M_P stands for the mass of a particle, further V_P and V_{pores} stands for the Volume of a particle and the pores.

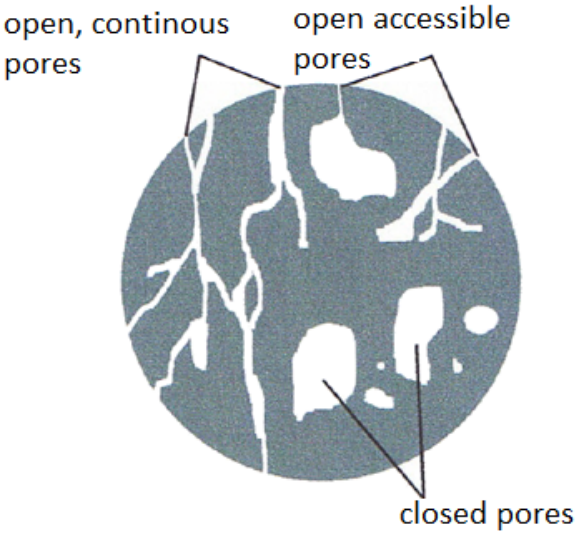

Figure 3.: *Particle with open and closed pores [7]*

Classification according to Geldart

Geldart [8] has made a classification of bulk materials in terms of fluidizability into four Groups A-D. The criteria for the classification are the particle diameter and the density difference between the particle and the fluid, see Fig.4

The characteristics of the Groups are presented in the following paragraphs [6]:

Group A

- homogeneous expansion after reaching the minimum fluidization velocity u_{mf}
- formation of bubbles at higher gas velocities, caused by slightly cohesive materials
- materials are usable for circulating fluidized beds and also for pneumatic transports
- fluidization of these materials have a high practical importance

Group B

- forces between particles are negligible
- formation of bubbles immediately after reaching the minimum fluidization velocity
- the dominant phenomenon is the formation of bubbles
- good solids mixture
- fluidization of these materials have the greatest practical importance

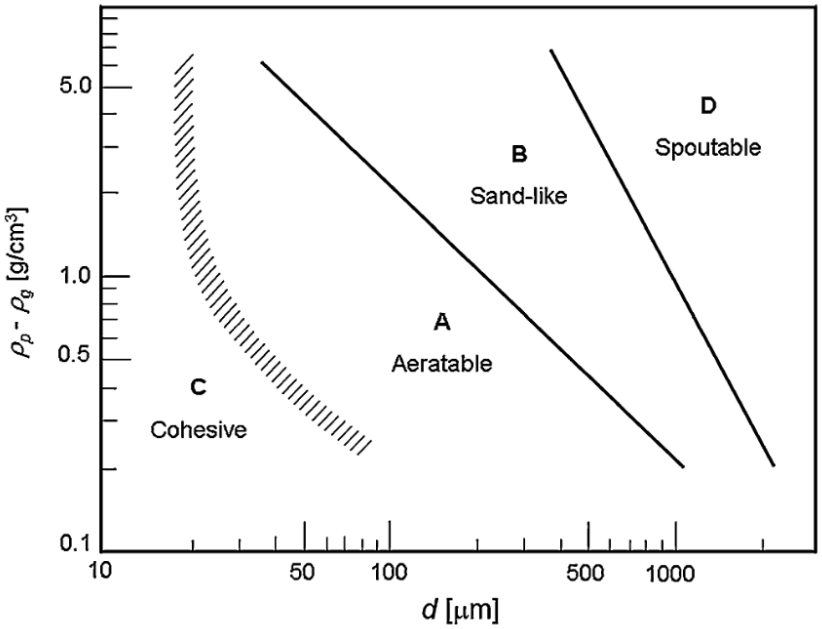

Figure 4.: *Classification diagram according to Geldart[9]*

Group C

- bulk materials with cohesive behaviour
- fluidization of these materials is extremely challenging
- fluidization tends to form plugs or channels
- forces between the particles are stronger than the force of the fluid on the particle
- wet and irregular shaped particles
- no use in practical applications

Group D

- particles with a large diameter or high density
- fluidized beds with these materials are mostly designed as bubble layer
- applications in the food industry and fluidized beds for agricultural products like coffee beans and grain

Particle size distribution

For the viability of technical powders it is necessary to consider the particle size distribution, as particles are usually not monodispers, but a more or less broad distribution of different particle sizes. Therefore, it is necessary to utilize the surface/volume related equivalent diameter d_{SV} which can be calculated from the number N_x and diameter d_x of the individual particles according to Eqn.(7).

$$d_{SV} = \frac{N_1 \cdot d_1^3 + N_2 \cdot d_2^3 + ...}{N_1 \cdot d_1^2 + N_2 \cdot d_2^2 + ...} \tag{7}$$

Porosity

The initial state of every fluidized bed is that of a fixed bed. The fluidized bed chamber is filled with a certain amount of the bulk material (Fig5). In this configuration the fixed bed has the fixed bed height L_m and a porosity $\epsilon_{fixedbed}$[10].

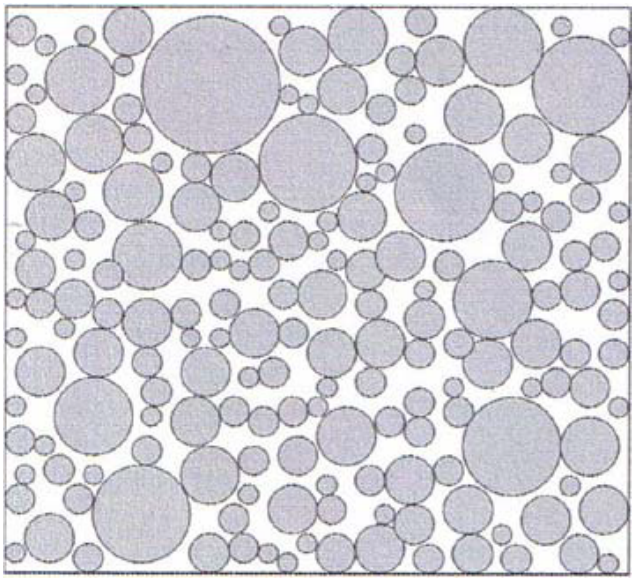

Figure 5.: *Porosity in the fixed bed[7].*

For a fluidized bed the porosity ϵ is defined in the following way[6][7]:

$$\epsilon = \frac{cavity\ volume}{bed\ volume} = \frac{bed\ volume - particle\ volume}{bed\ volume} \tag{8}$$

$$\epsilon = \frac{V_C}{V_B} = 1 - \frac{V_P}{V_B} = 1 - \frac{M_P}{\rho_P \cdot V_B} \tag{9}$$

In the previous equation(9), V_C, V_B and V_P are the volume of the cavity, the total bed and the particles. M_P and ρ_P are the total mass and the density of the particles.

The porosity of the fixed bed should be determined in this case in which it occurs under real conditions, because there is a difference between a loose bulk and a shaken bulk. Furthermore the fixed bed porosity depends on the following parameters[6]:

(a) particle shape: lower form factor leads to a higher fixed bed porosity

(b) particle size: larger particles leads to lower fixed bed porosity

(c) particle size distribution: a larger distribution leads to a lower fixed bed porosity

Bulk density

The bulk density ρ_B is the mass M of a bulk quantity divided by the bed Volume V_B, see Eqn.(10). The bulk density is always smaller than the particle density ρ_P, because the cavities between the particles which are included in the calculation. The bulk density increases when the bulk material is solidified, this means a force is applied to shrink the cavities[6][11].

$$\rho_B = \frac{M}{V_B} \tag{10}$$

The connection between the bulk density and the porosity can be seen when comparing Eqn.(9) and Eqn.(10) to get Eqn.(11).

$$\epsilon = 1 - \frac{\rho_B}{\rho_P} \tag{11}$$

2.1.3. Characterization of fluidized beds

The characterization of fluidized beds is very important as there are several influencing parameters like particle properties, fluidizing agent (gaseous or liquid), fluidization velocity. The manifestation of a fluidized bed can be divided into two different cases, homogeneous and heterogeneous. Knowledge of the relationship between the pressure loss in the fluidized bed and the fluidization velocity is also a crucial point for the correct design of a fluidized system.

Homogeneous fluidized beds

Homogeneous fluidized beds are characterized by a uniform volume expansion with increasing fluidization velocity (see Fig.6 a). Homogeneity of a fluidized bed means a uniform distribution of the particles. This is in reality only possible with same-size particles and a liquid as fluidizing agent [5].

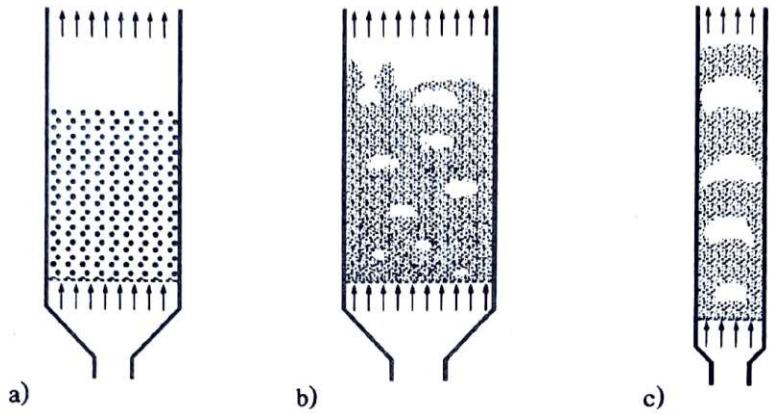

Figure 6.: *a)Homogeneous fluidized bed, b)Heterogeneous (bubbling) fluidized bed, c)Thrusting fluidized bed[5]*

Heterogeneous fluidized beds

Heterogeneous fluidized beds arise when the bulk material is unevenly distributed, then the larger and heavier particles are in the lower part of the fluidized bed. Instabilities in the flow lead to the formation of bubbles are also counted among the heterogeneous fluidized beds. The bubbles are nearly completely free from solids, unite (coalesce) during the rise and burst when they reach the top of the fluidized bed. Therefore, it looks like a bubbling liquid (see Fig.6b). In cases where the fluidized bed has a small cross sectional and a large height, the bubbling leads to a periodic and jerky lifting of the fluidized bed (thrusting fluidized bed - see Fig.6c). If the height of thrusting fluidized beds is not predictable and it is possible for a discharge of solids to occur, the use of a side mounted cyclone is necessary. The bed material is returned which is why it is called a circulating fluidized bed, see Fig.7a). For cohesive fine-grained bulk materials (Geldart Group C) a fluidization with gas is often impossible, because flow channels are formed and so the rest of the material is practically not flown through, see Fig.7b) [5].

2.1.4. Fundamentals of fluid mechanics in fluidized beds

In order to better understand the processes in a fluidized bed it is necessary to consider the fluid mechanical key points. The starting point for this is the pressure loss diagram and, as a result, the relationships between pressure loss and velocities, such as minimal fluidization velocity and transport velocity.

Pressure loss profile

The airflow through of the fluidized bed causes a pressure loss Δp, which depends on the superficial gas velocity u_0, which in turn is the velocity of the fluid in an empty vessel. The typical course of the pressure loss over the superficial gas velocity

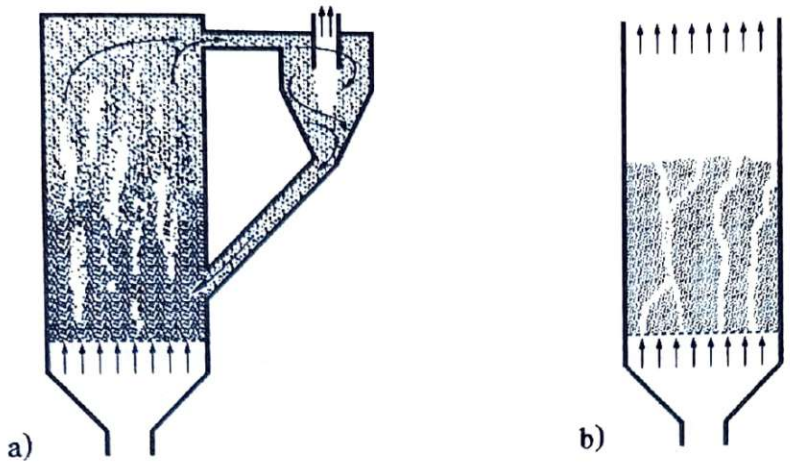

Figure 7.: *a)Circulating fluidized bed, b)Channel forming in fluidized beds[5]*

can be seen in Fig.8. Also, a hysteresis can be seen in the area of the fixed bed, which means a difference in the pressure loss for increasing or decreasing the velocity. Tab.3 as well as in Fig.8 show three gas/solid flow conditions which are mainly dependent on the superficial gas velocity [5].

Table 3.: *Gas/solid flow conditions[6].*

Area/Description	Particle	Pressure drop	Fluid velocity
I fixed bed	motionless	increasing	slightly
II fluidized bed	motion	constant	medium
III pneumatic transport	motion	slightly increasing	high

Minimal fluidization velocity

The minimal fluidization velocity is the limit velocity between the fixed bed (area I) and the fluidized bed (area II). The point of minimal fluidization and therefore the minimal fluidization velocity can be seen in the pressure loss profile (Fig.8) as the intersection of the pressure curves of the fixed bed and the fluidized bed. In real-world applications the transition from the fixed to the fluidized bed is smooth and not a hard cut. Only for materials with a narrow range of particle size the transition happens for the whole bed simultaneously (see Fig.9). For the experimental determination of the minimal fluidization velocity it must be observed, that the fixed bed is a loose bulk and not compacted, because otherwise other pressure losses and therefore other minimal fluidization velocities occur. Conventionally the experimental determination of the minimal fluidization velocity is carried out in such a way, that first the bed is completely fluidized and then the volume flow is

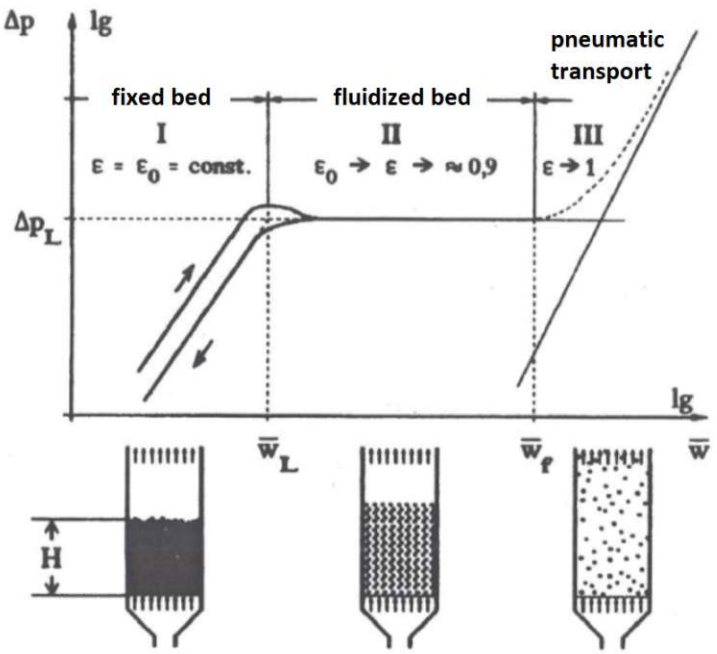

Figure 8.: *Pressure loss profile of a homogeneously fluidized bed [5]*

successively reduced in order to record the pressure loss profile [6].

In some literature the minimal fluidization velocity u_{mf} is calculated via an approximation Eqn.(12) and uses the Archimedes-number Ar (see Eqn.(13)).

$$u_{mf} = \frac{\mu}{\rho_F \cdot d_{SV}} \left(\sqrt{33.7^2 + 0.0408 \cdot Ar} - 33.7 \right) \tag{12}$$

$$Ar = \frac{\rho_g \cdot d_{SV}^3 \cdot (\rho_P - \rho_g) \cdot g}{\eta_g^2} \tag{13}$$

The approximation Eqn.12 is useable for Reynolds-numbers between 0.001 to 4000 and has proven its worth for different materials and particle diameters [6]. The Reynolds number is a dimensionless number which is used in fluid dynamics and can be understood as the ratio of inertial to viscous forces. The disadvantage is, that other influences such as internals or other operating temperatures are not included.

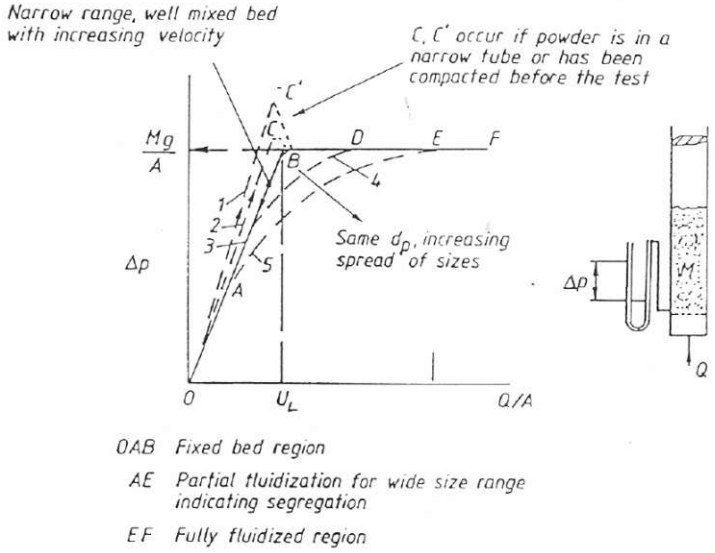

Figure 9.: *Determination of the point of minimal fluidization*

Transport velocity

The transport velocity is the limit velocity between the fluidized bed (area II) and the pneumatic transport (area III) (see Fig.Fig.8). The transport velocity can be calculated using an equilibrium of forces on the particle, in which the weight force minus the buoyancy force and the drag force is equal to the acceleration force[6].

Pressure loss in the fluidized bed

The fixed bed reaches the fluidized bed condition when the resistance of the gas flow against the bulk material is equal to the weight force of the whole particles minus the buoyancy force. This equilibrium can be seen in Eqn.(14)[6].

$$\Delta p \cdot A = A \cdot L_{mf} \cdot (1 - \epsilon_{mf}) \cdot (\rho_P - \rho_g) \cdot g \tag{14}$$

The Pressure loss in the fluidized bed (Eqn.(15)) can be expressed from Eqn.(14). Also, it is evident that the pressure loss is independent from the superficial gas velocity, which means that the pressure loss remains constant in the fluidized bed[6].

$$\Delta p = (1 - \epsilon) \cdot (\rho_P - \rho_g) \cdot g \cdot L \tag{15}$$

Degree of fluidization

The degree of fluidization is defined in Eqn.(16) as the ratio of the air velocity u_f in the fluidized bed to the minimum fluidization velocity u_{mf}. It is used to set the operating point.

$$FG = \frac{u_f}{u_{mf}} \tag{16}$$

2.1.5. Gas distributor trays

The main task of the gas distributor tray is to distribute the fluidization gas as evenly as possible over the fluidized bed cross-section. The better the gas is distributed, the better the fluidized bed can form, but care must be taken that the gas resignations are permitted in such a way that no particle can can enter the wind box or pipeline[6].

There are several possible designs for a gas distributor tray (see Fig10[6]):

- porous plates (sintered plates) 10a
- perforated plates, bottoms or pipes 10b
- nozzle plates with air boxes or pipe distributors 10c
- bell bottoms with air boxes or pipe distributors 10d

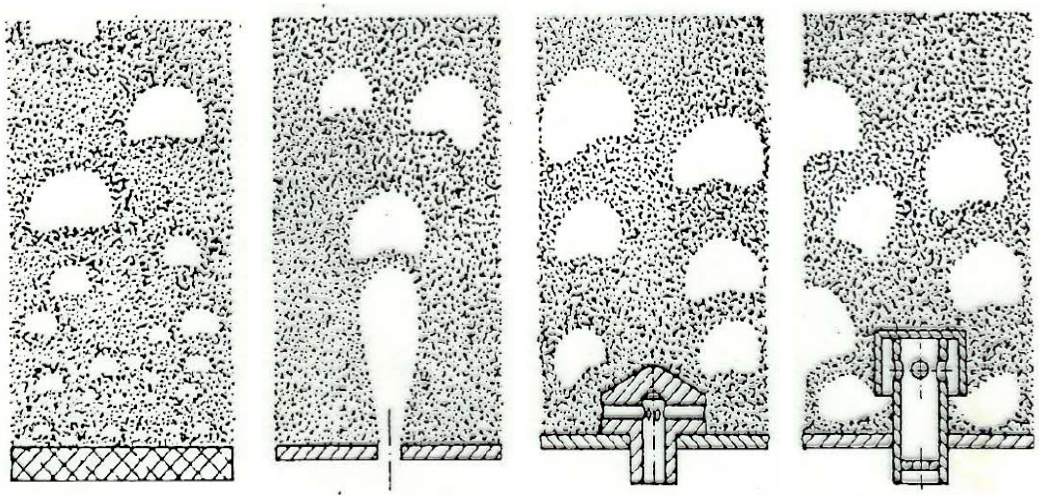

(a) *porous plate* (b) *perforated plate* (c) *nozzle plate* (d) *bell bottom*

Figure 10.: *gas distributor trays[6]*

2.1.6. Bubbling and mixing of solids

The formation of bubbles is relevant in gas-solid fluidized beds, specifically for the Group A and Group B according to Geldart [8]. Depending on the gas distributor system the bubbles form just above the system itself. During the rise the bubbles unite with each other, this is also called bubble coalescence, and thus the diameter and the rate of ascent of the bubbles increase [5].

The advantages of bubbling are the following[6][5]:

- mixing of the phases
- good heat and mass transport
- uniform temperature distribution over the entire fluidized bed
- better heat transfer to built-in heating or cooling surfaces

There are also some disadvantages which occur when bubbles form[6][5]:

- increased particle abrasion
- increased wear of walls and components

The shape of a gas bubble usually looks like an umbrella, because of a particle wake that forms behind the bubble. The bubble volume and the wake volume approximately forms a sphere[6]. During the rise of a bubble we differentiate between slow-bubbles and fast bubbles, which can be seen in Fig.11. Smaller bubbles rise more slowly in a fluidized bed than the gas flow in the suspension phase. For this reason, a circulating flow forms in the bubbles and they are also flowed through from the bottom up in the middle of the bubbles. If the bubbles rises faster, as is the case with larger bubbles, then there is a circulating flow inside the bubble with the formation of a cloud an less exchange to the outside. If an intensive exchange of the gas with the fluidized bed is to take place, small, slow bubbles are advantageous[5].

The mixing of solids in a fluidized bed is an important factor for several other operating parameters. The quality of the mixing affects the following processes[6]:

- gas/solid-contact
- temperature gradient between reaction zone and heat exchanger surface
- heat transfer coefficient
- number of the entry and exit points for solid materials

The process of mixing can be seen in Fig.12. During the rise of the bubble, particles of the particle wake are lost (wake shedding), see situation 5 in Fig.12. Likewise there are particles in the drag which are distributed during the rise (situation 4 in Fig.12). At last the bubble bursts on the surface of the fluidized bed and the particles are distributed horizontally (see situation 6 in Fig.12). In general the particles are mainly mixed in the vertical direction[6].

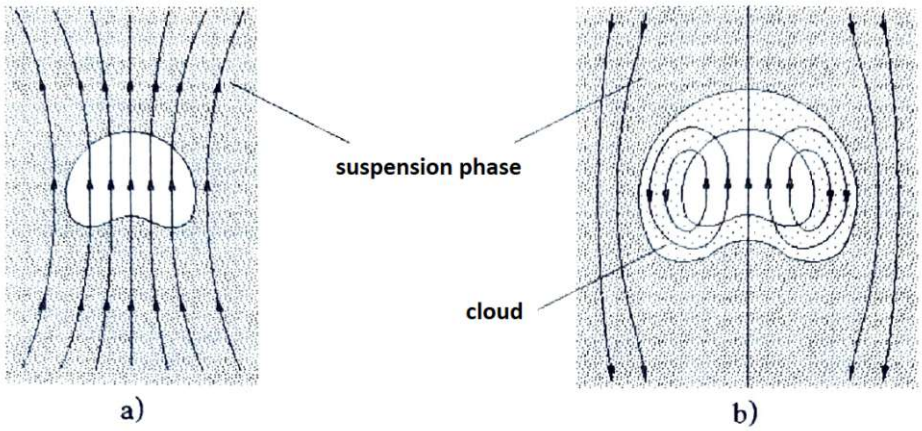

Figure 11.: *Relative flow in a) slow-bubbles and b) fast-bubbles[5]*

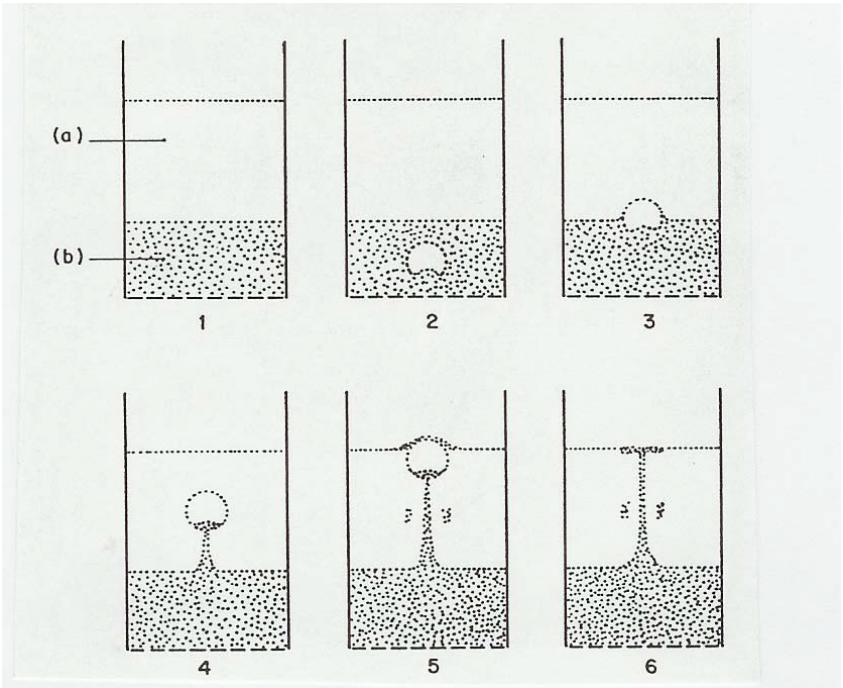

Figure 12.: *Mechanism of mixing in solids in bubbling fluidized beds[6].*

2.2. Erosion in fluidized beds

Erosion plays a major role for objects, such as heat exchanger tubes, in the fluidized bed. Since these internals are essential for the function, a defect would be fatal, as the costs for repairs and downtime for systems are substantial and sometimes only possible to a limited extent due to the construction of the system.

2.2.1. Influencing parameters

Erosion in fluidized beds is comparable to the sandblasting process, however undesirable in most applications. A precise description of the material removed by erosion is not possible, as there are several parameters which affect the behaviour and also each other.
The following parameters have a major effect on the erosion behaviour:

- fluid velocity
- particle properties (size, shape, abrasion resistance,...)
- position and shape of the internals/obstacles

Time

In most studies, time plays a subordinate role, as the erosion extent depends linearly on time. In some papers the incubation time is investigated for ductile materials, erosion occurs after an incubation time of 10 to 20 hours. For brittle materials there is no incubation time [12][13].

Fluid velocity

The most important parameter for the description of erosion in fluidized beds is the superficial gas velocity u_0, which is the velocity of the fluid in the empty vessel. Effenberger [14] describes the rate of erosion Δs, see Eqn.(17), over the superficial gas velocity u_0 and the particle diameter d_P, see also [15]. A Similar correlation is mentioned by Brötz [16].

$$\Delta s \approx K_1 \cdot u_0^3 \cdot d_P \tag{17}$$

According to Howes [12] and Zhu [13] the impact velocity u_I is the main characteristic.

$$\Delta s \approx k \cdot u_I^n \tag{18}$$

The Exponent n in Eqn.(18) is different compared to Eqn.(17) and has a value between 2 and 3. Especially for ductile materials it is about 2.3 or 2.4. For ceramic materials n also can reach values from 2 up to 4. In general, most sources describe that the rate of erosion increases with the fluid velocity [17].

Particle size

As already seen in Eqn.(17), the erosion rate also depends on the particle diameter, which also agrees with other literature [17]. Howes et al. claims that above the critical diameter of 100 µm the erosion rate remains constant [12].

Particle hardness

In most cases the erosion rate increases as the particle hardness increases, however if the particle hardness is lower than the material hardness of the installations the erosion rate decreases dramatically [12]. For non ferrous materials the erosion rate is significantly less influenced by the particle hardness [13].

Particle angularity

In the literature the shape of the particle impinge the erosion behaviour. The erosion rate increases when the form factor Ψ decreases, this means that the erosion rate for particles with a high angularity is higher than for round particles [12].

Particle flux

As particle flux (amount of flowing particles) increases there is an observed decrease in erosion rate, because the rebounding particles shield the objects [12].

Installation position

In the literature it has been reported that the angle in which the main flow direction reaches the installation has a huge impact on the erosion behaviour. Brötz [16] claims that the highest erosion rate occurs when the flow direction is inclined 20° in regard to the normal on the surface of impact. It is also mentioned that this erosion rate is twice as high as the erosion rate with a flow direction normal to the surface of impact. Wiman and Almstedt [17] made quite similar observations, as can also be seen in Fig.13. In many papers it is mentioned that the maximum erosion rate occurs at angles between 20 to 40° relative to the gravity vector (i.e. 140° and 220° in Fig.13.

Material properties

Predictions of the erosion rate based on the material hardness are contradictory in some studies. Another option described by Zhu [13] is that the erosion rate increases when the Youngs modulus decreases. Under a certain threshold value of hardness and Youngs modulus the erosion rate increases enormously.

Pressure in the fluidized bed

A raised pressure in the fluidized bed increases the erosion rate for the installations, as can be see in Fig.13 [17].

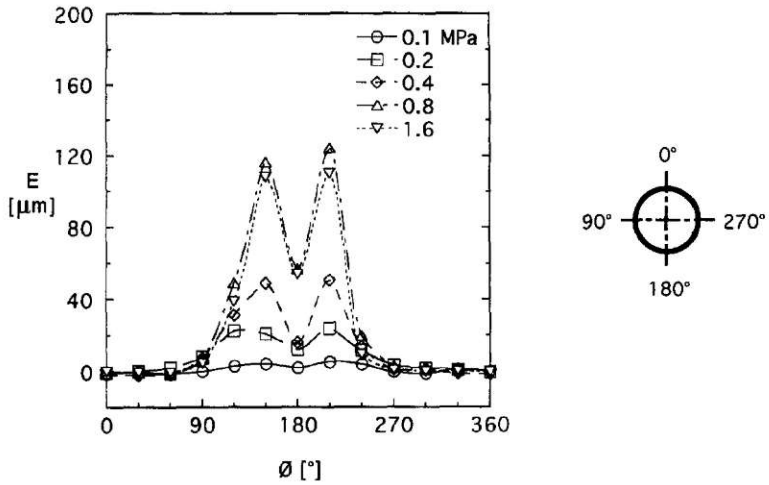

Figure 13.: *Dependence of the erosion of a tube on the angle of incidence for different bed pressures[17].*

2.3. Heat transfer in fluidized beds

One of the most important advantages of fluidized beds, as mentioned in 2.1 is the excellent heat transfer between the fluidized bed and internals. The very good heat and material transfer results from the large surface area that is available in the fluidized bed due to the use of small particles. A cubic meter of 100 µm particles has a surface area of approximately 30 000 m^2. Because of the predominantly vertical mixing the fluidized bed has a high effective thermal conductivity in the vertical direction, quickly dissipating temperature gradients [6].

2.3.1. Definition of the heat transfer coefficient

The heat transfer coefficien α between gas/solid fluidized beds an the surface of immersed heated or cooled internals (plates, tubes or tube bundles) A_O can be desribed with Eqn.(19) [6].

$$\alpha = \frac{\dot{Q}_{OB}}{A_O \cdot (T_O - T_B)} \tag{19}$$

In Eqn.(19) $\dot{Q}$ is the heat flow which is emitted from the surface of the internals A_O. T_O is the temperatures of the surface of the internals and T_B is the temperture of the bed in a sufficient distance of the heated or cooled internals.

2.3.2. Typical heat transfer coefficients

Fig.14 shows the heat transfer coefficient α between a vertical cylindrical heater and an air-fluidized bed of glass spheres (400 µm diameter) as a function of the fluid velocity. It can be seen that the heat transfer coefficient increases rapidly after the minimal fluidization velocity and reaches its maximum at the optimal fluidization as velocity u_{opt}. The fluidization velocity keeps increasing, the porosity ϵ also increases, leading to a decrease of the heat transfer coefficient. With increasing loosening of the fluidized bed after the minimal fluidization the particles begin to move and the heat transfer coefficient rises as a result of the particle-convective net energy transport from the heater surface to the bulk of the bed. The dotted curve in Fig.14 shows the increase of the heat transfer coefficient with gas velocity for a single-phase gas flow (without particles) [10].
Beside the particle convective transport, heat is also transferred directly to the gas (gas convective transport) and by radiation between heater surface and the particles. These three heat transport mechanisms can be viewed independently, although they are running in parallel. The total heat transport coefficient can be written as sum of these three parts (see Eqn.21).

$$\begin{aligned} \alpha &= \alpha_P + \alpha_G + \alpha_R \\ \text{total} &= \text{particle convection} + \text{gas convection} + \text{radiation} \end{aligned} \tag{20}$$

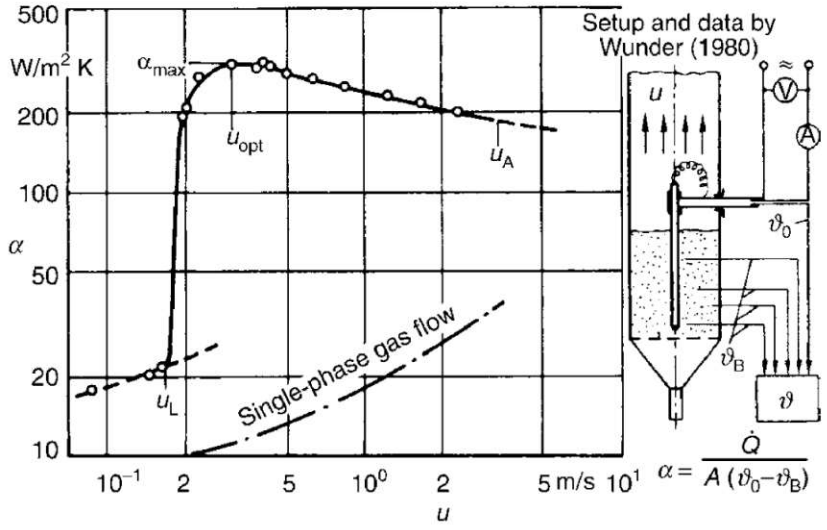

Figure 14.: *Heat transfer coefficient between immersed surface and fluidized bed of* 400 µm *glass spheres versus gas velocity [10]*

2.3.3. Parameters influencing the heat transfer coefficient

The heat transfer coefficient between gas fluidized particles and internals is mainly influenced by the particle properties, the gas properties and the operation parameters [10].

Particle properties

The following particle properties have an influence on the heat transfer coefficient[10]:

- particle diameter d
- porosity ϵ
- heat capacity c_p
- particle density ρ_P
- thermal conductivity of the particle λ_P

Fig.15 and Fig.16 show that the heat transfer coefficient changes with different configurations of the porosity ϵ (in Fig.15 ψ) and the particle diameter d. The maximum of the heat transfer coefficient is achieved by using particles with a small diameter. Above a certain particle diameter the heat transfer coefficient increases again. The reason for this is that the gas convective heat transport[10]. Fig.15 has to be used with great care, as the fluidization degree where the maximum heat transfer occurs is a strong function of the fluidization degree (FG).

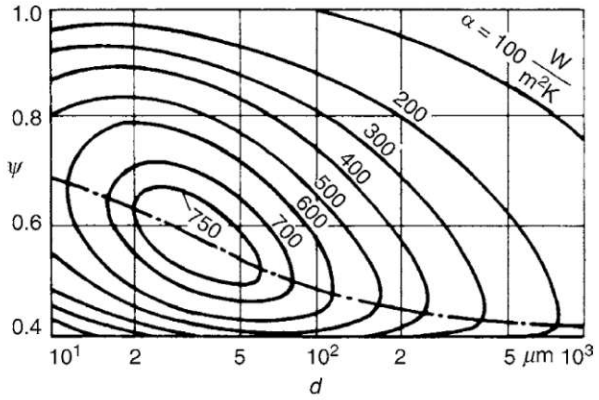

Figure 15.: *Maximum heat transfer coefficient map dependent on particle diameter and porosity, at variable FG [10].*

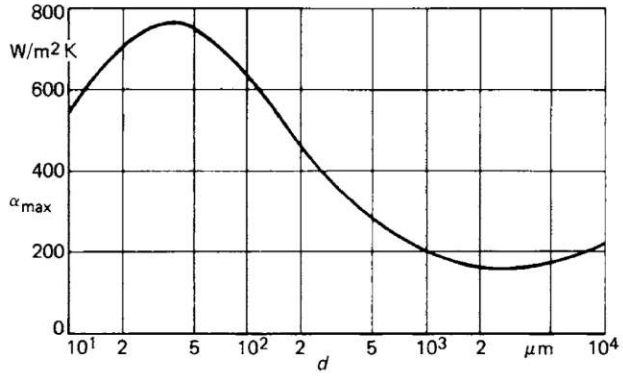

Figure 16.: *Maximum heat transfer coefficient dependent on the particle diameter, at variable FG [10]*

Gas Properties

The following gas properties have an influence on the heat transfer coefficient[10]:

- thermal conductivity of the gas λ_g
- modified mean free path of the molecules l
- density of the gas ρ_g
- viscosity of the gas η_g

Only the thermal coductivity and the modified mean free path of the molecules affect the particle convective component of the heat transfer coefficient. From an empirical equation the maximum heat transfer coefficients are found to be roughly proportional to $\lambda_g^{0.6}$ [10].

Operational Parameters

The following operational parmeters have an influence on the heat transfer coefficient[10]:

- gas flow rate
- pressure
- temperature
- shape and size of the arrangement and heater (or cooler)

The influence of the gas flow rate (along with the fluid velocity) can be seen in Fig.14 [10].

3. Requirements and design considerations for the erosion test rig

3.1. Structure and basic function

The main aim of this test rig and the test is the investigation of erosion on internals in dense fluidized beds. With these results it is possible to estimate the erosion rate of internals in fluidized beds over a long period of time. For the determination of the erosion rates under real conditions the erosion rate of the inspection elements is converted. Therefore a rather conservative approach is chosen, in order to overestimate the actual erosion rate.

The structure of the erosion test rig itself is kept rather simple, as can be seen in Fig.17. Air is conveyed into the wind box by means of a positive displacement blower. The wind box is necessary to ensure an even flow through the sintered plate. The sintered plate guarantees an even distribution of the air volume flow over the entire bed surface. After the sintered plate the air enters the fluidized bed chamber. The inspection elements are arranged side by side and are completely immersed in the fluidized bed. The air escaping from the fluidized bed collects in the free space and is then extracted.

For the evaluation of the results it is necessary that the flow regime as the test is the same as under real conditions. This means, that the bubbling fluidized bed that normally occurs in these applications must also be present in the test rig. The simplest way to check this is visually. The front and back wall of the test rig is made of plexiglas to be able to see the inside of the test rig in the area of the fluidized bed (see Fig.18).

3.2. Measuring principle

The test execution consists of three parts. The first part contains the recording of the pressure loss profile. The second part contains the long-term test under specific operating conditions. This approach is necessary to carry out the erosion tests, because the first part provides the data to be able to set the operating point exactly in the long-term test. The third part is the measurement of the inspection elements.

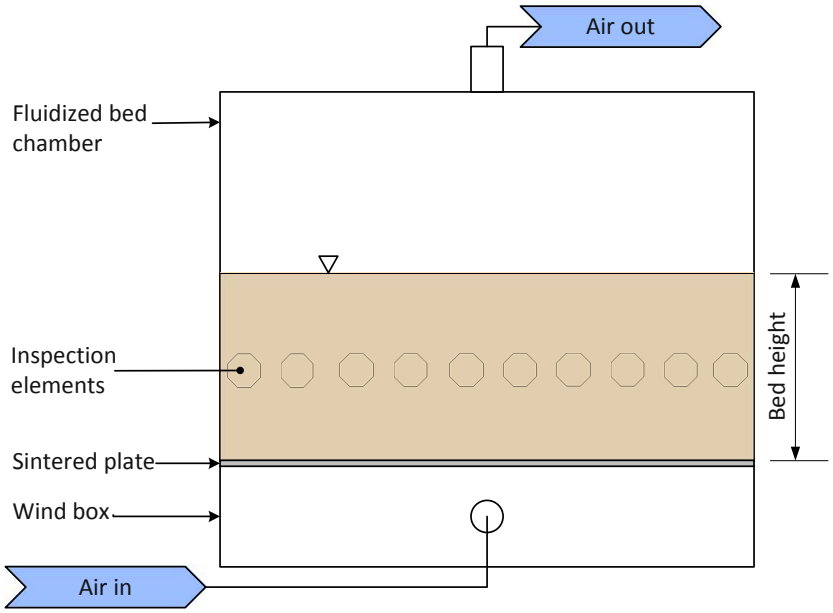

Figure 17.: *Structure erosion test rig.*

3.2.1. Measuring arrangement

For the effective execution of the measurements several pressure difference sensors and a flow sensor are necessary. In Fig.19 the layout of the measuring equipment can be seen. One of the key points of the measurement is the volume flow sensor (FS), because it is necessary to determine the real volume flow which enters the erosion test rig. An exact determination of the volume flow is important for the determination of the minimal fluidization velocity and also for the regulation in the long-term test. Tab.4 shows the measuring task and the connection points of the different differential pressure measuring sensors.

3.2.2. Recording of the pressure loss profile

The execution of this measurement task is paramount to get comparable results for the erosion rate. As already described in 2.1.4, the volume flow is successively reduced to record the pressure loss profile. It starts with full fluidization, which is controlled on the one hand by setting a multiple of the theoretical volume flow and On the other hand it it will be checked optically, whether a bubbling fluidized bed is present. The volume flow is continuously reduced via the frequency converter for the roots blower. However, since the roots blower delivers a very high minimal volume flow it is necessary to reduce the volume flow via a bypass valve (BV), as it can be seen in Fig.19. In order to also be able to record and evaluate the hysteresis

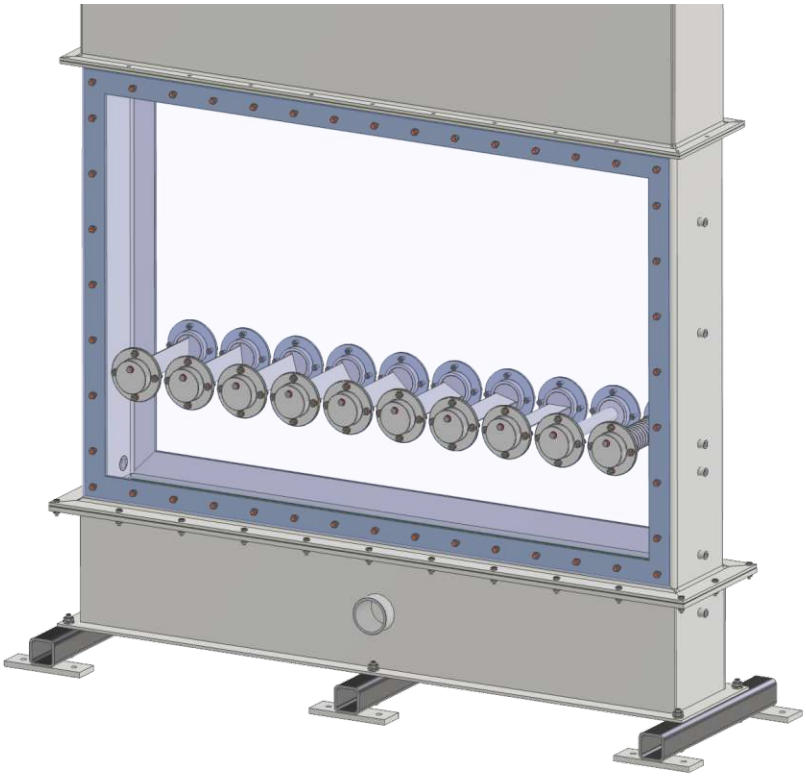

Figure 18.: *Plexiglas insert for front and back wall for the erosion test rig.*

of the pressure loss profile, tests in which the volume flow is continuously increased until full fluidization is achieved are also carried out.

3.2.3. Long-term test under specific operating conditions

The long-term test is planned for a period of one month. After this time the inspection elements are removed from the test rig and measured. During the whole test time the differential pressure of all sensors and the volume flow are documented. Likewise the frequency converter of the roots blower offers the possibility to control the volume flow and and can also kept constant over the entire test period. This is also very important, because of temperature differences the volume flow can fluctuate more or less. The temperature differences can occur due to the ambient temperature but also due to increased compressor work.

3.2.4. Measurement of the inspection elements

To get substantial results it is important to consider different configurations or flow conditions on the inspection elements in the fluidized bed. Small metal sheets are primarily used as erosion bodies/inspection elements. These metal sheets are

Table 4.: *Description of the pressure sensors in the erosion test rig.*

Pressure sensor	**Connection point 1**	**Connection point 2**	**Measuring task**
PD1	atmosphere	wind box	absolute pressure wind box
PD2	wind box	bottom of the fluidized bed chamber	pressure loss over the sintered plate
PD3	bottom of the fluidized bed chamber	top of the fluidized bed chamber	pressure loss over the fluidized bed
PD4	lower measuring point for porosity	upper measuring point for porosity	differential pressure for porosity determination
PD5	top of the fluidized bed chamber	atmosphere	absolute pressure above the fluidized bed

positioned at different angles in the fluidized bed. A tube and a fin tube are also used as erosion bodies. The characteristics and installation positions of the inspection elements are presented in Tab.5. The angle for the installation position of the metal sheets is measured away from the vertical, which is also the direction of the flow.

The mass and geometric dimensions are used as measured variables for determining the erosion rate. On this occasion the measured variables are determined before and after the long-term test. The determination of the mass is done with a scale calibrated to a thousandth of a gram. For the metal sheets the thickness is the measurement parameter for the geometric dimension. The measurement points for the thickness of the metal sheets can be seen in Fig.20. For the tube, the diameter is the measurement parameter and the measurement points can be seen in Fig.21

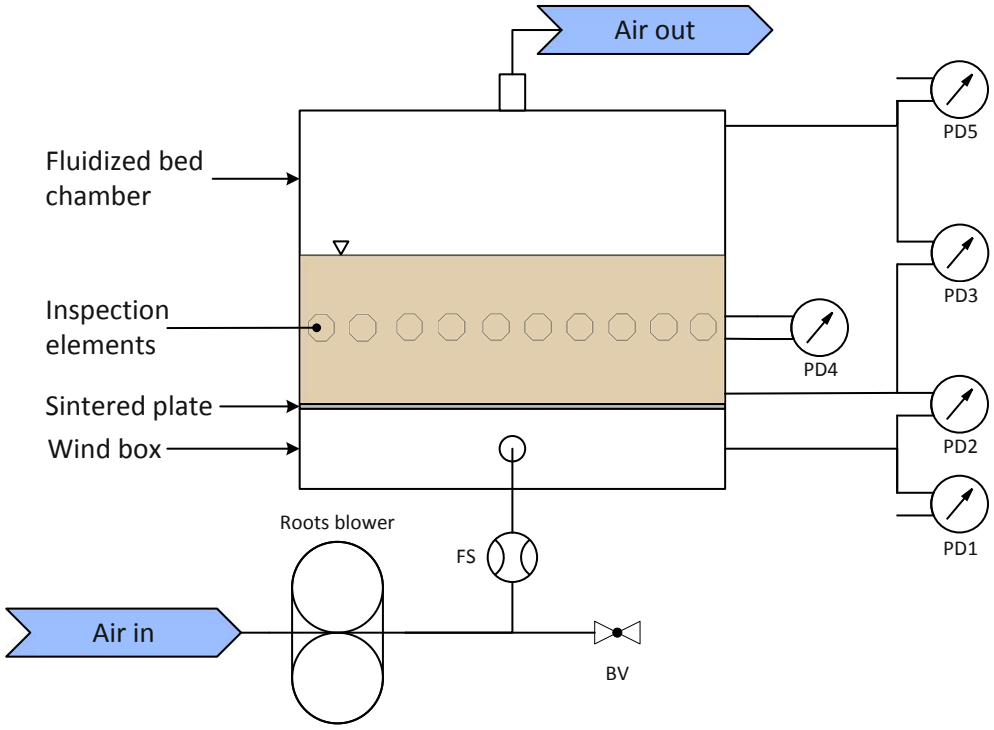

Figure 19.: *Measuring arrangement erosion test rig*

3.3. Design of the erosion experiments

For the erosion experiments quartz sand is used as the material for the fluidized bed.

3.3.1. Test duration

Reference values for real operating parameters

- Particle size: 146 µm
- Minimum fluidization velocity: $u_{mf} = 0.0215\ \frac{\mathrm{m}}{\mathrm{s}}$
- Degree of fluidization: FG4

Values for Erosion test 1

- Particle size: 330 µm
- Minimum fluidization velocity: $u_{mf} = 0.1057\ \frac{\mathrm{m}}{\mathrm{s}}$
- Degree of fluidization: FG5

Table 5.: *Characteristics inspection elements*

Number	Inspection element	Geometric dimensions	Installation positions
1-8	metal sheet	width $w_p = 40\,\text{mm}$ thickness $t_p = 2\,\text{mm}$	0°, 7°, 15°, 30°, 45°, 60°, 75°, 90°
9	tube	outer diameter tube $d_t = 25\,\text{mm}$ tube thickness $t_t = 2\,\text{mm}$	-
10	fin tube	outer diameter tube $d_t = 25\,\text{mm}$ outer diameter fin $d_f = 45\,\text{mm}$ fin spacing $s_f = 9\,\text{mm}$ fin thickness $t_f = 2\,\text{mm}$	-

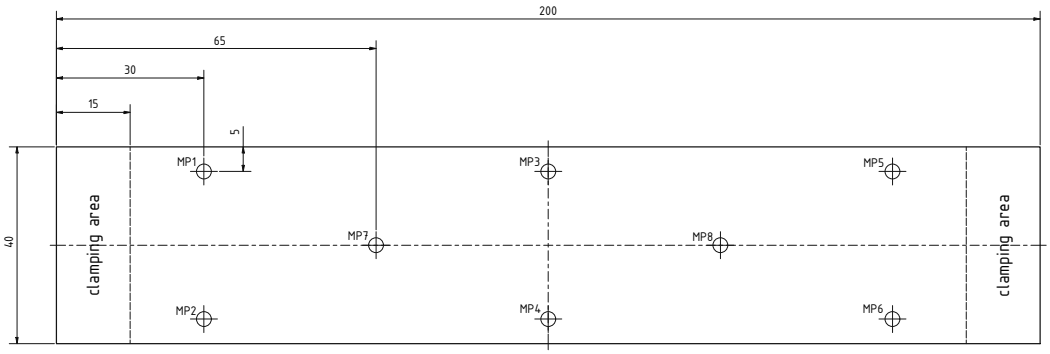

Figure 20.: *Measurement points metal sheets.*

Estimation of the test duration

The ratio of the minimum fluidization velocity can be calculated according to Eqn.(21).

$$R_{umf} = \frac{u_{mf}(330\,\mu\text{m})}{u_{mf}(146\,\mu\text{m})} = \frac{0,1057}{0,0215} = 4,916 \approx 5 \tag{21}$$

This ratio of the minimum fluidization velocity leads approximately to an $5^3 = 125$ times higher erosion rate, referenced to Eqn.(17)(18), for the same degree of fluidization.

$$\Delta s_{est} \approx \left(R_{umf} \cdot \frac{FG5}{FG4}\right)^3 \cdot \frac{330}{146} \approx 525 \tag{22}$$

The result of Eqn.(22) shows, that a test duration of one month with the operating parameters for the test will generate the same erosion rate like for a test duration

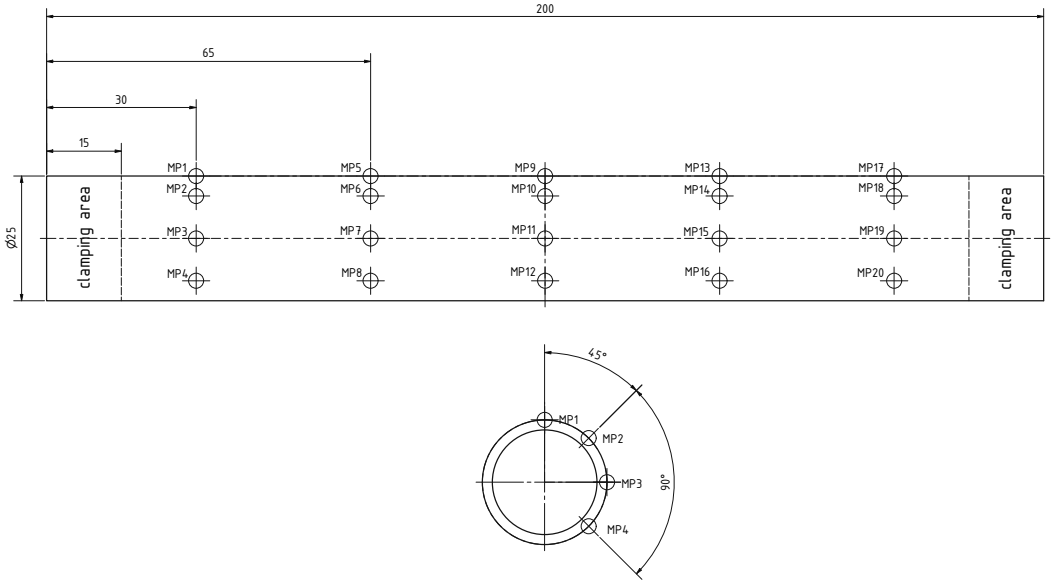

Figure 21.: *Measurement points tube.*

of approximately 44 years with the real operating parameters and the dependence on the particle diameter.

$$\Delta s_{cons.est} \approx \left(R_{umf} \cdot \frac{FG5}{FG4} \right)^3 \approx 232 \tag{23}$$

If the more conservative approach is used (Eqn.(23)) the test will generate an erosion rate which would be achieved with 19 years of operation.

All possible configuration for erosion tests are listed in Tab.6. This variety of possible test configurations makes it easier to choose the best variant for the specific test task.

3.3.2. Planned Experiments

Erosion test 1

The first test is used to generate general information about long time erosion behaviour. If the erosion rate values in this test are very small no more tests are needed, because the real erosion rate is also much smaller.

Test parameters

- Particle size: 330 µm
- Degree of fluidization: FG5
- Test duration: 1 month

Optional Erosion test 2

The second test serves to verify whether there is a particle size dependency.

Test parameters

- Particle size: 242 µm
- Degree of fluidization: FG9
- Test duration: 1 month

Optional Erosion test 3

The third test serves to check the dependency of the erosion rate on the superficial gas velocity to the third power.

Test parameters

- Particle size: 242 µm
- Degree of fluidization: FG4
- Test duration: 1 month

Table 6.: *Design table for erosion rate.*

Design table for erosion rate								
temp. (°C)	density air $\left(\frac{kg}{m^3}\right)$	viscosity air $(Pa \cdot s)$	particle size (µm)	minimum fluidization velocity $\left(\frac{m}{s}\right)$	size ratio of the minimum fluidization velocity	degree of fluidization	erosion rate multiplier based on the design point ($dp = 146$ µm, FG4)	conservative erosion rate multiplier based on the design point ($dp = 146$ µm, FG4)
20	1.189	0.00001821	146	0.0215	1	6	3.4	3.4
						7	5.4	5.4
						8	8.0	8.0
						9	11.4	11.4
						10	15.6	15.6
			242	0.0583	2.712	4	33.0	19.9
						5	64.5	38.9
						6	111.5	67.3
						7	177.1	106.9
						8	264.4	159.5
						9	376.4	227.1
						10	516.4	311.5
			330	0.1057	4.916	4	268.6	118.8
						5	524.6	232.1
						6	906.5	401.0
						7	1439.4	636.8
						8	2148.6	950.6
						9	3059.3	1353.5
						10	4196.5	1856.6

4. Requirements and design considerations for the heat transfer test rig

4.1. Structure and basic function

The main aim of the heat transfer test rig is the investigation of the heat transfer in dense fluidized beds. For industrial thermal energy storage applications, like sandTES, it is necessary to know the details of the heat transfer, because the particle and gas properties of the fluidized bed affect the heat transfer coefficient. For the determination of transfer coefficient a steady state is targeted in order to prevent influences of boundary conditions.

The structure of the heat transfer test rig, which was developed under the project name micro hot test rig, can be seen in Fig.22. The test rig itself mainly consists of the wind box, the fluidized bed chamber (FBC) and the sintered plate between. In order to be able to measure a heat transfer, it is necessary that there is a temperature difference between the heat source and the surrounding medium. This requirement is met by a stationary circulation between the heating and cooling side. The functionality of this consideration was already confirmed in advance by a simulation in Barracuda® [18].

The basic function of the test rig can also be seen in Fig.22. Compressed air from the air chamber is conveyed into each chamber of the wind box and then pushed through the sintered plate into the fluidized bed chamber. The subdivision of the wind box into two chambers is made to support the circulation in the fluidized bed. The airflow on the heating side is greater than on the cooling side. Therefore, the circulation process is designed in such a way, that cold particles flow from the cooling side to the heating side in the lower area of the fluidized bed. During the rise on the heating side the particles are heated up at the same time. In the upper area, the particles flow back onto the cooling side and will be cooled during the descent. The air escaping from the fluidized bed collects in the free space and is then extracted.

The advantage of this test rig is the simple structure without additional conveying equipment. Furthermore, there is also the possibility of examining different configurations of materials at different temperature levels.

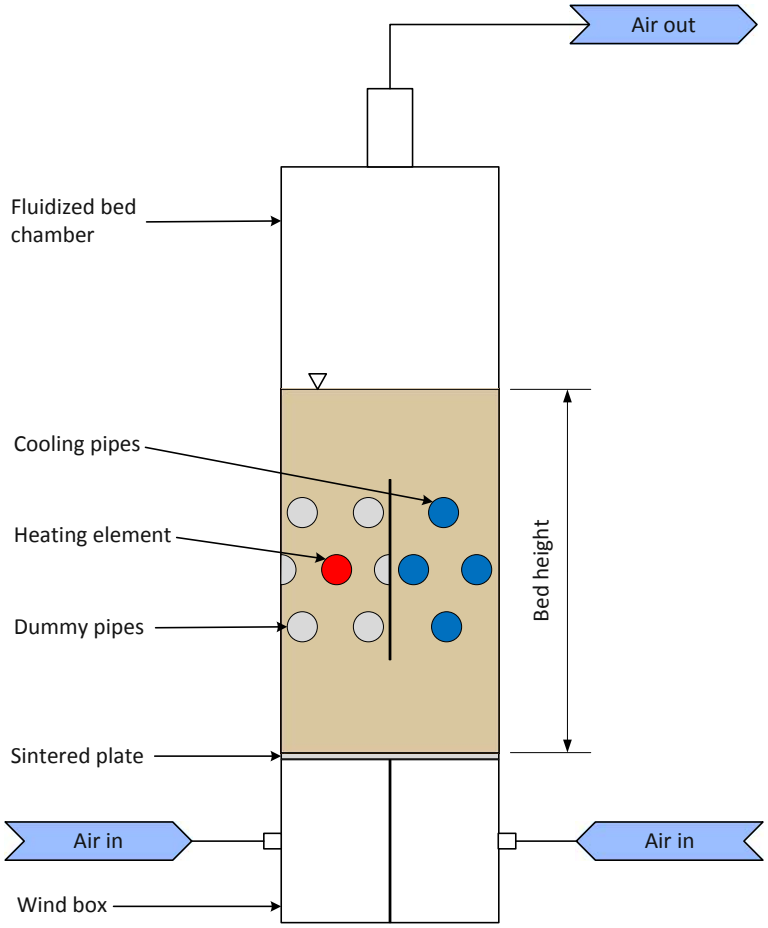

Figure 22.: *Structure of the heat transfer test rig.*

4.2. Measuring principle

The main task is the determination of the heat transfer coefficient. For meaningful results it is necessary, as with the erosion test rig, to determine the real minimal fluidization velocity for the test configuration. Therefore, the recording of pressure loss profile is the first step in the measuring procedure. With this result the operating parameters for the high temperature heat transfer tests can be set precisely. During heat transfer tests the temperature is measured at several positions and also the consumed heating power is detected. With these measured values, the heat transfer coefficient can be calculated. The tests are also carried out for two different heating elements, one element is designed like a plain tube and the second like a finned tube.

4.2.1. Measuring arrangement

Several temperature sensors are necessary, which on one hand measure the medium temperature at various points in the test rig and on the other hand also the surface temperature of the heating element. This arrangement is important, as the heat transfer coefficient is calculated by using the temperature difference between the heating element and the medium, as described in Eqn.(19). The positions of the individual temperature sensors can be seen in Fig.23 and in Tab.7 the measuring task is described in detail.

Table 7.: *Description of the temperature sensors for the heat transfer test rig.*

Temperature sensor	Measuring task
T1	Medium temperature under cooling side
T2	
T3	Medium temperature above cooling side
T4	
T5	Medium temperature under heating side
T6	
T7	Medium temperature under heating element
T8	
T9	Medium temperature above heating element
T10	
T11	Medium temperature above heating side
T12	
T13	Surface temperature heating element

For the effective execution of the measurements several pressure difference sensors and flow sensors are also necessary. In Fig.23 also the layout of the additional measuring equipment can be seen. One of the key points of the measurements are the two volume flow sensor (FS1 + FS2), because it is necessary to determine the real volume flow which enters each side (heating and cooling) of the micro hot test rig. An exact measurement of the volume flow is important for the determination of the minimal fluidization velocity and also for the regulation for the high temperature tests. Tab.8 shows the measuring task and the connection points of the different differential pressure measuring sensors. A control valve (CV) is required to set the total volume flow which is required for the test rig. Furthermore, two adjustment valves (AV1 + AV2) are required in order to be able to correctly distribute the total volume flow to the volume flows for the heating and cooling side (see Fig.22).

4.2.2. Recording of the pressure loss profile

The recording of the pressure loss profile is essential to ensure that the operating parameters are set correctly for the test configuration. As already described in 3.2.2

Table 8.: *Description of the pressure sensors heat transfer test rig.*

Pressure sensor	**Connection point 1**	**Connection point 2**	**Measuring task**
PD1	atmosphere	wind box cooling side	absolute pressure wind box cooling side
PD2	wind box cooling side	bottom FBC cooling side	pressure loss over the sintered plate cooling side
PD3	bottom FBC cooling side	center FBC cooling side	pressure loss over the fluidized and differential pressure for porosity bed cooling side
PD4	center FBC cooling side	top FBC cooling side	pressure loss over the fluidized bed cooling side
PD5	top FBC cooling side	atmosphere	absolute pressure above the fluidized bed
PD6	atmosphere	wind box heating side	absolute pressure wind box heating side
PD7	wind box heating side	bottom FBC heating side	pressure loss over the sintered plate heating side
PD8	bottom FBC heating side	center FBC heating side	pressure loss over the fluidized and differential pressure for porosity bed heating side
PD8	center FBC heating side	top FBC heating side	pressure loss over the fluidized bed heating side

the volume flow rate is successively reduced from a full fluidized bed to a fixed bed configuration to record the pressure loss profile. For this test rig attention should also be paid to the temperature of the medium for the recording of the pressure loss profile. The minimal fluidization velocity decreases with increasing temperature. In order to take this dependency into account, the minimum fluidization velocity must be determined at several temperatures. Also, the structure of the test rig (see Fig.22) offers the possibility to carry out two parallel measurements, by setting the volume flows equally on both sides (heating and cooling side).

4.2.3. High temperature heat transfer tests

The main task of the test rig is the determination of the heat transfer coefficient for high temperature fluidized beds. The tests are designed in such a way that the measured values for the stationary state are recorded for several temperatures which also require different heating capacities. Each operating point is approached several times in order to be able to calculate a meaningful mean value from the results. As already described in the test configurations the volume flow on the heating side is greater than on the cooling side. In this case the degree of fluidization is set to FG4.5 for the heating side and to FG2 for the cooling side. Also the simulations in Barracuda® were carried out with this setting and led to acceptable results.

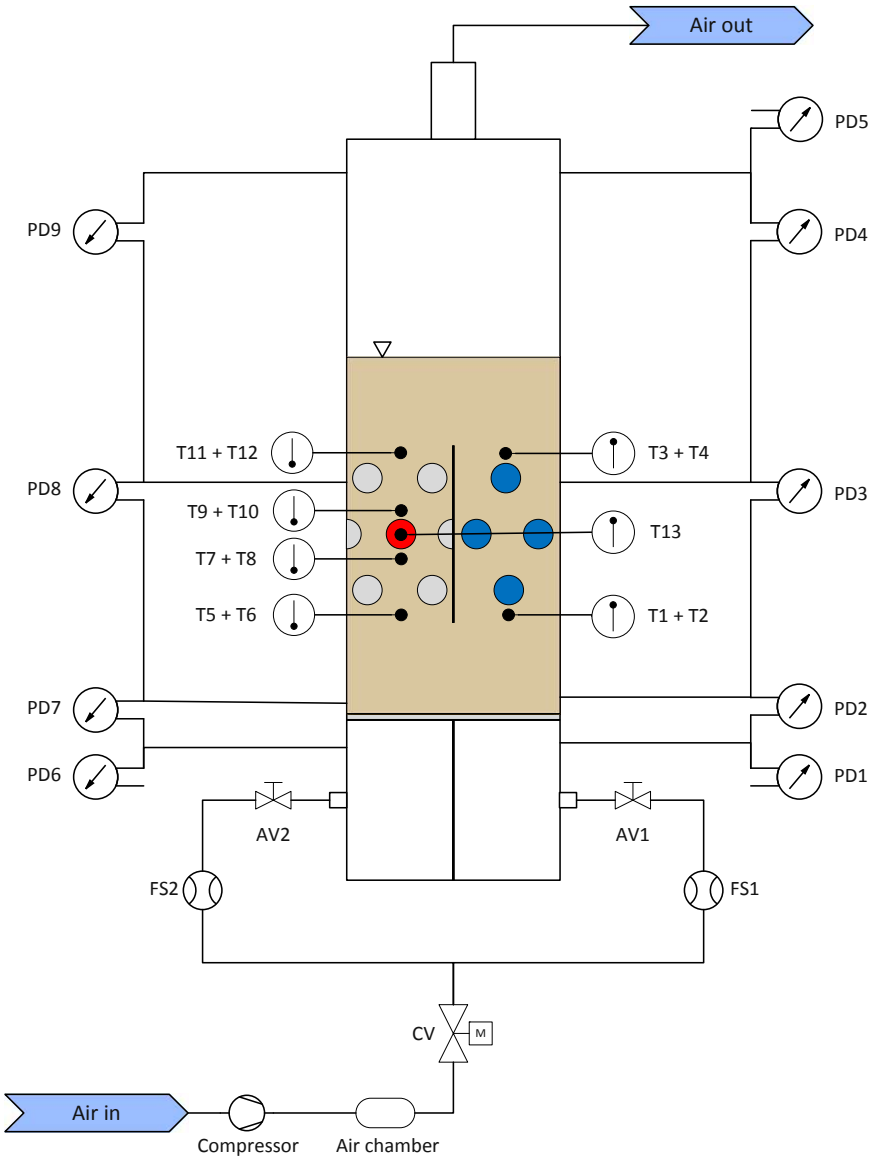

Figure 23.: *Measuring arrangement for heat transfer test rig.*

5. Design and Implementation of the erosion test rig

5.1. Calculations

5.1.1. Minimal fluidization velocity

For the calculation of the minimal fluidization velocity u_{mf} a ready-made calculation tool, developed by the supervisor Stefan Thanheiser, was used which is based on a correlation by Richardson [19]. The calculation tool is executed in MATLAB and needs the following three input parameters.

- particle diameter d_P
- particle density ρ_P
- fluidization temperature T_f

The the density ρ_g and the dynamic viscosity η_g of the dry air for the defined temperature are calculated by the tool, by interpolation of a table. With this data and the two constants C1 and C2 the minimal fluidization velocity is calculated using the Reynolds number Re and the Archimedes number Ar. The value of the constants $C1 = 25.7$ and $C2 = 0.0365$ is defined by Richardson.

5.1.2. Sintered plate

The sintered plate is one of the key elements in this test rig and ensures a uniform distribution of the fluidizing air flow. Beside the dimensional parameters and the strength of the material the permeability is the point via which the calculations according to ISO4022 are carried out.

The following input data must be known:

- cross-sectional area of the fluidized bed A_B
- height of the fixed bed h_B
- bulk density of the used sand ρ_{sand}
- density of the fluidizing air ρ_g
- dynamic viscosity of the fluidizing air η_g

- minimal fluidization velocity u_{mf}
- degree of fluidization FG
- viscosity coefficient Ψ_v
- permeability coefficient Ψ_p

The pressure drop across the fluidized bed Δp_B is calculated acoording to Eqn.(24) Then the volumetric flow rate in the fluidized bed is calculated according to Eqn.(25).

$$\Delta p_B = \rho_{sand} \cdot g \cdot h_{sand} \tag{24}$$

$$\dot{V}_B = A_B \cdot u_{mf} \cdot FG \tag{25}$$

For a homogeneous fluidization it is necessary for the required pressure drop across the sintered plate $\Delta p_{sinter.req}$ to be more than 30 % of the pressure drop across the fluidized bed (see Eqn.(26)) [20].

$$\Delta p_{sinter.req} = 0.3 \cdot \Delta p_B \tag{26}$$

The next step in the calculation is the required plate thickness $e_{sinter.req}$ (see Eqn.(27)).

$$e_{sinter.req} = \frac{\Delta p_{sinter.req}}{\frac{\dot{V}_B \cdot \eta_g}{A_b \cdot \Psi_v} + \frac{\dot{V}_B^2 \cdot \rho_g}{A_B^2 \cdot \Psi_p}} \tag{27}$$

The last step in the calculation is the calculation of the real pressure loss across the sintered plate Δp_{sinter} for a defined thickness e_{sinter} (see Eqn.(26)). The thickness of the sintered plate is selected based on the possible manufacturing thicknesses and the required applications. For a versatile test rig it is necessary to to investigate multiple applications without changing the hardware of the test rig. This means, that the sintered plate must be suitable for all test configurations and this in every case, the pressure drop of the sintered plate must be more than 30 % of the pressure drop of the fluidized bed (see Eqn.(29)). Furthermore, the total pressure drop for every configuration is calculated in Eqn.(30). All of the calculations as well as the sizing table can be found in appendix A.

$$\Delta p_{sinter} = e_{sinter} \cdot \left(\frac{\dot{V}_B \cdot \eta_g}{A_b \cdot \Psi_v} + \frac{\dot{V}_B^2 \cdot \rho_g}{A_B^2 \cdot \Psi_p} \right) \tag{28}$$

$$\frac{\Delta p_{sinter}}{\Delta p_B} \geq 30\% \tag{29}$$

$$\Delta p_{total} = \Delta p_{sinter} + \Delta p_B \tag{30}$$

A mistake was made in the initial calculation and selection of the sintered plate. For the calculation of the minimum fluidization velocity the bulk density of the sand was used instead of the particle density. This mistake leads to a higher pressure drop across the sintered plate for the real operating parameters. For the execution of the test this has no influence only the total pressure drop is higher and so a higher pressure must be provided by the roots blower.

5.2. Construction

The design and preparation of the production documents was one of the main tasks of this project. Starting with the requirements for the test rig, a concept was first created of how the basic structure could look. After a few consultations with the manufacturing companies, the laboratory team and the supervisors, the construction was started. After inquiries from suppliers, the detailed construction was changed in a few points to be able to manufacture more cost effectively and to better meet technical boundary conditions.

5.2.1. Basic structure

The basic structure of the final construction of the erosion test rig can be seen in Fig.24. The individual elements and their purpose are described below. Special construction details such as the integration of the sintered plate or the filter system are also described in detail in the following sections.

Air inlet The air inlet of the wind box is connected to the roots blower via the air line. In the air line a volume flow sensor is installed.

Wind box The wind box distributes the air in order to guarantee a uniform flow through the sintered plate. The wind box also forms the foundation for the entire test rig. The welded construction is made of 5 mm sheet steel and contains the welding sockets for the air inlet and pressure sensors.

Sintered plate The sintered plate is a custom-made product by GKN Powder Metallurgy (Radevormwald - Germany). Smaller standard plates are welded together and then reworked. This provides several advantages. On one hand, sealing has only to be done for one part and on the other hand, an even and complete fluidization of the bed can be guaranteed.

Inspection elements The inspection elements are the centerpieces of the erosion tests. The characteristics of the inspection elements are described in Tab.5. The attachment of the inspection is very important, as they have to remain firmly in position during the test period, even if large forces act on them in the fluidized bed. It is also necessary that the inspection elements ca be installed and removed easily without disassembling the entire test rig. The detailed construction can be seen in Fig.26.

Plexiglas insert The plexiglas insert is made from a transparent 12 mm PMMA-plate. The main reason for it´s use is to enable the observation of fluidized bed. The attachments for the inspection elements are screwed with the plexiglas insert and hold them firmly in position. The edge of the plexiglas insert has a milling so that the wall in the fluidized bed chamber has a flat surface. On the inside of the plexiglas insert a scratch protection film was applied to prevent the plexiglas insert from being worn down too much by the sand.

Fluidized bed chamber The fluidized bed chamber is also a welded construction made of 5 mm sheet steel. When the design was revised, it was changed so that the fluidized bed chamber can be made from bent sheet metal parts, which saves material and makes production cheaper.

Collar 1 + 2 Large bubbles in the fluidized bed fling sand particles very high up as they burst on the surface of the fluidized bed and these were sucked in by the extraction system. As a first step, it was necessary to increase the free board height with collars. Collar 1 is made out of 5 mm sheet steel and is 600 mm high. Collar 2 is 2000 mm high and is made out of 2 mm sheet steel as on the top of the fluidized chamber small forces act on it. Therefore, mass and the production costs can also be kept low.

Maintenance cover The maintenance cover was designed for maintenance and cleaning work on the filter system and to be able to refill sand. It is constructed of plexiglas, which offers the possibility to observe the fluidized bed from above.

Filter system The filter system was the second step to prevent the sand particles from being extracted. The detailed construction can be seen in Fig.28. In the first try only one filter cartridge was used. The problem with this construction was that the filter system clogged very fast. To prevent it from clogging the system uses two filter cartridges with alternating blow-out system with automatically closable flaps.

Air extraction The air extraction is realized with an standalone extraction system which is connected to the test rig via pipeline. The extraction system can be set manually using a frequency converter.

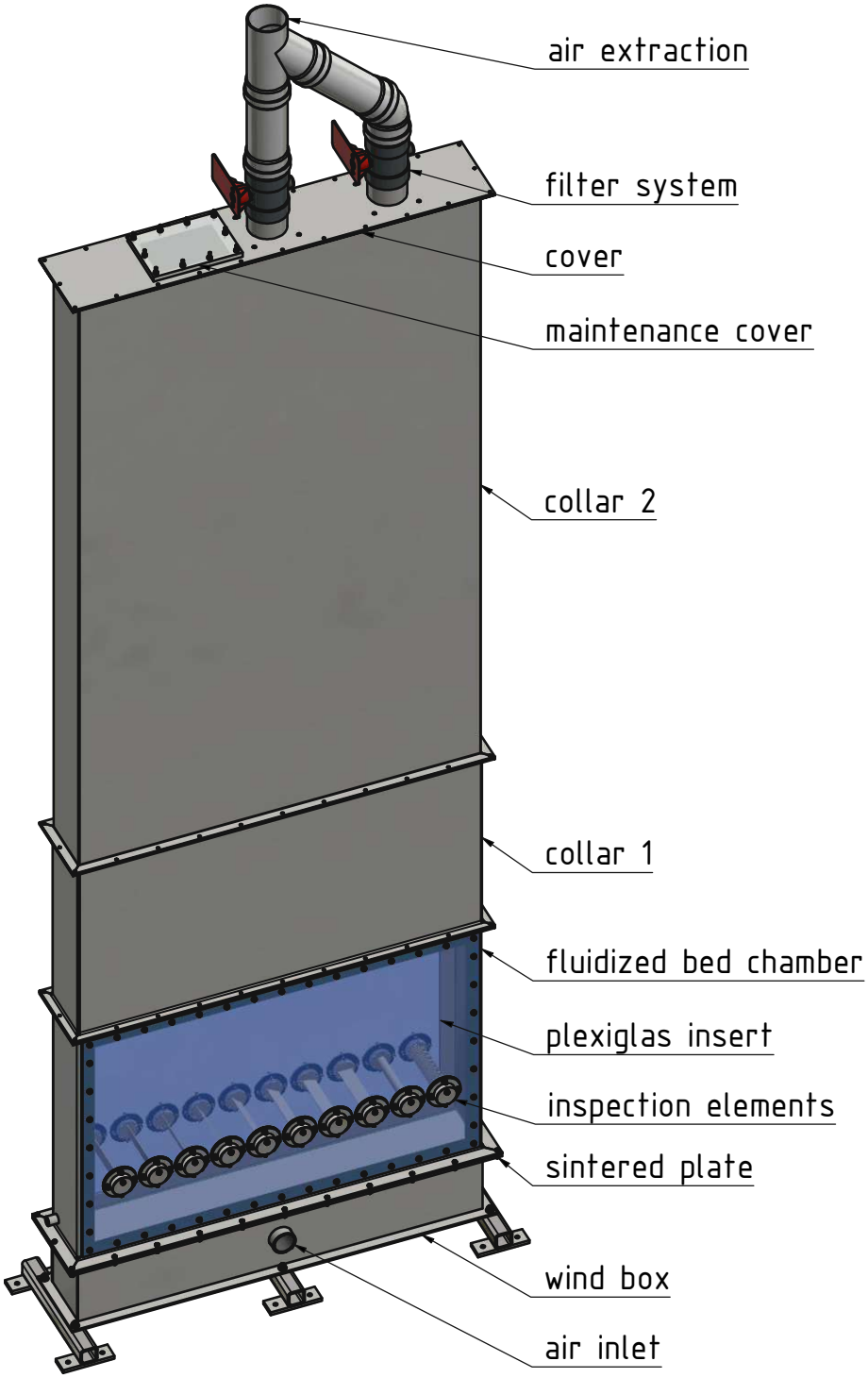

Figure 24.: *Basic structure of the erosion test rig.*

5.2.2. Integration of the sintered plate

The sintered plate is clamped between the wind box and the fluidized bed chamber (see Fig.25). It is sealed from below against the wind box and from above against the fluidized bed chamber. The seals are designed that way that the cross-sectional area of the fluidized bed is consistently without change. This approach of a constant cross-sectional area of the fluidized bed is realized over the entire test rig. Due to manufacturing inaccuracies, the originally planned Klingersil-C4400 seal for the seal above the sintered plate was replaced with a foam rubber seal to ensure tightness.

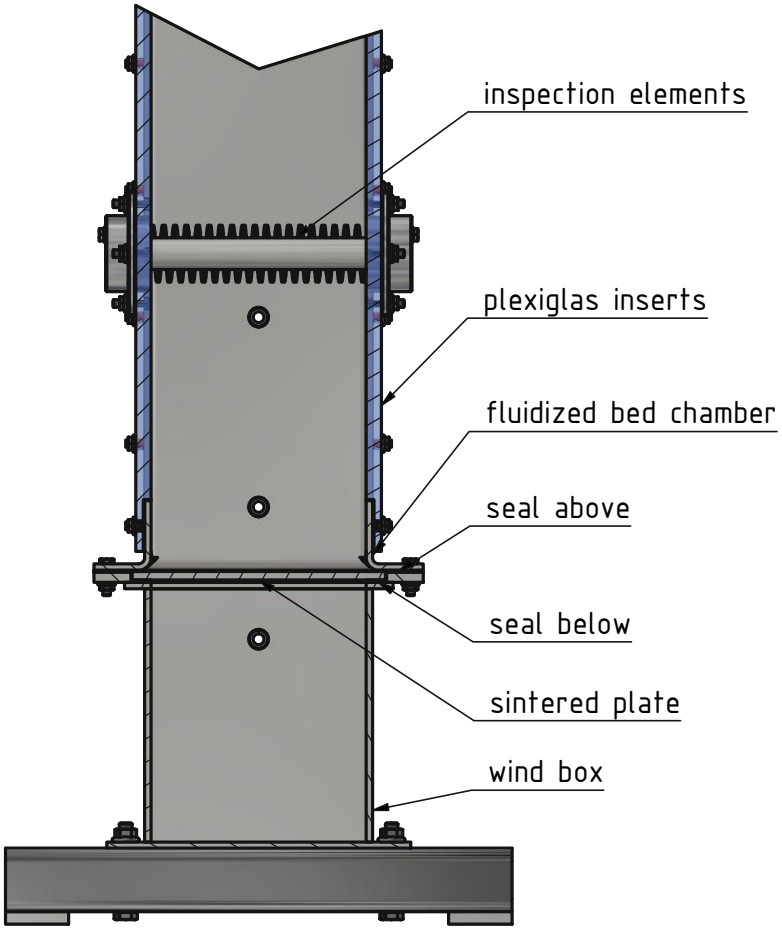

Figure 25.: *Integration of the sintered plate erosion test rig.*

5.2.3. Incorporation and attachment of the inspection elements

The ulterior motive for the construction of the attachment of the inspection elements was to enable a stable, secure and reusable attachment. It was also important to install and remove the inspection elements in a fast and easy way.

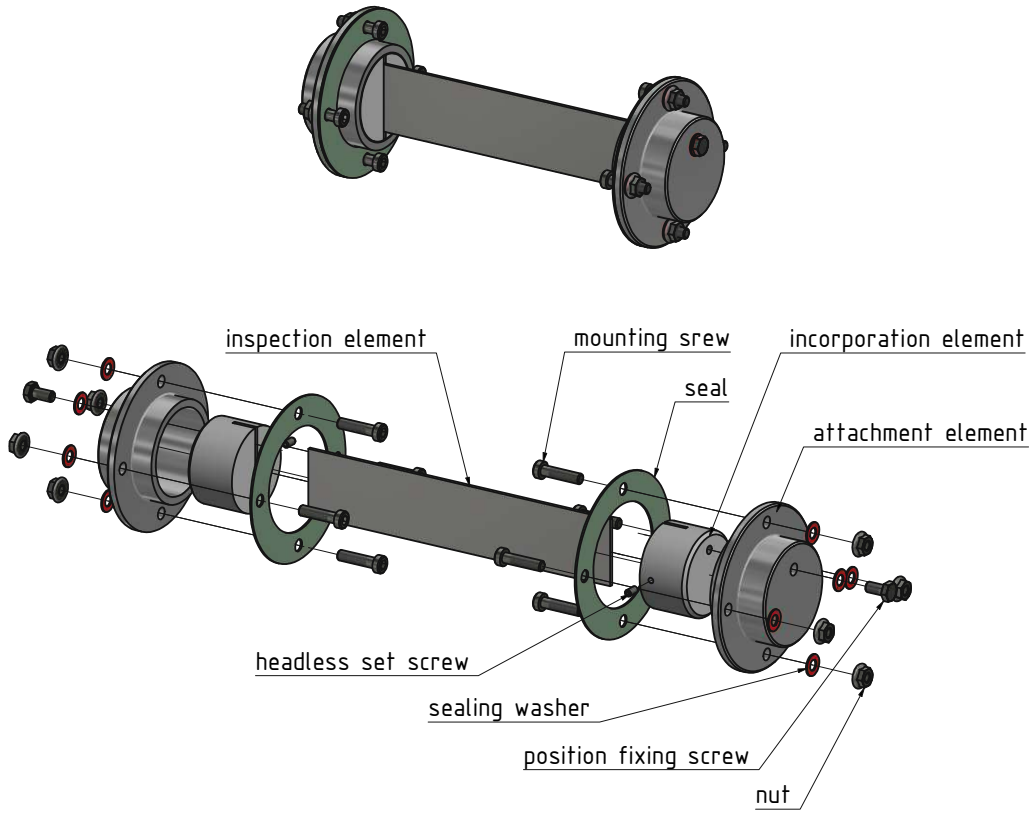

Figure 26.: *Incorporation of the inspection element.*

In Fig.26 the basic structure of the incorporation of the inspection elements can be seen in the assembled state and as exploded view. For assembly, the incorporation elements are placed on the inspection element and secured with headless set screws. The mounting screws are screwed to the plexiglas insert which have threaded holes. This allows an assembly only from the outside. On one side of the test stand the attachment element can already be screwed to the plexiglas insert with the seal (see Fig.27). The second attachment element and the pre-assembled inspection element are placed in the test bench together with the seal. Lastly, the position fixing screws are screwed in and all screws are tightened. The disassembly is working exactly in reverse order.

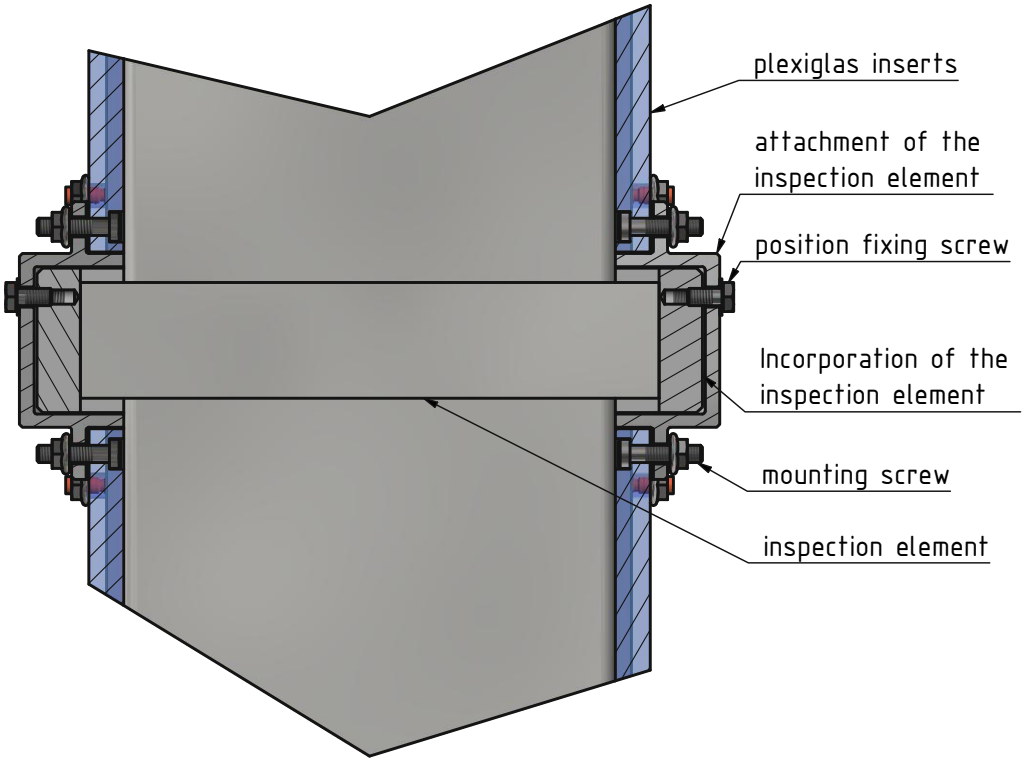

Figure 27.: *Sectional view of the attachment of the inspection element.*

5.2.4. Filter system

The filter system is kept rather simple. It consists of two filter cartridges and two closable flaps which are connected and sealed against the cover (see Fig.28). The air extraction pipe system connects the two filter cartridges and leads the air to the extraction system where it is filtered again by special filters before being released into the environment. For the filter cartridge several grooves are milled into a Ø140 mm pipe, leaving approximately 60 % of the pipe surface open for air flow. On the outside of the pipe a metal mesh with a grid size of 150 µm is applied and fixed with clamps. The connections for the flush process with compressed air are on the cover for each filter cartridge and can be seen in Fig.30.

The cleaning process for the filter cartridges runs according to the following procedure:

- close flap 1
- flush filter cartridge 1 with compressed air
- open flap 1

- waiting time (adjustable)
- close flap 2
- flush filter cartridge 2 with compressed air
- open flap 2
- waiting time (adjustable)
- restart of the procedure

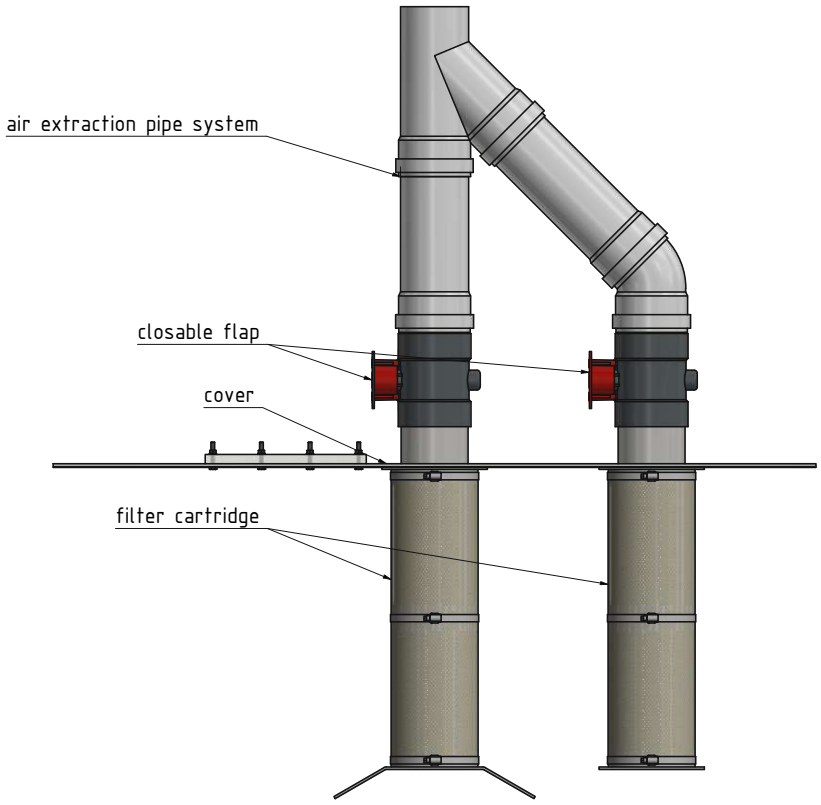

Figure 28.: *Filter system.*

5.3. Manufacture and assembly

5.3.1. Air supply

The fluidization air is the only component which is required for operation of the test rig. Compared to other applications the erosion test rig requires a high volume flow and a lower pressure difference, therefore it was possible to use the existing roots blower in the laboratory.

The whole air supply consists of the following three main parts:

Roots blower The roots blower, from the company Ochsner, can be controlled centrally via the APROL control system. A frequency converter is also integrated, which allows for the almost stepless coverage of a large volume flow range. At 100 % engine power a volume flow rate of 3420 m^3/h and compression pressure of 1.3 bar at an intake pressure of 1 bar can be achieved. The data sheet of the Ochsner roots blower can be found in appendix A.

Air supply line For the air supply line the existing line made of PP-Mega 8 plug-in pipes from the company Bauernfeind GmbH (Waizenkirchen - Austria) was used to a large extent. The existing supply line with a diameter DN250 was extended to the test stand and shortly before reduced to a 2 inch hose line that leads directly into the wind box. The bypass valve is also located just before the reduction (see Fig.29).

Bypass valve The bypass valve is necessary, as the roots blower delivers too much volume flow even in the lowest configuration. The bypass valve consists of a y-junction and shut-off ball valves which are screwed into a cover, which can be seen in Fig.29. The advantage of this system is, that a rough presetting via the ball valves is possible and thus, the roots blower can always be operated in a low power range.

5.3.2. Mechanical components

The mechanical components of the erosion test rig were manufactured almost entirely by subcontractors, only some repairs and conversion work were carried out by the staff in the laboratory. The steel construction parts, including the wind box, the fluidized bed chamber, collars 1 & 2, and the cover were fabricated by the company Innoweld Metallverarbeitung GmbH (Mürzzuschlag - Austria). The inncorporation and attachment of the inspection elements were manufactured by the company ORLIK & Co GmbH (Wöllersdorf - Austria) and the plexiglas inserts were manufactured by the company Acrystudio GmbH (Laxenburg - Austria). Production and assembly were carried out in cooperation with the laboratory staff. The manufacturing and assembly drawings can be found in appendix A.

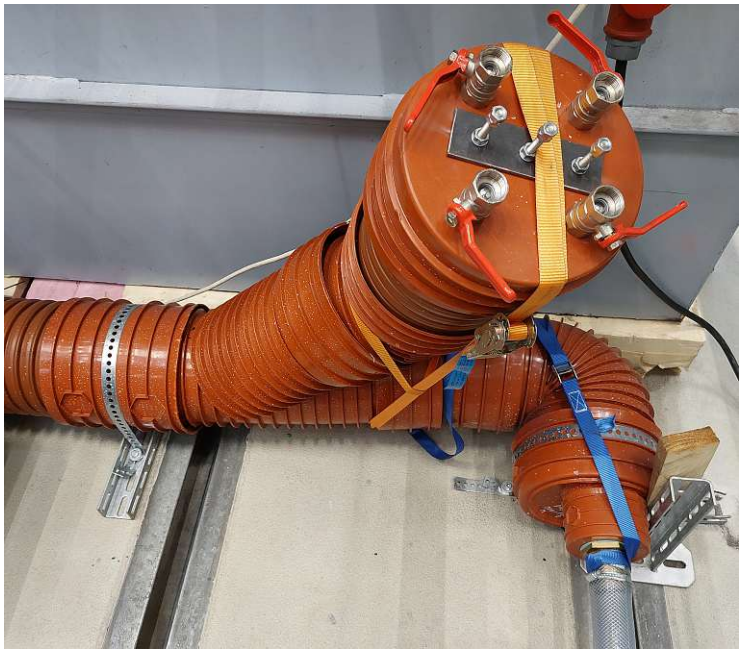

Figure 29.: *Bypass valve in air supply line.*

5.3.3. Pneumatic and electrical components

Beside to the sensors, the pneumatic and electrical components are limited to the filter system and the differential pressure switch for over-pressure shutdown.

The closable flaps of the filter system are the main components of the flush process (see 5.2.4). The flap including the actuator is a premade assembly and was purchased from VentilationNord GmbH (Lauenburg/Elbe - Germany). The actuator Belimo CM24 has the advantage of being able to be controlled directly by the controller with 24 V. This flush process lasts about 5 s and is clocked by the controller via magnetic valves. The required compressed air is taken from the house air system and adjusted to a pressure of approximately 8 bar with a pressure control valve. The flush air arrives via compressed air hoses that are connected to the flush air connections and is injected into the filter cartridges (see Fig.30).

The differential pressure switch is crucial to prevent an over pressure in the fluidized bed chamber. The used pressure switch PSW-A3-50 has a variable adjustable pressure cut-off point between 10 to 50 mbar and is integrated into the emergency shut-off of the roots blower to ensure shutdown even in the event of a control failure. The datasheet can be found in the appendix A.

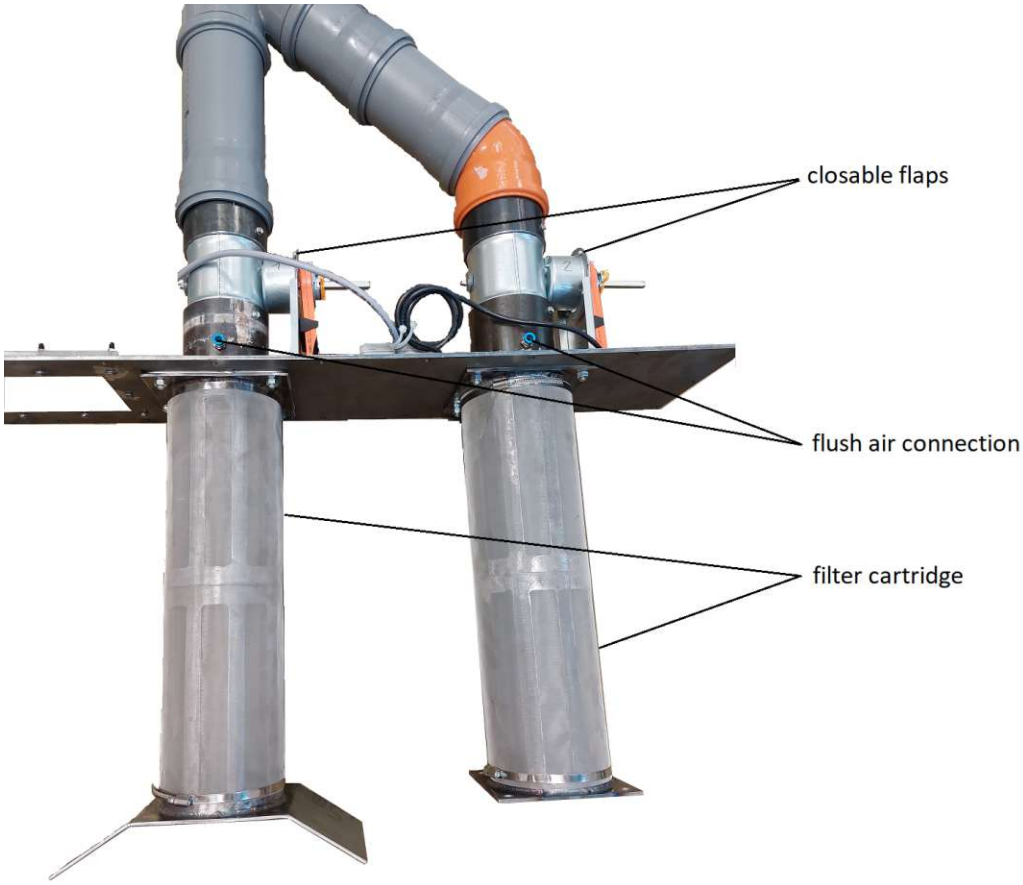

Figure 30.: *Pneumatic and electrical components of the filter system.*

5.3.4. Air extraction

As described in 5.2.4, air leaving the erosion test rig is directed into a extraction and filter system via a pipeline (see Fig.31). The extraction has the advantage that the differential pressure over the fluidized bed can be lowered. The system itself is independent from the control and can be continuously adjusted and is an existing assembly, available at the test site, which is also used for other test rigs. The special filter in the extraction system is also crucial to prevent particles smaller than 150 µm, that would pass the filter cartridge, from being released to the environment.

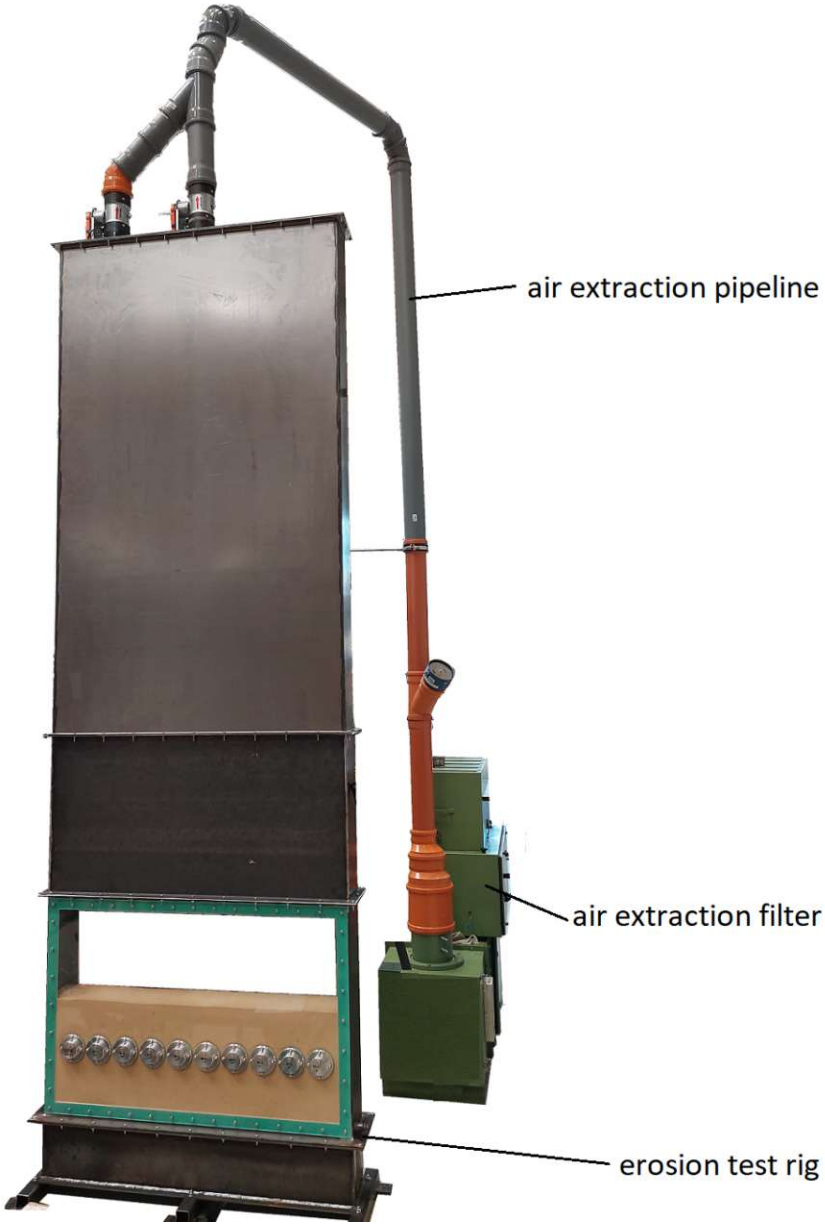

Figure 31.: *Erosion test rig with air extraction.*

5.4. Measurement setup and sensors

The measurements taken during the runtime of the test rig ensure consistent test conditions. As described in 3.2.1, a volume flow sensor and five pressure sensors are used. The data sheet of the used flow sensor and the pressure sensors can be found in appendix A.

The used volume flow sensor IL30.020 MPM from SCHMIDT Technology GmbH (St. Georgen - Germany) was screwed in directly at the entrance to the wind box and connected to the hose line of the air supply line on the other side (see Fig.32). The sensor has a measuring range of 0 to 710 m^3/h and also determines the medium temperature. The big advantage of this sensor is the possibility to use the Multi-Point-Measurement. Due to the four simultaneously measured values in connection with intelligent algorithms for evaluating the measurement results, flow values can also be determined for uneven flow conditions.

Figure 32.: *Built-in volume flow sensor IL30.020.*

The used pressure sensors DS2 from the company Kalinsky Sensor Elektronik GmbH & Co.KG (Erfurt - Germany) have a simple structure, high reliability and accuracy. They were connected to the measuring points on the test rig via compressed air hoses. The 4 to 20 mA output signal is passed directly to the controller. In order to increase the accuracy, the pressure sensors were adapted to their measuring task, which are listed in Tab.9 based on the description of the pressure sensors Tab.4.

Table 9.: *Measuring range pressure sensors erosion test rig*

Pressure sensor	Measuring range
PD1	0 to 500 mbar
PD2	0 to 500 mbar
PD3	0 to 100 mbar
PD4	0 to 10 mbar
PD5	−25 to 25 mbar

5.5. Challenges and solution approaches

5.5.1. Bypass valve

At the beginning of the assembling the bypass valve was positioned immediately after the roots blower with an adjustment flap for regulation. In this configuration the approximately 40 m long air supply line generate too much flow resistance and whole air flowed through the bypass valve. To prevent this, the bypass valve was positioned just before the reduction of the air supply line.

5.5.2. Air supply line

The plug in pipes of the air supply line have the disadvantage that there is no axial securing of the plugged connections. With increasing flow rate the pressure in the air supply line increases because of the increasing pressure losses over the sintered plate as well as the flow losses in the air supply line itself. This causes the air supply line to split apart at the plug connections. This problem unfortunately occurred several times. The only solution that was practical was to fix the pipes firmly to the ground with perforated straps or other fixing elements.

5.5.3. Transport disengagement height

The area between the surface of the fluidized bed and the air outlet is called freeboard. Particles are entrained above the fluidized bed by the air flow. The suspension density of the particles decreases with increasing altitude and above a certain level, the transport disengagement height (TDH), the entrainment remains constant.

The first configuration of the erosion test rig was designed without collars and filter system, compare with Fig.24. During the first test runs a considerable part of the quartz sand was extracted from the test stand and collected in the filter of the air extraction. The main reason for this was that the TDH was smaller than the freeboard height. Another possible cause for the problem could have been the strongly energetic ejections of the bursting screen bubbles as can be seen in Fig.33

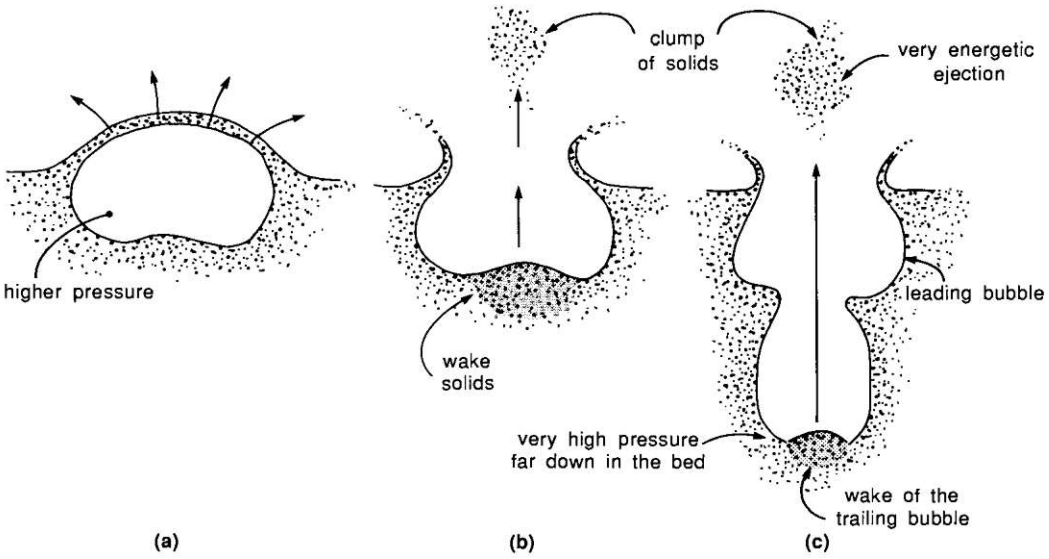

Figure 33.: *Mechanism of ejection of solids from a fluidized bed into the freeboard [20].*

In the **first approach**, the first collar was designed and manufactured to increase the freeboard height. The volume of the extracted quartz sand was lower than before, but if a bubble collapsed direct under the air extraction the ejected particles was extracted.

In the **second approach**, a filter cartridge was used to prevent the entrained particles from being discharged. However, the filter cartridge clogged very quickly.

To be on the safe side with the **third approach**, the freeboard height was increased with a second collar and a filter system with flushing device, as described in 5.2.1 and 5.2.4, was installed. This improvements led to good results with a low discharge rate.

5.5.4. Impermissible over-pressure in the fluidized bed chamber

A chain of unforeseeable events resulted in the simultaneous closing of both flaps in the filter system. Due to the failure of the connection between the controller and the APROL control system the programmed over-pressure shutdown could not intervene and pressure built up in the fluidized bed chamber. The high pressure resulted in shattering of the plexiglas inserts. At this point 22.5 % of the test duration had been reached. After this incident the plexiglas inserts had to be replaced and repairs to the steel structure were necessary before the erosion test could be restarted.

5.5.5. scratch protection film

After about 500 hours of running time, the scratch protection film was worn down at the transition point between the fluidized bed and the freeboard. Almost the entire scratch protection film was then detached from the plexiglas insert. Therefore it was necessary to disassemble the plexiglas inserts and remove the detached film from the fluidized bed.

5.5.6. Static charge

The rubbing of the quartz sand against the plexiglas insert caused static charge. To prevent this. the attachment elements were connected via a perforated metal tape to the wind box. The windbox itself stands on the clamping field which is electrically grounded.

6. Design and Implementation of the heat transfer test rig

6.1. Calculations

6.1.1. Sintered plate

The calculation of the sintered plate for the heat transfer test rig was done similar to the erosion test rig, which can be seen in section 5.1.2. As well as the calculation of the minimal fluidization velocity, which can be seen in section 5.1.1. The particularity of the sintered plate for the heat transfer test rig is the construction out of plates with different filter properties (viscosity and permeability coefficient). The reason therefore is the different volume flow rate for the heating and cooling side which would generate a different pressure drop across a sintered plate with same filter properties. In order to achieve a similar pressure drop the approach with different filter properties was chosen. Furthermore, the plate is made of Hastelloy C276 (2.4819) to withstand the possible high temperatures inside the test rig. All of the calculations as well as the production drawing from the of the sintered plate can be found in appendix B.

6.1.2. Design of the heating elements

The design of the heating elements was done in cooperation with the company VULCANIC S.A.S (Neuilly/Marne - France), which also carried out the production of the heating elements. The challenge here was the high operating temperature, which on one hand effects the material of the heating element casing an on the other hand requires a high performance level. The heating elements have an electrical power of 10.6 kW and an integrated temperature measurement to avoid overheating. The temperature range of the heating elements is between 10 to 800 °C. The active length of the heating element is 360 mm, this means the surface area of the heating elements which is immersed in the fluidized bed is completely heated. The tube diameter of the heating elements is 25 mm and the sheath is made of Inconel 600. The fins for the finned tube were designed from disk which were welded onto the tube. All further parameter and information can be found in the data sheets and the production drawings of the two different heating elements in appendix B.

6.2. Construction

The design and preparation of the production documents was one of the main tasks of this project. Starting with the requirements for the test rig, a concept was first created of how the basic structure could look. Additionally the structure was confirmed by the results of the simulations. After a few consultations with the manufacturing companies, the laboratory team and the supervisors, the construction was started.

6.2.1. Basic structure

The basic structure of the final construction of the heat transfer test rig can be seen in Fig.34. The individual elements and their purpose are described below. Special construction details such as the integration of the sintered plate or the design of the cooling lines are also described in detail in the following sections. After assembly and the first tests, the test bench will be completely thermally insulated. Therefore, the sockets and supply lines are also longer in order to be able to apply the insulation with sufficient thickness.

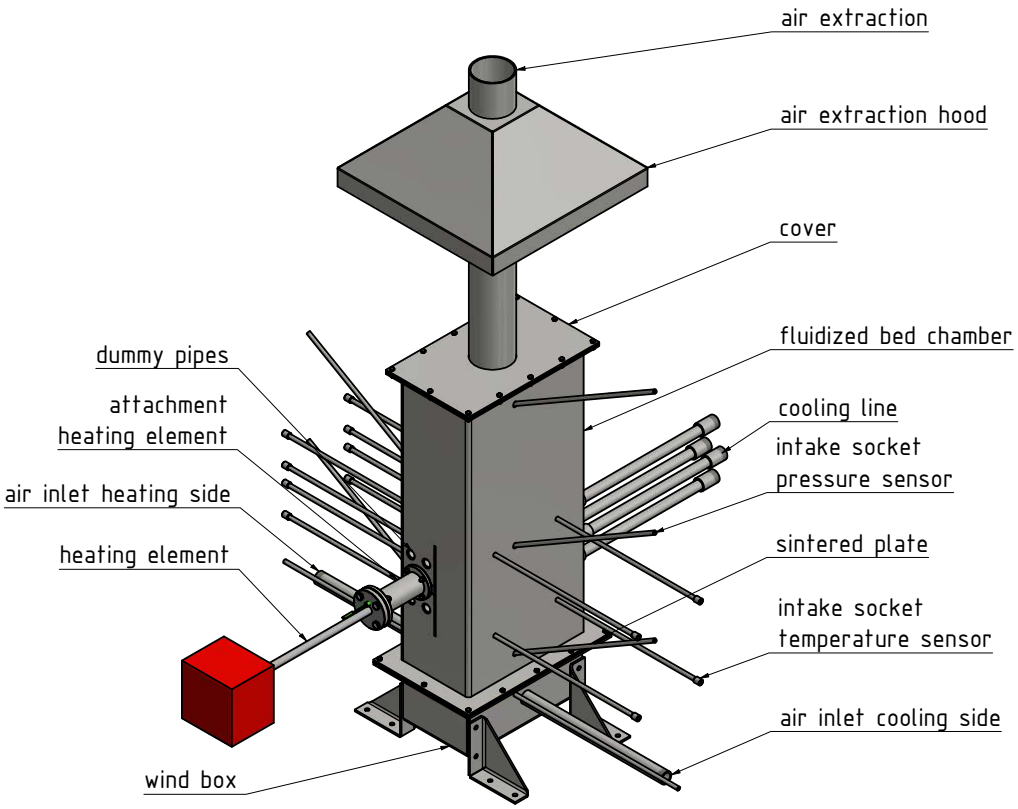

Figure 34.: *Basic structure of the heat transfer test rig.*

Air inlets The fluidization air inlets on both sides, the heating and the cooling side, are designed as a pipe with a G1 inch external thread connection. The adjustment valves, volume flow sensors and the air supply line are further connected to these air inlets.

Wind box The wind box distributes the air in order to guarantee a uniform flow through the sintered plate. The wind box also forms the foundation for the entire test rig and is divided into two chambers for the heating and cooling side. The welded construction is made of 5mm sheet steel and contains the welding sockets for the air inlets and pressure sensors. Because of the high temperatures, a heat-resistant chromium-nickel steel X15CrNiSi25-21 (1.4841) was used for the construction.

Sintered plate The sintered plate is a custom-made product by GKN Powder Metallurgy (Radevormwald - Germany). Smaller standard plates are welded together and then reworked. As described in 6.1.1 the sintered plate is divided into two sections with different filter properties. The sintered plate is made out of Hastelloy C276 (2.48190), to withstand the high temperatures.

Fluidized bed chamber The fluidized bed chamber is also a welded construction made of 5mm chromium-nickel sheet steel (1.4841). The fluidized bed chamber is made from bent sheet metal parts and the recesses and bores for pipes and fixtures were designed in such a way that production is simpler and therefore cheaper.

Cooling line The cooling line is made out of pipes and have a G1 inch external thread connection. The detailed construction and the integration to the fluidized bed chamber can be seen in Fig.39, 40.

Intake sockets for sensors The intake sockets for the temperature and pressure sensors are essential in order to be able to connect the sensors with the test rig through the applied thermal insulation. The intake socket for the temperature sensors have a Rp1/8 inch internal thread for the compression fittings of the temperature sensors. The intake sockets for the pressure sensors have a R1/8 inch external thread for the compressed air hose connections.

Cover The cover is also made out of heat-resistant chromium-nickel steel (1.4841) and is screwed to the fluidized bed chamber. The air outlet pipe is connected to the air extraction hood and guides the air from the test bench into the extraction.

Air extraction hood Due to the high operating temperatures, the exhaust air is also very hot which would have several disadvantages for the air extraction system. To prevent this problem, the air extraction hood was developed, which aspires and mixes the exhaust air from the test rig and the ambient air. This approach has the main advantage that the temperature in the air extraction system can be kept low. However, the extracted air volume is much higher and has to be managed by the system.

Heating element The main component for the operation of the test rig is the heating element. The amount of heat introduced into the test stand is made available entirely by the heating element. The detailed information can be seen in section 6.1.2 and in appendix B.

Attachment of the heating element The attachment of the heating element is important to secure the position during operation and also to thermally isolate the heating element from other components. The detailed construction of the attachment of the heating elements can be seen in Fig.36, 37, 38.

Dummy pipes Dummy pipes are installed around the heating element in order to generate similar flow conditions as in industrial applications. The dummy pipes have a diameter of 25 mm which is the same as for the main tube of the heating element. The arrangement of the dummy pipes has a horizontal pitch of 2 times the pipe diameter $p_{hor} = 50\,\text{mm}$ and a vertical pitch of 2.5 times the pipe diameter $p_{vert} = 62.5\,\text{mm}$. Furthermore, the dummy pipes are staggered as can be seen in Fig.35.

Air extraction The air extraction is realized with an standalone extraction system which is connected to the test rig via pipeline. The extraction system can be set manually using a frequency converter.

6.2.2. Integration of the sintered plate

The sintered plate is clamped between the wind box and the fluidized bed chamber, which can be seen in Fig.35. It is sealed from below against the wind box and from above against the fluidized bed chamber. The sealing against the wind box is special because also the sealing between the two chambers of the wind box must be realized with this in order to enable the different volume flows on the heating and cooling side. The challenge for the seals as well as for the other components is the high operating temperature. Therefore the KLINGER® milam PSS is used for the sealings, which is specially designed for dry gas high temperature applications. For all gaskets the PSS130 with a thickness of 1.3 mm is used. The data sheet for the KLINGER® milam PSS can be seen in appendix B.

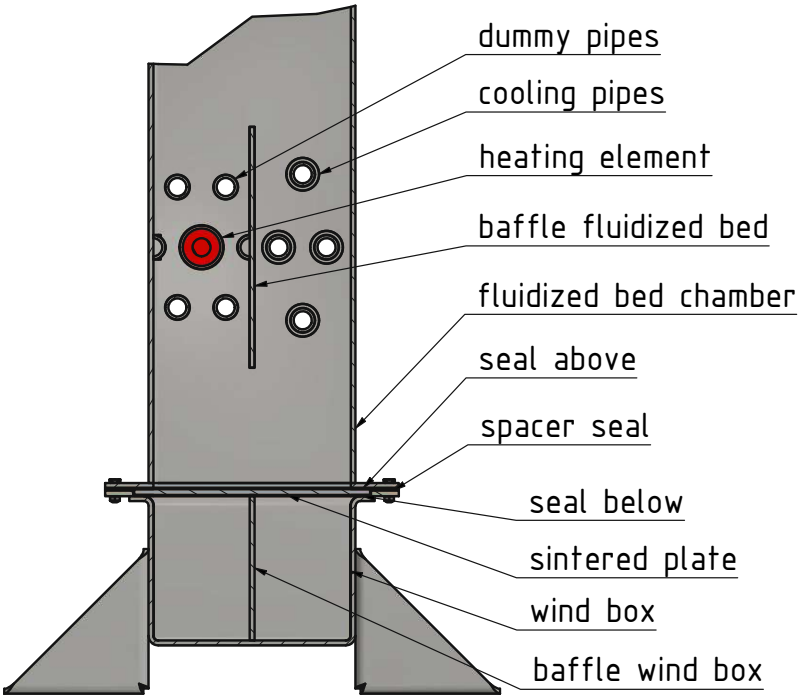

Figure 35.: *Integration of the sintered plate heat transfer test rig.*

6.2.3. Incorporation and attachment of the heating elements

A safe and secure mounting of the heating element is a basic requirement for a proper execution of the experiment. The heating element is attached to the front and rear of the fluidized bed chamber as it can be seen in Fig.36. The assembly consists the following steps.

- Assembly of the attachment for the rear side
- Pre-assembly of the attachment for the front side on the heating element
- Plug in of the pre-assembled heating element and screw with the fluidized bed chamber

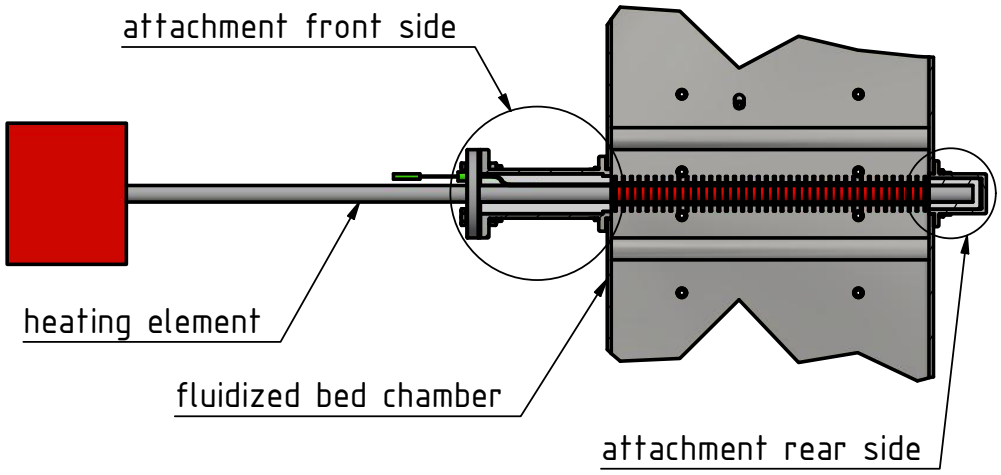

Figure 36.: *Atachment of the heating element.*

The attachment on the rear side of the heat transfer test rig mainly consists of the rear mounting flange and the inserted rear ceramic socket, which are connected to the welding studs of the fluidized bed chamber with hex nuts (see Fig.37). The rear flange gasket made out of KLINGER® milam PSS is used to seal the flange with the fluidized bed chamber. Ceramic sockets are used to thermally insulate the heating element from the other directly adjacent components. The thermal insulation is very important to ensure that heat is only introduced into the fluidized bed via the heating element and the losses are kept small. This is necessary in order not to falsify the measured input power and consequently also the heat transfer coefficient. The sockets are made from Macor® a glass ceramic with low thermal conductivity and operating temperatures up to 800 °C. The possibility of customizing existing semi-finished products makes this material so unique for use in the heat transfer test rig. The material data sheet of the Macor® glass ceramic can bee seen in appendix B.

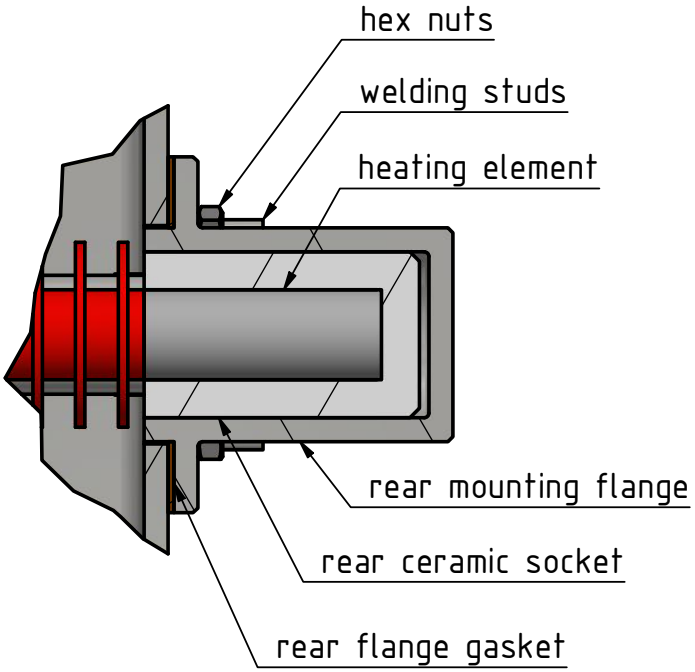

Figure 37.: *Attachment rear side.*

The attachment on the front side of the heat transfer test rig has to fulfill several tasks, which are the connection of the heating element to the fluidized bed chamber, the thermal insulation of the heating element and the embedding of the temperature sensor (see Fig.38). The connection of the front mounting flange with the fluidized bed chamber is executed in the same way as with the rear mounting flange. The fixation between the heating element and the front mounting flange is done with hex bolts and hex nuts. The ceramic socket for the attachment on the front side is also made out of Macor® glass ceramic and divided into two halves. This is necessary on one hand because of the reusability for both types of heating elements (plain tube and finned tube) and on the other hand because of the cable bushing of the temperature sensor into the test rig. One half of the front ceramic socket has a groove where the sheathed thermocouple is routed. through. The sealing is also done with flange gaskets made out of KLINGER® milam PSS.
The pre-assembly of the attachment for the front side is carried out according to the following procedure.

- Screw and glue the sheathed thermocouple
- Putting on the ceramic socket halves
- Slide on of the front mounting flange and fixation with the heating element

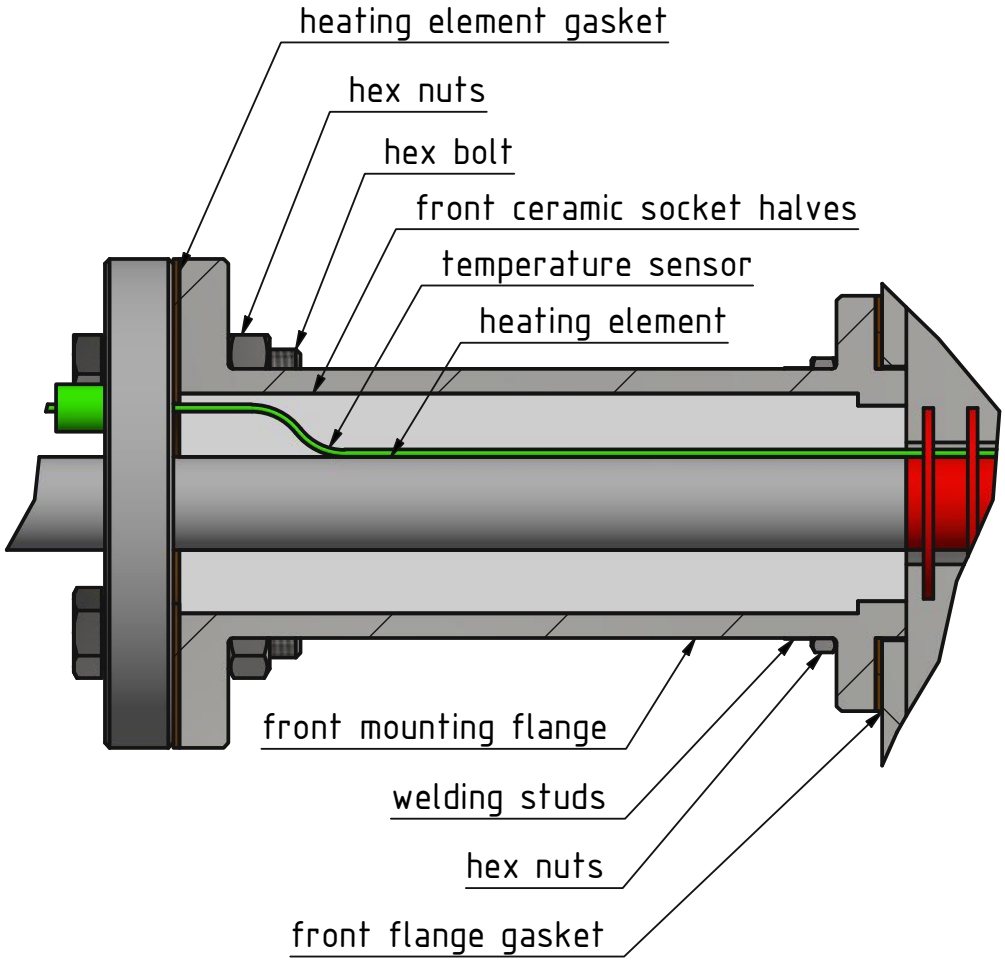

Figure 38.: *Attachment front side.*

6.2.4. Design of the cooling lines

The cooling system is essential for the operation of the test rig to ensure a steady state. The cooling is realized via the recooling circuit of the laboratory. The structure of the cooling lines can be seen in Fig.39. In order to prevent thermal stresses in the structure there are two u-bends, which offers the possibility to connect the two cooling lines in parallel or in series. The cooling pipe u-bends are made out of heat-resistant chromium-nickel steel X15CrNiSi25-21 (1.4841) and have threaded bushings at the end with a G1 inch external thread where the recooling circuit is connected with hoses.

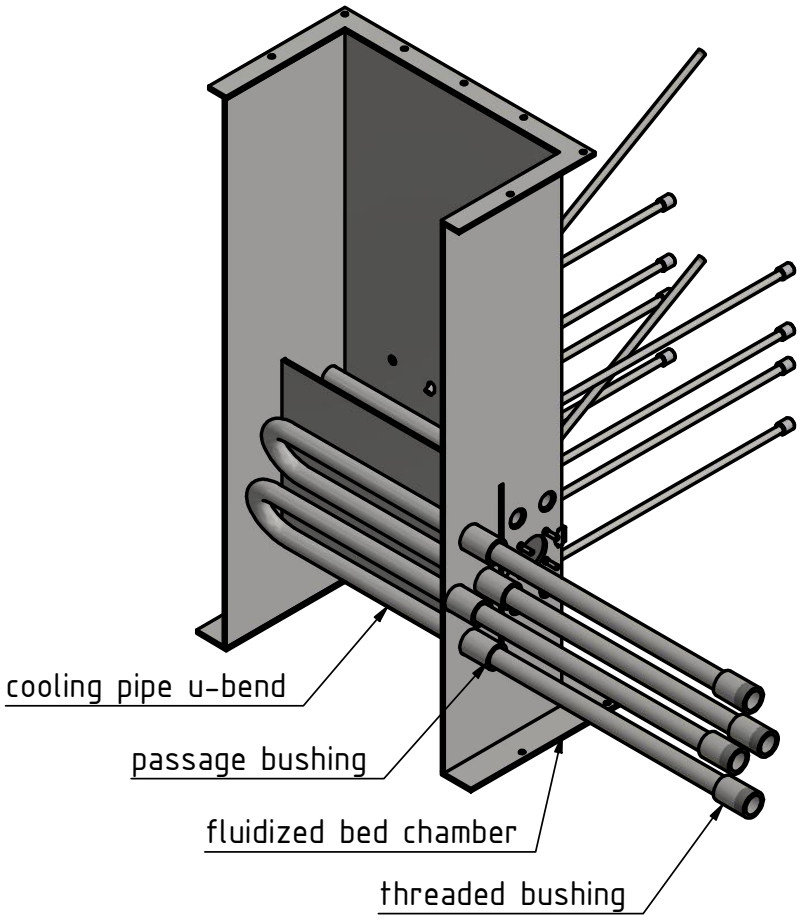

Figure 39.: *Structure of the cooling lines.*

The high operation temperatures also have a major effect on the design of the cooling lines. Due to the temperature difference between the cooling line and the rest of the test rig and the resulting uneven thermal expansion of the components a design with u-bends is necessary, otherwise impermissible thermal stresses would arise. A passage bushing is also used to reduce the thermal stresses in the cooling pipe, which can be seen in Fig.40. A vertical pitch of 2.5 times the pipe diameter as on the heating side is not possible due to manufacturing limitations. The minimum bending diameter of the u-bend bend with 98 mm specifies the vertical pitch with 94.8 mm.

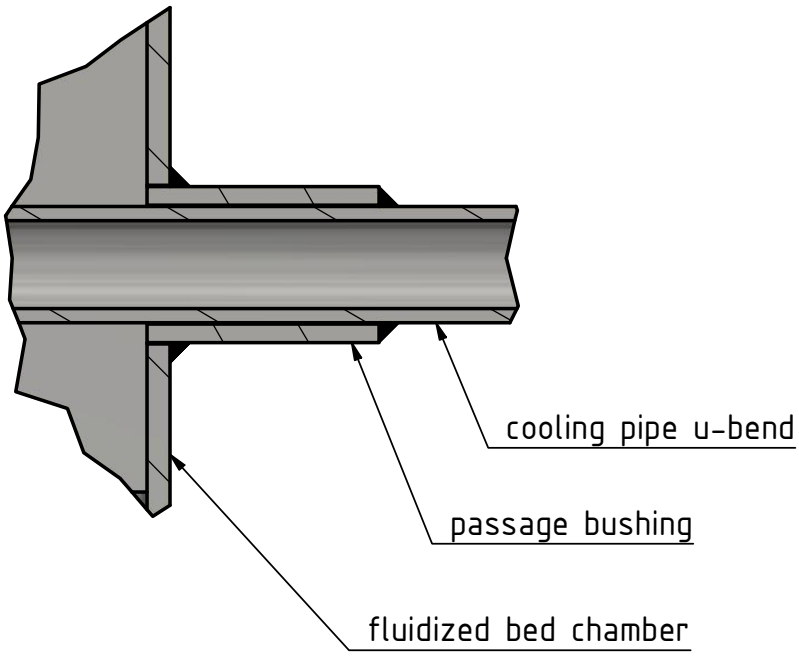

Figure 40.: *Integration of the cooling lines.*

The design of the cooling lines with two u-bends also offers the opportunity to use them not only in series or parallel but also to cool only one strand and keep the other hot. However, it must be taken into account that this can result in a rather asymmetrical cooling effect due to the arrangement of the u-bends. Theoretically it would also be possible to use air instead of water for cooling. However, the hot exhaust air would also have to be discharged in order to be able to comply with all safety-related boundary conditions.

6.3. Manufacturing and assembling

6.3.1. Air supply

The air supply is a main requirement for the fluidization of the operating medium. As it can be seen in Fig.23 the compressed air is stored in the air chamber from which it is taken for the test rig. A 2 inch steel pipe conducts the compressed air to the control valve (CV) with electric actuator from the company FLUVIUS Flow Control GmbH (Wiener Neustadt - Austria), which adjusts the total volume flow. After the control valve the supply line splits into two 0.5 inch steel pipes which are connected to the flow sensors. The individual air supply lines made out of compressed air hoses for the heating and cooling side connects the adjustment valves (AV) at the inlets of the test rig with the flow sensors.

6.3.2. Mechanical components

The mechanical components of the heat transfer test rig were manufactured entirely by subcontractors. The steel construction parts, including the wind box, the fluidized bed chamber, the cover and the air extraction hood were fabricated by the company Innoweld Metallverarbeitung GmbH (Mürzzuschlag - Austria). The mounting flanges for the attachment of the heating element were manufactured by the company ORLIK & Co GmbH (Wöllersdorf - Austria) and the ceramic sockets were manufactured by the company Präzisions Ceramik Nord GmbH Co. OHG (Bönningstedt - Germany). Production and assembly were carried out in cooperation with the laboratory staff. The manufacturing and assembly drawings can be found in appendix B.

6.3.3. Air extraction

The air flowing out of the heat transfer test rig is directed into a air cooling tower and then in the extraction and filter system via a pipeline, which can be seen in Fig.41. The control independent system can be continuously adjusted and is an existing assembly, available at the test site, which is also used for other test rigs. The special filter in the extraction system is also crucial to prevent particles from being released to the environment. The air cooling tower is also an existing assembly at the test site and consist of a heat exchanger on the top and the basic construction made out of steel. The heat exchanger is also connected to the recooling circuit of the laboratory. Additionally, the air is cooled over the large surface of the steel base construction.

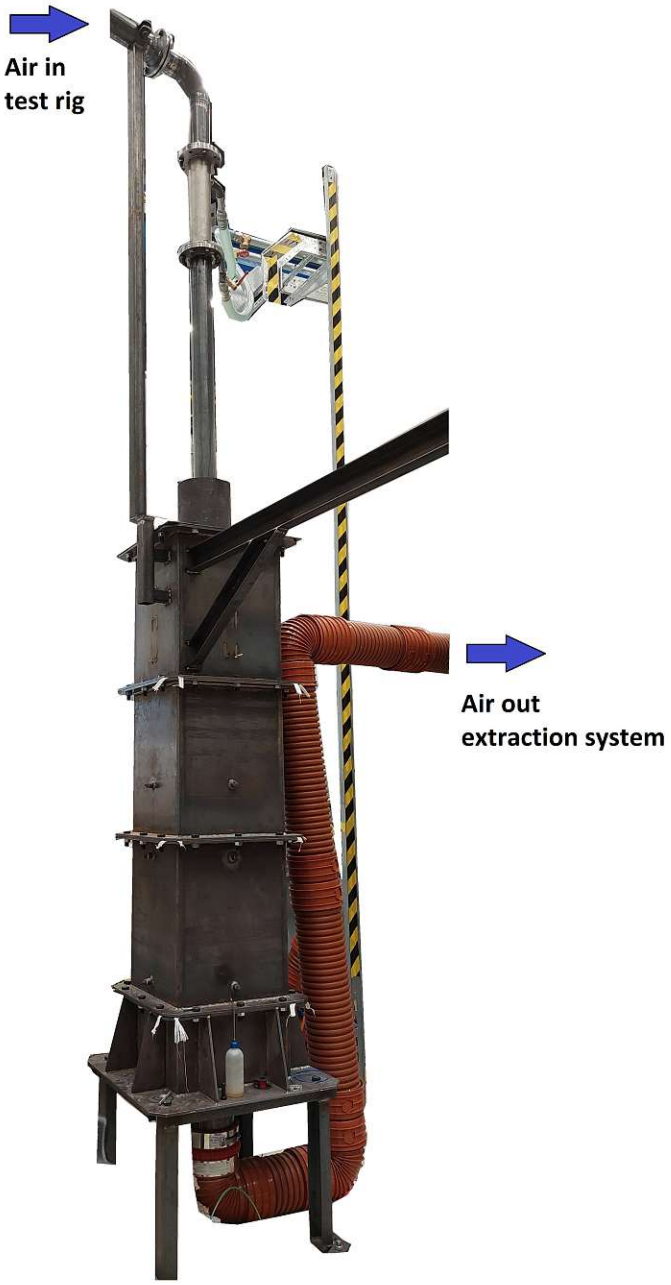

Figure 41.: *Air extraction cooling tower.*

6.4. Measurement setup and sensors

The measurements which are taken during the runtime of the test rig on one hand ensure consistent test conditions and on the other hand are the basis for evaluating the heat transfer coefficient. As described in section 4.2.1 two volume flow sensors, 13 temperature sensors and nine pressure sensors are used. The used volume flow and pressure sensor are similar or the same as for the erosion test rig and the data sheets can be seen in appendix A. The data sheet for the temperature sensors can be seen in appendix B.

The used volume flow sensors IL30.005 from SCHMIDT Technology GmbH are screwed in directly at the air supply lines. The sensors have a measuring range of 0 to 76.3 m^3/h and also determines the medium temperature. The used pressure sensors DS2 from the company Kalinsky are adapted to their measuring task, which are listed in Tab.10 based on the description of the pressure sensors Tab.8. For the temperature sensor sheathed thermocouples type 12, K (NiCr/NiAl) are used and are manufactured by the company TC Mess- und Regeltechnik GmbH (Mönchengladbach - Germany). The used thermocouples have a measuring range between 0 to 700 °C. For T1-T12 the measuring transducer is integrated in the connection head and the 4 to 20 mA analog output signal is passed directly to the controller. For this sensors the sheathed thermocouple 12-K-450-310-4,5-2I-3P11-TXLTC is used. For the measurement of the surface temperature of the heating element the sheathed thermocouple 12-K-400-310-1,5-2I-3P3LB-4M C40 KX with a measuring transducer installed in the control cabinet is used. The temperature sensors are fastened with compression fittings in the sockets provided for this purpose.

Table 10.: *Measuring range pressure sensors heat transfer test rig*

Pressure sensor	**Measuring range**
PD1	0 to 500 mbar
PD2	0 to 500 mbar
PD3	0 to 100 mbar
PD4	0 to 50 mbar
PD5	−25 to 25 mbar
PD6	0 to 500 mbar
PD7	0 to 500 mbar
PD8	0 to 100 mbar
PD9	0 to 50 mbar

7. Results and Discussion

7.1. Erosion test rig

7.1.1. Recording of the pressure loss profile

The recording procedure of the pressure loss profile has already been described in section 3.2.2. During the recording of the pressure loss profile a fixed bed height L_m of 500 mm was realized. For the long-time-test the fixed bed height L_m was reduced to 400 mm to decrease the entrainment of particles. In order to obtain a meaningful mean value, five recordings with rising volume flow and five recordings with falling volume flow were taken. A typical course of the pressure loss profile can be seen in Fig.42.

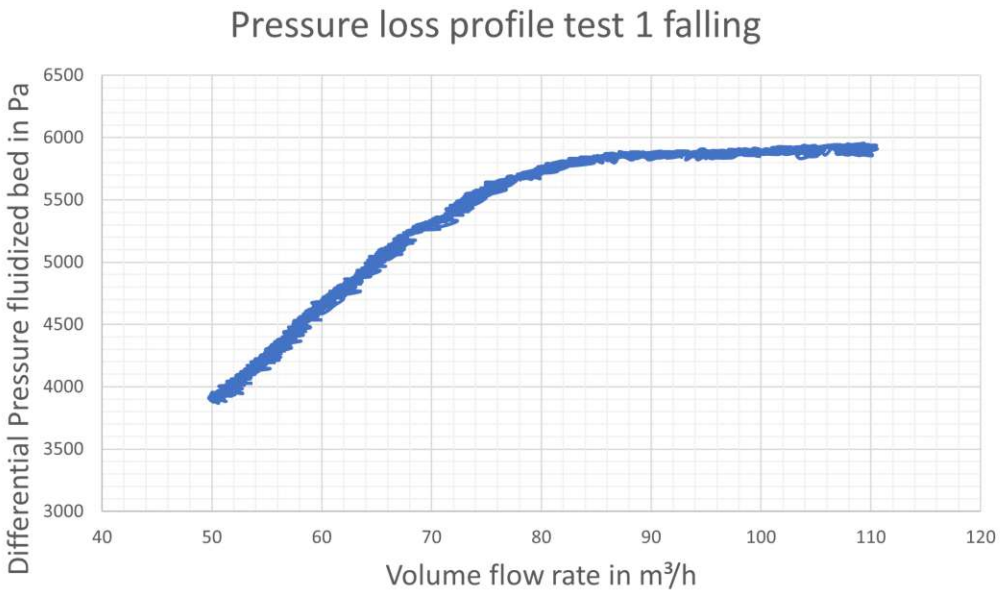

Figure 42.: *Pressure loss profile for falling volume flow rate.n*

7.1.2. Calculation of the minimal fluidization velocity

For the calculation of the minimal fluidization volume flow rate the intersection of two regression lines was determined, as it can be seen in Fig.43. The first regression

line was determined for the linear pressure increase across the fluidized bed. For this a sufficiently stable area under the minimal fluidization volume flow rate was selected and a linear trend line was generated for the pressure increase. The constant pressure p_{const} for a fully developed fluidized bed was determined from the mean value of the measured values for a sufficiently stable area above the minimal fluidization volume flow rate. Likewise the linear function for the trend line was evaluated, which can be seen in Eqn.(31). Using the linear function (Eqn.(31)) and the value of the constant pressure at higher volume flow rates $p_B = p_{const}$ the minimal fluidization volume flow rate can be calculated (see Eqn.(32)).

$$p_B = c_1 \cdot \dot{V} + c_2 \tag{31}$$

$$\dot{V}_{mf} = \frac{p_{const} - c_2}{c_1} \tag{32}$$

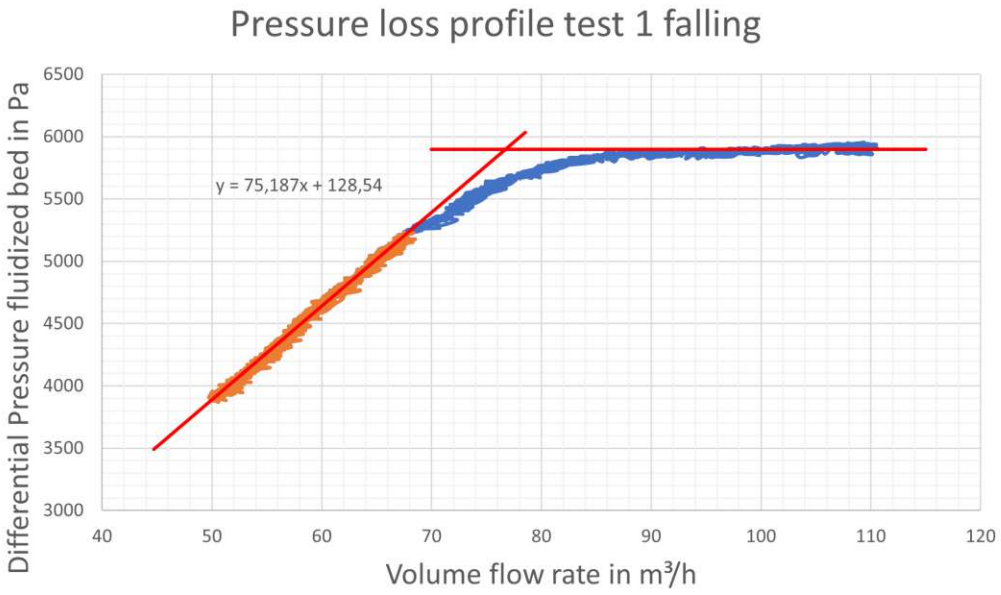

Figure 43.: *Determination of the minimal fluidization volume flow rate*

In Tab.11 the values of the constants c_1, c_2 and the value of the constant pressure p_{const} for the different test procedures are collected. The underlying pressure loss profiles can be found in appendix A.

The average minimal fluidization volume flow rate for the falling test procedure $\dot{V}_{mf} = 76.2\,\mathrm{m}^3/\mathrm{h}$, with a cross sectional are of the fluidized bed $A_B = 0.1989\,\mathrm{m}^2$ gives a real minimal fluidization velocity $u_{mf.real} = 0.1064\,\frac{\mathrm{m}}{\mathrm{s}}$ which is similar to the theoretical value $u_{mf.theor} = 0.1057\,\frac{\mathrm{m}}{\mathrm{s}}$. The value of the real minimal fluidization velocity was used for setting the volume flow rate for the long-term test.

Table 11.: *Calculation of the minimal fluidization volume flow rate*

Test configuration	Constant $c_1 \left(\frac{Pa \cdot h}{m^3}\right)$	Constant $c_2(Pa)$	Constant pressure $p_{const}(Pa)$	Minimal fluidization volume flow rate $V_{mf} \left(\frac{m^3}{h}\right)$
Test 1 rising	86,309	-504,54	5885,1	74,03
Test 1 rising	84,661	-370,16	5889,1	73,93
Test 3 rising	91,354	-903,26	5766,2	73,01
Test 4 rising	85,702	-511,48	5751,6	73,08
Test 5 rising	82,624	-362,24	5708,0	73,47
			Average rising test	**73,50**
Test 1 falling	75,187	128,54	5896,3	76,71
Test 2 falling	73,691	203,33	5869,6	76,89
Test 3 falling	76,652	-58,769	5763,6	75,96
Test 4 falling	76,192	-72,606	5738,5	76,27
Test 5 falling	78,985	-249,82	5687,5	75,17
			Average falling test	**76,20**

7.1.3. Mass loss evaluation of the inspection elements

The mass of the inspection elements was determined before and after the long-term test by weighing on a balance (MSA2203S-OCE-DE from Satorius) which has an accuracy of 1 µg. The measured values of the mass and the calculated mass and material loss of the inspection elements can be seen in Tab.12. In order to achieve better comparability of the results, the mass loss was related to the inspection element surface, which results in mass loss values between 7.5 to 27.6 g/m^2. The inspection element surface is the entire surface of the inspection element immersed in the fluidized bed, i.e. the surface that is touched by the sand. In order to illustrate the loss of mass geometrically, the material density was used to calculate the removal thickness in relation to the surface of the inspection elements. The material loss thicknesses are, as presented in Tab.12, very low. This also means that the calculated loss of material is an average value and may possibly higher real values at certain points on the inflow side can occur. The low erosion rates in the long-time-test are very positive, as they suggest that real lifetime erosion rates will also be low.

Table 12.: *Mass loss evaluation of the inspection elements*

Inspection element	Installation angle (°)	Mass before test (g)	Mass after test (g)	Mass difference (g)	Inspection element surface (m^2)	Mass loss $\left(\frac{g}{m^2}\right)$	Material loss (µm)
metal sheet 1	0	125,802	125,408	0,394	0,01428	27,591	3,515
metal sheet 2	7	125,792	125,411	0,381	0,01428	26,681	3,399
metal sheet 3	15	125,770	125,444	0,326	0,01428	22,829	2,908
metal sheet 4	30	125,783	125,480	0,303	0,01428	21,218	2,703
metal sheet 5	45	125,828	125,581	0,247	0,01428	17,297	2,203
metal sheet 6	60	125,726	125,531	0,195	0,01428	13,655	1,740
metal sheet 7	75	125,780	125,629	0,151	0,01428	10,574	1,347
metal sheet 8	90	125,781	125,635	0,146	0,01428	10,224	1,302
tube		202,614	202,416	0,198	0,01335	14,829	1,889
fin tube		1096,763	1096,338	0,425	0,05693	7,465	0,951

As can be seen in Fig.44 the mass loss decreases with increasing installation angle. An installation angle of 0° means that the inspection element is vertical and oriented in the direction of flow and an installation angle of 90° means that it is horizontal and transverse to the direction of flow. This behavior is different from what is described in the literature [17] and section 2.2. A possible explanation for this case is the atmospheric bed pressure. With atmospheric bed pressure it can assumed, that the material removal is done mostly abrasively. If this case is compared to Fig.13 it can be seen, that the influence of the angle of attack for low bed pressure is no longer clearly recognizable. This also leads to the hypothesis that at higher bed pressures, erosion is strongly based on the impact of the particles on the surface. In the configuration with low installation angles, this means the metal sheet lies in the direction of flow, the particles have a longer way to act abrasively. This means that erosion mainly occurs on flow-guiding components and less on transverse installations that impede the flow.

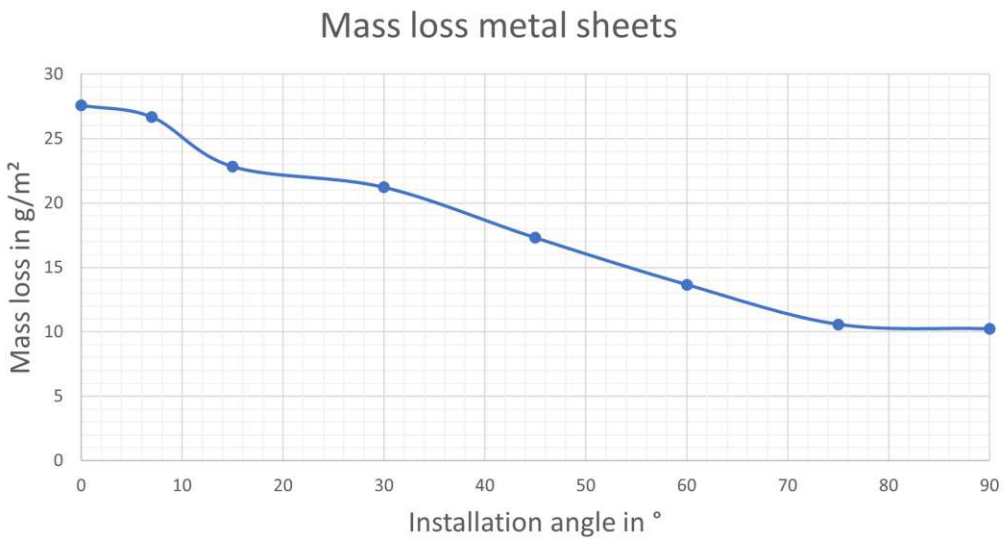

Figure 44.: *Mass loss over installation angle (0°-vertical / 90°-horizontal) of the metal sheets*

7.1.4. Geometry change evaluation of the inspection elements

The measurement of the inspection elements was carried out at the defined measuring points (see Fig.20, 21). The measurement itself was carried out with a slide gauge and an outside micrometer. The full geometric measurement data of the inspection elements can be found in appendix A in Tab.15 16.

The reduction in the thickness of the metal sheets due to erosion is shown in Tab.13. When comparing these results to the arrangement of the measuring points (see Fig.20), one can see that erosion occurs mainly in the middle of the inspection elements. In the middle of the fluidized bed the flow is fully developed, whereas in the edge area the influence of wall friction or other flow influences have an importance. Fig.45 shows a heatmap of the geometrical material loss of metal sheet 1 (installation angle 0°). However, in a comparison with the calculated loss of material from the loss of mass, attention must be paid to the related surface area. For the geometry change evaluation the total material loss is measured, which refers to the front and back of the metal sheets, which means twice the area. In order to compare the results from Tab.13 with Tab.12, the values have to be halved. Furthermore, it must be ensured that the determined measuring points are selective measured values and that these result in average values, which are similar to those that are determined from the mass loss.

Table 13.: *Geometry change of the metal sheet inspection elements*

Inspection element	Difference of the measuring points in µm							
	MP1	MP2	MP3	MP4	MP5	MP6	MP7	MP8
metal sheet 1	0	0	-10	-10	0	0	-10	-10
metal sheet 2	0	0	-10	-10	0	0	-10	-10
metal sheet 3	0	0	-10	-10	0	0	-10	-10
metal sheet 4	0	0	-10	-10	0	0	-10	-10
metal sheet 5	0	0	-10	-10	0	0	-10	-10
metal sheet 6	0	0	-10	-10	0	0	0	-10
metal sheet 7	0	0	-10	0	0	0	-10	-10
metal sheet 8	0	0	-10	-10	0	0	0	0

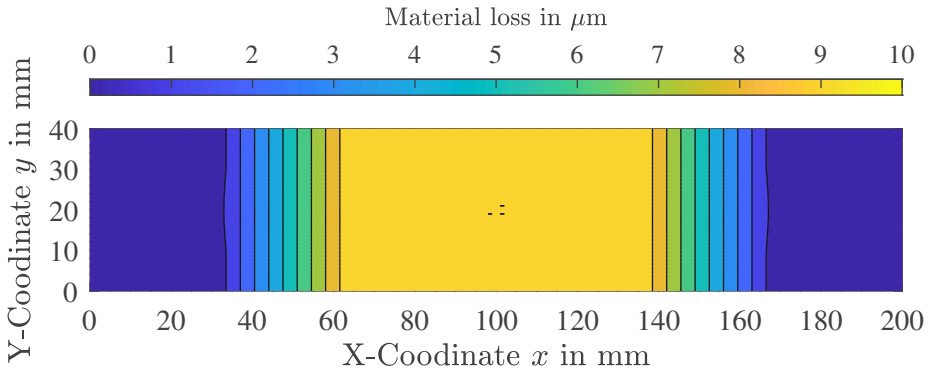

Figure 45.: *Heatmap of geometric material loss of metal sheet 1.*

The geometry changes of the measuring points of the tube can be seen in Tab.14. For some measuring points of the tube a material increase was detected. A possible explanation in this case are measurement inaccuracies. The tube itself is not perfectly circular, as can be seen in Tab.16 in appendix A. Therefore small angle errors in the measurement can effect the result. In general, the measurement results for the tube give less information about the erosion behavior.

Table 14.: *Geometry change of the tube inspection element*

Inspection element	Difference of the measuring points in µm						
tube	MP1	MP2	MP3	MP4	MP5	MP6	MP7
	-10	-10	-10	-50	10	10	-50
	MP8	MP9	MP10	MP11	MP12	MP13	MP14
	0	10	20	0	0	0	10
	MP15	MP16	MP17	MP18	MP19	MP20	
	0	0	20	30	-50	-30	

7.1.5. Wear and tear of the resource sand

During the long-term-test a total amount of 20 kg sand was extracted from the erosion test rig. At the beginning 105 kg of sand were in the test rig. The level of the sand was checked in regular intervals and if necessary refilled. After the long-term test, the sand had a different composition, so it was suspected that wear has occurred in the sand itself. Thus a particle analysis was carried out in order to be able to compare the values with the starting values. As a starting point for the experiments quartz sand with a average particle size of 330 µm from Strobel Quarzsand GmbH was used. The data sheet of the used quartz sand can be found in the appendix A.

A sieve analysis of the used sand was carried out in cooperation with the E166-01 Research area "Mechanical Process Engineering and Clean Air Technology". The entire measurement data of the sieve analysis can be found in appendix A. The distribution of the particle can be seen in Fig.46. There, the volumetric amount of sand in % is plotted against the particle size. The average particle size is determined via the d(0,5)-Median. The d(0.5)-Median is the particle size where 50 % of the sand volume are below this value and 50 % are above this value. For the used used sand the determined d(0,5)-Median is 330.5 µm. Furthermore, a laser diffraction analysis measurement using the Mastersizer 2000 was performed. The measurement data and results are also attached in the appendix A. A total of 4 measurements were carried out in order to be able to form an average. The averaged d(0,5)-Median which was determined with this method is 339.6 µm.

If we compare the values of the average particle size, we can see that there is practically no difference between the starting sand with 330 µm and the used sand with 330.5 µm. The average particle size of the laser diffraction 339.6 µm differs only slightly from that of the sieve analysis. However, it has to be considered that nearly 20 % of the quartz sand volume has been entrained. Therefore, it is possible for the sand to be worn down and the resulting finer fraction to be extracted from the test rig. It also has to be noted that the sand changed optically, meaning that the initially sharp-edged particles appeared more rounded after the long-term test.

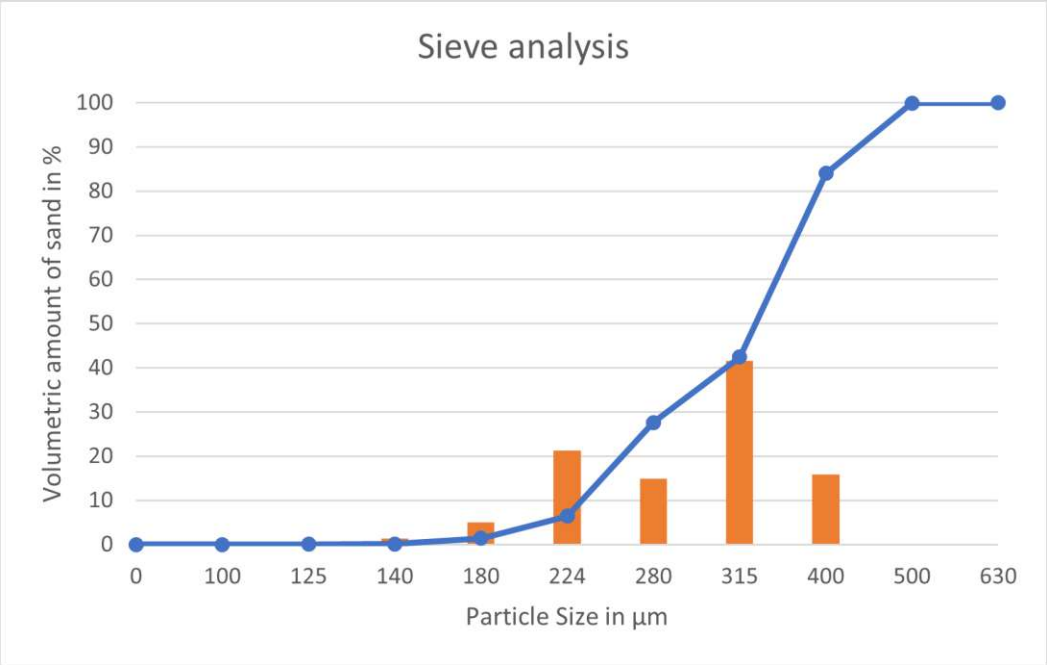

Figure 46.: *Sieve analysis of the used sand.*

7.2. Heat transfer test rig

The construction and production of all components is finished and the assembly is largely complete. Due to the use of the air supply and air extraction system for a different test rig, the assembly can be completed at the earliest in December 2022.

8. Conclusion and Outlook

The main work of this thesis was the development and construction of the erosion test rig and the heat transfer test rig. Furthermore the commissioning and the execution of a long-term test for the erosion test rig was another big part. During the assembly and the commissioning of the erosion test rig several adaptions were necessary in order to be able to carry out the tests as desired.

An important finding gained by conducting the erosion tests is the relatively high transport disengagement height (TDH) for larger average particle size. For the case of large particle sizes and high degree of fluidization (FG) the TDH can not be calculated exactly analytically. The existing equations for the TDH are often limited to small particle sizes or fluid velocities. Especially very energetic ejections are problematic for large average particle sizes. This must be taken into account for future designs to prevent particle extraction. The used solutions of an increased freeboard height or a filter system are very practicable and cost effective and should be considered.

The recording of the pressure loss profile was performed using a frequency converter and resulted in consistent curves. The precise pressure loss profiles enabled a good determinability of the minimal fluidization velocity. The determined minimal fluidization velocity value agreed very well with the theoretical value.
As expected the erosion rates are very low. The mass loss values were between 7.5 to 27.6 g/m^2. These mass loss values were achieved after one month operation at test conditions, which translates to about 19 years at operating conditions. A very interesting finding results from the dependence of the erosion rate on the installation angle. It turns out that an increasing installation angle (inclination to the flow direction) leads to an decreased mass loss.

The results of the first long-term test are exactly what was expected. However, some dependencies cannot be determined precisely without further tests. Further test directions and their background are listed below.

- **Particle size dependency** In the correlation for the appraisal of the erosion rate for operating conditions, the particle size may also have an impact. In order to be able to determine this dependency more precisely, tests with other particle sizes are necessary.

- **Superficial gas velocity** The correlation for the estimation of the erosion rate mainly depends on the superficial gas velocity with with a power factor. This power factor is normally 3, but in some papers there are differences. In order to be able to determine this power factor more precisely, tests with different degrees of fluidization under otherwise identical test conditions are possible.
- **Installation angle** The dependency of the erosion rate on the installation angle is different to the literature, see 7.1.3. Therefore, the arrangement of the inspection elements in the test rig should also be considered. Also maybe boundary conditions have an influence. This case should be considered in more detail as it also has a significant impact on the construction of internals.

The assembly of the heat transfer test rig can be completed in December 2022 after the completion of the tests of the other test rig. The test rig probably can be put into operation at the beginning of 2023 and afterwards the heat transfer tests can be stared.

Bibliography

[1] Institut für Energietechnik und Thermodynamik, *Institut für Energietechnik und Thermodynamik Forschungsgebiet Energiespeicher*. [Online]. Available: https://www.tuwien.at/mwbw/iet/e302-01-forschungsbereich-thermodynamik-und-waermetechnik/forschungsgebiete/energiespeicherung.

[2] K. B. Schwaiger, *Development of a novel particle reactor/heat-exchanger technology for thermal energy storages*. 2016.

[3] J. P. Filipic, "Experimentelle Untersuchungen am Kaltmodell einer Wirbelschichtverbrennungsanlage im Technikumsmaßstab", Ph.D. dissertation, University of Leoben, 2006.

[4] Y. Liu, "Two-fluid modeling of gas-solid and gas-liquid flows: solver development and application", Ph.D. dissertation, Technische Universität München, 2014.

[5] M. Stieß, *Mechanische Verfahrenstechnik : 2(1997)*, ger, [Nachdr.]. Berlin [u.a.]: Springer, 1997, ISBN: 3540558527.

[6] Hermann Hofbauer, "Unterlagen zur Vorlesung Wirbelschichttechnik (159.220)", Vienna.

[7] Matthias Stiess, *Mechanische Verfahrenstechnik - Partikeltechnologie 1*. Berlin, Heidelberg: Springer Berlin Heidelberg, 2009, ISBN: 978-3-540-32551-2. DOI: 10.1007/978/3-540-32552-9.

[8] D. Geldart, "Types of gas fluidization", *Powder Technology*, vol. 7, no. 5, pp. 285–292, May 1973, ISSN: 00325910. DOI: 10.1016/0032-5910(73)80037-3.

[9] E. Tsotsas, "M5 Wärmeübergang in Wirbelschichten", in 2019, pp. 1719–1730. DOI: 10.1007/978-3-662-52989-8{_}100.

[10] S. Kabelac, M. Kind, H. Martin, D. Mewes, K. Schaber, and P. Stephan, *VDI-Wärmeatlas, 11. Auflage*. 2013.

[11] D. Schulze, *Pulver und Schüttgüter*. Berlin, Heidelberg: Springer Berlin Heidelberg, 2014, ISBN: 978-3-642-53884-1. DOI: 10.1007/978-3-642-53885-8.

[12] T. E. Howes, "Erosion-oxidation of mild steel in a fluidized bed environment", Ph.D. dissertation, University of Cambridge, 1997.

[13] J. Zhu, J. R. Grace, and C. J. Lim, "Tube wear in gas fluidized beds—I. Experimental findings", *Chemical engineering science*, vol. 45, no. 4, pp. 1003–1015, 1990.

[14] H. Effenberger, *Dampferzeugung*. Springer-Verlag, 2013.

[15] R. Chalupnik, W. Kaiman, M. Vogt, and D. Wiese, "Optimierung und Weiterentwicklung einer stationären Wirbelschichtfeuerung", in *VDI-Bericht*, VDI-Verlag, 1987, pp. 209–218.

[16] W. Brötz, "Grundlagen der wirbelschichtverfahren", *Chemie Ingenieur Technik*, vol. 24, no. 2, pp. 60–81, 1952.

[17] J. Wiman and A.-E. Almstedt, "Hydrodynamics, erosion and heat transfer in a pressurized fluidized bed: influence of pressure, fluidization velocity, particle size and tube bank geometry", *Chemical Engineering Science*, vol. 52, no. 16, pp. 2677–2695, 1997.

[18] N. Ladner, "CPFD-Simulation einer einfachen blasenbildenden quaderförmigen Wirbelschicht mit zwei unterschiedlich fluidisierten Querschnitten", E302 - Institut für Energietechnik und Thermodynamik, Tech. Rep., 2021.

[19] RICHARDSON, "Sedimentation and fluidisation: Part I", *Chemical engineering research & design : transactions of the Institution of Chemical Engineers.*, vol. 32, p. 35, 1954, ISSN: 0263-8762.

[20] Kunii and Levenspiel, *Fluidization Engineering*. Elsevier, 1991, ISBN: 9780080506647. DOI: 10.1016/C2009-0-24190-0.

A. Erosion test rig

Calculation of the sintered plate

Input data:

Cross sectional area of the fluidized bed: $A_B := 1170mm \cdot 170mm = 0.1989\,m^2$

Bedheight of the silica sand: $h_B := 0.4m$

Bulk density of the silica sand: $\rho_{Sand} := 1325 \frac{kg}{m^3}$

Temperature of the air: $T_{Luft} := 20\,°C$

Density of the airt: $\rho_{Luft} := 1.189 \frac{kg}{m^3}$

Dynamic viscosity of the fluidizing air: $\eta_{Luft} := 1.821 \cdot 10^{-5} Pa \cdot s$

Minimal fluidization velocity
(particle diameter, particle density, Temperatur) $u_{mf} := 0.1057 \frac{m}{s}$

Degree of fluidization: $FG := 5$

Keydata of the sintered plate material

Material: SIKA-R 10 AX

Viscosity coefficient: $\psi_v := 3.9 \cdot 10^{-12} m^2$

Permeability coefficient $\psi_p := 24 \cdot 10^{-7} m$

Calculation:

Pressure drop bed: $\Delta p_B := \rho_{Sand} \cdot g \cdot h_B = 5197.5245\,Pa$

Volumetric flow rate: $V_{Punkt.B} := A_B \cdot u_{mf} \cdot FG = 378.4271 \cdot \frac{m^3}{h}$

Required pressure drop sintered plate: $\Delta p_{sinter.req} := 0.3 \cdot \Delta p_B = 1559.2573\,Pa$

Sintered plate thickness according to DIN EN ISO 4022:

Required plate thickness:

$$e_{sinter.req} := \frac{\Delta p_{sinter.req}}{\frac{V_{Punkt.B} \cdot \eta_{Luft}}{A_B \cdot \psi_v} + \frac{V_{Punkt.B}^2 \cdot \rho_{Luft}}{A_B^2 \cdot \psi_p}} = 0.5983 \cdot mm$$

Defined plate thickness:

$$e_{sinter} := 6.5mm$$

Pressure drop across the sintered plate:

$$\Delta p_{sinter} := e_{sinter} \cdot \left(\frac{V_{Punkt.B} \cdot \eta_{Luft}}{A_B \cdot \psi_v} + \frac{V_{Punkt.B}^2 \cdot \rho_{Luft}}{A_B^2 \cdot \psi_p} \right)$$

$$\Delta p_{sinter} = 16939.4186\,Pa$$

Relative pressure drop:

$$\frac{\Delta p_{sinter}}{\Delta p_B} = 3.2591$$

Total pressure drop

$$\Delta p_{Gesamt} := \Delta p_{sinter} + \Delta p_B = 0.2214 \cdot bar$$

Sizing table sintered plate erosion test rig

Used sintered plate material	SIKA-R 10 AX
Temperature (°C)	20
Density air (kg/m³)	1,189
Dynamic viscosity air (Pa·s)	0,00001821
Pressure drop fluidized bed (Pa)	5197,5245
Plate thickness (mm)	6,5
Cross sectional area of the fluidized bed (m²)	0,1989
Viscosity coefficient (m²)	0,0000000000039
Permeability coefficient (m)	0,0000024

Particle diameter silica sand (µm)	Minimal fluidization velocity (m/s)	Degree of fluidization (-)	Volumetric flow rate (m³/s)	Pressure drop sintered plate (Pa)	Relative pressure drop (-)	Total pressure drop (Pa)
146	0,0215	6	0,0257	3968,7375	0,7636	9166,2620
		7	0,0299	4640,6135	0,8929	9838,1380
		8	0,0342	5315,4666	1,0227	10512,9911
		9	0,0385	5993,2968	1,1531	11190,8213
		10	0,0428	6674,1041	1,2841	11871,6286
242	0,0583	4	0,0464	7252,7421	1,3954	12450,2666
		5	0,0580	9120,6533	1,7548	14318,1778
		6	0,0696	11010,4548	2,1184	16207,9793
		7	0,0812	12922,1466	2,4862	18119,6711
		8	0,0928	14855,7286	2,8582	20053,2531
		9	0,1044	16811,2008	3,2345	22008,7253
		10	0,1160	18788,5634	3,6149	23986,0879
330	0,1057	4	0,0841	13407,6239	2,5796	18605,1484
		5	0,1051	16939,4186	3,2591	22136,9431
		6	0,1261	20543,1688	3,9525	25740,6933
		7	0,1472	24218,8745	4,6597	29416,3990
		8	0,1682	27966,5357	5,3807	33164,0602
		9	0,1892	31786,1524	6,1156	36983,6769
		10	0,2102	35677,7245	6,8644	40875,2490

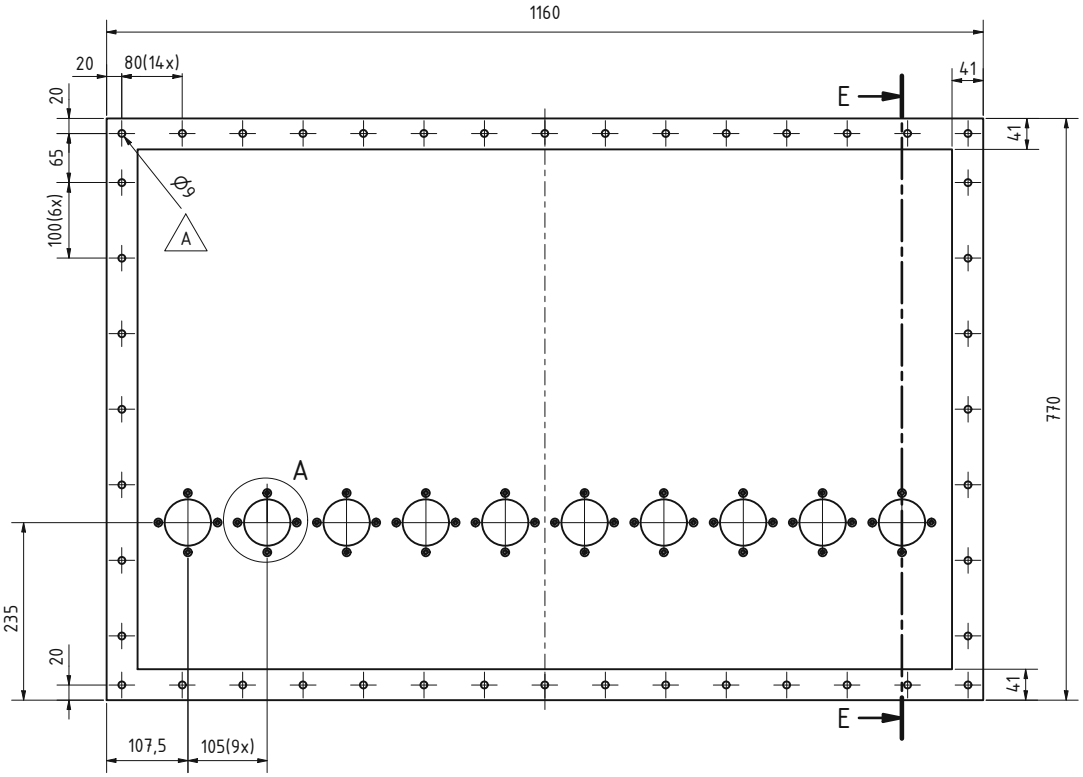

E-E (1 : 5)

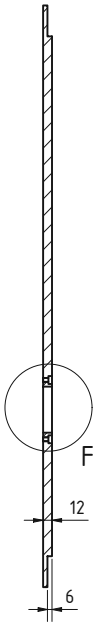

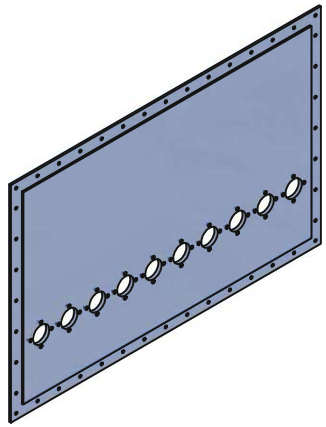

A (1/1)

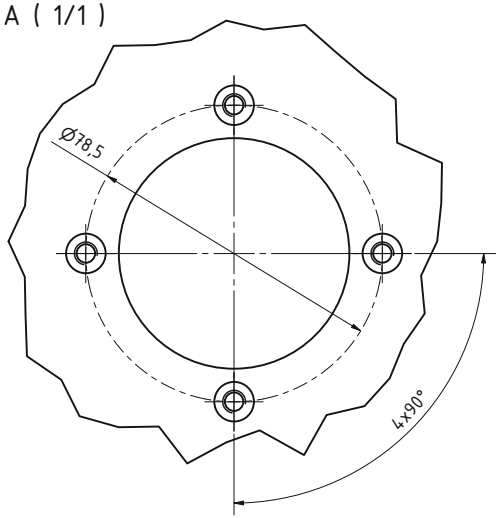

F (1:1)

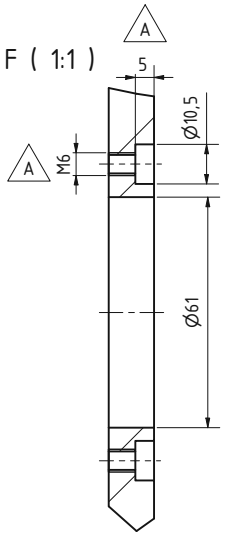

REVISIONSVERLAUF				
ZONE	REV.	BESCHREIBUNG	DATUM	GENEHMIGT
	A	Bohrung Gewind und Größ	05.07.2022	

unbemaßte Werkstückkanten DIN ISO 13715 | ISO 128 | Allgemeintoleranz ISO2768 mK | Maßstab: 1 : 5 | Masse: –

Oberflächenbehandlung: | Material: PMMA-Kunststoff

	Datum	Name
Gezeichn.	17.11.2021	Philipp Mayer
Kontroll.		
Norm		

Benennung: Plexiglaseinsatz

Projekt: Erosionsprüfstand

INSTITUT FÜR ENERGIETECHNIK UND THERMODYNAMIK
Institute for Energy Systems and Thermodynamics

Z-Nummer: ER001

Blatt 1/1 A2

Status | Änderungen | Datum | Name

A-A (1 : 1)

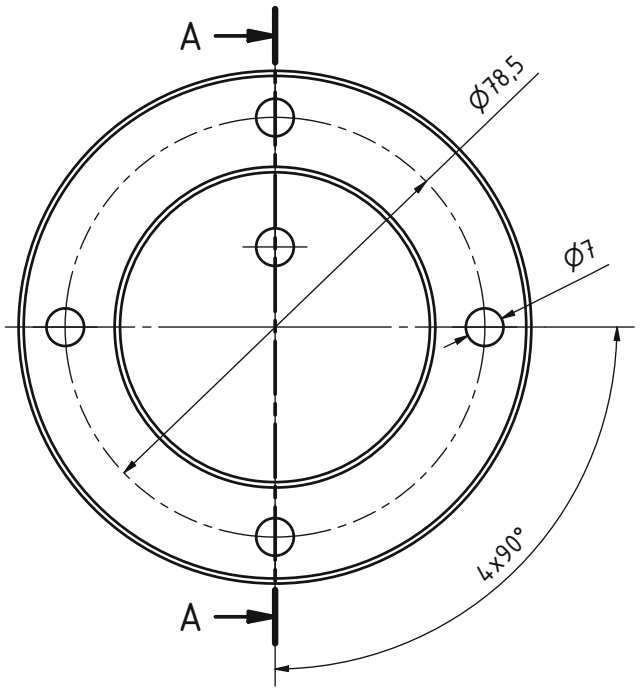

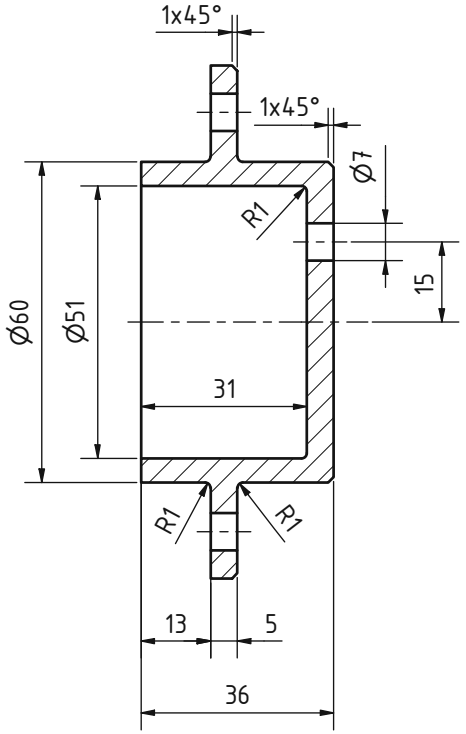

unbemaßte Werkstückkanten DIN ISO 13715	ISO 128	Allgemeintoleranz ISO2768 mK	Maßstab: 1 : 1
		Oberflächenbehandlung:	Masse: 0,160 kg
			Material: Aluminium
	Datum	Name	Benennung: Einbautenträger
Gezeichn	17.11.2021	Philipp Mayer	
Kontroll			Projekt: Erosionsprüfstand
Norm			
INSTITUT FÜR ENERGIETECHNIK UND THERMODYNAMIK Institute for Energy Systems and Thermodynamics			Z-Nummer: ER002
Status Änderungen Datum Name			Blatt 1/1 A3

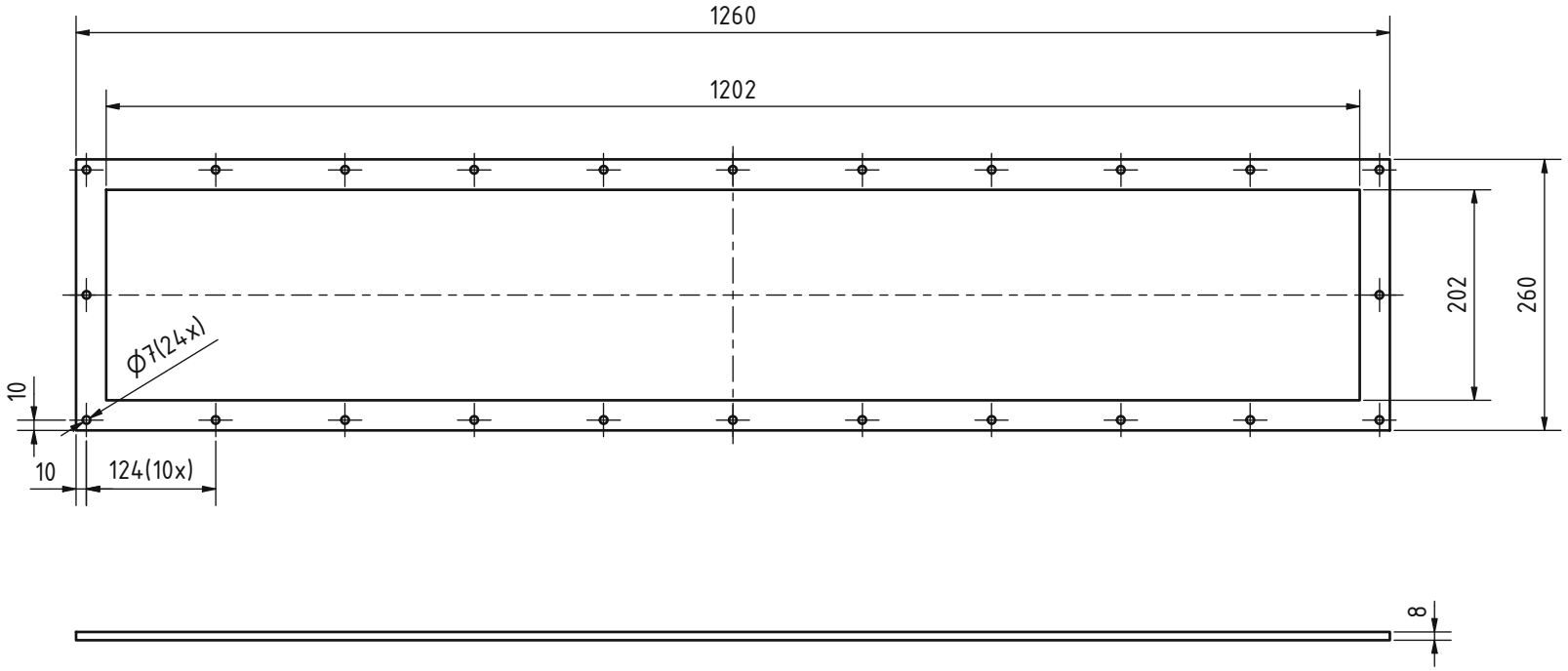

unbemaßte Werkstückkanten DIN ISO 13715	ISO 128	Allgemeintoleranz ISO2768 mK	Maßstab: 1 : 5
		Oberflächenbehandlung:	Masse: 5,267 kg
			Material: Stahl S235 JR
	Datum	Name	Benennung: Windkasten Flansch oben
Gezeichn	18.11.2021	Philipp Mayer	
Kontroll			
Norm			Projekt:
Status / Änderungen / Datum / Name	INSTITUT FÜR ENERGIETECHNIK UND THERMODYNAMIK Institute for Energy Systems and Thermodynamics	Z-Nummer: ER009	Blatt 1/1 A3

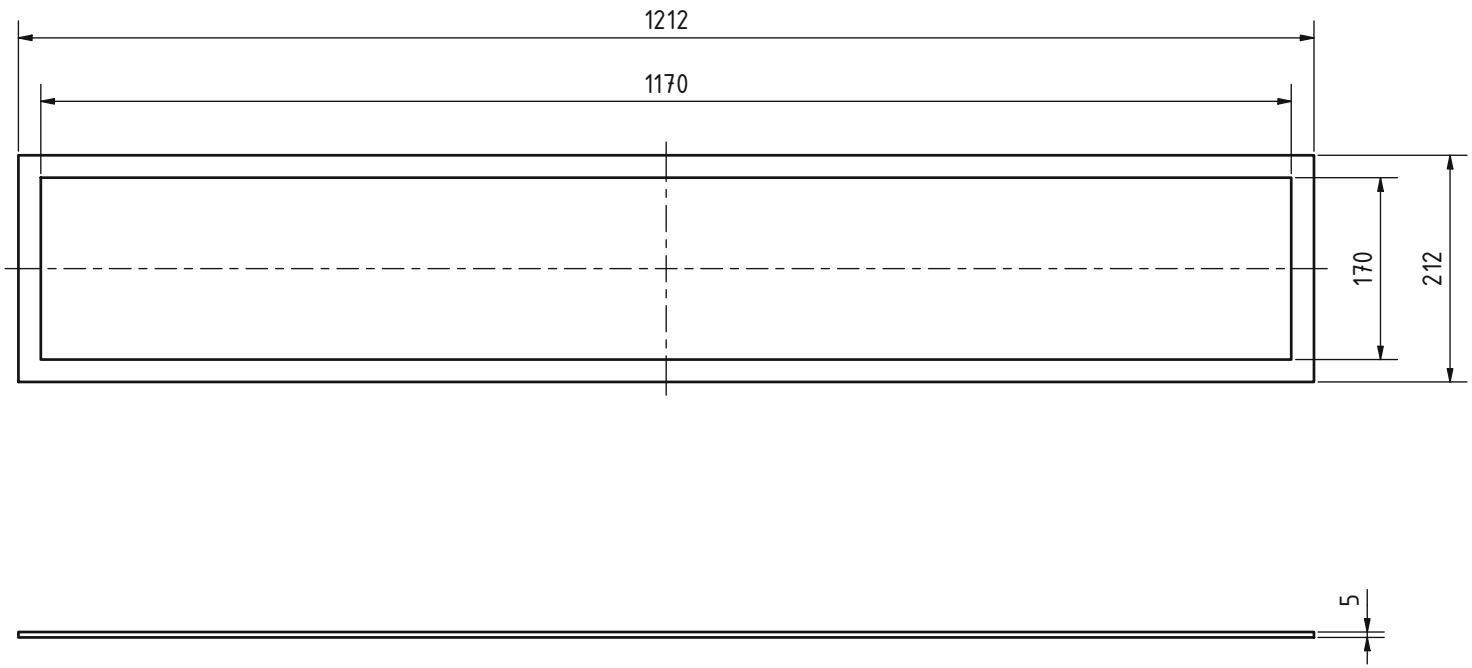

unbemaßte Werkstückkanten DIN ISO 13715	ISO 128	Allgemeintoleranz ISO2768 mK	Maßstab: 1 : 5
		Oberflächenbehandlung:	Masse: 2,278 kg
			Material: Stahl S235 JR
	Datum	Name	Benennung: Windkasten Auflage-Sinterplatte
Gezeichn	18.11.2021	Philipp Mayer	
Kontroll			Projekt: Erosionsprüfstand
Norm			
INSTITUT FÜR ENERGIETECHNIK UND THERMODYNAMIK			Z-Nummer: ER010
Status / Änderungen / Datum / Name			Blatt 1/1 A3

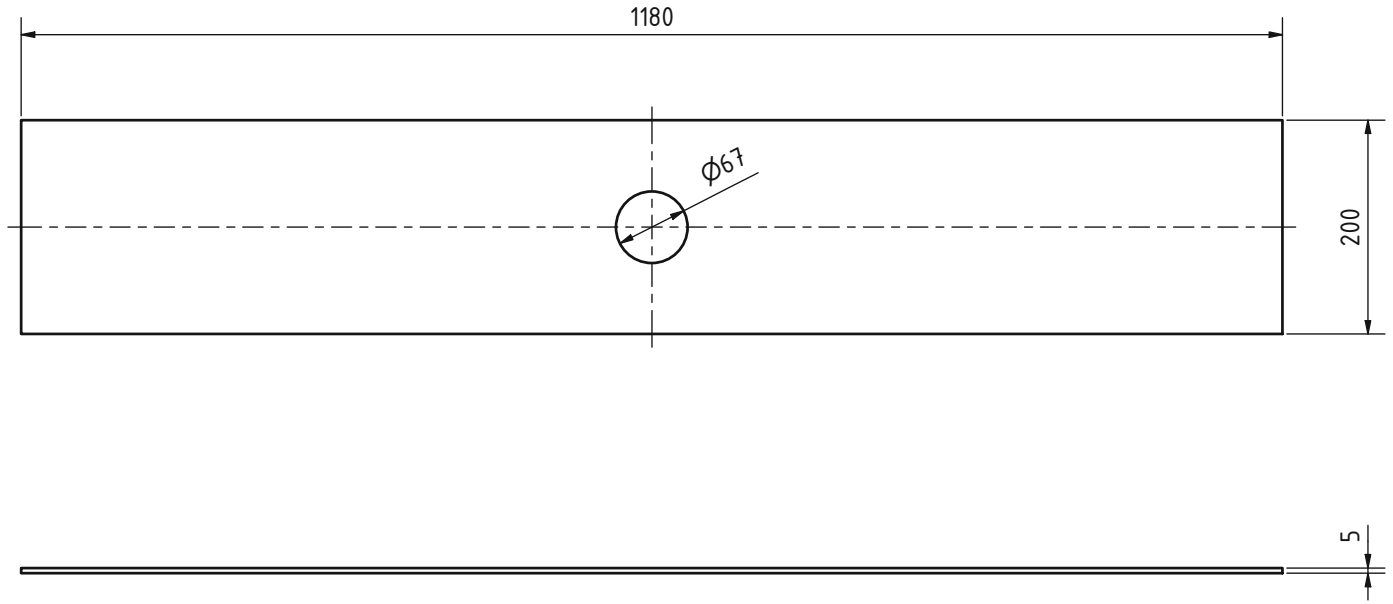

unbemaßte Werkstückkanten DIN ISO 13715	ISO 128	Allgemeintoleranz ISO2768 mK	Maßstab: 1 : 5
		Oberflächenbehandlung:	Masse: 9,125 kg
			Material: Stahl S235 JR

	Datum	Name
Gezeichn	18.11.2021	Philipp Mayer
Kontroll		
Norm		

Benennung:
Windkasten Vorderwand
Projekt: Erosionsprüfstand

INSTITUT FÜR ENERGIETECHNIK UND THERMODYNAMIK
Institute for Energy Systems and Thermodynamics

Z-Nummer: ER011

Blatt 1/1
A3

Status	Änderungen	Datum	Name

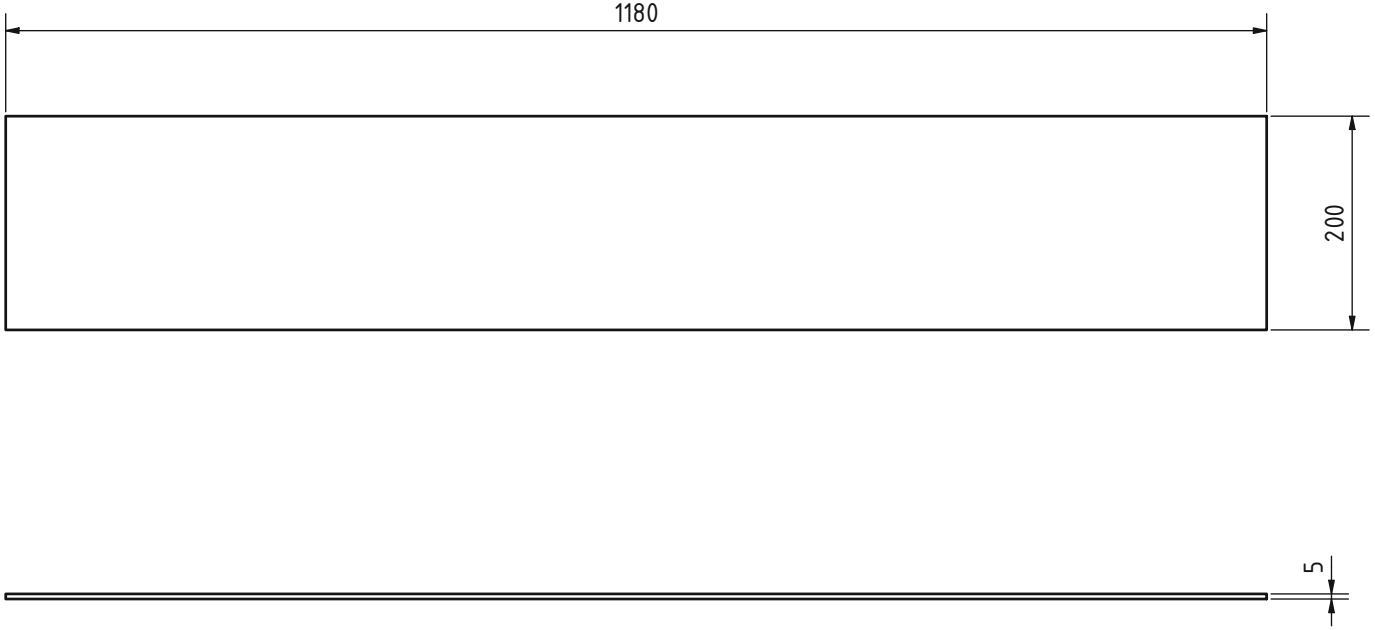

unbemaßte Werkstückkanten DIN ISO 13715	ISO 128	Allgemeintoleranz ISO2768 mK	Maßstab: 1 : 5
		Oberflächenbehandlung:	Masse: 9,263 kg
			Material: Stahl S235 JR
	Datum	Name	Benennung: Windkasten Rückwand
Gezeichn	18.11.2021	Philipp Mayer	
Kontroll			Projekt: Erosionsprüfstand
Norm			
INSTITUT FÜR ENERGIETECHNIK UND THERMODYNAMIK Institute for Energy Systems and Thermodynamics			Z-Nummer: ER012
			Blatt: 1/1 A3

Status	Änderungen	Datum	Name

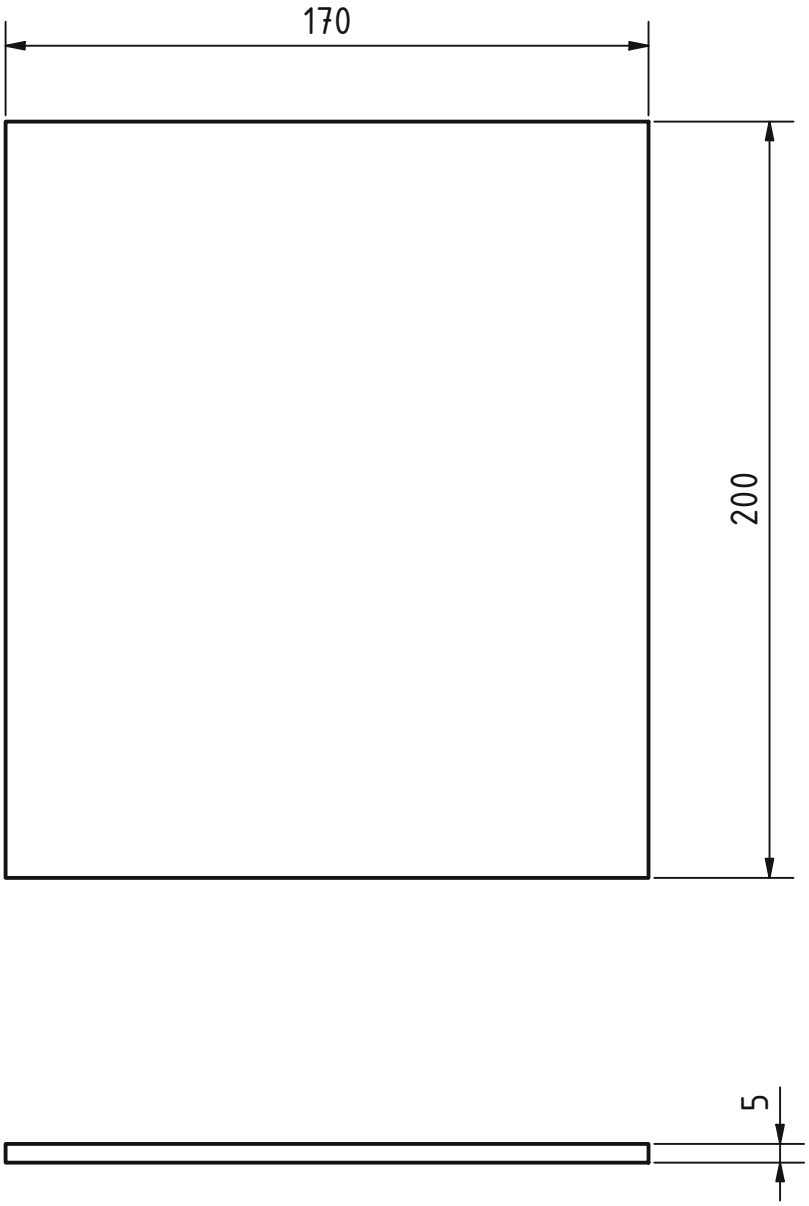

unbemaßte Werkstückkanten DIN ISO 13715 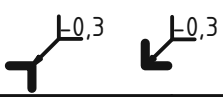	ISO 128 	Allgemeintoleranz ISO2768 mK	Maßstab: 1 : 2
			Oberflächenbehandlung:
			Masse: 1,335 kg
			Material: Stahl S235 JR

	Datum	Name
Gezeichn	18.11.2021	Philipp Mayer
Kontroll		
Norm		

INSTITUT FÜR ENERGIETECHNIK UND THERMODYNAMIK
Institute for Energy Systems and Thermodynamics

Benennung: Windkasten Seitenwand links

Projekt: Erosionsprüfstand

Z-Nummer: ER013

Blatt 1/1

A4

Status	Änderungen	Datum	Name

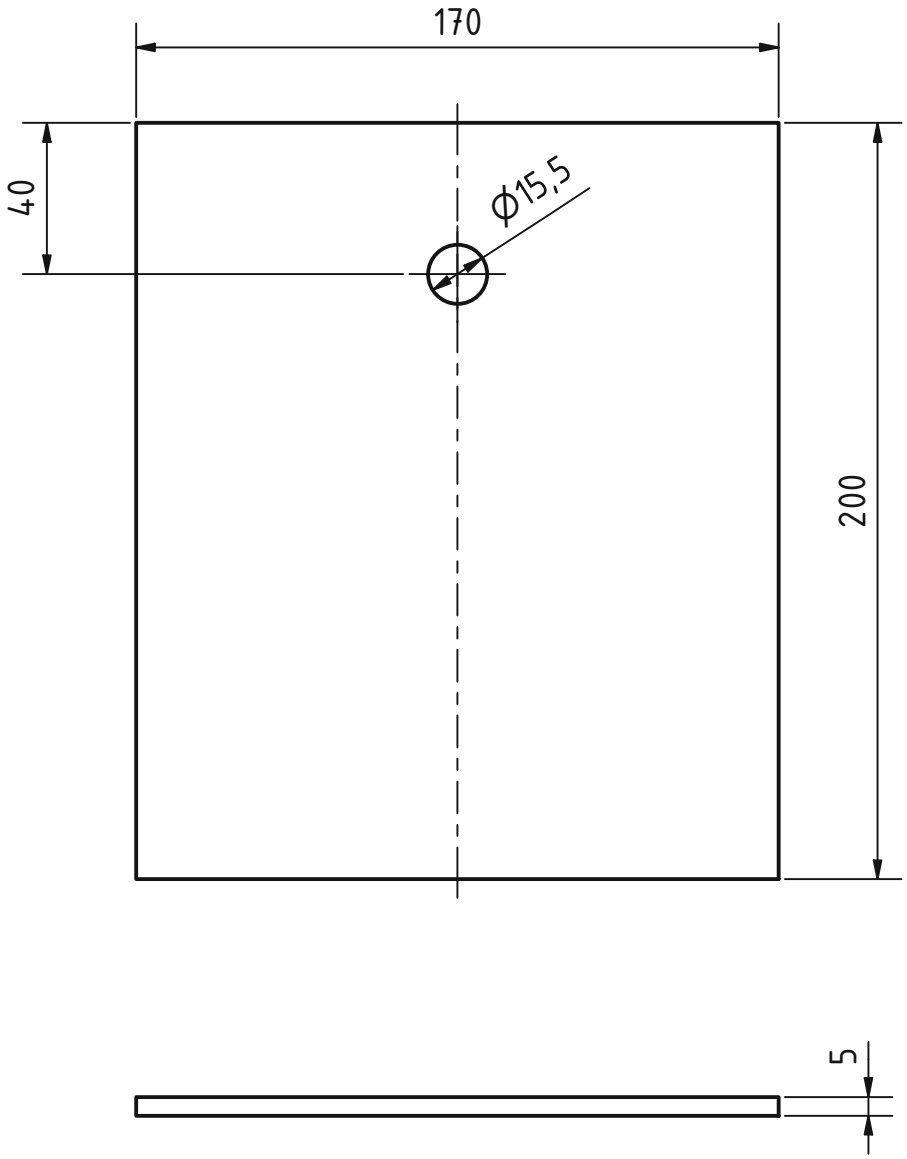

unbemaßte Werkstückkanten DIN ISO 13715 ⌊0,3 ⌊0,3	ISO 128	Allgemeintoleranz ISO2768 mK	Maßstab: 1 : 2
			Masse: 1,327 kg
			Oberflächenbehandlung:
			Material: Stahl S235 JR

	Datum	Name
Gezeichn	18.11.2021	Philipp Mayer
Kontroll		
Norm		

Benennung:
Windkasten Seitenwand rechts
Projekt: Erosionsprüfstand

INSTITUT FÜR ENERGIETECHNIK UND THERMODYNAMIK
Institute for Energy Systems and Thermodynamics

Z-Nummer: ER014

Blatt 1/1
A4

Status	Änderungen	Datum	Name

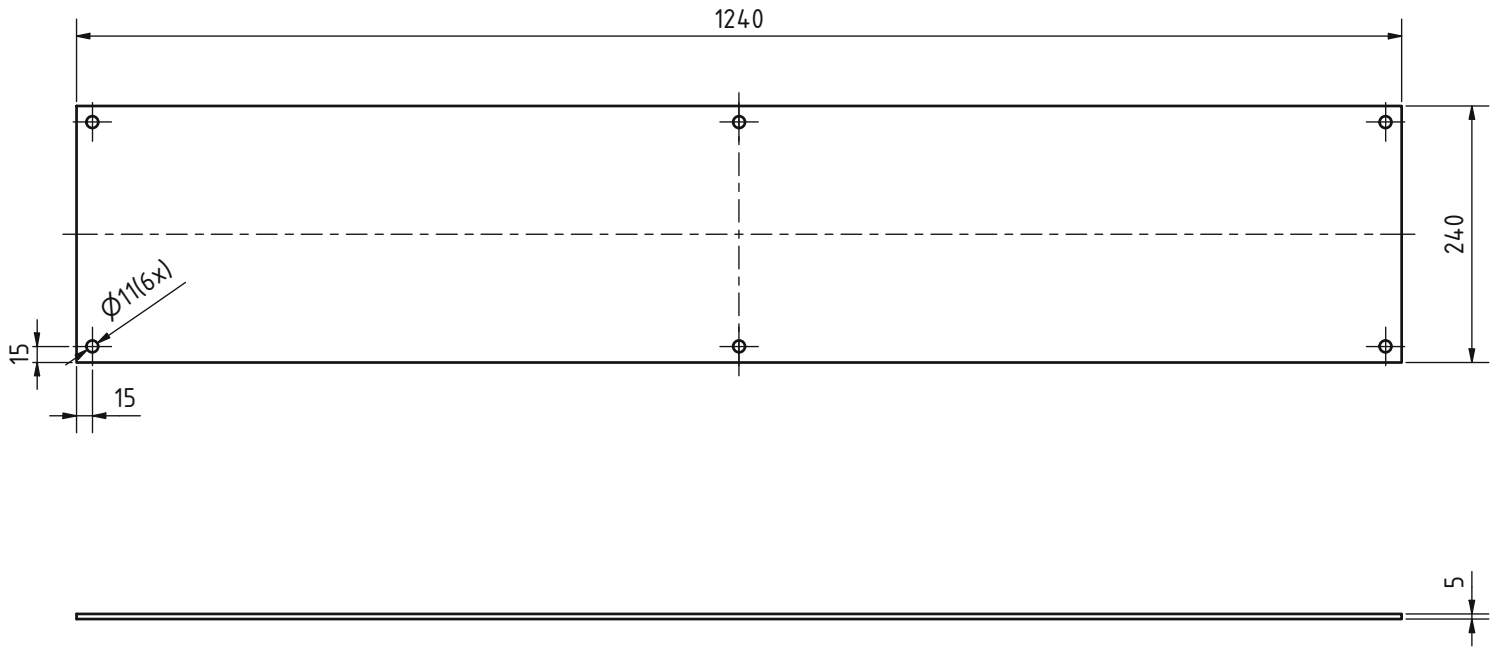

unbemaßte Werkstückkanten DIN ISO 13715	ISO 128	Allgemeintoleranz ISO2768 mK	Maßstab: 1 : 5
		Oberflächenbehandlung:	Masse: 11,658 kg
			Material: Stahl S235 JR
	Datum	Name	Benennung: Windkasten Bodenplatte
Gezeichn	18.11.2021	Philipp Mayer	
Kontroll			
Norm			Projekt: Erosionsprüfstand
INSTITUT FÜR ENERGIETECHNIK UND THERMODYNAMIK Institute for Energy Systems and Thermodynamics			Z-Nummer: ER015
			Blatt: 1/1 A3
Status	Änderungen	Datum	Name

A-A (1 : 5)

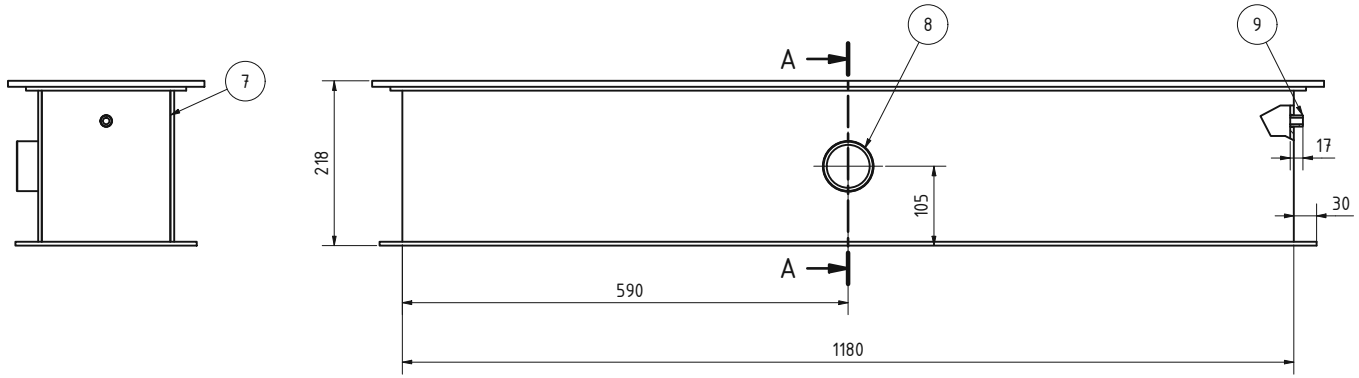

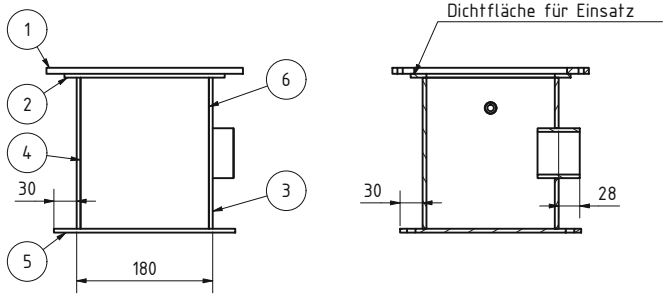

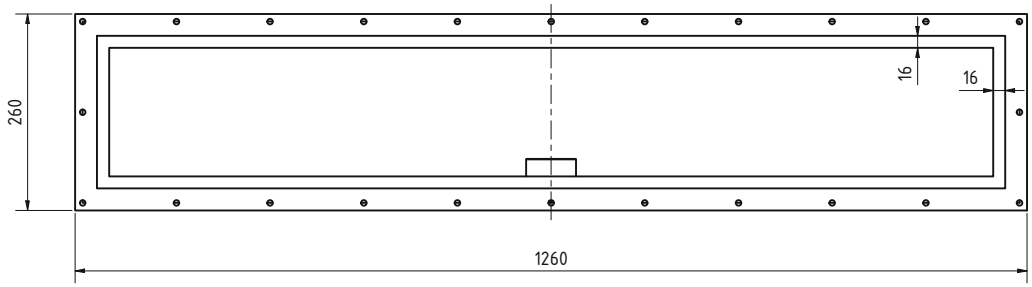

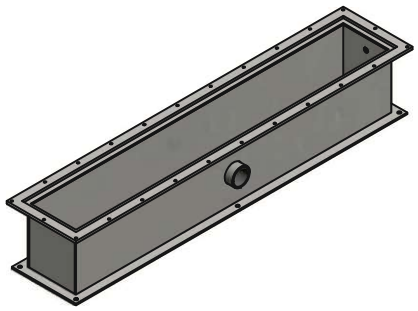

Fertigungshinweis:
Bauteile mit Kehlnähten gasdicht verschweißen

STÜCKLISTE

OBJEKT	ANZAHL	BAUTEILNUMMER	Z-NUMMER	BESCHREIBUNG
1	1	Windkasten Flansch oben	ER009	
2	1	Windkasten Auflage Sinterplatte	ER010	
3	1	Windkasten Vorderwand	ER011	
4	1	Windkasten Rückwand	ER012	
5	1	Windkasten Bodenplatte	ER015	
6	1	Windkasten Seitenwand links	ER013	
7	1	Windkasten Seitenwand rechts	ER014	
8	1	Gewindemuffe Rp2	MUR 20 AS ST	Landefeld, DIN EN 10241
9	1	Gewindemuffe Rp1/8	MUR 18 AS ST	Landefeld, DIN EN 10241

unbemaßte Werkstückkanten DIN ISO 13715 | ISO 128 | Allgemeintoleranz ISO2768 mK | Maßstab: 1 : 5 | Masse: 40,307 kg

Oberflächenbehandlung: | Material:

	Datum	Name
Gezeichn	18.11.2021	Philipp Mayer
Kontroll		
Norm		

Benennung: Windkasten Schweißbaugruppe
Projekt: Erosionsprüfstand

INSTITUT FÜR ENERGIETECHNIK UND THERMODYNAMIK
Institute for Energy Systems and Thermodynamics

Z-Nummer: ER016

Blatt 1/1 A2

Status | Änderungen | Datum | Name

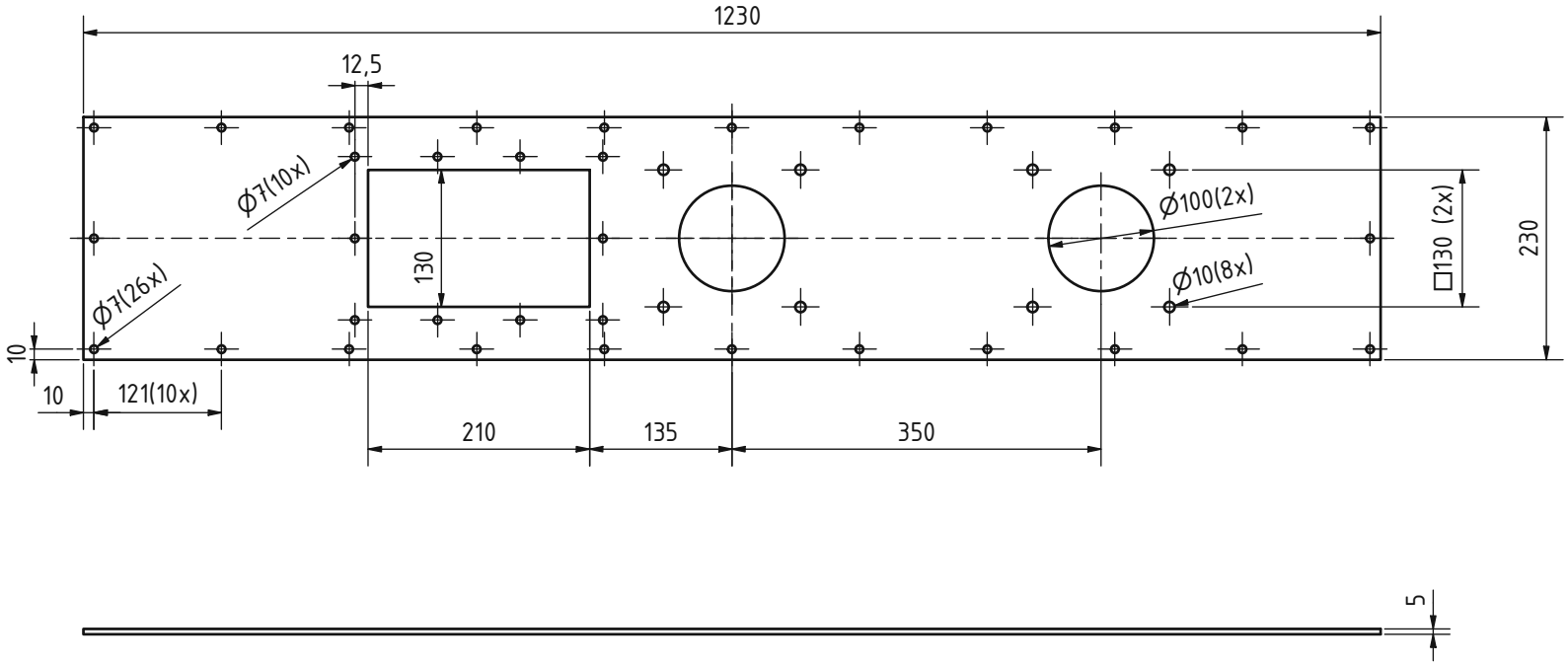

unbemaßte Werkstückkanten DIN ISO 13715	ISO 128	Allgemeintoleranz ISO2768 mK	Maßstab: 1 : 5
		Oberflächenbehandlung:	Masse: 9,340 kg
			Material: Stahl S235 JR
	Datum	Name	Benennung: Wirbelschichtkammer Deckel oben
	Gezeichn 18.11.2021	Philipp Mayer	Projekt: Erosionsprüfstand
	Kontroll		
	Norm		
Status Änderungen Datum Name	INSTITUT FÜR ENERGIETECHNIK UND THERMODYNAMIK Institute for Energy Systems and Thermodynamics		Z-Nummer: ER017
			Blatt 1/1 A3

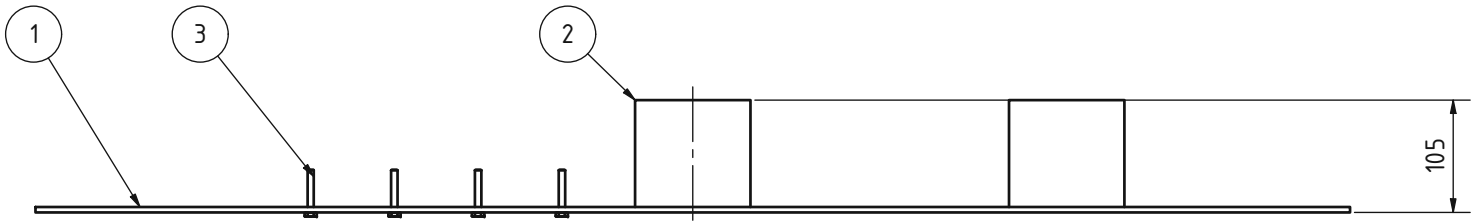

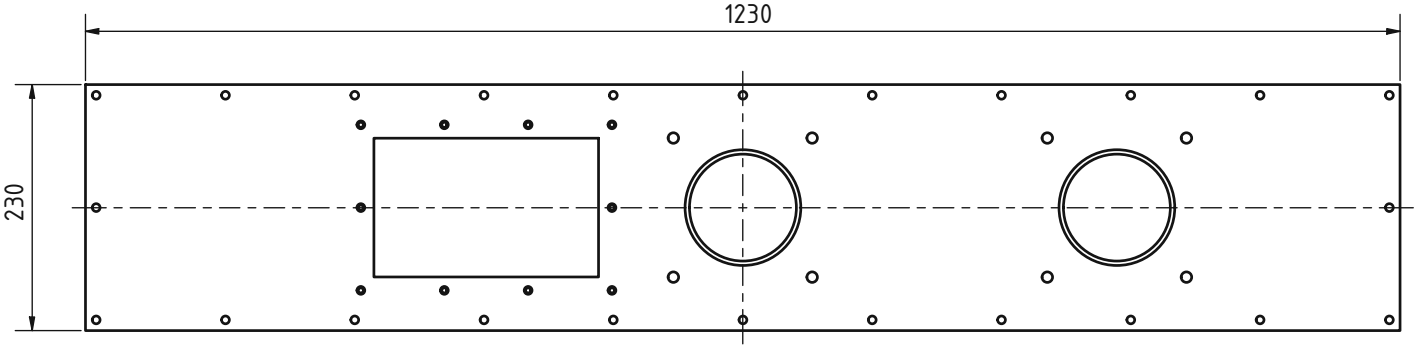

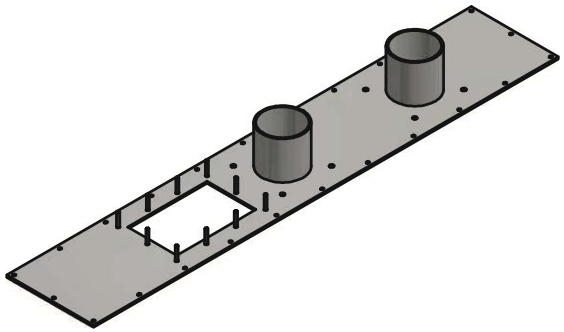

Fertigungshinweis:
Bauteile mit Kehlnähten gasdicht verschweißen
Schraubenkopf an Deckelunterseite anschweißen

STÜCKLISTE

OBJEKT	ANZAHL	BAUTEILNUMMER	Z-NUMMER	BESCHREIBUNG
1	1	Wirbelschichtkammer Deckel oben	ER017	
2	2	Rohr – 108 × 4 – EN 10216-2 – P235GH		Länge 100mm
3	10	BS EN ISO 4017 - M6 x 40		Sechskantschrauben - Produktklasse A und B

unbemaßte Werkstückkanten DIN ISO 13715 — 0,3 — 0,3

ISO 128

Allgemeintoleranz: ISO2768 mK

Maßstab: 1 : 5

Masse: -

Oberflächenbehandlung:

Material:

	Datum	Name
Gezeichn	18.11.2021	Philipp Mayer
Kontroll		
Norm		

Benennung:
Wirbelschichtkammer Deckel Schweißbaugruppe
Projekt: Erosionsprüfstand

INSTITUT FÜR ENERGIETECHNIK UND THERMODYNAMIK
Institute for Energy Systems and Thermodynamics

Z-Nummer: ER018

Blatt: 1/1
A3

Status	Änderungen	Datum	Name

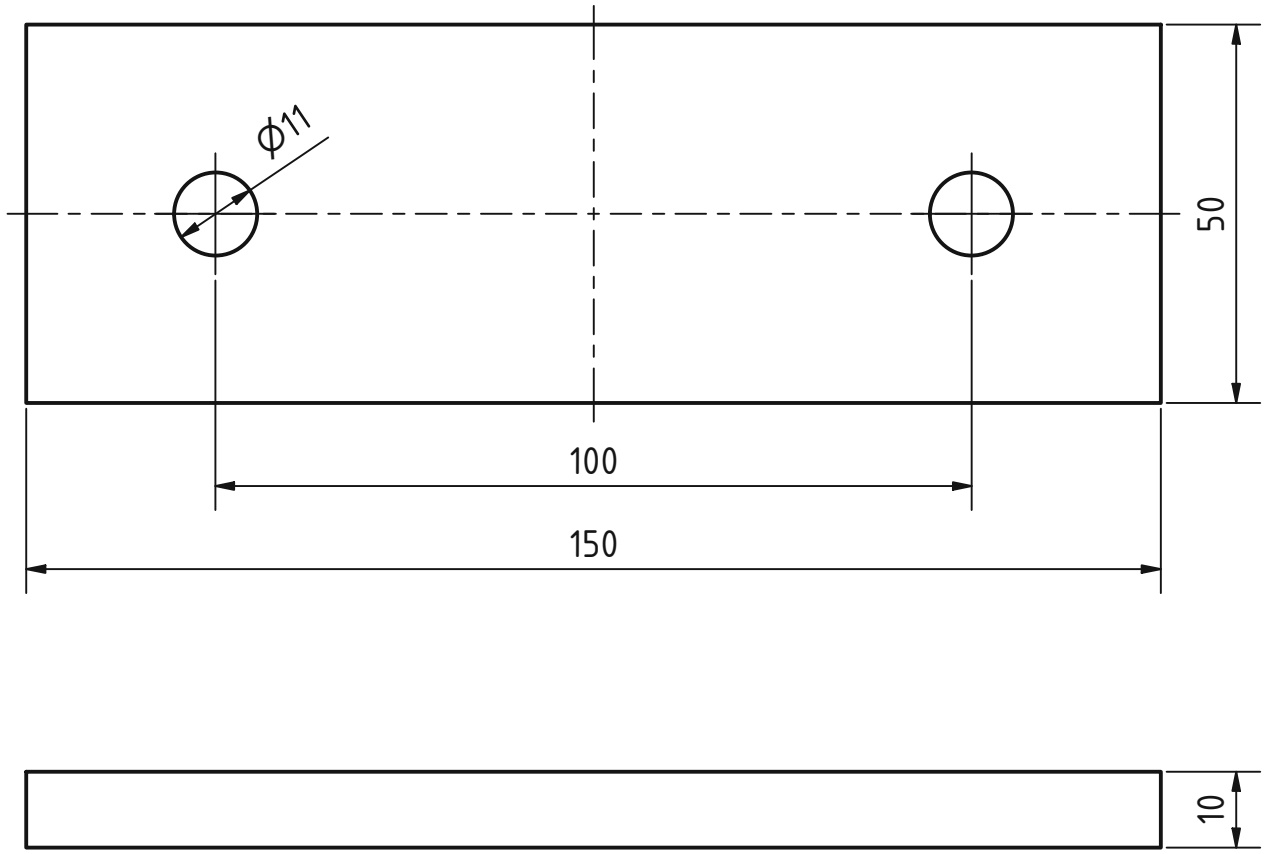

unbemaßte Werkstückkanten DIN ISO 13715	ISO 128	Allgemeintoleranz ISO2768 mK	Maßstab: 1 : 1
			Masse: 0,574 kg
			Oberflächenbehandlung:
			Material: Stahl S235 JR

	Datum	Name
Gezeichn	18.11.2021	Philipp Mayer
Kontroll		
Norm		

INSTITUT FÜR ENERGIETECHNIK UND THERMODYNAMIK
Institute for Energy Systems and Thermodynamics

Benennung: Aufstandsfuß Fußplatte

Projekt: Erosionsprüfstand

Z-Nummer: ER019

Blatt 1/1

A4

Status	Änderungen	Datum	Name

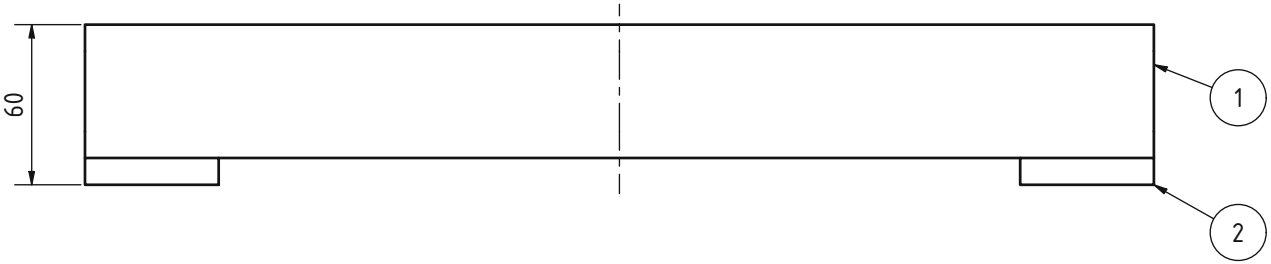

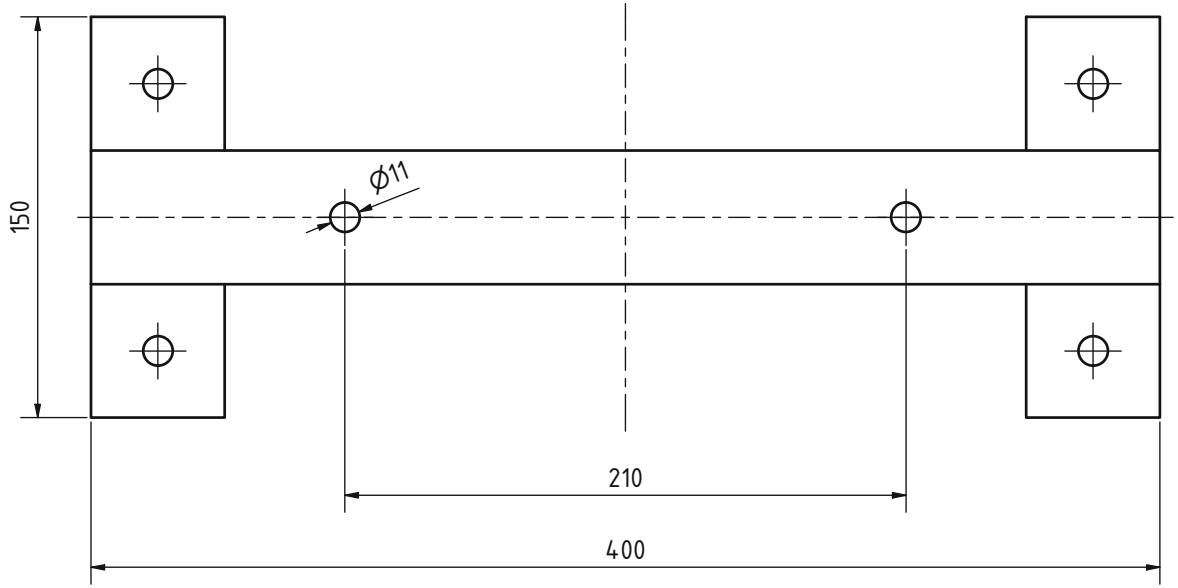

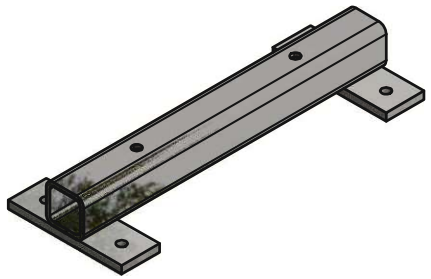

STÜCKLISTE				
OBJEKT	ANZAHL	BAUTEILNUMMER	Z-NUMMER	BESCHREIBUNG
1	400,000 mm	BS EN 10219-2 - 50 x 50 x 5		
2	2	Aufstandsfuß Fußplatte	ER019	

unbemaßte Werkstückkanten DIN ISO 13715 | ISO 128 | Allgemeintoleranz ISO2768 mK | Maßstab: 1 : 2 | Masse: 3,757 kg

Oberflächenbehandlung: | Material:

	Datum	Name
Gezeichn	18.11.2021	Philipp Mayer
Kontroll		
Norm		

Benennung: Aufstandsfuß Schweißbaugruppe

Projekt:

INSTITUT FÜR ENERGIETECHNIK UND THERMODYNAMIK
Institute for Energy Systems and Thermodynamics

Z-Nummer: ER020

Blatt 1/1 A3

Status	Änderungen	Datum	Name

Fertigungshinweis:
Bauteile mit Kehlnähten verschweißen

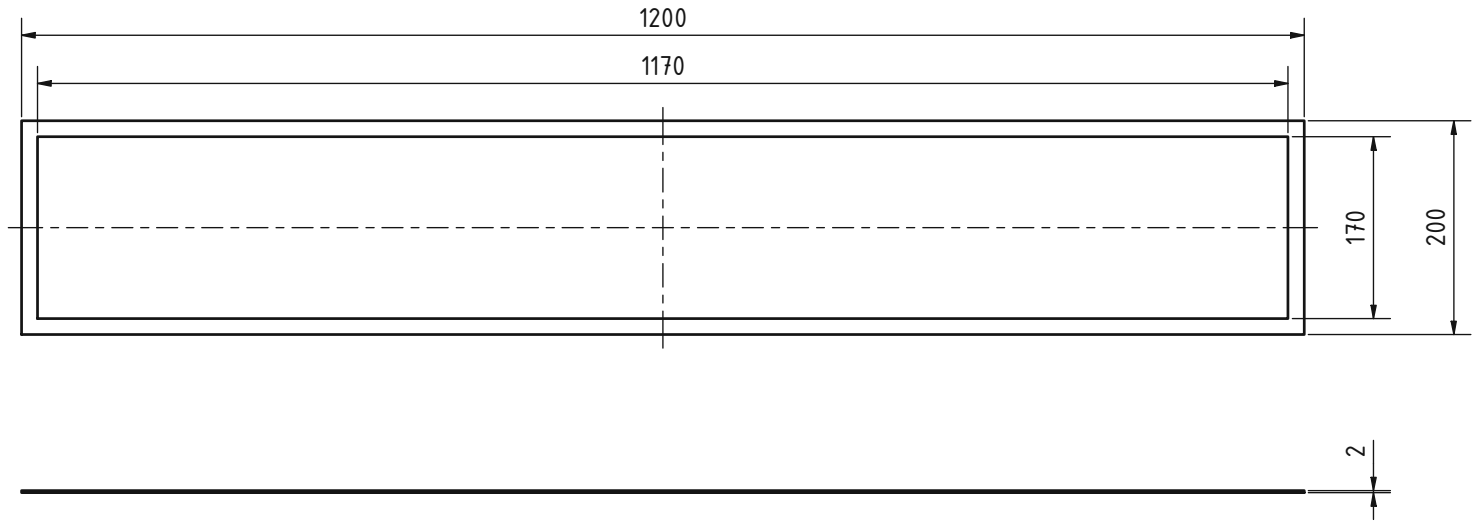

unbemaßte Werkstückkanten DIN ISO 13715	ISO 128	Allgemeintoleranz ISO2768 mK	Maßstab: 1 : 5
		Oberflächenbehandlung:	Masse: 0,099 kg
			Material: Klingersil C4400
	Datum	Name	Benennung: Dichtung Sinterplatte unten
Gezeichn	18.11.2021	Philipp Mayer	
Kontroll			
Norm			Projekt: Erosionsprüfstand
INSTITUT FÜR ENERGIETECHNIK UND THERMODYNAMIK			Z-Nummer: ER021
			Blatt 1/1 A3

Status	Änderungen	Datum	Name

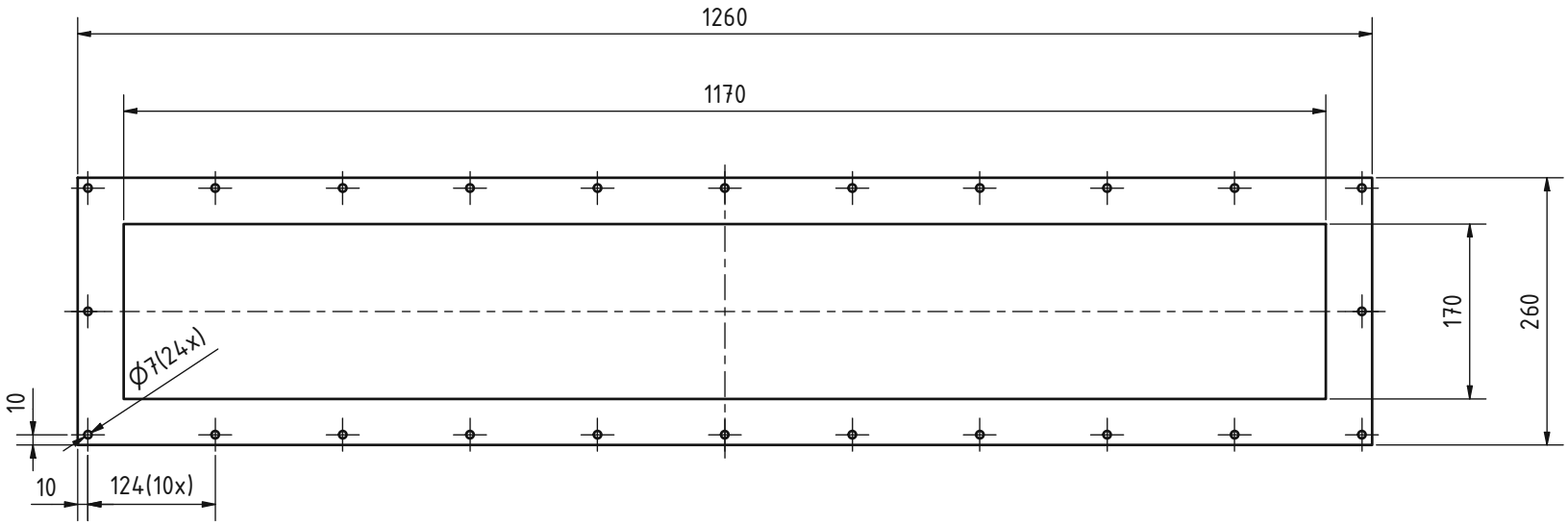

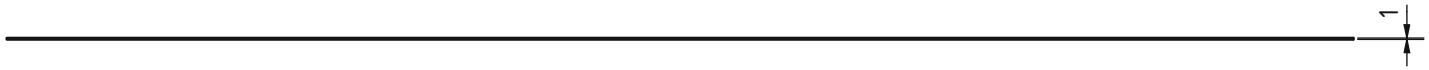

unbemaßte Werkstückkanten DIN ISO 13715	ISO 128	Allgemeintoleranz ISO2768 mK	Maßstab: 1 : 5
		Oberflächenbehandlung:	Masse: 0,153 kg
			Material: Klingersil C4400
	Datum	Name	Benennung: Dichtung Sinterplatte oben
	Gezeichn 18.11.2021	Philipp Mayer	
	Kontroll		Projekt: Erosionsprüfstand
	Norm		
Status Änderungen Datum Name	INSTITUT FÜR ENERGIETECHNIK UND THERMODYNAMIK Institute for Energy Systems and Thermodynamics		Z-Nummer: ER022
			Blatt 1/1 A3

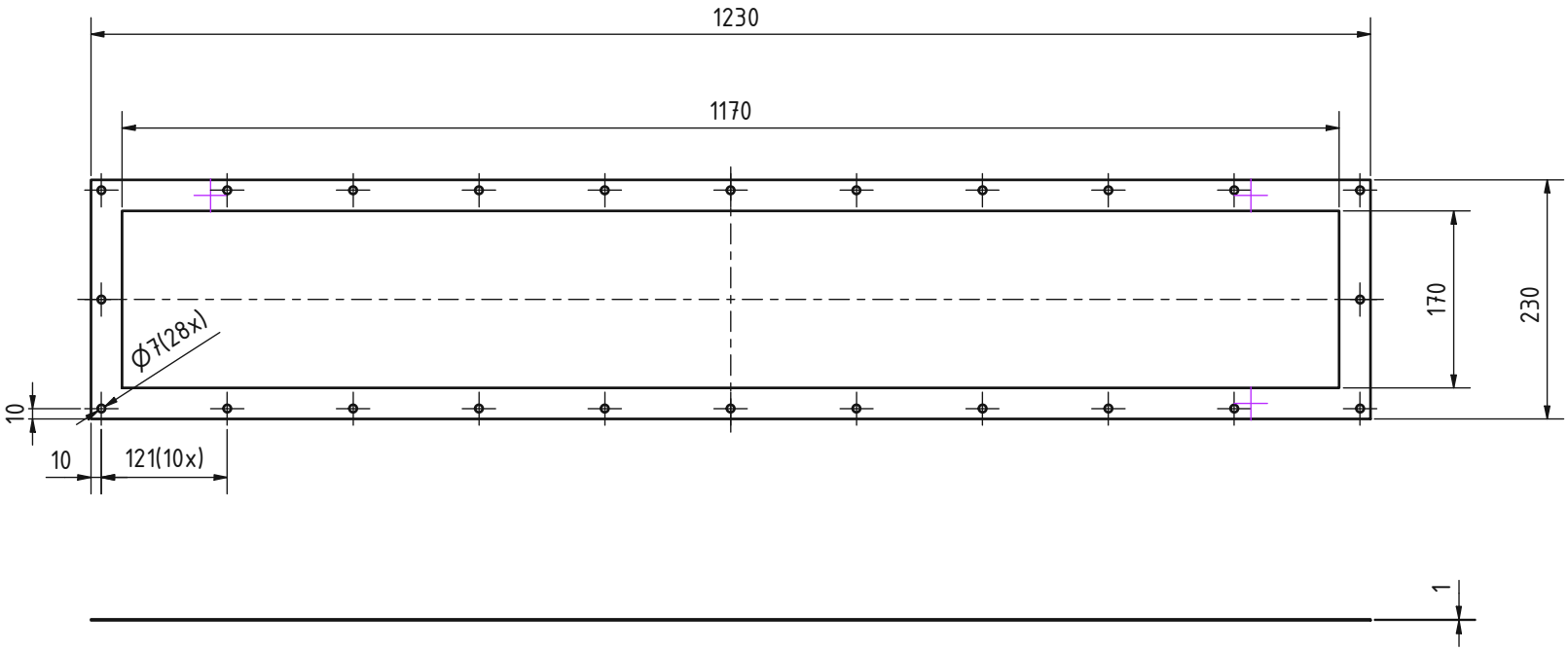

unbemaßte Werkstückkanten DIN ISO 13715	ISO 128	Allgemeintoleranz ISO2768 mK	Maßstab: 1 : 5
		Oberflächenbehandlung:	Masse: 0,100 kg
			Material: Klingersil C4400

	Datum	Name
Gezeichn	18.11.2021	Philipp Mayer
Kontroll		
Norm		

Benennung:
Dichtung Wirbelschichtkammer Flansch oben
Projekt: Erosionsprüfstand

INSTITUT FÜR ENERGIETECHNIK UND THERMODYNAMIK
Institute for Energy Systems and Thermodynamics

Z-Nummer: ER023

Blatt 1/1
A3

Status	Änderungen	Datum	Name

D-D (1 : 1)

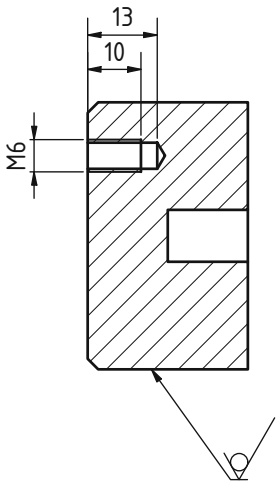

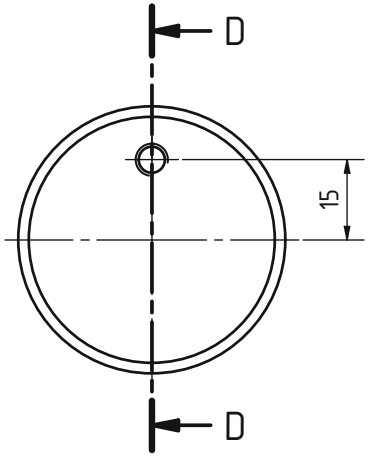

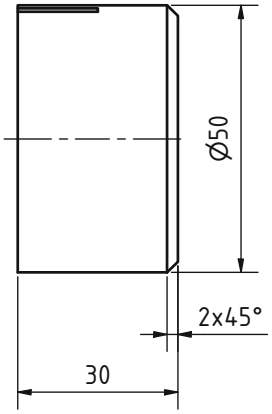

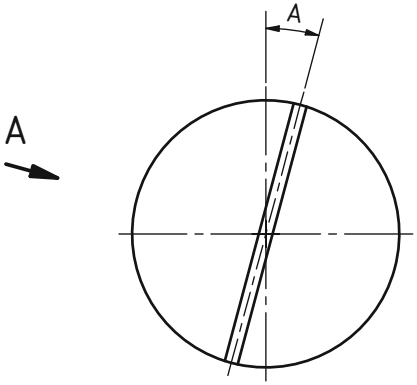

A (1 : 1)

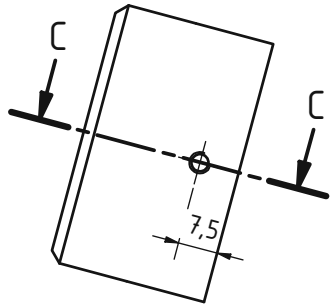

C-C (1 : 1)

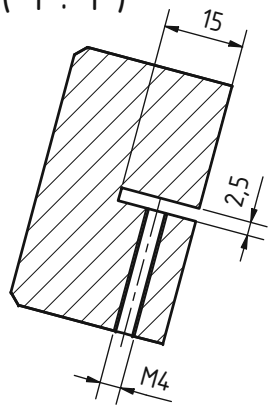

Bauteilvarianten	
Winkel A	Stückzahl
0	2
7	1
-7	1
15	1
-15	1
30	1
-30	1
45	1
-45	1
60	1
-60	1
75	1
-75	1
90	2

Ra 6,3 ( )

unbemaßte Werkstückkanten DIN ISO 13715 0,3 0,3

ISO 128

Allgemeintoleranz ISO2768 mK

Maßstab: 1 : 1

Masse: 0,152 kg

Oberflächenbehandlung:

Material: Aluminium

	Datum	Name
Gezeichn	18.11.2021	Philipp Mayer
Kontroll		
Norm		

Benennung: Einsatzträger Blech

Projekt: Erosionsprüfstand

INSTITUT FÜR ENERGIETECHNIK UND THERMODYNAMIK
Institute for Energy Systems and Thermodynamics

Z-Nummer: ER024

Blatt 1/1 A3

Status	Änderungen	Datum	Name

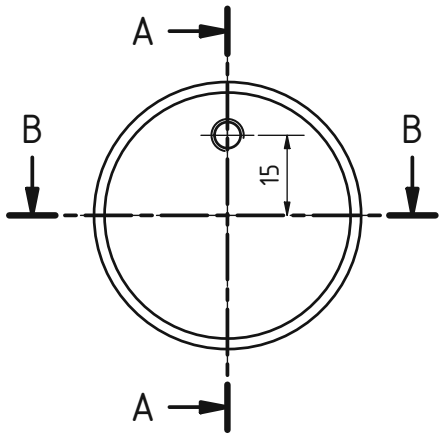

A-A (1 : 1)

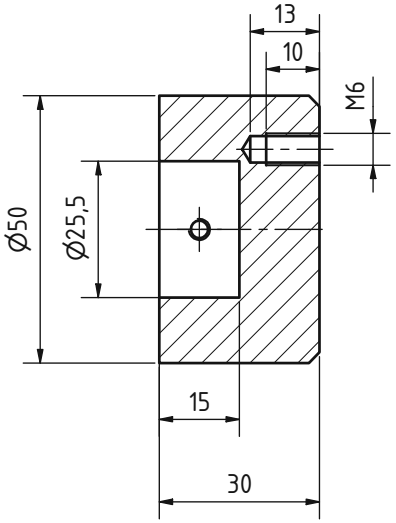

B-B (1 : 1)

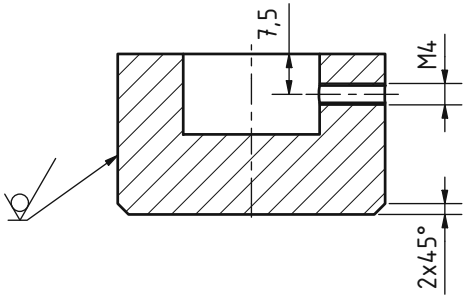

Ra 6,3 ( )

unbemaßte Werkstückkanten DIN ISO 13715 ⌊0,3 ⌊0,3	ISO 128	Allgemeintoleranz ISO2768 mK	Maßstab: 1 : 1 / Masse: 0,137 kg
		Oberflächenbehandlung:	Material: Aluminium
	Datum / Name		Benennung: Einsatzträger Rohr
	Gezeichn 19.11.2021 Philipp Mayer		
	Kontroll		Projekt: Erosionsprüfstand
	Norm		
Status / Änderungen / Datum / Name	INSTITUT FÜR ENERGIETECHNIK UND THERMODYNAMIK, Institute for Energy Systems and Thermodynamics		Z-Nummer: ER025 / Blatt 1/1 / A3

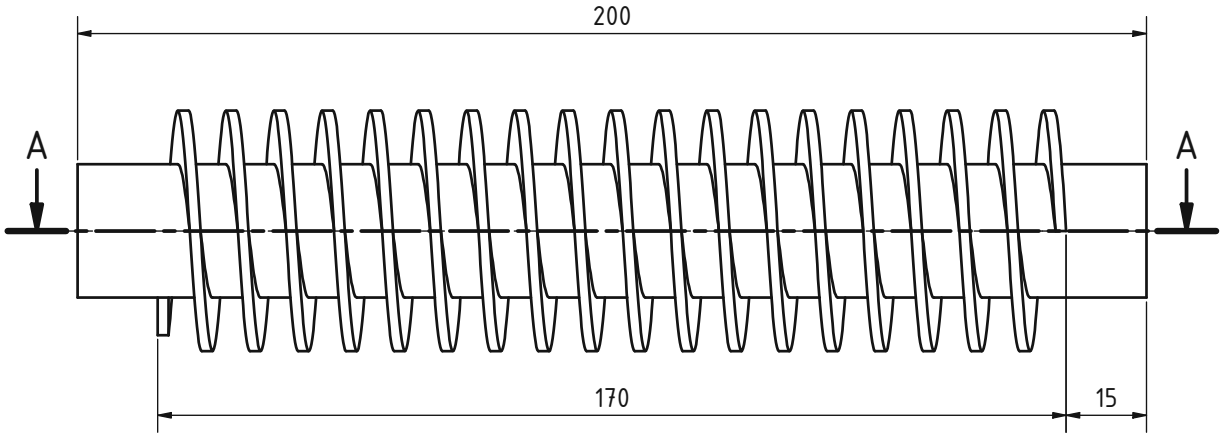

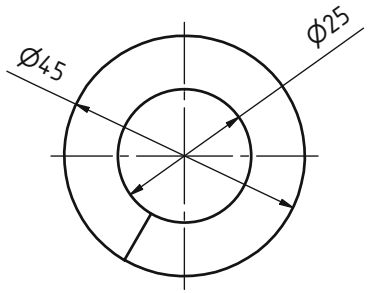

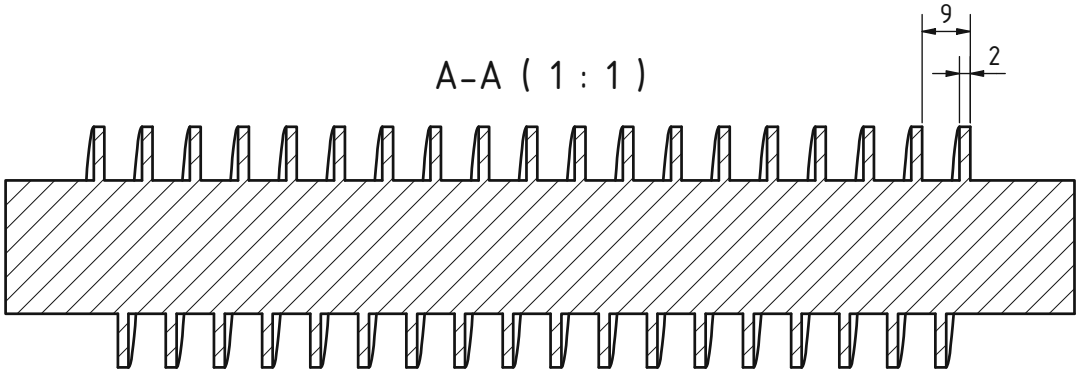

Fertigungshinweis Spirale:
Steigung: 9mm
Stärke: 2mm
Länge: 170mm
Umschlingungen: 18,6666
Umschlingungswinkel gesamt: 6720°

unbemaßte Werkstückkanten DIN ISO 13715	ISO 128	Allgemeintoleranz ISO2768 mK	Maßstab: 1 : 1
		Oberflächenbehandlung:	Masse: 1,093 kg
			Material: Stahl
	Datum	Name	Benennung: Erosionskörper Spiralrohr
	Gezeichn 19.11.2021	Philipp Mayer	
	Kontroll		Projekt: Erosionsprüfstand
	Norm		
Status Änderungen Datum Name	INSTITUT FÜR ENERGIETECHNIK UND THERMODYNAMIK Institute for Energy Systems and Thermodynamics		Z-Nummer: ER026
			Blatt 1/1 A3

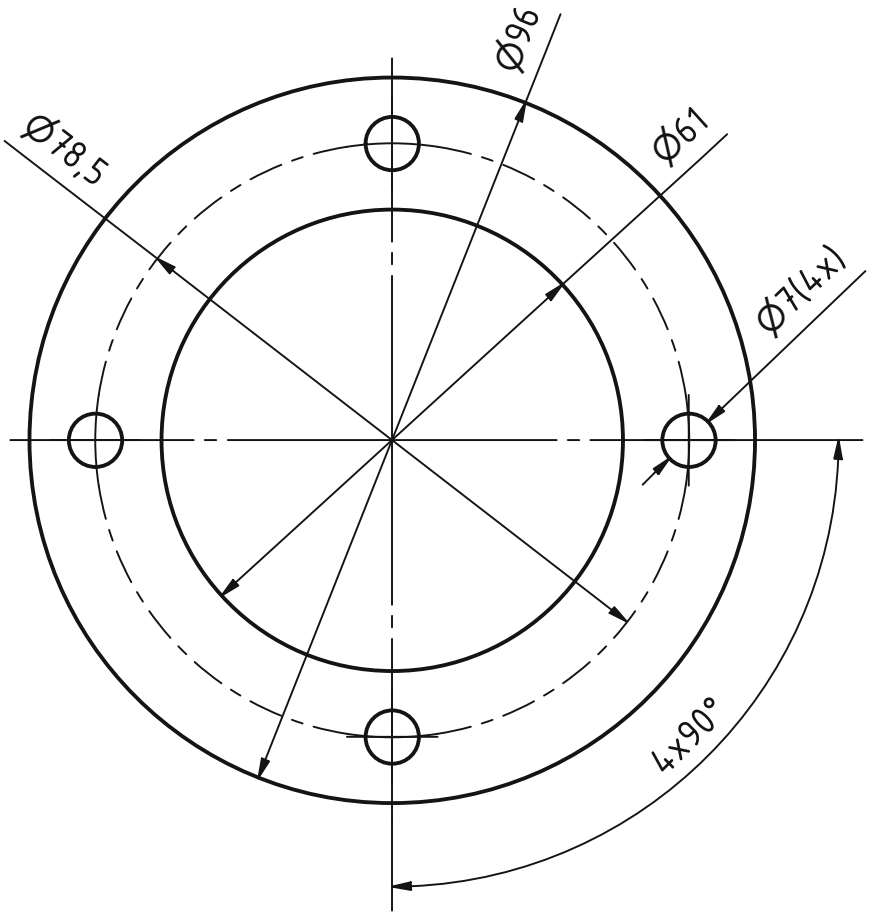

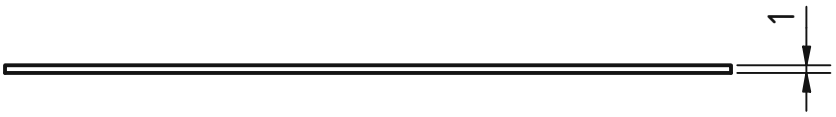

Fertigungshinweis:
Als Rohteil kann die Flachdichtung EN 1514-1 (Teile-Nr.: 261685) von der Firma Haberkorn verwendet werden

unbemaßte Werkstückkanten DIN ISO 13715 ⌐0,3 ⌐0,3	ISO 128	Allgemeintoleranz ISO2768 mK	Maßstab: 1 : 1 / Masse: -
			Oberflächenbehandlung: / Material: Klingersil C4400
	Datum / Name		Benennung: Dichtung Einbautenträger
	Gezeichn 19.11.2021	Philipp Mayer	
	Kontroll		Projekt: Erosionsprüfstand
	Norm		
	INSTITUT FÜR ENERGIETECHNIK UND THERMODYNAMIK Institute for Energy Systems and Thermodynamics		Z-Nummer: ER027 / Blatt 1/1 / A4
Status / Änderungen / Datum / Name			

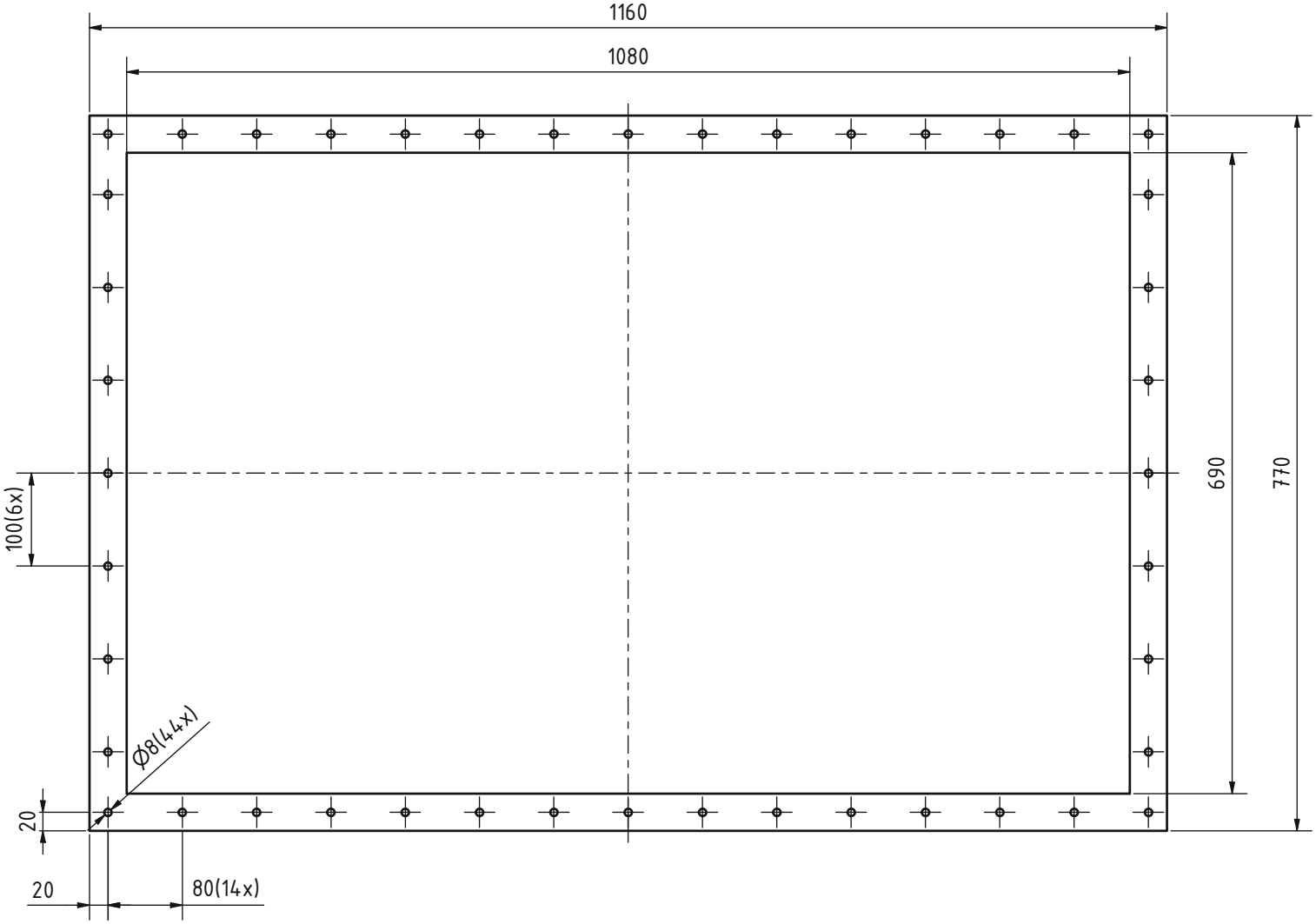

unbemaßte Werkstückkanten DIN ISO 13715 | ISO 128 | Allgemeintoleranz ISO2768 mK

	Datum	Name
Gezeichn	19.11.2021	Philipp Mayer
Kontroll		
Norm		

Maßstab: 1 : 5 | Masse: 0,175 kg

Oberflächenbehandlung: | Material: Klingersil C4400

Benennung: Dichtung Plexiglaseinsatz

Projekt: Erosionsprüfstand

INSTITUT FÜR ENERGIETECHNIK UND THERMODYNAMIK
Institute for Energy Systems and Thermodynamics

Z-Nummer: ER028

Blatt 1/1 A3

Status	Änderungen	Datum	Name

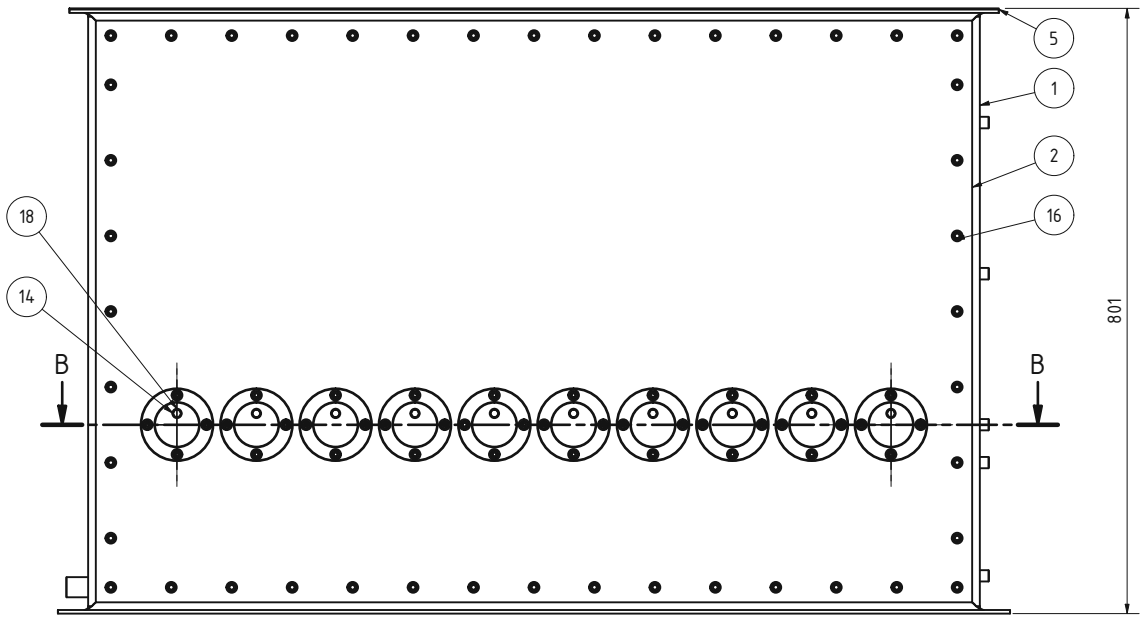

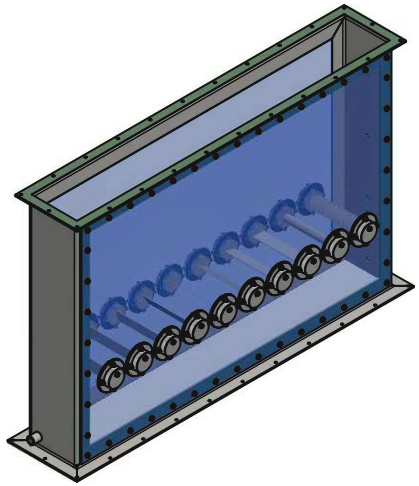

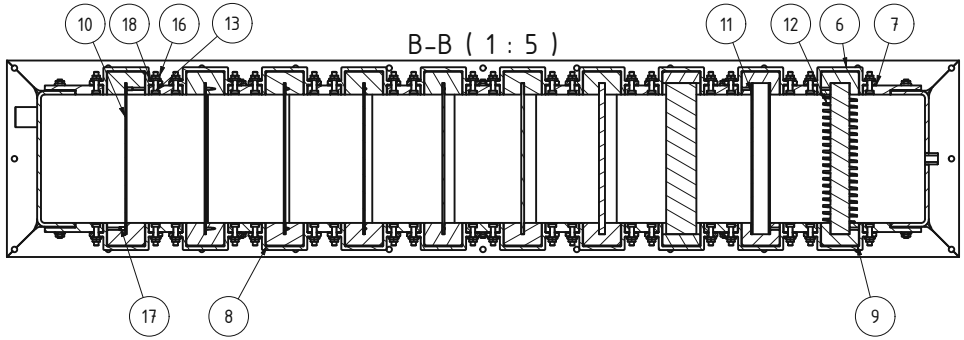

STÜCKLISTE

OBJEKT	ANZAHL	BAUTEILNUMMER	Z-NUMMER	BESCHREIBUNG
1	1	Wirbelschichtkammer Blech Schweißbaugruppe	ER036	
2	2	Plexiglaseinsatz	ER001	
3	2	Dichtung_Plexiglaseinsatz	ER028	
5	1	Dichtung Wirbelschichtkammer Flansch oben	ER023	
6	20	Einbautenträger	ER002	
7	20	Dichtung Einbautenträger	ER027	
8	16	Einsatzträger Blech	ER024	
9	4	Einsatzträger Rohr	ER025	
10	8	Erosionskörper Blech	ER037	Blech 200x40x2
11	1	Erosionskörper_Rohr	ER038	Rohr 25x2mm
12	1	Erosionskörper Spiralrohr	ER026	
13	80	DIN 6912 - M6 x 25		Zylinderkopfschraube
14	20	ISO 4017 - M6 x 12(3)		Sechskantschrauben mit Ganzgewinde
16	168	DIN 6923 - M6		Sechskantmutter
17	20	AS 1421 - M4 x 8 Kegelstumpf		ISO metrische Gewindestifte mit Innensechskant
18	100	M6 Dichtscheibe		RS Pro, Best.-Nr. 526-388

unbemaßte Werkstückkanten DIN ISO 13715 | ISO 128 | Allgemeintoleranz ISO2768 mK | Maßstab: 1 : 5 | Masse: -

Oberflächenbehandlung: | Material:

	Datum	Name
Gezeichn.	19.11.2021	Philipp Mayer
Kontroll.		
Norm		

Benennung: Wirbelschichtkammer Zusammenbauzeichnung

Projekt: Erosionsprüfstand

INSTITUT FÜR ENERGIETECHNIK UND THERMODYNAMIK
Institute for Energy Systems and Thermodynamics

Z-Nummer: ER029

Blatt 1/1 A2

Status | Änderungen | Datum | Name

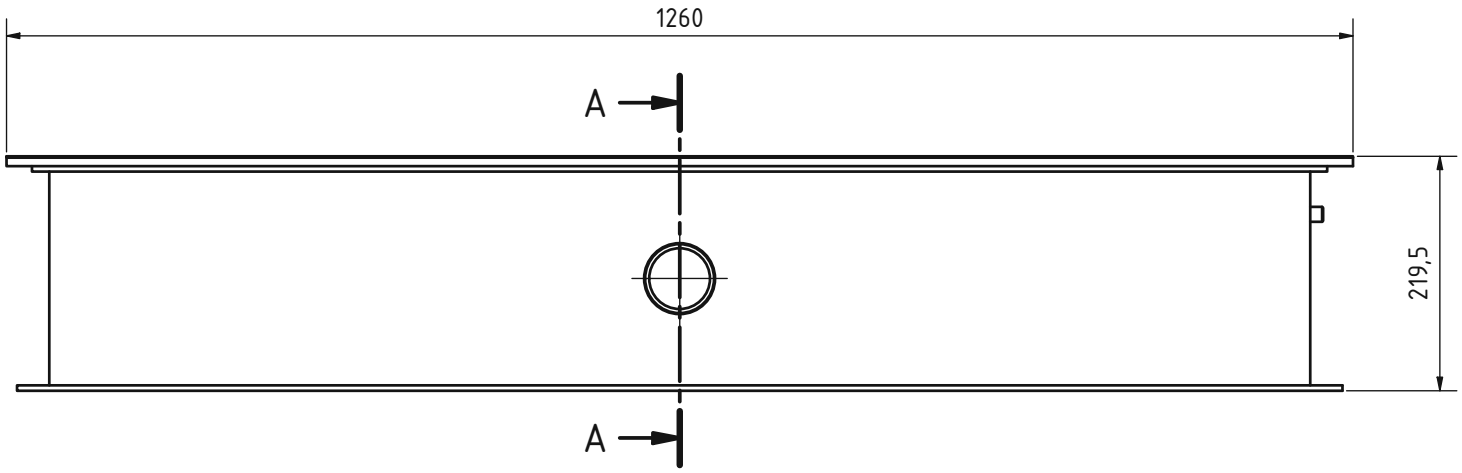

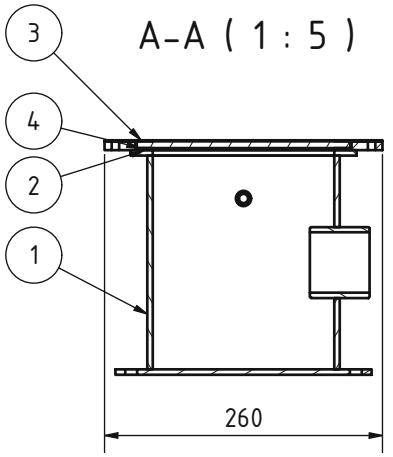

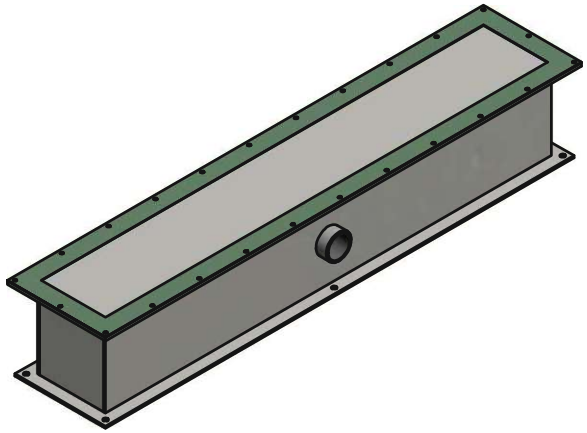

STÜCKLISTE				
OBJEKT	ANZAHL	BAUTEILNUMMER	Z-NUMMER	BESCHREIBUNG
1	1	Windkasten Schweißbaugruppe	ER016	
2	1	Dichtung Sinterplatte unten	ER021	
3	1	Dichtung Sinterplatte oben	ER022	
4	1	Sinterplatte Erosionsprüfstand		GKN Sinter Metals Filters GmbH, SIKA-R 10

unbemaßte Werkstückkanten DIN ISO 13715 — 0,3 — 0,3

ISO 128

Allgemeintoleranz ISO2768 mK

Maßstab: 1 : 5

Masse: 42,123 kg

Oberflächenbehandlung:

Material:

	Datum	Name
Gezeichn	23.11.2021	Philipp Mayer
Kontroll		
Norm		

Benennung:

Windkasten Zusammenbauzeichnung

Projekt: Erosionsprüfstand

INSTITUT FÜR ENERGIETECHNIK UND THERMODYNAMIK
Institute for Energy Systems and Thermodynamics

Z-Nummer: ER030

Blatt 1/1

A3

Status	Änderungen	Datum	Name

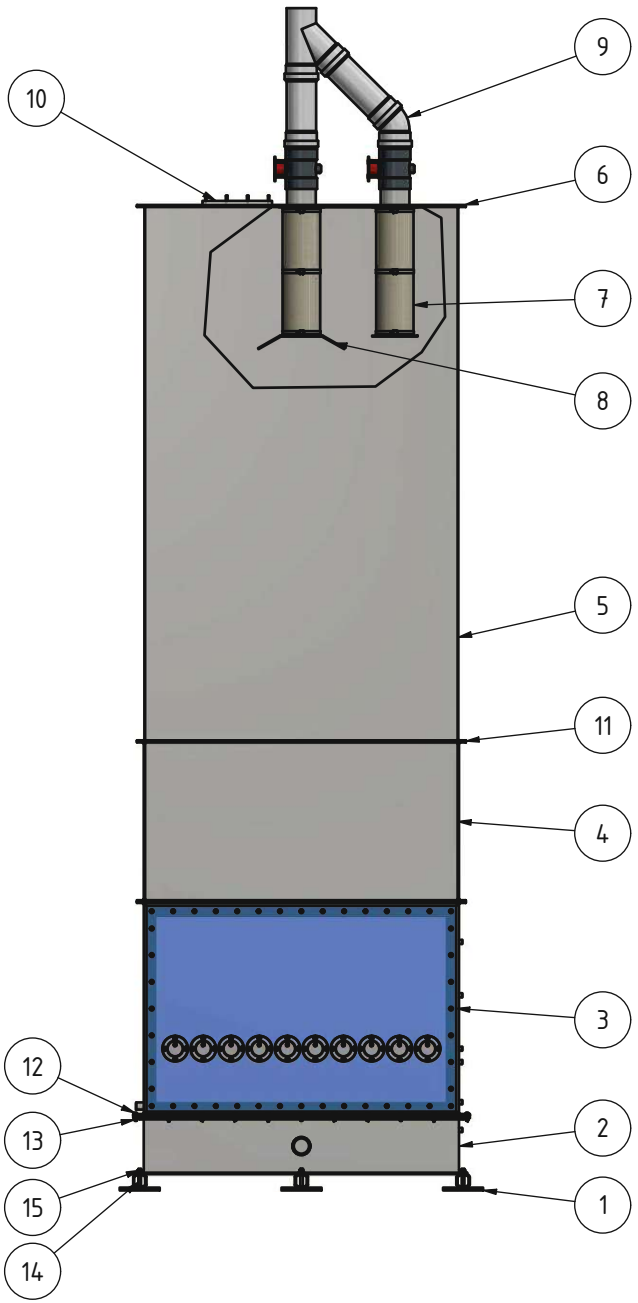

STÜCKLISTE

OBJEKT	ANZAHL	BAUTEILNUMMER	Z-NUMMER	BESCHREIBUNG
1	3	Aufstandsfuß Schweißbaugruppe	ER020	
2	1	Windkasten	ER030	
3	1	Wirbelschichtkammer	ER029	
4	1	Aufsatzrahmen Schweißbaugruppe	ER041	
5	1	Aufsatzrahmen hoch Schweißbaugruppe	ER044	
6	1	Wirbelschichtkammer Deckel Schweißbaugruppe	ER018	
7	1	Filtereinsatz		
8	1	Filtereinsatz mit Prallblech		
9	1	Rohrleitungen und Absperrklappen		
10	1	Deckel Sichtdeckel Plexiglas		
11	3	Dichtung Wirbelschichtkammer Flansch oben	ER023	
12	96	ISO 4017 - M6 x 25		Sechskantschraube
13	96	DIN 6923 - M6		Sechskantmutter
14	6	ISO 4017 - M10 x 70		Sechskantschraube
15	6	DIN 6923 - M10		Sechskantmutter

unbemaßte Werkstückkanten DIN ISO 13715 — 0,3 — 0,3

ISO 128

Allgemeintoleranz ISO2768 mK

Maßstab: 1 : 20

Masse: -

Oberflächenbehandlung:

Material:

	Datum	Name
Gezeichn	20.10.2022	Philipp Mayer
Kontroll		
Norm		

Benennung: Erosionspruefstand

Projekt:

INSTITUT FÜR ENERGIETECHNIK UND THERMODYNAMIK
Institute for Energy Systems and Thermodynamics

Z-Nummer: ER031

Blatt 1/1

A3

Status	Änderungen	Datum	Name

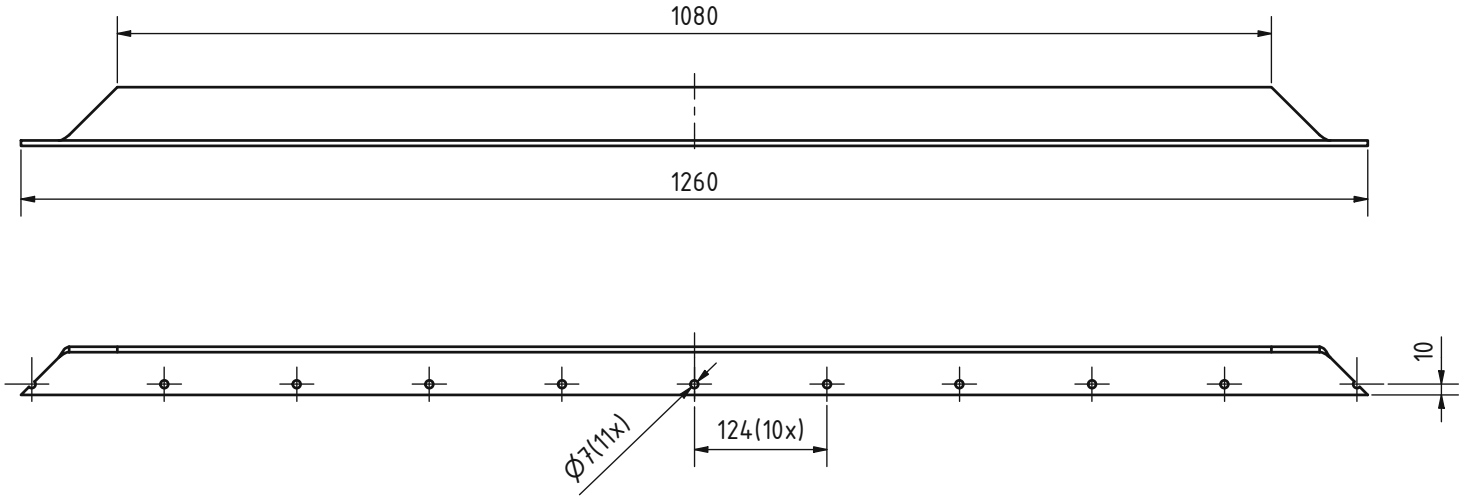

Abwicklung (1 : 5)

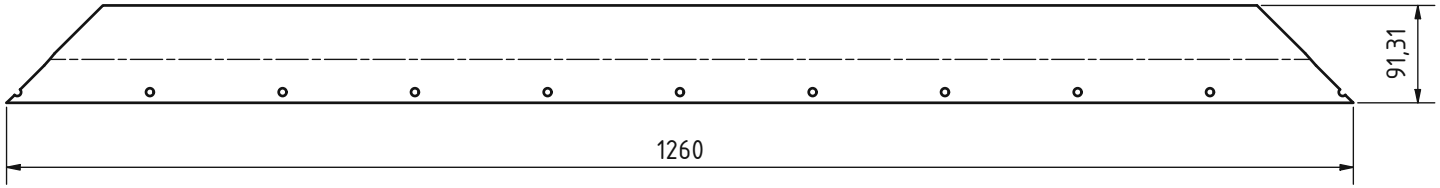

unbemaßte Werkstückkanten DIN ISO 13715 0,3 0,3	ISO 128	Allgemeintoleranz ISO2768 mK	Maßstab: 1 : 5
Oberflächenbehandlung:			Masse: 4,200 kg
			Material: Stahl S235 JR

	Datum	Name
Gezeichn	01.12.2021	Philipp Mayer
Kontroll		
Norm		

Benennung:
Wirbelschichtkammer Stegblech unten
Projekt: Erosionsprüfstand

INSTITUT FÜR ENERGIETECHNIK UND THERMODYNAMIK
Institute for Energy Systems and Thermodynamics

Z-Nummer: ER032

Blatt 1/1
A3

Status	Änderungen	Datum	Name

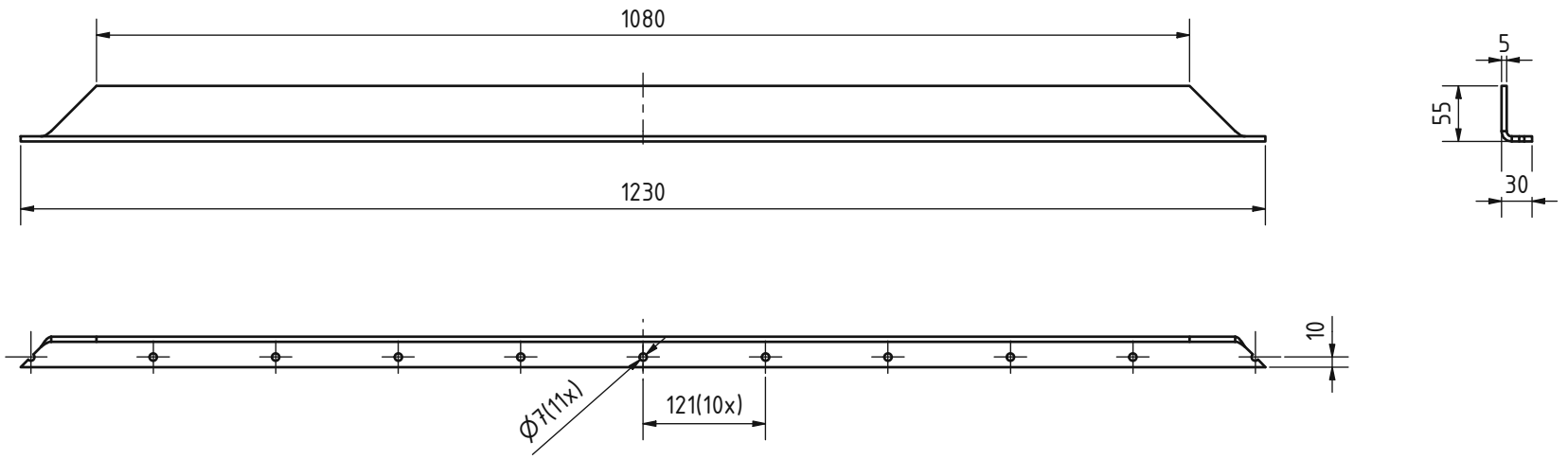

Abwicklung (1 : 5)

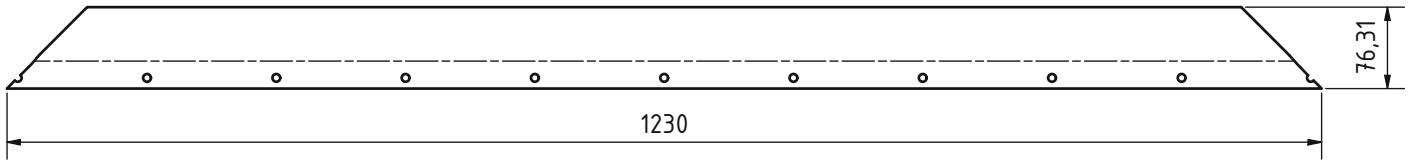

unbemaßte Werkstückkanten DIN ISO 13715 (0,3 / 0,3)	ISO 128	Allgemeintoleranz ISO2768 mK	Maßstab: 1 : 5
Oberflächenbehandlung:			Masse: 3,467 kg
			Material: Stahl S235 JR
	Datum	Name	Benennung: Wirbelschichtkammer Stegblech oben
Gezeichn	01.12.2021	Philipp Mayer	Projekt: Erosionsprüfstand
Kontroll			
Norm			
INSTITUT FÜR ENERGIETECHNIK UND THERMODYNAMIK, Institute for Energy Systems and Thermodynamics			Z-Nummer: ER033
			Blatt 1/1, A3
Status	Änderungen	Datum / Name	

Abwicklung (1 : 5)

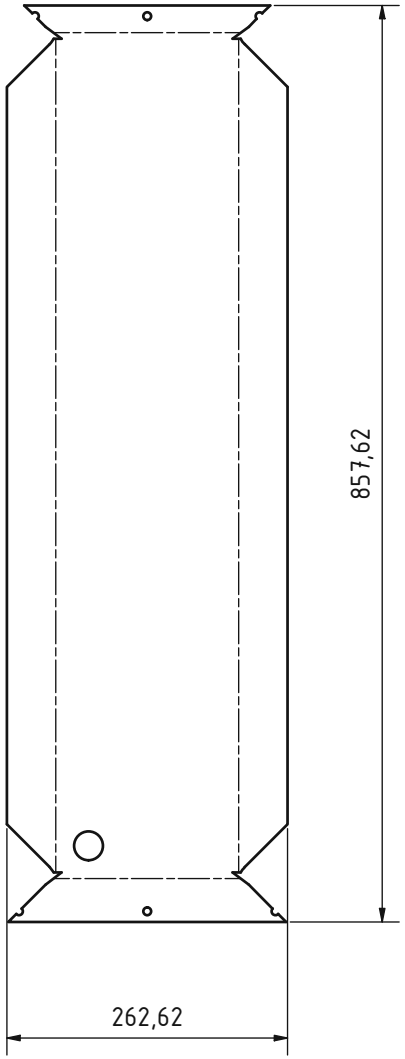

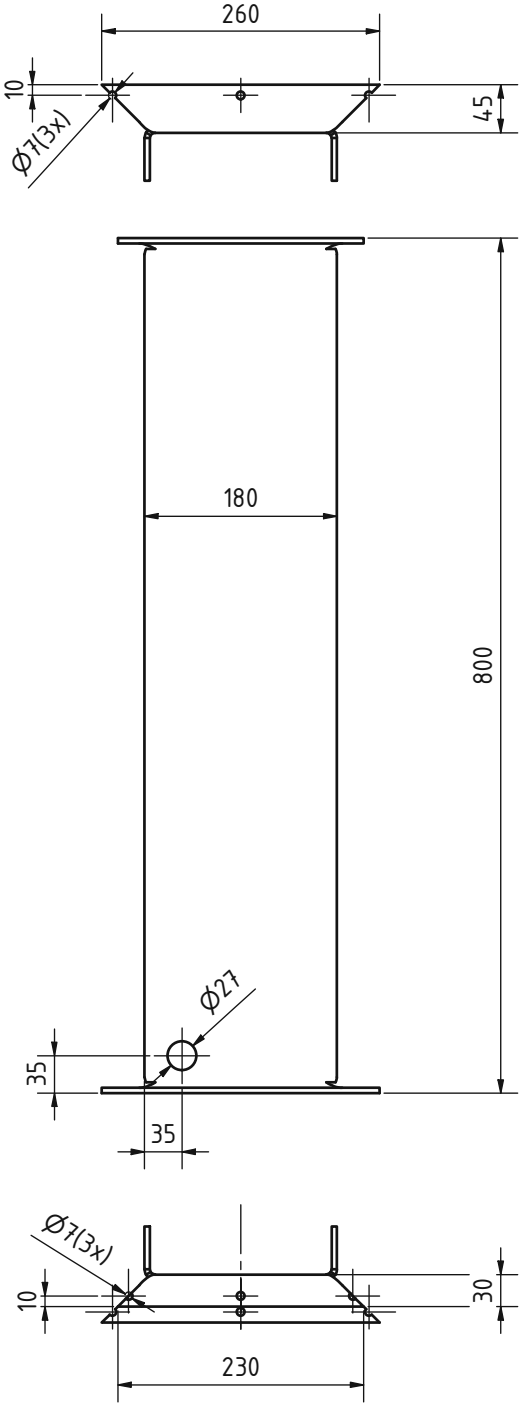

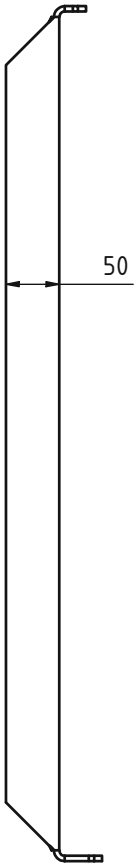

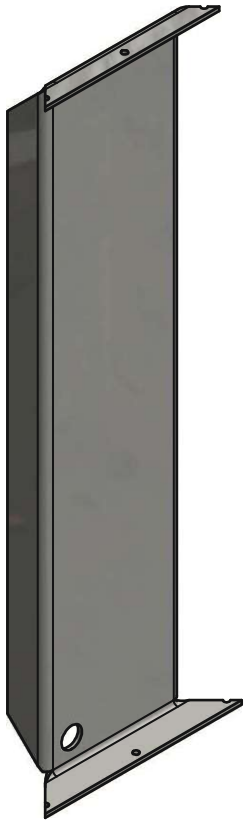

unbemaßte Werkstückkanten DIN ISO 13715	ISO 128	Allgemeintoleranz ISO2768 mK	Maßstab: 1 : 5
		Oberflächenbehandlung:	Masse: 8,518 kg
			Material: Stahl S235 JR
	Datum	Name	Benennung: Wirbelschichtkammer Seitenwand links Blech
	Gezeichn 01.12.2021	Philipp Mayer	Projekt: Erosionsprüfstand
	Kontroll		
	Norm		
Status Änderungen Datum Name	INSTITUT FÜR ENERGIETECHNIK UND THERMODYNAMIK Institute for Energy Systems and Thermodynamics		Z-Nummer: ER034
			Blatt 1/1 A3

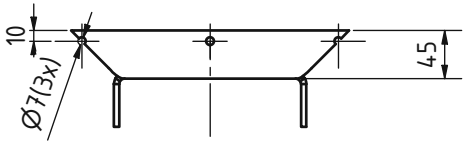

Abwicklung (1 : 5)

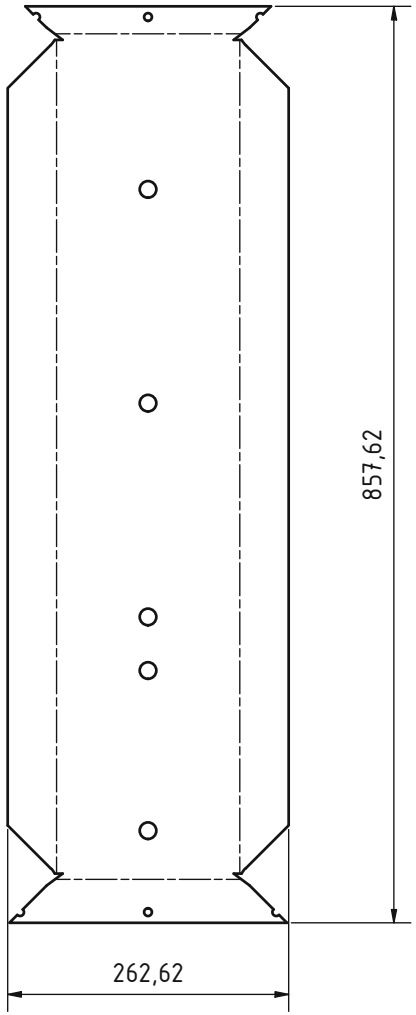

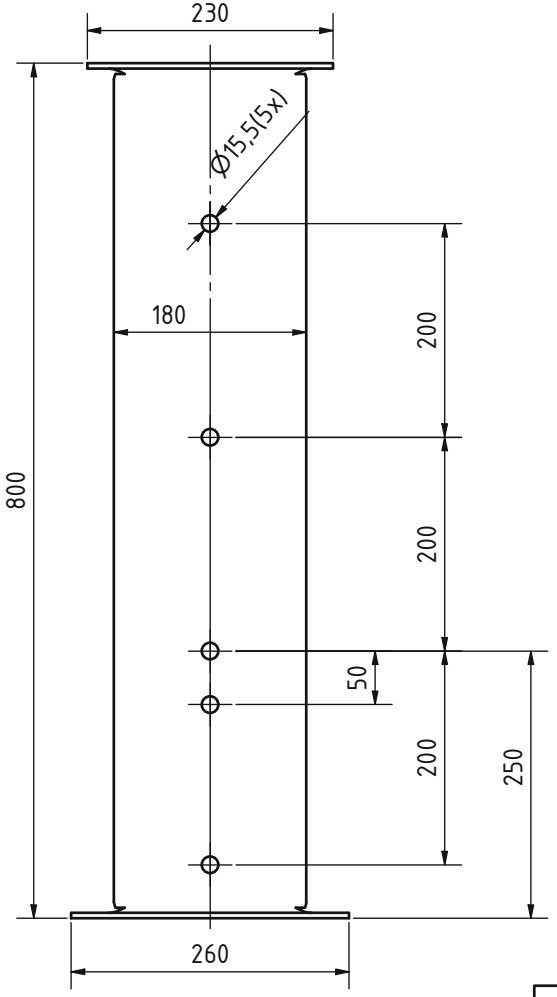

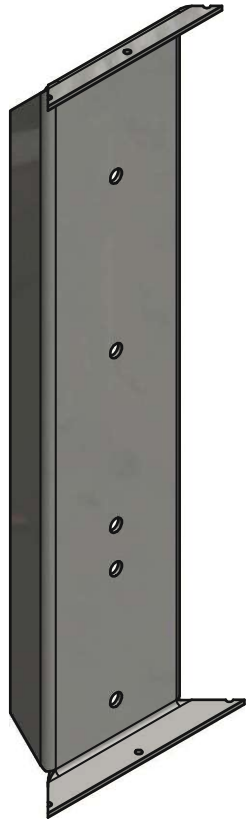

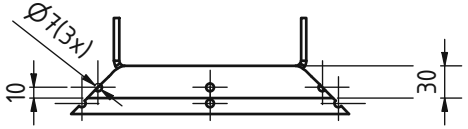

unbemaßte Werkstückkanten DIN ISO 13715	ISO 128	Allgemeintoleranz ISO2768 mK	Maßstab: 1 : 5
			Masse: 8,503 kg
		Oberflächenbehandlung:	Material: Stahl S235 JR
	Datum	Name	Benennung: Wirbelschichtkammer Seitenwand rechts Blech
	Gezeichn 01.12.2021	Philipp Mayer	
	Kontroll		Projekt: Erosionsprüfstand
	Norm		
INSTITUT FÜR ENERGIETECHNIK UND THERMODYNAMIK Institute for Energy Systems and Thermodynamics			Z-Nummer: ER035
Status Änderungen Datum Name			Blatt 1/1 A3

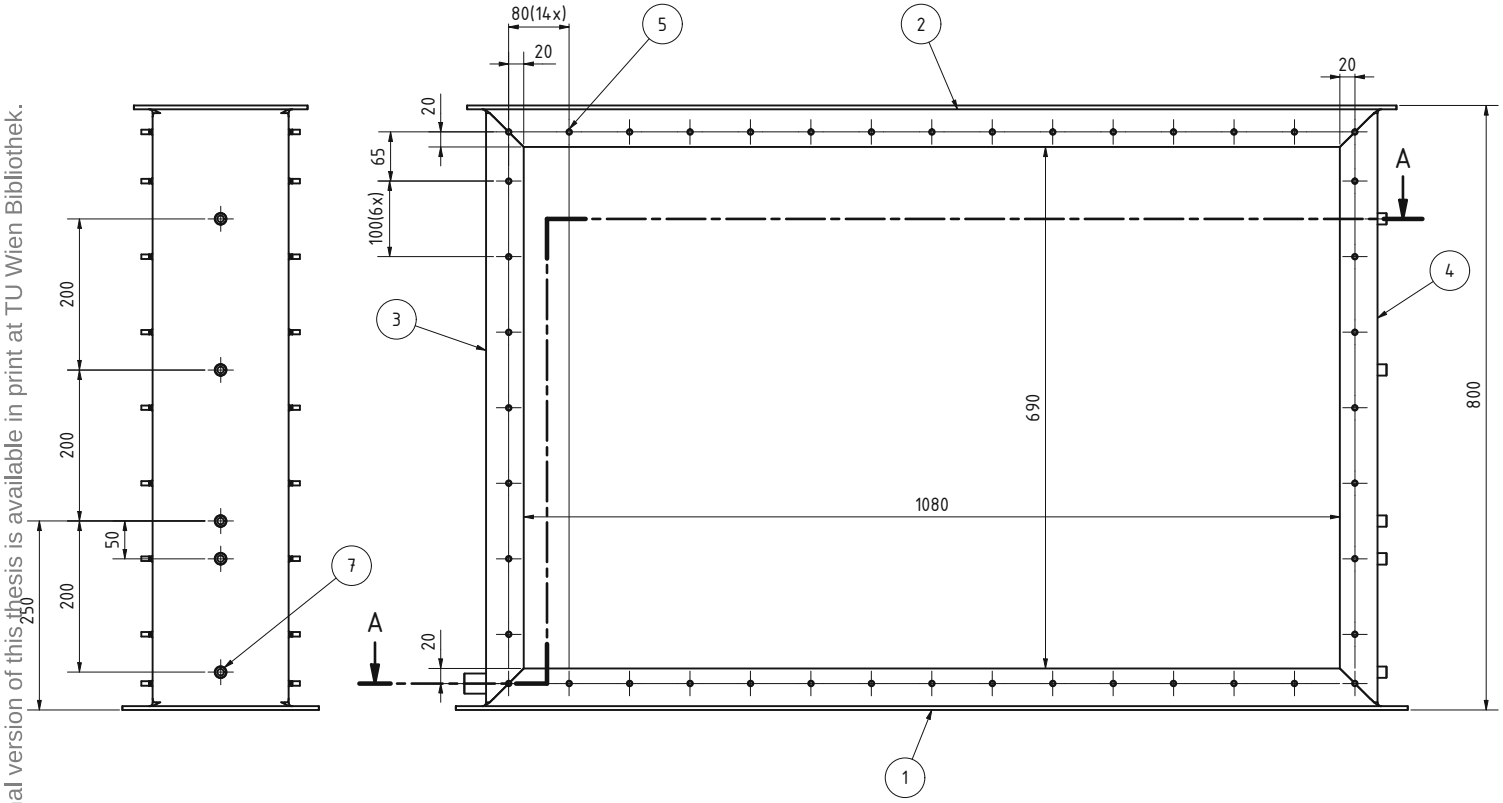

A-A (1 : 5)

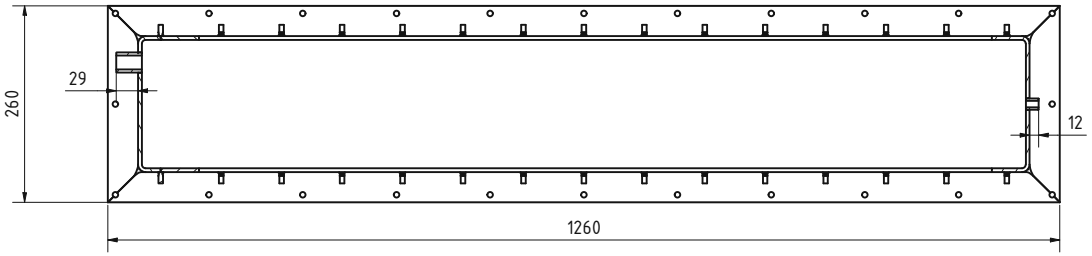

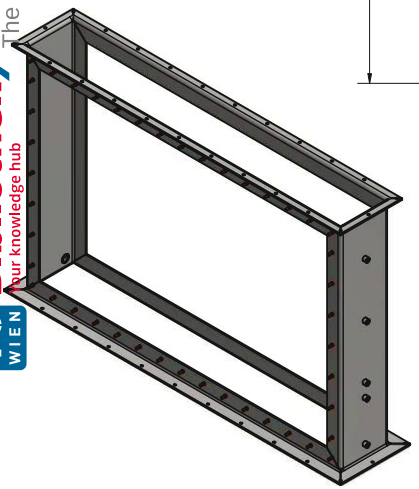

STÜCKLISTE				
OBJEKT	ANZAHL	BAUTEILNUMMER	Z-NUMMER	BESCHREIBUNG
1	2	Wirbelschichtkammer Stegblech unten	ER032	
2	2	Wirbelschichtkammer Stegblech oben	ER033	
3	1	Wirbelschichtkammer Seitenwand links Blech	ER034	
4	1	Wirbelschichtkammer Seitenwand rechts Blech	ER035	
5	88	Bolzen ISO 13918 – PT M6×15 – 4.8		Würth, Art.-Nr. 44766 15
6	1	Gewindemuffe Rp1/2	MUR 12 AS ST	Landefeld, DIN EN 10241
7	5	Gewindemuffe Rp1/8	MUR 18 AS ST	Landefeld, DIN EN 10241

unbemaßte Werkstückkanten DIN ISO 13715 | ISO 128 | Allgemeintoleranz ISO2768 mK | Maßstab: 1 : 5 | Masse: 32,412 kg

Oberflächenbehandlung: | Material:

	Datum	Name
Gezeichn.	01.12.2021	Philipp Mayer
Kontroll.		
Norm		

Benennung: Wirbelschichtkammer Blech Schweißbaugruppe

Projekt: Erosionsprüfstand

INSTITUT FÜR ENERGIETECHNIK UND THERMODYNAMIK
Institute for Energy Systems and Thermodynamics

Z-Nummer: ER036

Blatt 1/1 A2

Status | Änderungen | Datum | Name

Fertigungshinweis: Bauteile gasdicht verschweißen

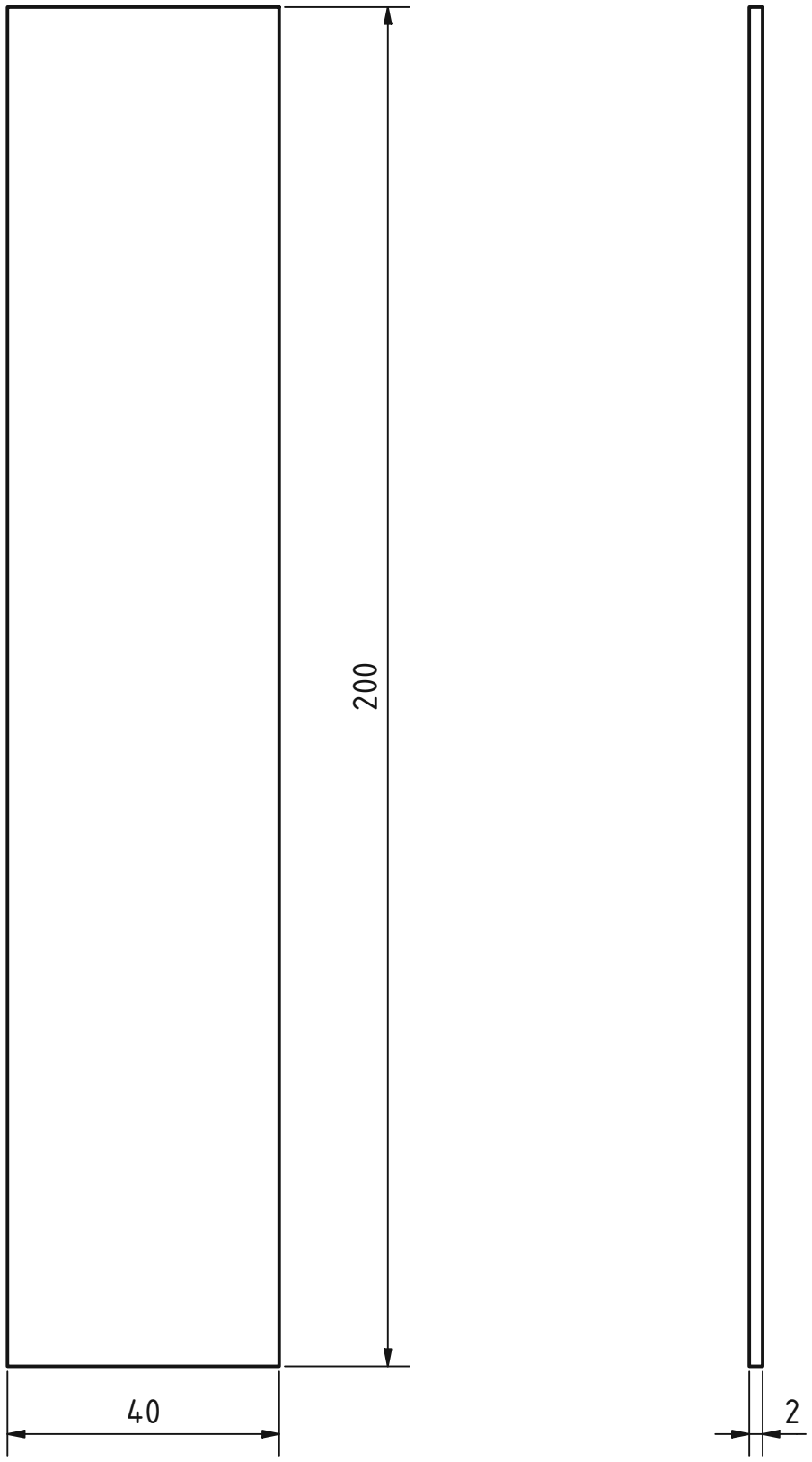

unbemaßte Werkstückkanten DIN ISO 13715

0,3 0,3

ISO 128

Allgemeintoleranz ISO2768 mK

Maßstab: 1 : 1

Masse: 0,126 kg

Oberflächenbehandlung:

Material: Stahl S235 JR

	Datum	Name
Gezeichn	18.01.2022	Philipp Mayer
Kontroll		
Norm		

Benennung:

Erosionskörper Blech

Projekt: Erosionsprüfstand

INSTITUT FÜR ENERGIETECHNIK UND THERMODYNAMIK
Institute for Energy Systems and Thermodynamics

Z-Nummer: ER037

Blatt 1/1

A4

Status	Änderungen	Datum	Name

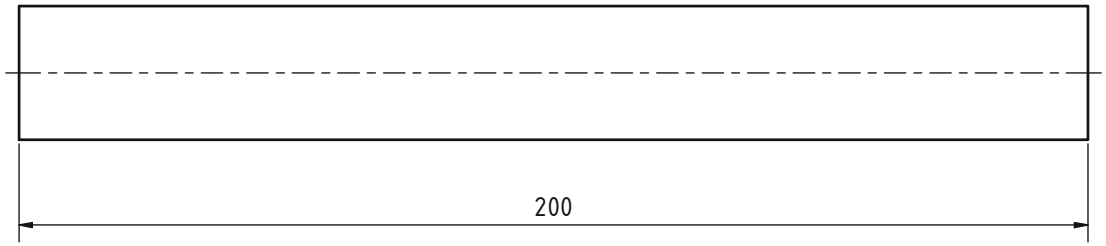

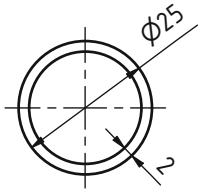

Fertigungshinweis:
Rohr – 25x2 – EN10216-2 – P265GH

unbemaßte Werkstückkanten DIN ISO 13715	ISO 128	Allgemeintoleranz ISO2768 mK	Maßstab: 1 : 1
		Oberflächenbehandlung:	Masse: 0,227 kg
			Material: Stahl S235 JR
	Datum	Name	Benennung: Erosionskörper Rohr
	Gezeichn 18.01.2022	Philipp Mayer	
	Kontroll		Projekt: Erosionsprüfstand
	Norm		
INSTITUT FÜR ENERGIETECHNIK UND THERMODYNAMIK Institute for Energy Systems and Thermodynamics			Z-Nummer: ER038
Status Änderungen Datum Name			Blatt 1/1 A3

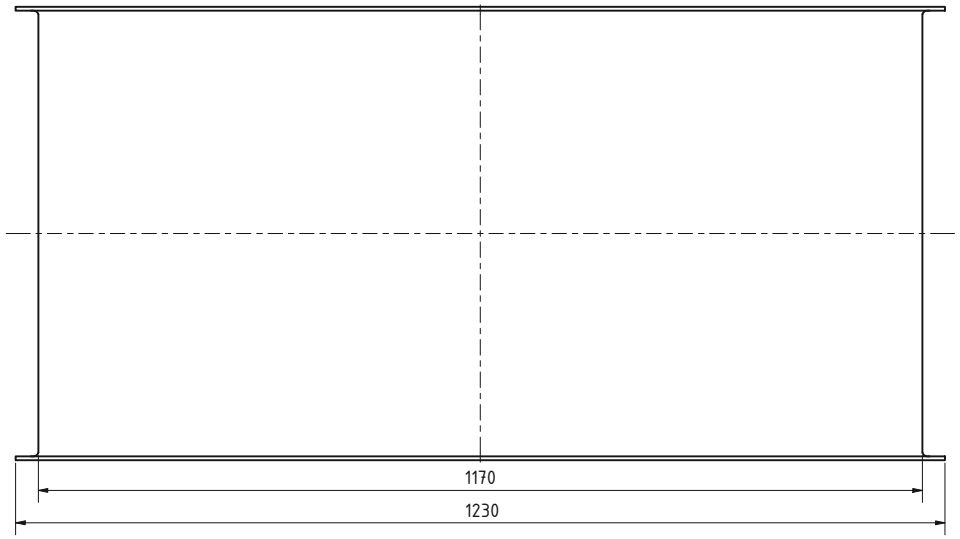

Abwicklung (1 : 5)

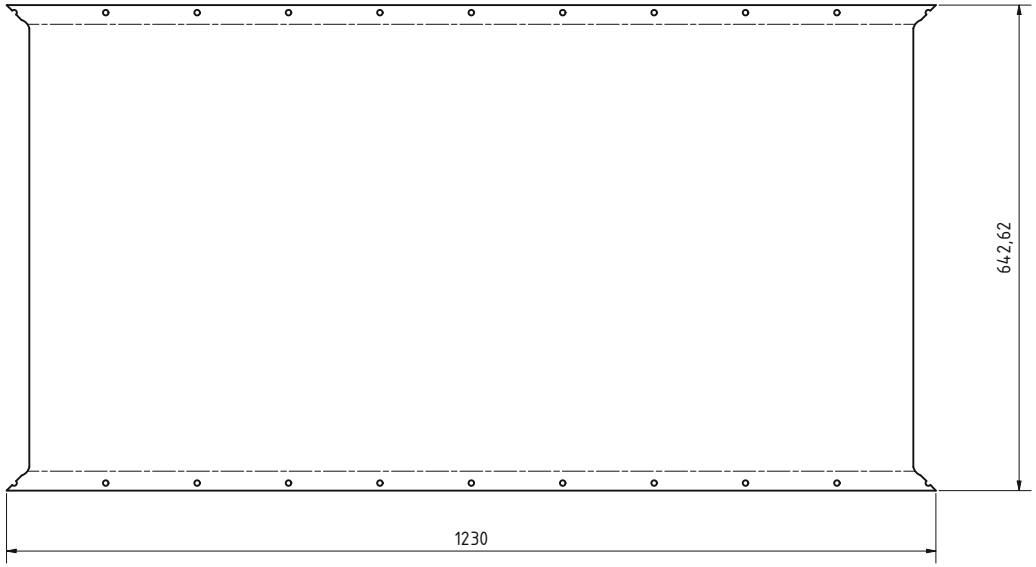

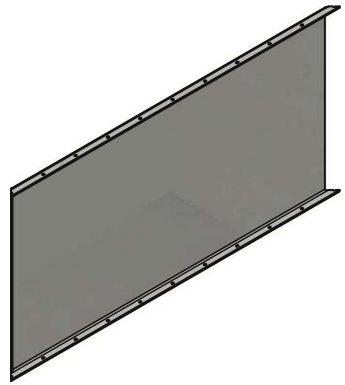

unbemaßte Werkstückkanten DIN ISO 13715	ISO 128	Allgemeintoleranz ISO2768 mK	Maßstab: 1 : 5	Masse: 29,592 kg	
			Oberflächenbehandlung:	Material: Stahl S235 JR	
	Datum	Name	Benennung: Aufsatzrahmen Längswand		
Gezeichn.	03.05.2022	Philipp Mayer			
Kontroll			Projekt: Erosionsprüfstand		
Norm					
INSTITUT FÜR ENERGIETECHNIK UND THERMODYNAMIK Institute for Energy Systems and Thermodynamics			Z-Nummer: ER039	Blatt 1/1 A2	
Status	Änderungen	Datum	Name		

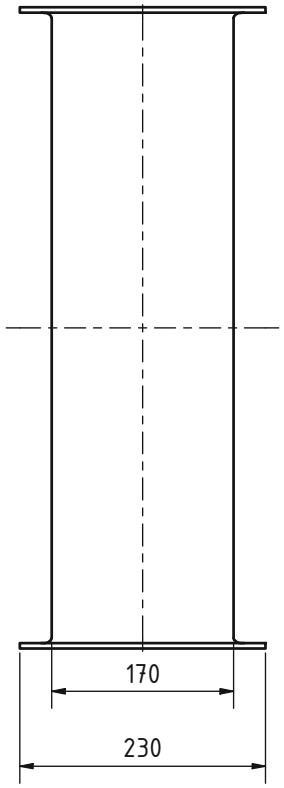

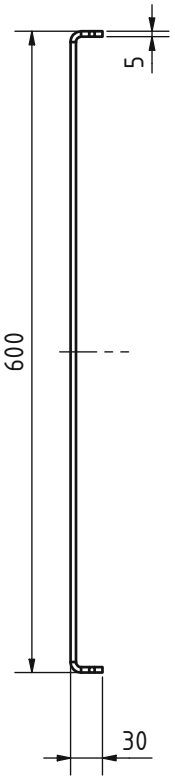

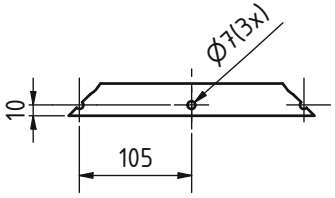

Abwicklung (1 : 5)

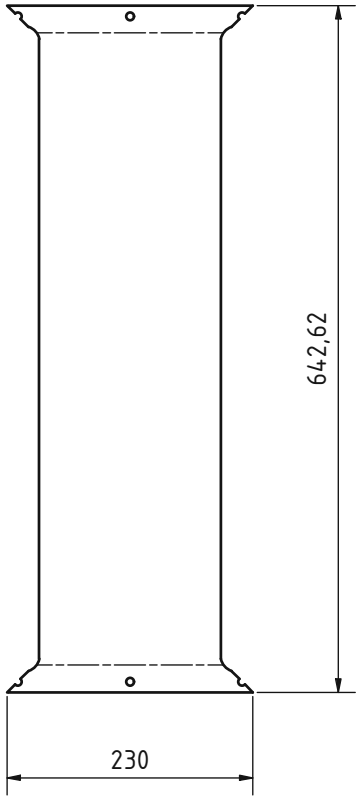

unbemaßte Werkstückkanten DIN ISO 13715	ISO 128	Allgemeintoleranz ISO2768 mK	Maßstab: 1 : 5
		Oberflächenbehandlung:	Masse: 4,357 kg
			Material: Stahl S235 JR
	Datum	Name	Benennung: Aufsatzrahmen Seitenwand
	Gezeichn 03.05.2022	Philipp Mayer	
	Kontroll		
	Norm		Projekt: Erosionsprüfstand
INSTITUT FÜR ENERGIETECHNIK UND THERMODYNAMIK Institute for Energy Systems and Thermodynamics			Z-Nummer: ER040
Status Änderungen Datum Name			Blatt 1/1 A3

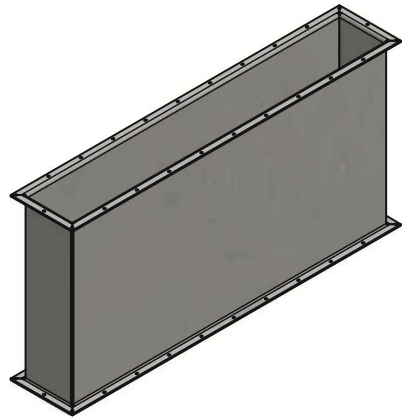

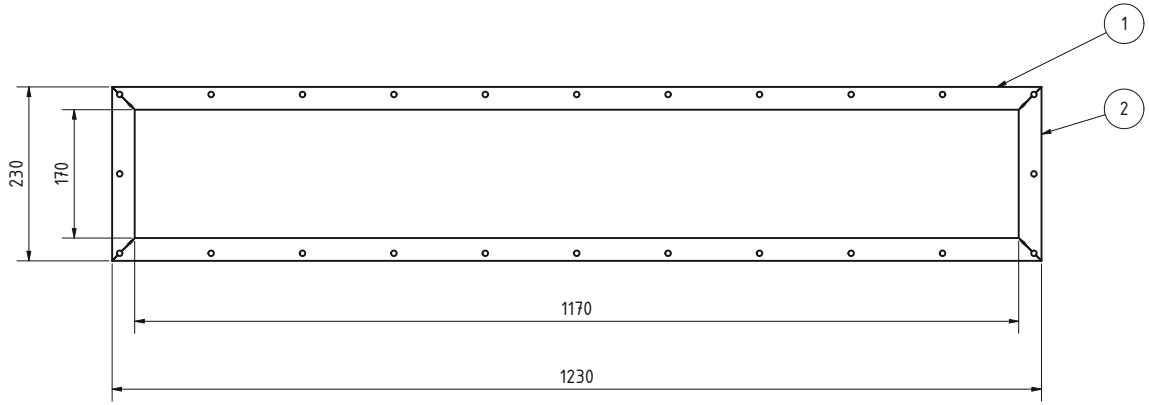

Fertigungshinweis: Bauteile gasdicht verschweißen

STÜCKLISTE

OBJEKT	ANZAHL	BAUTEILNUMMER	Z-NUMMER	BESCHREIBUNG
1	2	Aufsatzrahmen Längswand	ER039	
2	2	Aufsatzrahmen_Seitenwand	ER040	

unbemaßte Werkstückkanten DIN ISO 13715 | ISO 128 | Allgemeintoleranz ISO2768 mK | Maßstab: 1 : 5 | Masse: 67,898 kg

Oberflächenbehandlung: | Material:

	Datum	Name
Gezeichn.	03.05.2022	Philipp Mayer
Kontroll.		
Norm		

Benennung: Aufsatzrahmen Schweißbaugruppe

Projekt: Erosionsprüfstand

INSTITUT FÜR ENERGIETECHNIK UND THERMODYNAMIK
Institute for Energy Systems and Thermodynamics

Z-Nummer: ER041

Blatt 1/1 A2

Status | Änderungen | Datum | Name

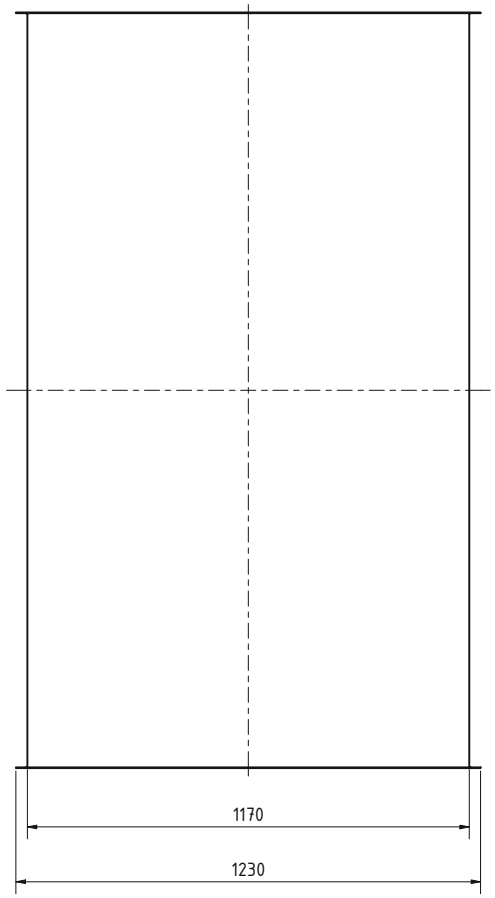

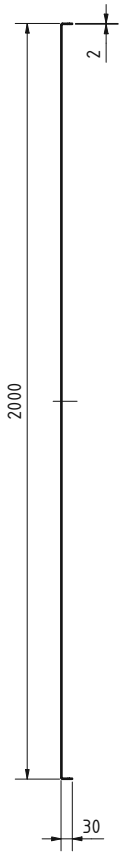

Abwicklung (1 : 10)

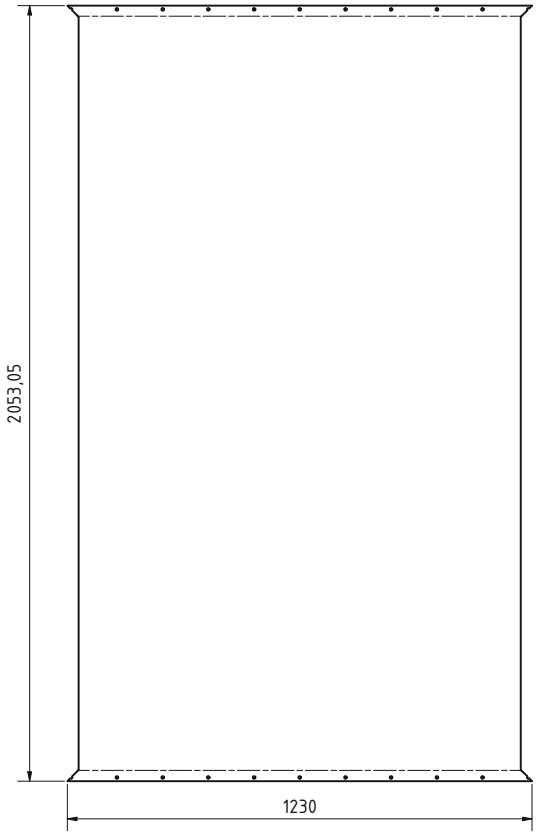

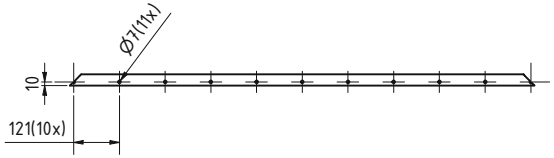

unbemaßte Werkstückkanten DIN ISO 13715	ISO 128	Allgemeintoleranz ISO2768 mK	Maßstab: 1 : 10	Masse: 37,736 kg	
			Oberflächenbehandlung:	Material: Stahl S235 JR	
	Datum	Name	Benennung: Aufsatzrahmen hoch Laengswand		
	Gezeichn. 27.05.2022	Philipp Mayer	Projekt: Erosionsprüfstand		
	Kontroll.				
	Norm		INSTITUT FÜR ENERGIETECHNIK UND THERMODYNAMIK Institute for Energy Systems and Thermodynamics	Z-Nummer: ER042	Blatt 1/1 A2
Status Änderungen	Datum	Name			

Abwicklung (1 : 10)

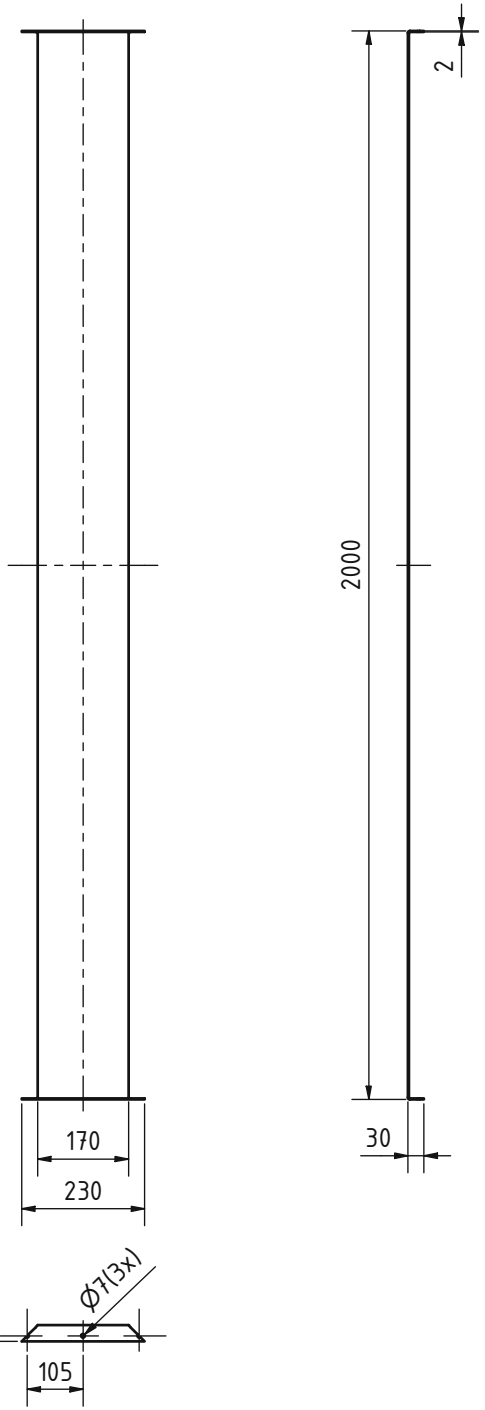

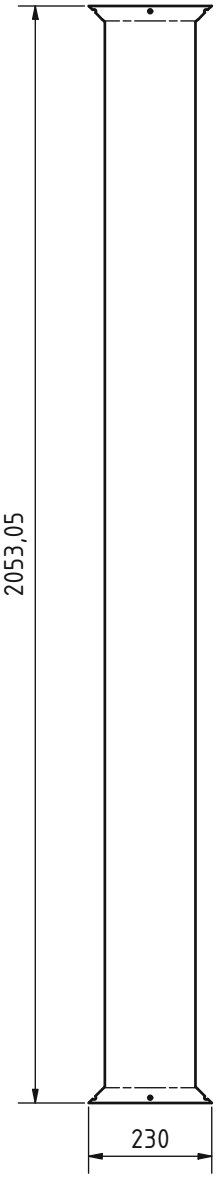

unbemaßte Werkstückkanten DIN ISO 13715	ISO 128	Allgemeintoleranz ISO2768 mK	Maßstab: 1 : 10
		Oberflächenbehandlung:	Masse: 5,506 kg
			Material: Stahl S235 JR
	Datum	Name	Benennung: Aufsatzrahmen hoch Seitenwand
	Gezeichn 27.05.2022	Philipp Mayer	Projekt: Erosionsprüfstand
	Kontroll		
	Norm		
INSTITUT FÜR ENERGIETECHNIK UND THERMODYNAMIK Institute for Energy Systems and Thermodynamics			Z-Nummer: ER043
Status Änderungen Datum Name			Blatt 1/1 A3

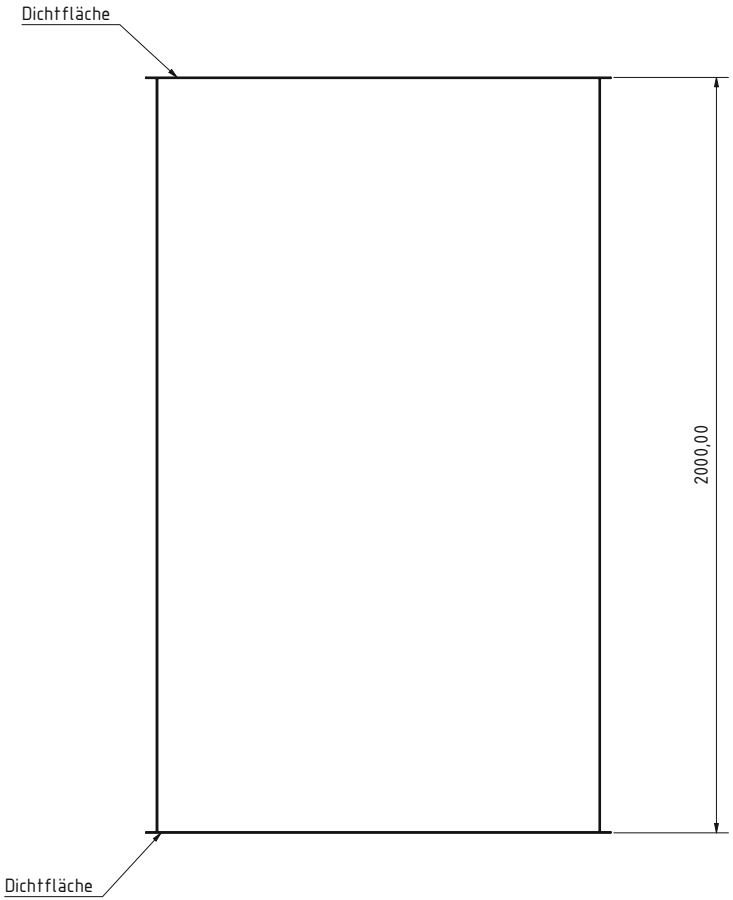

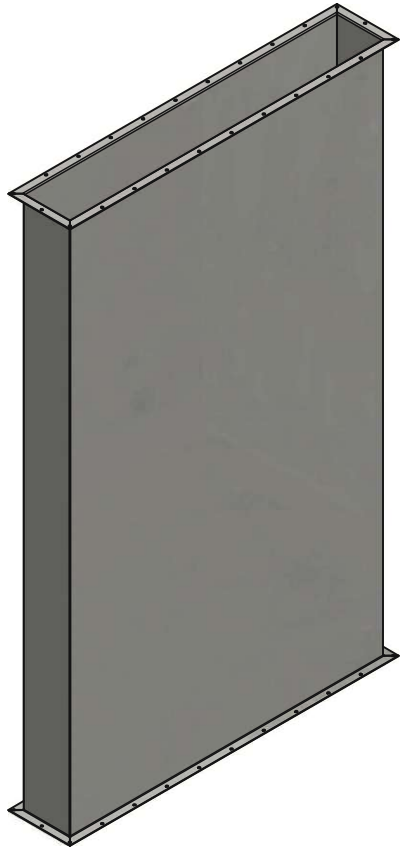

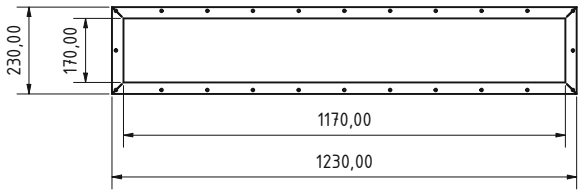

Fertigungshinweis: Bauteile gasdicht verschweißen

unbemaßte Werkstückkanten DIN ISO 13715	ISO 128	Allgemeintoleranz ISO2768 mK	Maßstab: 1 : 10	Masse: 86,484 kg	
			Oberflächenbehandlung:	Material:	
	Datum	Name	Benennung: Aufsatzrahmen hoch Schweißbaugruppe		
	Gezeichn. 27.05.2022	Philipp Mayer			
	Kontroll		Projekt: Erosionsprüfstand		
	Norm				
INSTITUT FÜR ENERGIETECHNIK UND THERMODYNAMIK Institute for Energy Systems and Thermodynamics			Z-Nummer: ER044	Blatt 1/1 A2	
Status Änderungen	Datum	Name			

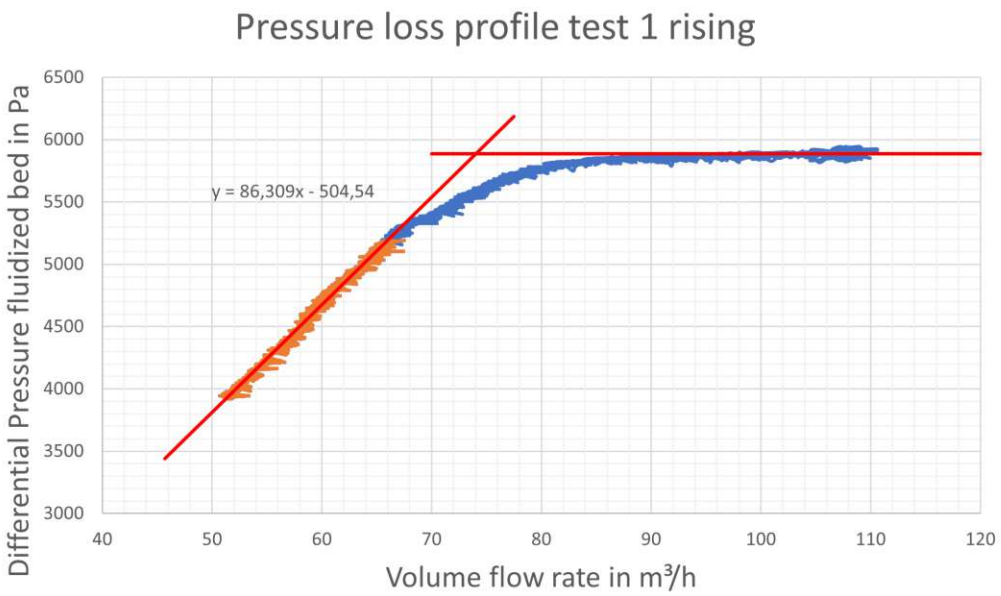

(a) *Rising test Nr.1*

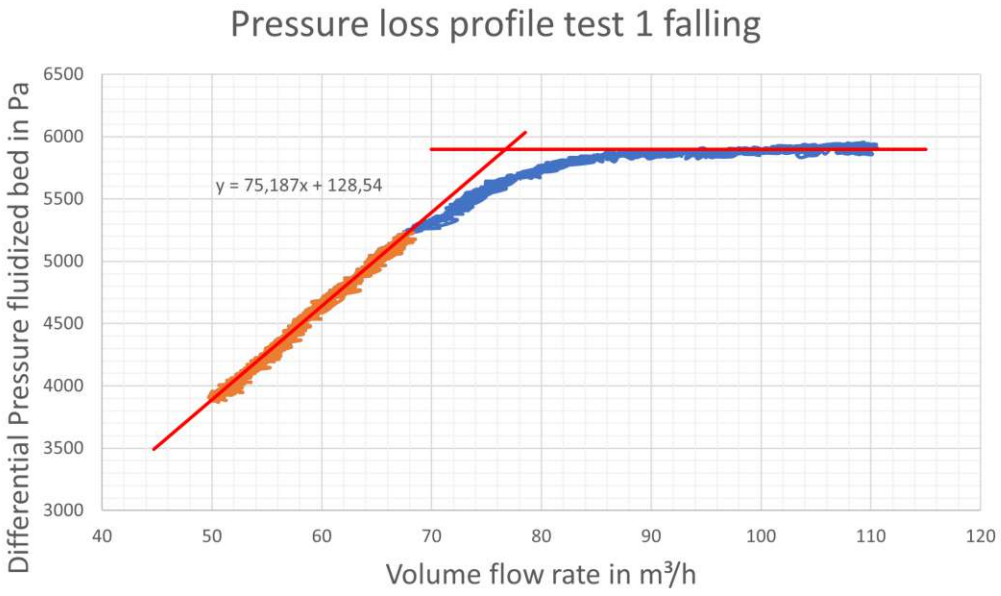

(b) *Falling test Nr.1*

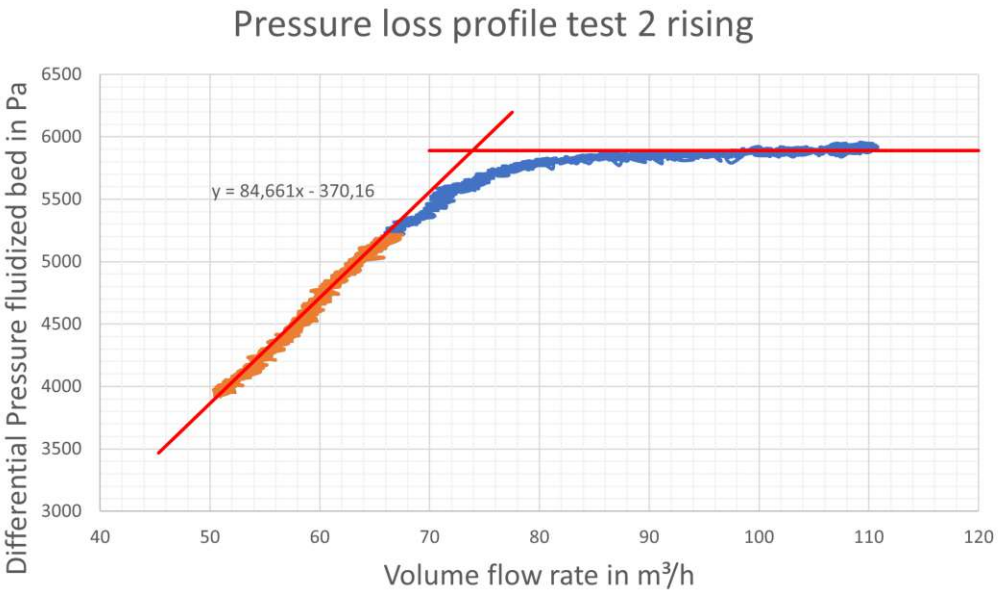

(c) *Rising test Nr.2*

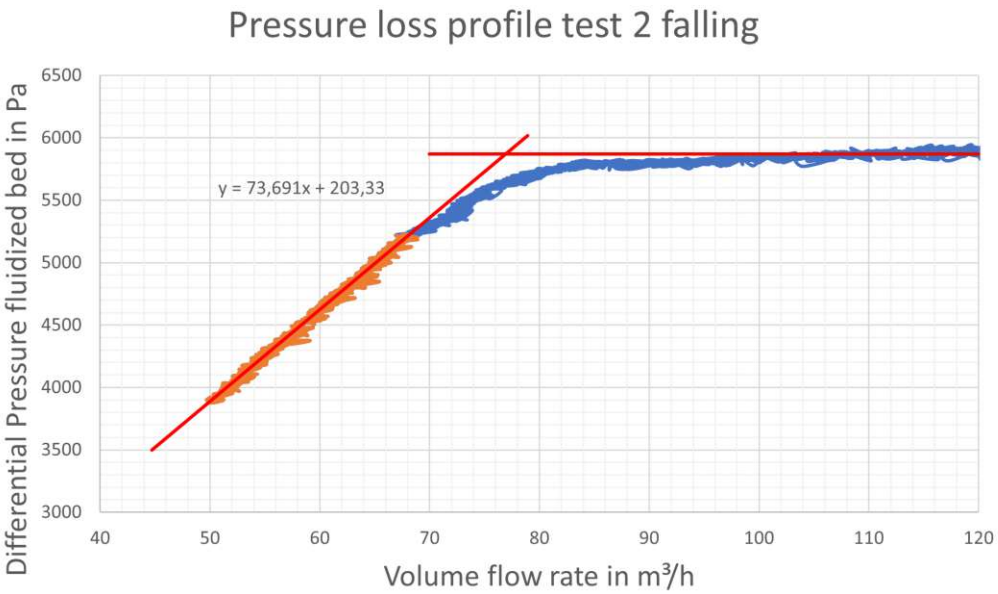

(d) *Falling test Nr.2*

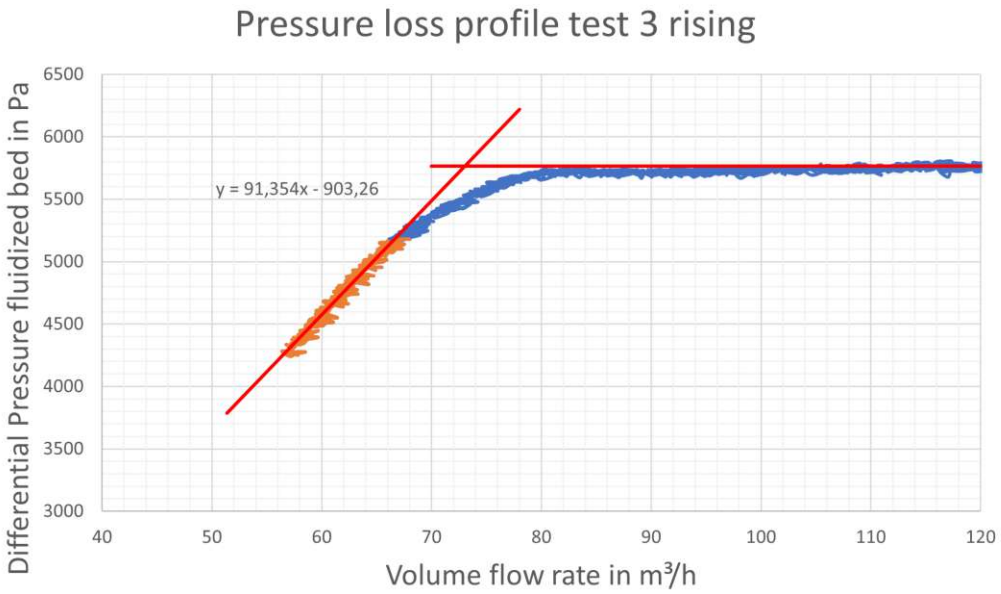

(e) *Rising test Nr.3*

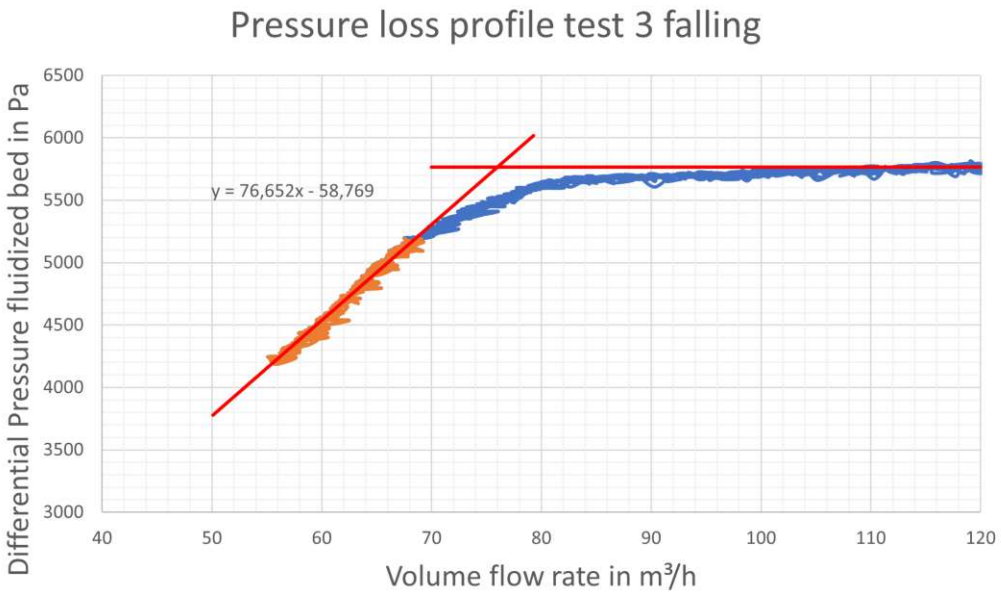

(f) *Falling test Nr.3*

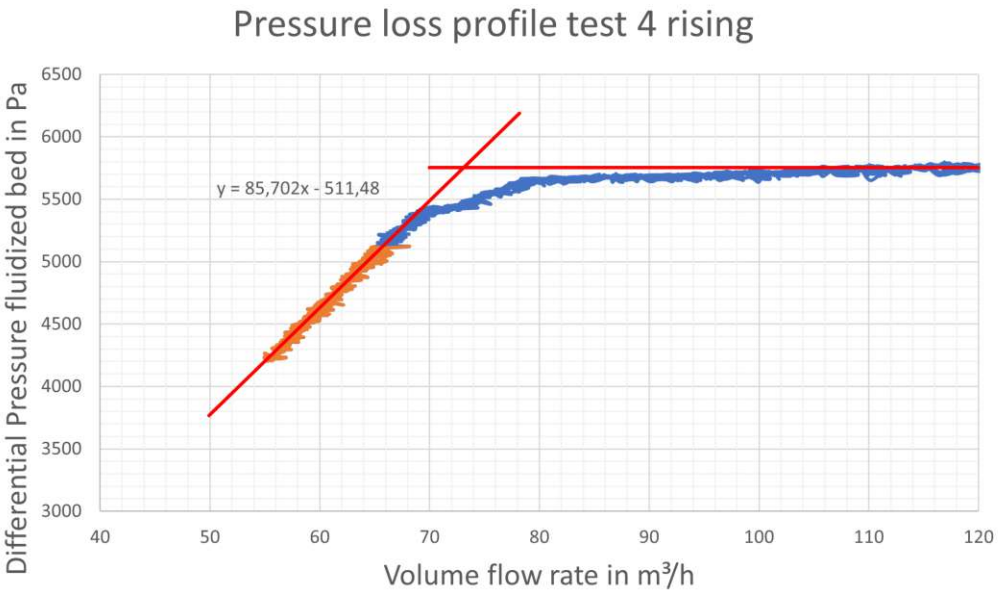

(g) *Rising test Nr.4*

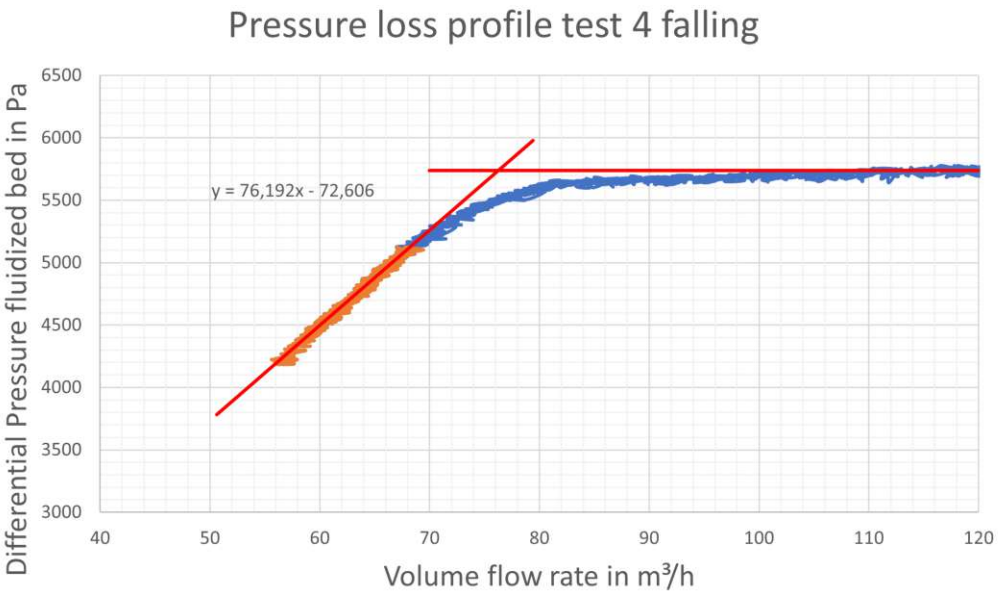

(h) *Falling test Nr.4*

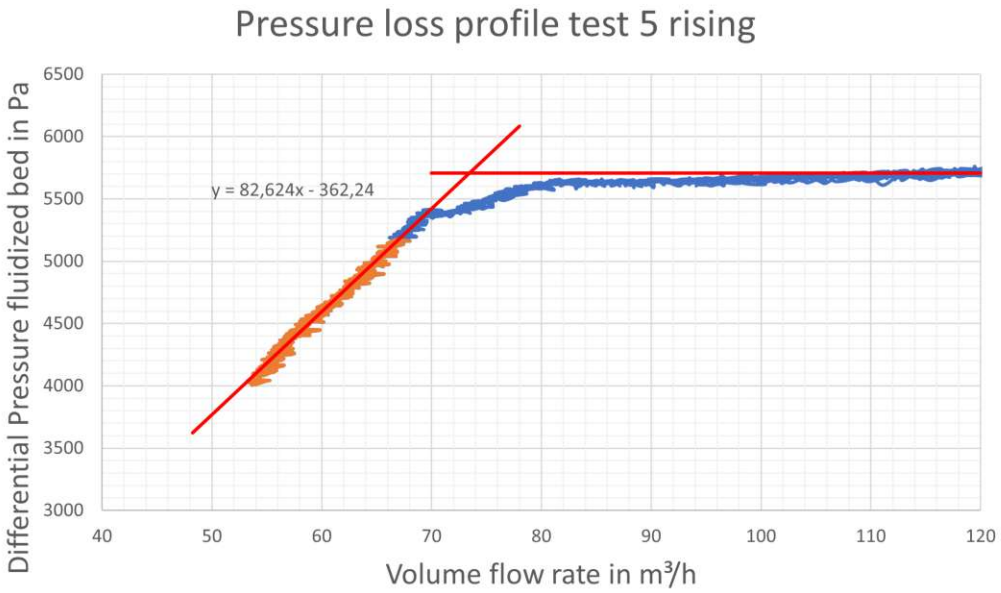

(i) *Rising test Nr.5*

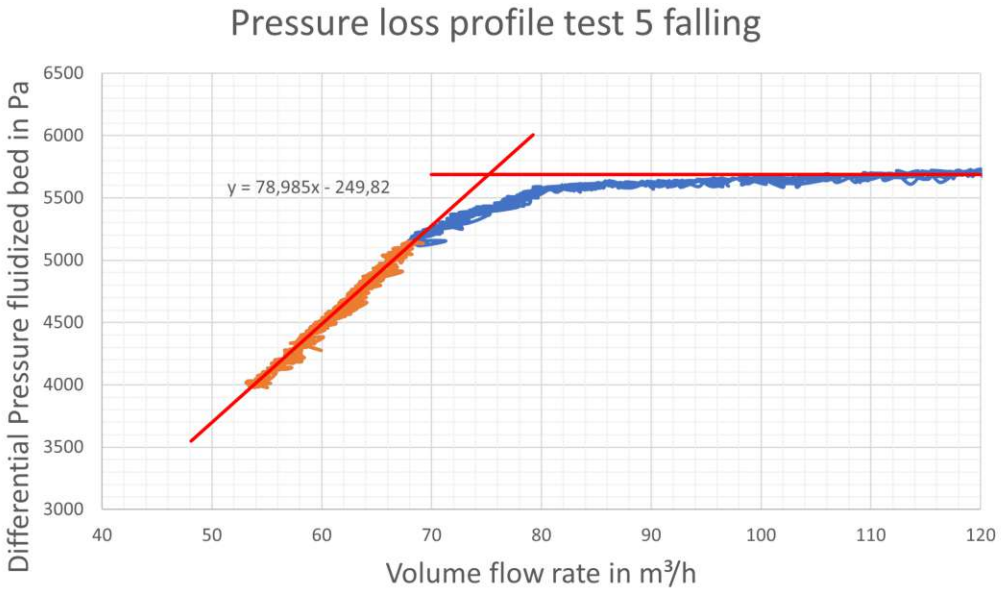

(j) *Falling test Nr.5*

Figure 47.: *Calculation of the minimal fluidization volume flow rate for the different test configurations.*

Inspection element	Installation angle (°)	Measurement	Measurement point							
			MP1	MP2	MP3	MP4	MP5	MP6	MP7	MP8
metal sheet 1	0	Before test in mm	2,00	2,00	2,00	2,00	2,00	2,00	2,00	2,00
		After test in mm	2,00	2,00	1,99	1,99	2,00	2,00	1,99	1,99
		Difference in µm	0,00	0,00	-10,00	-10,00	0,00	0,00	-10,00	-10,00
metal sheet 2	7	Before test in mm	2,00	2,00	2,00	2,00	2,00	2,00	2,00	2,00
		After test in mm	2,00	2,00	1,99	1,99	2,00	2,00	1,99	1,99
		Difference in µm	0,00	0,00	-10,00	-10,00	0,00	0,00	-10,00	-10,00
metal sheet 3	15	Before test in mm	2,00	2,00	2,00	2,00	2,00	2,00	2,00	2,00
		After test in mm	2,00	2,00	1,99	1,99	2,00	2,00	1,99	1,99
		Difference in µm	0,00	0,00	-10,00	-10,00	0,00	0,00	-10,00	-10,00
metal sheet 4	30	Before test in mm	2,00	2,00	2,00	2,00	2,00	2,00	2,00	2,00
		After test in mm	2,00	2,00	1,99	1,99	2,00	2,00	1,99	1,99
		Difference in µm	0,00	0,00	-10,00	-10,00	0,00	0,00	-10,00	-10,00
metal sheet 5	45	Before test in mm	2,00	2,00	2,00	2,00	2,00	2,00	2,00	2,00
		After test in mm	2,00	2,00	1,99	1,99	2,00	2,00	1,99	1,99
		Difference in µm	0,00	0,00	-10,00	-10,00	0,00	0,00	-10,00	-10,00
metal sheet 6	60	Before test in mm	2,00	2,00	2,00	2,00	2,00	2,00	2,00	2,00
		After test in mm	2,00	2,00	1,99	1,99	2,00	2,00	2,00	1,99
		Difference in µm	0,00	0,00	-10,00	-10,00	0,00	0,00	0,00	-10,00
metal sheet 7	75	Before test in mm	2,00	2,00	2,00	2,00	2,00	2,00	2,00	2,00
		After test in mm	2,00	2,00	1,99	2,00	2,00	2,00	1,99	1,99
		Difference in µm	0,00	0,00	-10,00	0,00	0,00	0,00	-10,00	-10,00
metal sheet 8	90	Before test in mm	2,00	2,00	2,00	2,00	2,00	2,00	2,00	2,00
		After test in mm	2,00	2,00	1,99	1,99	2,00	2,00	2,00	2,00
		Difference in µm	0,00	0,00	-10,00	-10,00	0,00	0,00	0,00	0,00

Table 15.: *Geometric measurement data metal sheet inspection elements*

Inspection element	Measurement	Measurement point						
tube		MP1	MP2	MP3	MP4	MP5	MP6	MP7
	Before test in mm	25,04	24,93	25,11	25,01	24,99	24,88	25,14
	After test in mm	25,03	24,92	25,10	24,96	25,00	24,89	25,09
	Difference in µm	-10,00	-10,00	-10,00	-50,00	10,00	10,00	-50,00
		MP8	MP9	MP10	MP11	MP12	MP13	MP14
	Before test in mm	24,96	25,00	24,88	25,14	24,95	25,00	24,88
	After test in mm	24,96	25,01	24,90	25,14	24,95	25,00	24,89
	Difference in µm	0,00	10,00	20,00	0,00	0,00	0,00	10,00
		MP15	MP16	MP17	MP18	MP19	MP20	
	Before test in mm	25,14	24,96	24,98	24,87	25,14	25,00	
	After test in mm	25,14	24,96	25,00	24,90	25,09	24,97	
	Difference in µm	0,00	0,00	20,00	30,00	-50,00	-30,00	

Table 16.: *Geometric measurement data tube inspection element*

GS35

GIESSEREISANDE | FOUNDRY SANDS

STROBEL QUARZSAND

Chemische Analyse | Chemical analysis

Fe_2O_3	< 0,2 %
Al_2O_3	< 0,2 %
TiO_2	< 0,2 %
SiO_2	> 99,1 %

Physikalische Kenndaten | Physical characteristics

Mittlere Körnung | Medium grain size	0,33 mm
AFS Kennzahl | AFS number	43
Theoretische spezifische Oberfläche | Theoretic specific surface area	71 cm^2/g
Gleichmäßigkeitsgrad | Uniformity ratio	99 %
Glühverlust | Loss on ignition	< 0,2 %
Sinterbeginn | Sintering point	> 1550 °C
Schüttdichte feuergetrocknet | Bulk density fire dried	1,37 to/m^3

Korngrößenverteilung | Grain size distribution

Maschenweite | Mesh Size (mm)	Rückstand | Residue (%)	Summe | Sum (%)	Toleranzbereich | Tolerance range (%)
> 0,710	0,0	100,0	0–1
0,500–0,710	0,5	100,0	0–5
0,355–0,500	40,0	99,5	30–50
0,250–0,355	45,0	59,5	35–50
0,180–0,250	14,0	14,5	5–25
0,125–0,180	0,5	0,5	0–3
0,090–0,125	0,0	0,0	0–1
0,063–0,090	0,0	0,0	0–0,2
0,000–0,063	0,0	0,0	0–0,1

Die angegebenen Daten stellen Jahresdurchschnittswerte dar, eine Verbindlichkeit kann daraus nicht abgeleitet werden.

The shown data represent annual averages, a liability can not be deduced.

STROBEL QUARZSAND GmbH | Freihungsand | 92271 Freihung | Germany | www.strobel-quarzsand.de | info@strobel-quarzsand.de | T: 09646 92010 | F: 09646 1257

STAND 10/2016 | REVISION 10

Siebnummer/ Kornklasse	Maschenweite/ Korngröße	Kornklassen-breite	mittlere Korngröße der i-ten Kornklasse	Leermasse (Sieb)	Leermasse (Sieb) mit Korn	Überkornmasse	relative Überkorn-masse	relative Häufigkeit der Kornklassen	relative Rückstands-summe
i	x_i /[µm]	Δx_i / [µm]	$x_{i\,mittel}$ / [µm]	m_0 / [g]	m_i / [g]	Δm_i / [g]	$\Delta m_i / \sum m_i$ / [ ]	q_i / [µm]	Q_i / [ ]
1	800	-	-	383,33	383,33	0,00	0,0000	-	0,0000
2	630	170	715	255,24	255,24	0,00	0,0000	0,000000	0,0000
3	500	130	565	244,00	244,26	0,26	0,0012	0,000009	0,0012
4	400	100	450	236,95	272,42	35,47	0,1589	0,001589	0,1601
5	315	85	358	224,74	317,50	92,76	0,4155	0,004888	0,5756
6	280	35	298	346,52	379,64	33,12	0,1484	0,004239	0,7239
7	224	56	252	451,79	499,17	47,38	0,2122	0,003790	0,9362
8	180	44	202	330,69	341,80	11,11	0,0498	0,001131	0,9859
9	140	40	160	333,79	336,69	2,90	0,0130	0,000325	0,9989
10	125	15	133	324,48	324,69	0,21	0,0009	0,000063	0,9999
11	100	25	113	216,55	216,58	0,03	0,0001	0,000005	1,0000
12	80	20	90	353,18	353,18	0,00	0,0000	0,000000	1,0000
13	63	17	72	228,73	228,73	0,00	0,0000	0,000000	1,0000
14	40	23	52	261,03	261,03	0,00	0,0000	0,000000	1,0000
Pfanne	0	40	20	192,56	192,56	0,00	0,0000	0,000000	1,0000
Summe (∑)						223,24	1,0000		

Einwaage / [g]	223,59
Fehlkornmasse / [g]	0,35
Siebzeit / [min]	20
Siebintensität / [%]	30

Auftraggeber:	Mauschitz
Projektnummer:	-
Analysedatum:	03. Oktober 2022
Analysesubstanz:	Quarzsand

MASTERSIZER 2000

Analyse Report

Probenname:	Gemitteltes Ergebnis	**SOP Name:**	SiO2 Mikrorinne (Mayschitz, Mayer) 5	**Gemessen:**	Monday, October 03, 2022 9:31:52 AM
Probenherkunft:	Factory = Mayer	**Operator:**	gmausch	**Berechnet:**	Monday, October 03, 2022 9:31:53 AM
Probenreferenz:	A			**Datenursprung:**	Gemittelt

Probenmaterial:	Silica 0.1			**Dispergiermodul:**	Scirocco 2000 (B)	**Abschattung:**	1.47 %
Partikel RI:	1.544	**Absorption:**	0.1	**Analysemodell:**	Monomodale Verteilung		
Dispergierfluid:				**Meßbereich:**	0.020 to 2000.000 um	**Fit(gewichtet):**	1.534 %
Fluid RI:	1.000			**Emulation:**	Aus		

Konzentration:	0.0138	%Vol	**Vol. Mittelwert D[4,3]:**	342.278	um	**Spezifische Oberfläche:**	0.0214 m²/g
Breite :	0.851		**Gleichförmigkeit:**	0.268		**D[3,2]:**	279.893 um
Verteilungsart:	Volumen						

d(0.1): 202.309 um **d(0.5): 339.622 um** d(0.9): 491.422 um

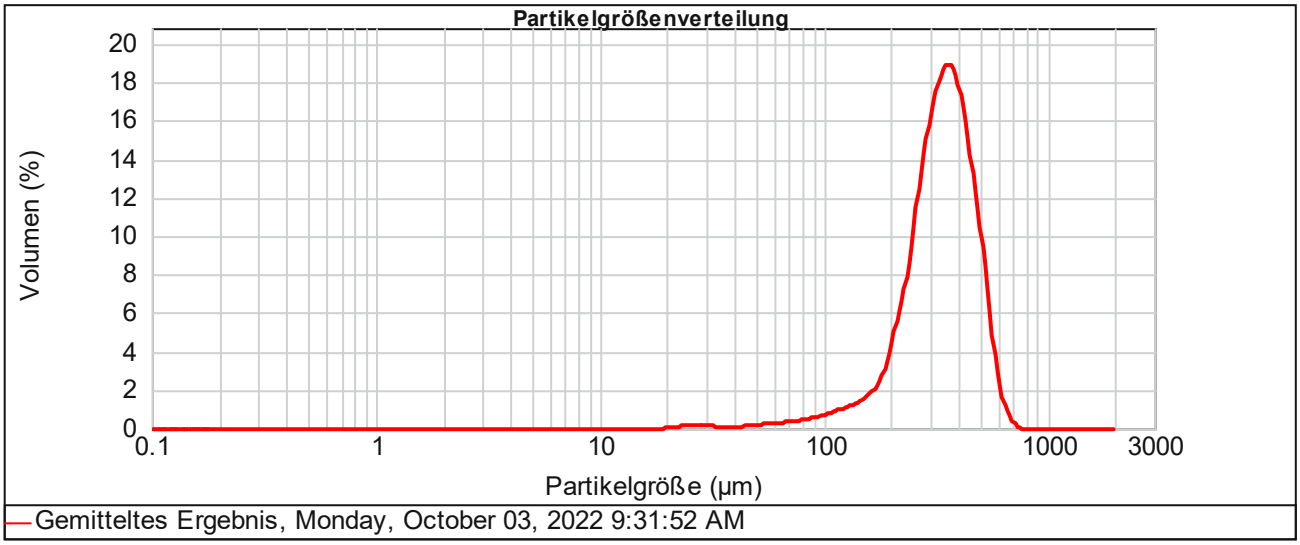

Größen-	Häufigkeit (%)	Größen-	Häufigkeit (%)	Größen-	Häufigkeit (%)	Größen-	Häufigkeit (%)	Größen-	Häufigkeit (%)	Größen-	Häufigkeit (%)
0.020	0.00	0.142	0.00	1.002	0.00	7.096	0.00	50.238	0.16	355.656	14.12
0.022	0.00	0.159	0.00	1.125	0.00	7.962	0.00	56.368	0.20	399.052	12.37
0.025	0.00	0.178	0.00	1.262	0.00	8.934	0.00	63.246	0.24	447.744	9.32
0.028	0.00	0.200	0.00	1.416	0.00	10.024	0.00	70.963	0.29	502.377	5.91
0.032	0.00	0.224	0.00	1.589	0.00	11.247	0.00	79.621	0.36	563.677	2.00
0.036	0.00	0.252	0.00	1.783	0.00	12.619	0.00	89.337	0.47	632.456	0.55
0.040	0.00	0.283	0.00	2.000	0.00	14.159	0.00	100.237	0.60	709.627	0.00
0.045	0.00	0.317	0.00	2.244	0.00	15.887	0.00	112.468	0.75	796.214	0.00
0.050	0.00	0.356	0.00	2.518	0.00	17.825	0.00	126.191	0.90	893.367	0.00
0.056	0.00	0.399	0.00	2.825	0.00	20.000	0.00	141.589	1.14	1002.374	0.00
0.063	0.00	0.448	0.00	3.170	0.00	22.440	0.03	158.866	1.54	1124.683	0.00
0.071	0.00	0.502	0.00	3.557	0.00	25.179	0.10	178.250	2.39	1261.915	0.00
0.080	0.00	0.564	0.00	3.991	0.00	28.251	0.11	200.000	4.23	1415.892	0.00
0.089	0.00	0.632	0.00	4.477	0.00	31.698	0.10	224.404	6.12	1588.656	0.00
0.100	0.00	0.710	0.00	5.024	0.00	35.566	0.07	251.785	9.52	1782.502	0.00
0.112	0.00	0.796	0.00	5.637	0.00	39.905	0.06	282.508	12.20	2000.000	0.00
0.126	0.00	0.893	0.00	6.325	0.00	44.774	0.07	316.979	13.98		
0.142	0.00	1.002	0.00	7.096	0.00	50.238	0.11	355.656			

Kommentar: *Mittelwert der 4-Messungen aus SiO2 Wärmeträger*

OCHSNER

Bitte sofort weiterleiten !

OCHSNER Gesellschaft mbH & CoKG
Oberfeldstraße 8 , A- 4024 Linz

TELEFON: (0732) 47 2 88
TELEX : 021439OCHSNR A
TELETEX: 232-3732305 OCHSNER
TELEFAX: (0732) 46 3 40

****
* T E L E F A X *
****

DATUM: 1990-07-05

SEITE 1 VON 2

VON: OCHSNER / Hr. Habinger
AN: INSTITUT FÜR TECHNISCHE WÄRMELEHRE
Hr. D.I. Haider

BETRIFFT: Ihre Anfrage Drehkolbengebläse
Unser Angebot Nr. 1/4662/13

Wir danken für Ihre Anfrage und bieten zu den Allgem. Liefer - bedingungen der Firma Ochsner GesmbH an:

DREHKOLBENGEBLÄSEAGGREGAT

Type		RB101V	RB120V
Stückzahl		1	1
Volumenstrom	m3/h	3420	
Fördermedium		Luft	
Ansaugdruck	bar abs	1	
Verdichtungsdruck	bar abs	1,3	
Ansaugtemperatur	Grad C	20	
Förderrichtung		vertikal	
Gebläsedrehzahl	1/min	2210	1560
Antrieb		Keilriemen	
eff. Wellenleistung	kW	34.5	35.9
erf. Motorleistung	kW	45	55 (45)
Motordrehzahl	1/min	3000	1500
Motorbaugröße		225M	250M
Geräuschpegel	ca. dB(A)	95	93
Temperaturerhöhung	ca.Grad C	28	28
Flanschanschluß	DN mm	200	250
Gewicht der Stufe	ca. kg	400	620
Gewicht des Aggregats	ca. kg	1600	2550

Gebläseaggregat bestehend aus:
Gebläsestufe, Grundrahmen mit integriertem Druckschalldämpfer, Ansaugschalldämpfer mit integriertem Ansaugfilter(bei Gebläse RB101V in gerader Ausführung,bei Geblase RB120V winkelig), Rueckschlagklappe, Sicherheitsventil, Kompensator mit Schlauchanschluß, elastische Maschinenfüsse

OCHSNER

Bitte sofort weiterleiten !

OCHSNER Gesellschaft mbH & CoKG
Oberfeldstraße 8 , A- 4024 Linz

TELEFON: (0732) 47 2 88
TELEX : 021439OCHSNR A
TELETEX: 232-3732305 OCHSNER
TELEFAX: (0732) 46 3 40

****
* T E L E F A X *
****

DATUM: 1990-07-05

SEITE 1 VON 2

VON: OCHSNER / Hr. Habinger
AN: INSTITUT FÜR TECHNISCHE WÄRMELEHRE
Hr. D.I. Haider

BETRIFFT: Ihre Anfrage Drehkolbengebläse
Unser Angebot Nr. 1/4662/13

Wir danken für Ihre Anfrage und bieten zu den Allgem. Liefer - bedingungen der Firma Ochsner GesmbH an:

DREHKOLBENGEBLÄSEAGGREGAT

Type		RB101V	RB120V
Stückzahl		1	1
Volumenstrom	m3/h	3420	
Fördermedium		Luft	
Ansaugdruck	bar abs	1	
Verdichtungsdruck	bar abs	1,3	
Ansaugtemperatur	Grad C	20	
Förderrichtung		vertikal	
Gebläsedrehzahl	1/min	2210	1560
Antrieb		Keilriemen	
eff. Wellenleistung	kW	34.5	35.9
erf. Motorleistung	kW	45	55 (45)
Motordrehzahl	1/min	3000	1500
Motorbaugröße		225M	250M
Geräuschpegel	ca. dB(A)	95	93
Temperaturerhöhung	ca.Grad C	28	28
Flanschanschluß	DN mm	200	250
Gewicht der Stufe	ca. kg	400	620
Gewicht des Aggregats	ca. kg	1600	2550

Gebläseaggregat bestehend aus:
Gebläsestufe, Grundrahmen mit integriertem Druckschalldämpfer, Ansaugschalldämpfer mit integriertem Ansaugfilter(bei Gebläse RB101V in gerader Ausführung,bei Gebläse RB120V winkelig), Rueckschlagklappe, Sicherheitsventil, Kompensator mit Schlauchanschluß, elastische Maschinenfüsse

Druckschalter
Top-Qualität
zu fairen Preisen

SKV-tec

PSW-A3

Dieser Druckschalter ist mit einem Drehregler zur einfachen Einstellung des Schaltpunktes ausgestattet. Üblicherweise wird dieser Schalter zur Überwachung des Luftstromes in Lüftungsanlagen und Wärmetauschern eingesetzt. Die Schalthysterese kann mit einer Schraube eingestellt werden. Durch die mitgelieferte Kunststoffabdeckung wird die Schutzklasse IP54 erreicht. Der Schalter ist als Wechselschalter verfügbar. Montage mit Membran in vertikaler Position, die Anschlüsse sind beschriftet.
Achtung: Durch den geringen Bauraum sind gewinkelte 6,3 mm Stecker notwendig. Gerade 6,3 mm Stecker können den Schalter beschädigen. Die Kontakte dürfen nicht verbogen werden!

Technische Daten

Medium	Luft, andere, nicht brennbare und nicht aggressive, Gase
Druckschaltpunkt	0,2 – 50 mbar (voreingestellte Hysterese: 0,1, 0,2, 1, 1,5 und 2,5 mbar)
Maximaler Betriebsdruck	100 mbar
Schutzart	IP54 (mit Abdeckung)
Betriebstemperaturbereich	-20 °C - +85°C
Elektrische Bauweise	Einpoliger Wechselschalter
Elektrische Anschlüsse	6,3 mm
Anschluss Medium	6,0 mm Außendurchmesser
Zulässige Stromstärke	1,5A (0,4A) bei 250V
Elektrischer Anfangswiderstand	< 50 mΩ
Montageposition	Membran in vertikaler Position
Toleranz	±15%
Größe	104x86x57mm

Modell	**Druckbereich**	**Hysterese**
PSW-A3-02	0,2 ~ 2 mbar	0,1 mbar
PSW-A3-03	0,3 ~ 3 mbar	0,1 mbar
PSW-A3-04	0,4 ~ 4 mbar	0,2 mbar
PSW-A3-05	0,5 ~ 5mbar	0,2 mbar
PSW-A3-10	2 ~ 10 mbar	1 mbar
PSW-A3-25	5 ~ 25 mbar	1,5 mbar
PSW-A3-50	10 ~ 50 mbar	2,5 mbar

Anschlussset

Stand: 11/2020; Änderung vorbehalten, Right of modification reserved, Sous réserve des modifications

SKV-tec GmbH
Forchheimer Str. 4
91338 Igensdorf - Germany
Tel.: +49 – (0) 9192- 995314 / Fax: 995268

Geschäftsführer:
Dipl.-Ing. (FH) Thomas Jakob und Dipl.-Ing.(FH) Robert Krämer
Handelsregister:
Bamberg, HRB 6436

www.druckschalter.shop
info@skv-tec.de
Onlineshop:
www.druckschalter.shop

Anschlussschema:

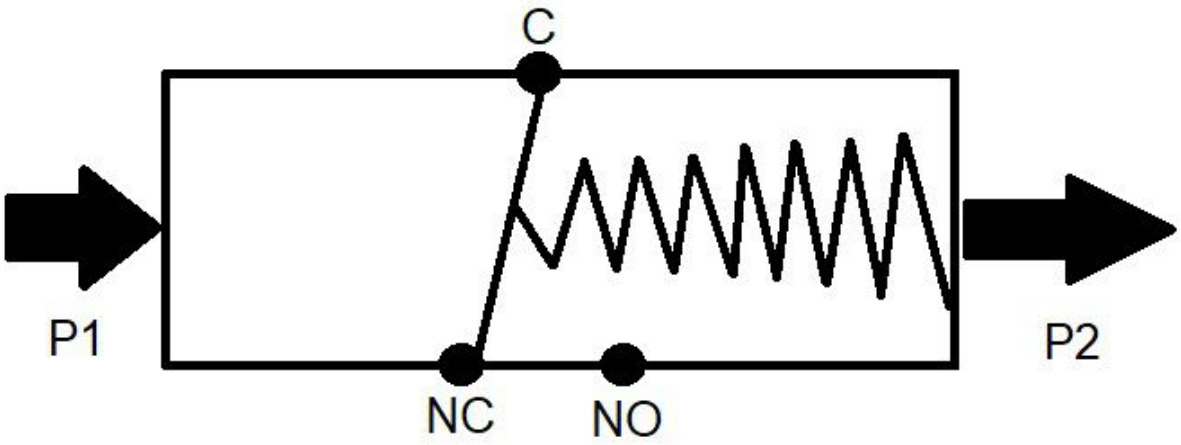

P1, P2: Mediumanschlüsse
C, NC, NO: elektrische Anschlüsse
Diese Anschlussbezeichnungen sind auf dem Druckschalter lesbar.

SKV-tec GmbH
Forchheimer Str. 4
91338 Igensdorf - Germany
Tel.: +49 – (0) 9192- 995314 / Fax: 995268

Geschäftsführer:
Dipl.-Ing. (FH) Thomas Jakob und Dipl.-Ing.(FH) Robert Krämer
Handelsregister:
Bamberg, HRB 6436

www.druckschalter.shop
info@skv-tec.de
Onlineshop:
www.druckschalter.shop

Einfach
besser messen

SCHMIDT® Technology

SCHMIDT® InLine-Volumenstromsensor

Kürzeste Ein- und Auslaufstrecken durch Multi-Point-Measurement

- Direkte Messung von Normvolumenstrom und Mediumstemperatur
- Geringer Druckverlust
- Modular erweiterbar
- Einfacher Einbau, integrierte Mess-Strecke
- **Höchste Messgenauigkeit**, selbst in Verbindung mit **Strömungshindernissen**

Optimaler Einsatz zur Verbrauchs- und Durchflussmessung bei Gasen und für druckluftbetriebene Werkzeuge und Maschinen

Multi-**P**oint-**M**easurement – Funktionsprinzip

Das bewährte und bekannte Messverfahren der thermischen Anemometer wurde in den neuen **SCHMIDT® InLine-Volumenstromsensor** gleich vierfach integriert.

Durch die vier parallel erzeugten Messwerte in Verbindung mit intelligenten Algorithmen zur Bewertung der Messergebnisse können **selbst für unzureichende Ein- und Auslaufstrecken** korrekte und verlässliche Strömungswerte ermittelt und ausgegeben werden.

Die radiale Anordnung der vier Messpunkte verbessert die Erfassung bei nicht optimal ausgebildetem Strömungsprofil. Die Strömungselemente sind dabei geschützt in der Mess-Strecke positioniert.

Auf zwei parallel verlaufenden Sensorträgern sind vier hochgenaue und voneinander unabhängig arbeitende Strömungsfühler im Sensorrohr untergebracht. Das Temperatursensorelement zur Ermittlung der Mediumstemperatur sitzt auf einer separaten, zentral angeordneten Sensorzunge.
Jeder der Strömungsfühler wird mittels elektrischer Beheizung auf eine feste Übertemperatur zur Umgebung gebracht. Die benötigte Leistung zur Aufrechterhaltung der Übertemperatur ist ein Maß für die Strömungsgeschwindigkeit des Mediums, die der Sensor als „Normvolumenstrom" ausgibt (lineares Strom- / Impulssignal).
Dies ist ein großer Vorteil des Messprinzips: Eine zusätzliche Messung von Druck oder Temperatur des Mediums und damit einhergehende Berechnungen sind nicht erforderlich.

Der Profi für Industrieprozesse und Druckluft-Technik

Der thermische **SCHMIDT® InLine-Volumenstromsensor** ist die robuste Lösung für anspruchsvolle Industrieeinsätze. Er kann für unterschiedliche Anwendungen wie Druckluftüberwachung, Gasüberwachung bei Prozess-Brennern, Verbrauchserfassung von Gasen und vieles mehr eingesetzt werden (nicht für ATEX-Anwendungen bzw. brennbare Gase). Der Sensor erfasst neben dem Volumenstrom auch Medientemperaturen von -20 °C bis +60 °C.

Der **SCHMIDT® InLine-Volumenstromsensor** verfügt über vier integrierte Duo-LEDs als quasi-analoge Anzeige der Strömung sowie zur Darstellung des Betriebszustands des Sensors. Die Messwerte für Volumenstrom und Mediumstemperatur werden parallel über zwei Signalausgänge zur Verfügung gestellt. Über einen zweiten Steckverbinder können diverse, als Zubehör erhältliche Module zur Anzeige oder Weitergabe der Daten angeschlossen werden.

Der **Einbau des Sensors ist denkbar einfach**: Einschrauben des Sensors in die vorhandene Druckleitung, elektrisch anschließen – fertig. Der Sensor arbeitet ohne bewegliche Teile und aufgrund des Messprinzips gibt es keinerlei Drift- oder Alterungserscheinungen. Somit reduziert sich der Wartungsaufwand.

Sensor	Außendurchmesser	Messbereich
IL 30.005	DN 15	76,3 Norm-m³/h [1]
IL 30.010 MPM	DN 25	229 Norm-m³/h [1]
IL 30.015 MPM	DN 40	417 Norm-m³/h [1]
IL 30.020 MPM	DN 50	712 Norm-m³/h [1]

[1] Bezogen auf Normbedingungen: T_N = 20 °C und p_N = 1.013,25 hPa

Betriebstemperatur	-20 … +60 °C
Messgenauigkeit Flow	±(3 % vom MW + 0,3 % vom MB)
Messgenauigkeit Temperatur	≤ ±2 °C (bei Volumenstrom > 2 % v. E.)
Ausgang 1 (OUT 1)	4 … 20 mA Volumenstrom
Ausgang 2 (OUT 2)	4 … 20 mA Mediumstemperatur
Impulsausgang	Anschluss eines Verbrauchszählers
Druckfestigkeit	16 bar
Medium	saubere Druckluft, Stickstoff, andere Gase auf Anfrage (nicht für ATEX-Anwendungen geeignet); nicht kondensierend (bis 95 % rF)

Haben wir Ihr Interesse geweckt? Weitere Informationen erhalten Sie auf unserer Homepage **www.schmidt-sensoren.de** oder von Herrn Oliver Joos, Telefon 07724/899198, o.joos@schmidttechnology.de

Form 1112/01/2020/500/2 · Art.-Nr. 560580.01 · Technische Änderungen vorbehalten.

Bestellinformation SCHMIDT® InLine-Volumenstromsensor

Typ	Artikel Nr.	Messbereiche	Anschluss	Länge ohne Rohre
SCHMIDT IL 30.005	550 250	76,3 Norm-m³/h	DN 15 / R 1/2	100 mm
SCHMIDT IL 30.010 MPM	550 251	229 Norm-m³/h	DN 25 / R 1	100 mm
SCHMIDT IL 30.015 MPM	550 252	417 Norm-m³/h	DN 40 / R 1 1/2	100 mm
SCHMIDT IL 30.020 MPM	550 253	712 Norm-m³/h	DN 50 / R 2	100 mm
Zubehör	523 565	Anschlusskabel 5-polig, Kabellänge 5 m, offene Kabelenden		
	523 566	Anschlusskabel 5-polig, Länge wählbar, mit Aderendhülsen, halogenfrei (2 … 100 m; 1 m-Schritte)		
	523 562	Kupplungsdose, 5-polig, mit Schraubklemmen, Kabel-Ø 4 ... 6 mm		
	535 282	Netzteil 24 V / 1 A DC (geregelt), Versorgung 115 / 230 V AC, Klemmleistenanschluss		
	556 954	Messstreckenverlängerungsrohr DN 15 (1 Satz)		
	556 955	Messstreckenverlängerungsrohr DN 25 (1 Satz)		
	556 956	Messstreckenverlängerungsrohr DN 40 (1 Satz)		
	556 957	Messstreckenverlängerungsrohr DN 50 (1 Satz)		
	559 340	Austauschrohrsatz DN 15 für Ersatz Vorgänger-Modell SS 30.300		
	559 341	Austauschrohrsatz DN 25 für Ersatz Vorgänger-Modell SS 30.301		
	559 550	Austauschrohrsatz DN 40 für Ersatz Vorgänger-Modell SS 30.302		
	559 551	Austauschrohrsatz DN 50 für Ersatz Vorgänger-Modell SS 30.303		
	531 394	Montagesatz für Rohranbau passend für MD 10.010 / 10.015, mit Schlauchschellen und Band zum Anpassen an den Rohr-Durchmesser		
	554 900	Messwert-Anzeige-Modul MD 10.020, 7-Segment-Anzeige, inkl. 0,6 m Anschlusskabel zum Anschluss am Modulstecker		
	527 320	LED-Anzeige MD 10.010; im Wandgehäuse zur Visualisierung von Volumenstrom und Strömungsgeschwindigkeit, 85 … 230 V AC und Sensorspeisung		
	528 240	LED-Anzeige MD 10.010; wie 527 320, jedoch mit 24 V DC Spannungsversorgung		
	527 330	LED-Anzeige MD 10.015; wie 527 320, jedoch mit zusätzlicher Summenfunktion und 2. Messeingang		
	528 250	LED-Anzeige MD 10.015; wie 527 330, jedoch mit 24 V DC Spannungsversorgung		
ISO Kalibrier-Zertifikat	556 958-1	IL 30.005 / 76,3 Norm-m³/h		4 Kalibrierpunkte
	556 959-1	IL 30.010 MPM / 229 Norm-m³/h		4 Kalibrierpunkte
	556 960-1	IL 30.015 MPM / 417 Norm-m³/h		4 Kalibrierpunkte
	556 961-1	IL 30.020 MPM / 712 Norm-m³/h		4 Kalibrierpunkte

Kalinsky Sensor Elektronik
GmbH & Co. KG
Drucksensortechnik
Mittelhäuser Strasse 87 D-99089 Erfurt
Telefon: 0361 / 7451311
Fax: 0361 / 7917813
E-Mail: dietrich.kalinsky@t-online.de
Internet: www.drucksensorik.de

Datenblatt Drucksensor DS2

Beschreibung:
Die Baureihe DS2 wird für Anwendungen mit Druckbereichen zwischen 2,5 mbar und 1 bar angeboten. Die Drucksensoren der Reihe DS2 messen Differenz-, Über- und Unterdruck oder Volumenstrom in Luft und nicht aggressiven Gasen. Die Messwerte werden als 0-10 V, 4-20 mA- oder 0-10 kHz- Signal ausgegeben.
Piezoresistive Messelemente sichern eine hohe Zuverlässigkeit und Genauigkeit. Das robuste Aluminium-Druckgussgehäuse garantiert eine hohe mechanische Stabilität und gute EMV-Eigenschaften.

Anwendung:

- Ansteuerung von Gebläsen
- Überwachung von Luftfiltern
- Maschinen- und Anlagenbau
- Umwelttechnik
- Niveauüberwachung von Flüssigkeiten
- Überwachung von Luftströmungen

Bestellschlüssel:

- DS2-010 0-10 V-Ausgang
- DS2-420 4-20 mA-Ausgang

Technische Daten für Typ DS 2-010 und DS 2-420 (Differenzdruck):

Druck-bereich [mbar]	Druck-bereich [kPa]	Über-last-barkeit [mbar]	Lineari-tätsfehler max. [± % v. EW]	Temperatur-fehler max. [± % v. EW] 0-50 °C	Langzeit-stabilität [% v. EW /Jahr]	Wiederhol-genauigkeit [% v. EW]	Ansprech-zeit [s] mit Dämpfung
0 - 2.5	0 - 0.25	350	1.0	3.5	2	0.3	2,5
0 - 5	0 - 0.5	350	1.0	2.5	2	0.3	2,5
0 - 10	0 - 1	350	1.0	1	0.5	0.2	2,5
0 - 25	0 - 2.5	350	0.8	1	0.5	0.1	2,5
0 - 50	0 - 5	350	0.8	1	0.5	0.1	2,5
0 - 100	0 - 10	350	0.8	1	0.5	0.1	2,5
0 - 250	0 - 25	4-fach	0.5	1	0.1	0.1	2,5
0 - 500	0 - 50	4-fach	0.5	1	0.1	0.1	2,5
0 - 1000	0 - 100	2-fach	0.5	1	0.1	0.1	2,5

Technische Daten DS 2 mit elektron. Korrektur des Linearitätsfehlers (Differenzdruck):

0 - 100	0 - 10	350	0.2	1	0.1	0.1	2,5
0 - 250	0 - 25	4-fach	0.2	1	0.1	0.1	2,5
0 - 500	0 - 50	4-fach	0.2	1	0.1	0.1	2,5
0 - 1000	0 - 100	2-fach	0.2	1	0.1	0.1	2,5

Ansprechzeit ohne Dämpfung: ca. 50 ms Für Sonderbereiche erbitten wir Ihre Anfrage

Kalinsky Sensor Elektronik
GmbH & Co. KG
Drucksensortechnik
Mittelhäuser Strasse 87 D-99089 Erfurt
Telefon: 0361 / 7451311
Fax: 0361 / 7917813
E-Mail: dietrich.kalinsky@t-online.de
Internet: www.drucksensorik.de

Datenblatt Drucksensor DS2

Betriebstemperaturbereich: -20 bis +50 °C

Hysterese: 0.1%

Medium: Luft, alle nicht aggressiven Gase

Ausgangssignale und Versorgungsspannungen:

DS 2-010:	0-10 V	R_L >= 2 kΩ	24 VDC/AC +/-10%
DS 2-420:	4-20 mA	R_B <= 400 Ω	15-30 VDC

Anschlüsse:
Elektrisch: Schraubklemmen für 0.14-1.5 mm^2
Pneumatisch: 2 Anschlüsse für Schlauch mit 6 mm oder 4 mm Innendurchmesser
Kabelverschraubung: PG7

Anschlussbelegung DS 2-010: Printklemme:
1 : + 24 VDC/AC
2 : Output 0 - 10 V
3 : GND

Anschlussbelegung DS 2- 420: Printklemme:
1 : + 24 VDC *
2 : output 4-20 mA *

* Durch eine spezielle Zusatzschaltung kann es nicht zur Beschädigung des Sensors durch falsche Anschlussbelegung kommen. Die beiden Anschlüsse sind daher vertauschbar. Zwischen Anschluss 2 und dem Masseanschluss der Spannungsversorgung muss bei einer Spannung von + 24 V DC ein Bürdenwiderstand R_B <= 400 Ω geschaltet werden.

Gewicht: ca. 170 g

Schutzart: IP65

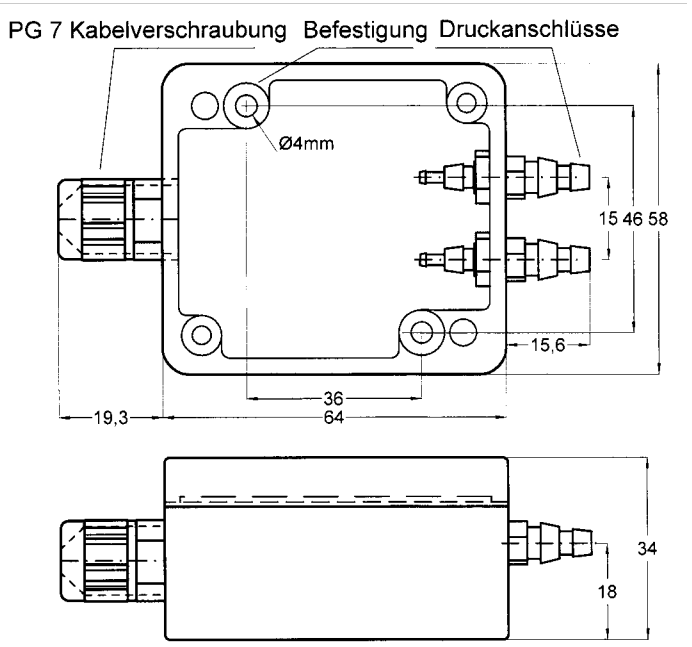

B. Heat transfer test rig

Calculation of the sintered plate heat transfer test rig

Input data:

Cross sectional area of the fluidized bed: $A_B := \frac{200mm \cdot 360mm}{2} = 0.036\,m^2$

Bedheight of the silica sand: $h_B := 0.5m$

Bulk density of the silica sand: $\rho_{Sand} := 1325 \frac{kg}{m^3}$

Temperature of the air: $T_{Luft} := 640\,°C$

Density of the airt: $\rho_{Luft} := 0.3815 \frac{kg}{m^3}$

Dynamic viscosity of the fluidizing air: $\eta_{Luft} := 4.0776 \cdot 10^{-5} Pa \cdot s$

Minimal fluidization velocity
(particle diameter, particle density, Temperatur) $u_{mf} := 0.0096 \frac{m}{s}$

Keydata of the sintered plate heating side

Degree of fluidization: $FG_{heat} := 4.5$

Material: SIKA-R 7 AX

Viscosity coefficient: $\psi_{v.heat} := 2.5 \cdot 10^{-12} m^2$

Permeability coefficient $\psi_{p.heat} := 15 \cdot 10^{-7} m$

Keydata of the sintered plate cooling side

Degree of fluidization: $FG_{cool} := 2$

Material: SIKA-R 5 AX

Viscosity coefficient: $\psi_{v.cool} := 0.8 \cdot 10^{-12} m^2$

Permeability coefficient $\psi_{p.cool} := 2 \cdot 10^{-7} m$

Calculation:

Pressure drop bed:

$$\Delta p_B := \rho_{Sand} \cdot g \cdot h_B = 6496.9056\ Pa$$

Required pressure drop sintered plate:

$$\Delta p_{sinter.req} := 0.3 \cdot \Delta p_B = 1949.0717\ Pa$$

Volumetric flow rate heating side:

$$V_{Punkt.heat} := A_B \cdot u_{mf} \cdot FG_{heat} = 0.00156 \cdot \frac{m^3}{s}$$

Volumetric flow rate heating side:

$$V_{Punkt.cool} := A_B \cdot u_{mf} \cdot FG_{cool} = 0.00069 \cdot \frac{m^3}{s}$$

Sintered plate thickness according to DIN EN ISO 4022:

Defined plate thickness:

$$e_{sinter} := 6mm$$

Pressure drop across the sintered plate heating side:

$$\Delta p_{sinter.heat} := e_{sinter} \cdot \left(\frac{V_{Punkt.heat} \cdot \eta_{Luft}}{A_B \cdot \psi_{v.heat}} + \frac{V_{Punkt.heat}^2 \cdot \rho_{Luft}}{A_B^2 \cdot \psi_{p.heat}} \right)$$

$$\Delta p_{sinter.heat} = 4230.5036\ Pa$$

Relative pressure drop heating side:

$$\frac{\Delta p_{sinter.heat}}{\Delta p_B} = 0.6512$$

Total pressure drop heating side:

$$\Delta p_{Gesamt.heat} := \Delta p_{sinter.heat} + \Delta p_B = 0.1073 \cdot bar$$

Pressure drop across the sintered plate cooling side:

$$\Delta p_{sinter.cool} := e_{sinter} \cdot \left(\frac{V_{Punkt.cool} \cdot \eta_{Luft}}{A_B \cdot \psi_{v.cool}} + \frac{V_{Punkt.cool}^2 \cdot \rho_{Luft}}{A_B^2 \cdot \psi_{p.cool}} \right)$$

$$\Delta p_{sinter.cool} = 5875.9631\ Pa$$

Relative pressure drop cooling side:

$$\frac{\Delta p_{sinter.cool}}{\Delta p_B} = 0.9044$$

Total pressure drop cooling side:

$$\Delta p_{Gesamt.cool} := \Delta p_{sinter.cool} + \Delta p_B = 0.1237 \cdot bar$$

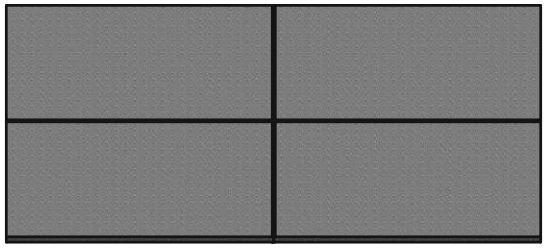

(1:4)

SIKA-HC5/HC7

Pos	Menge	Sachnummer	Benennung	Material	Teile-Nr.
2	2	WZ 3549	Platte 122,5x200	Hastelloy C276 (2.4819)	
1	2	WZ 3549	Platte 122,5x200	Hastelloy C276 (2.4819)	

Maße ohne Toleranzangabe für gesinterte Werkstoffe nach ISO 2768-v

Maße ohne Toleranzangabe nach ISO 2768-m

	Datum	Name
Gez.	07.01.2022	K.Bozaci
Gepr.		
Norm		

Maßstab 1:2 | Masse 3,64111 kg

Material:

Material:

Platte 245x400

GKN SINTER METALS FILTERS

Angebotszeichung | 1 von 1 | A3

Status | Änderungen | Datum | Name

Kundenzeichnung:

		Project	Electrical High Temperature Sand Heater for Laboratory Test Rig	
		Equipment	Electrical High Flux Heating Rods	
		Vulcanic Ref	A670908A1	
		Date	28.01.2022	
		Revision	A	
1	Datasheet No.	UNIT	112331-91	
2	Inquiry Number / Customer Data sheet		Specification No. 2	
3	Product		High flux heating rod - Finned Element	
4	Installation		Laboratory Rig	
5	Quantity		1	
6	PROCESS DATA			
7	Heated Fluid		Sand	
8	Fluid state		Solid	
9	Nominal flow rate	kg/h	To be Defined	
10	Min. Operating Temperature	°C	400	
11	Max. Operating Temperature	°C	650	
12	Operating pressure	bar (g)	atmospheric	
13	Specific Heat	kJ/kg.°C @ T	N/A	
14	Density ρ	kg/m3 @ T	N/A	
15	Thermal Conductivity λ	Wx(m°.C)	N/A	
16	Viscosity μ	cP @ T	N/A	
17	Minimum required heat duty	W	1 000	
18	Maximum required heat duty (kW)	W	7 065	
19	Power Voltage Supply	**1ph+N (Single phase)**	230	
20	Notes		the overall task is to heat up sand at varying temperature differences between fin tube surface temperature and sand bulk temperature. • Design point 1: T-sand=400 /T-tube=700°C => max. Power = 7kW • Design point 2: T-sand=500 /T-tube=700°C • Design point 3: T-sand=600 /T-tube=800°C • Design point 4: T-sand=650 /T-tube=800°C • Design point 5: T-sand=650 /T-tube=700°C => min Power = 1.2 kW	
21			The tube heater temperature should be controllable to a constant value comprised between 500°C and 800°C.	
22			Depending on the bed temperature and the heater surface temperature, the electric duty of one heater tube will vary in the range from 1. to 7. kW.	
23			Number of cycle (ON/OFF): around 200	
24	DESIGN DATA			
25	Heating rod heating capacity (+/-5%)	W	10 600	
25	Heater Mounting		Horizontal	
26	Area		Safe area - Laboratory	
27	Location		Indoor	
29	Extreme ambient temperature limits	°C	10 / 30	
32	Design current for the whole heater	A	54	
33	Design Temperature of the heating part	°C	10 / 800	
34	Design pressure	bar (g)	Atmospheric (to be confirmed)	
35	Min/Max. Voltage Variation		To be Defined	
36	Min/Max. Frequency Variation		To be Defined	
37	Design and Construction code		as per manufacturer standards	
38	U-Stamp		N/A	
40	Certification		N/A	
41	Corrosion allowance (mm)	mm	0	
42	FITTING FEATURES			
43	Mounting		Onto a frame (by Others)	
44	Heater flange/Fitting type		Flange Standard: DIN EN 1092-1 / Type: 05 / Size: DN25 / Rating: PN6	
45	Flange Machining/Drilling		As per client's requirements and drawing	
46	Lifting Lugs		Not fitted	
47	HEATING ELEMENT FEATURES			
48	Heating element total quantity per bundle		1	
49	Heating element type		High-Flux type	
50	Heating element power	W	10 600,00	
51	Unit voltage supply	1ph+N (Single phase)	230	
52	Heating Element Outer Diameter (OD)	mm	19	
53	Heating length Lc	mm	360	
54	Inactive length Nct (Terminal connection side)	mm	150	
55	Inactive length Ncp (heating rod end side)	mm	50	

		Project	Electrical High Temperature Sand Heater for Laboratory Test Rig	
		Equipment	Electrical High Flux Heating Rods	
		Vulcanic Ref	A670908A1	
		Date	28.01.2022	
		Revision	A	
1	Datasheet No.	UNIT	112331-91	
2	Inquiry Number / Customer Data sheet		Specification No. 2	
3	Product		High flux heating rod - Finned Element	
4	Installation		Laboratory Rig	
5	Quantity		1	
56	Surface load on the sheath @ installed power	W/cm2	49,35	
57	Heating element features		80-20 Ni/Cr Resistive wire	
58	Electrical Insulator		High compacted BN	
59	Heating element Terminal sealing		Weather-proof epoxy seals	
60	Finned element		Yes	
61	Type		Washer type	
62	Fin OD1	mm	39	
63	Fin ID	mm	19	
64	Fin Thickness	mm	2	
65	Pitch P	mm	9	
66	Fins Qty		40	
67	Exchange surface (Plain tube)	cm2	215	
68	Exchange surface (tube with fins)	cm2	1 098	
69	Surface load on the sheath @ installed power	W/cm2	49,4	
70	Surface load on the fins @ installed power	W/cm2	9,7	
71	OFFSET ASSEMBLY AND HEATER ENCLOSURE			
72	Junction box offset length (B)	mm	400	
73	Construction type		N/A	
74	Anti-radiation Shield		Not fitted	
75	Heater Enclosure Type		as per Manufacturer Standards	
76	Power Stage Quantity Per Flange Heater		1	
77	Design current	A	54	
78	IP rating		IP54	
79	Space heater	W	N/A	
80	Cable gland(s) for power connection		Fitted	
81	Size and type		To be defined	
83	Cable gland(s) for space heater		N/A	
84	Size and type		N/A	
81	Breather / Drain		Not fitted	
82	Notes		The area "B" between flange and terminal box can be hot in operating conditions. There is risk of burns in case of accidental contact. Precautions shall be taken by Client to protect the personal against accidental contact when the heating rod is in operation.	
83	INSTRUMENTATION			
84	Heating rod wire over temperature safety		1 Piece	
86	Location		in thermowell located in the center of the heating rod	
85	Measuring the temperature of		resistive wire(s)	
86	Distance of the sensing point from flange face		310	
87	Heating rod internal sheath over temperature safety		1 Piece	
88	Location		in thermowell located onto the internal wall of the of the heating rod sheath	
89	Measuring the temperature of		internal skin temperature	
90	Distance of the sensing point from flange face		310	
91	Sensors type		K-type metal sheathed mineral insulated cable	
92	Hot junction style		ungrounded - Simplex	
93	Standard		IEC 60584, Class 1	
93	Removable sensors		**Yes**	
94	Connection of the sensors		K-type therminals in the main terminal box of the heating rod	
95	Temperature transmitter		N/A	
97	MATERIAL			
98	Heating rod sheath		Inconel 600 - Seamless type	
99	Sheath thickness	mm	2,60	
100	Sheath tip		Inconel 600 (machined and welded to the rod sheath)	
101	Rod fitting / Flange		Inconel 600	
102	Fins		Inconel 600	
106	Heater enclosure		Aluminium or painted carbon steel or Stainless steel (C1 type)	
107	Name plate		Aluminium or stainless steel	
108	Thermocouple Sheath		Inconel 600	
109	Thermowell for Thermocouple		Inconel 600	

		Project	Electrical High Temperature Sand Heater for Laboratory Test Rig	
		Equipment	Electrical High Flux Heating Rods	
		Vulcanic Ref	A670908A1	
		Date	28.01.2022	
		Revision	A	
1	Datasheet No.	UNIT	112331-91	
2	Inquiry Number / Customer Data sheet		Specification No. 2	
3	Product		High flux heating rod - Finned Element	
4	Installation		Laboratory Rig	
5	Quantity		1	
111	Instrument Cable Glands		Polyamide	
112	Power Cable Glands		Polyamide	
111	Bolting and nuts		N/A	
112	Gasket		N/A	
113	SURFACE TREATMENT / COATING			
114	Heater enclosure		Painted as per Manufacturer standard (if not stainless steel)	
115	Offset between flange and terminal box		Unpainted	
116	Flange / Fittings		N/A	
116	Bolts and Nuts		N/A	
117	Rod sheath		Unpainted	
118	Thermal insulation cladding		N/A	
120	OTHERS			
121	Testing		• Dimensional and visual check • Insulation measurement at 500 VDC (in cold conditions) • ohm value (in cold conditions) • high voltage (2xU + 1000V) • 3.1 material certificated for heating rod sheath	
122	Approx. Bundle Weight (kg)		To be defined	
123	Others		Fins are washer type	
124			Continious welds of the fins to the element sheath	
125			Heating element power is controlled by a thyristor unit (recommended cycle time: 1 second)	
125			Maximum allowed temperarture of the resistive wire : 950°C	
127			Maximum allowed temperarture of the element tube : 800°C	
128				
129				
130				
131				
126				

Heating rod Preliminary GA Drawing:

Drawing not to scale

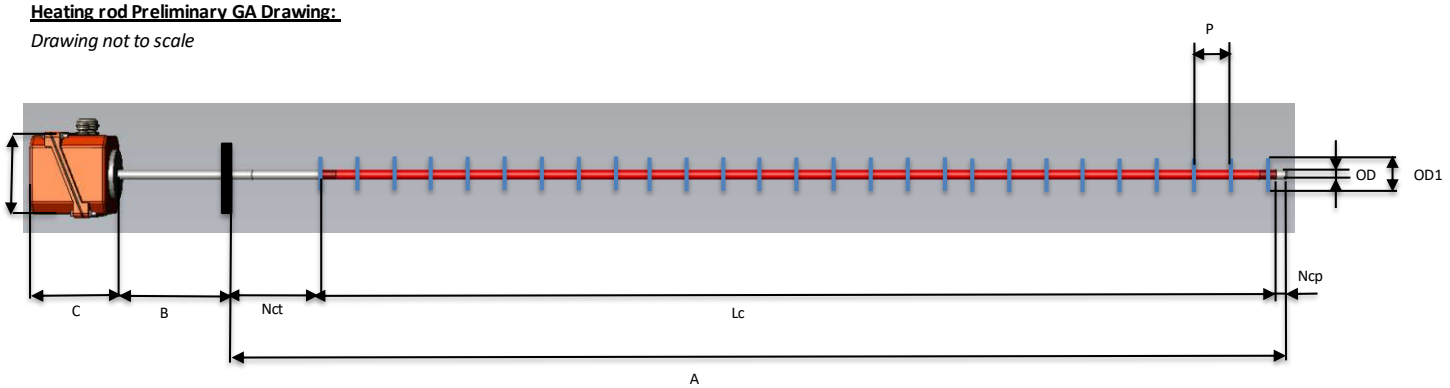

Preliminary dimensions (mm) To be confirmed at detailed engineering

A (immersed length)	560
B (offset length)	400
C	135
D	To be defined
Lc (Active length)	360
Nct (inactive length)	150
Ncp (inactive length)	50
OD	19
OD1	39
P (pitch)	9

All confirmed and validated dimensions are the ones indicated in the corresponding General Arrangement Drawing No. 112331-01

		Project	Electrical High Temperature Sand Heater for Laboratory Test Rig	
		Equipment	Electrical High Flux Heating Rods	
		Vulcanic Ref	A670908B1	
		Date	28.01.2022	
		Revision	A	
1	Datasheet No.	UNIT	112331-92	
2	Inquiry Number / Customer Data sheet		Specification No. 2	
3	Product		High flux heating rod - Plain Tube Element	
4	Installation		Laboratory Rig	
5	Quantity		1	
6	PROCESS DATA			
7	Heated Fluid		Sand	
8	Fluid state		Solid	
9	Nominal flow rate	kg/h	To be Defined	
10	Min. Operating Temperature	°C	400	
11	Max. Operating Temperature	°C	650	
12	Operating pressure	bar (g)	atmospheric	
13	Specific Heat	kJ/kg.°C @ T	N/A	
14	Density ρ	kg/m3 @ T	N/A	
15	Thermal Conductivity λ	Wx(m°.C)	N/A	
16	Viscosity μ	cP @ T	N/A	
17	Minimum required heat duty	W	1 000	
18	Maximum required heat duty (kW)	W	7 065	
19	Power Voltage Supply	**1ph+N (Single phase)**	230	
20	Notes		the overall task is to heat up sand at varying temperature differences between fin tube surface temperature and sand bulk temperature. • Design point 1: T-sand=400 /T-tube=700°C => max. Power = 7kW • Design point 2: T-sand=500 /T-tube=700°C • Design point 3: T-sand=600 /T-tube=800°C • Design point 4: T-sand=650 /T-tube=800°C • Design point 5: T-sand=650 /T-tube=700°C => min Power = 1.2 kW	
21			The tube heater temperature should be controllable to a constant value comprised between 500°C and 800°C.	
22			Depending on the bed temperature and the heater surface temperature, the electric duty of one heater tube will vary in the range from 1. to 7. kW.	
23			Number of cycle (ON/OFF): around 200	
24	DESIGN DATA			
25	Heating rod heating capacity (+/-5%)	W	10 600	
25	Heater Mounting		Horizontal	
26	Area		Safe area - Laboratory	
27	Location		Indoor	
29	Extreme ambient temperature limits	°C	10 / 30	
32	Design current for the whole heater	A	54	
33	Design Temperature of the heating part	°C	10 / 800	
34	Design pressure	bar (g)	Atmospheric (to be confirmed)	
35	Min/Max. Voltage Variation		To be Defined	
36	Min/Max. Frequency Variation		To be Defined	
37	Design and Construction code		as per manufacturer standards	
38	U-Stamp		N/A	
40	Certification		N/A	
41	Corrosion allowance (mm)	mm	0	
42	FITTING FEATURES			
43	Mounting		Onto a frame (by Others)	
44	Heater flange/Fitting type		Flange Standard: DIN EN 1092-1 / Type: 05 / Size: DN25 / Rating: PN6	
45	Flange Machining/Drilling		As per client's requirements and drawing	
46	Lifting Lugs		Not fitted	
47	HEATING ELEMENT FEATURES			
48	Heating element total quantity per bundle		1	
49	Heating element type		High-Flux type	
50	Heating element power	W	10 600,00	
51	Unit voltage supply	1ph+N (Single phase)	230	
52	Heating Element Outer Diameter (OD)	mm	19	
53	Heating length Lc	mm	360	
54	Inactive length Nct (Terminal connection side)	mm	150	
55	Inactive length Ncp (heating rod end side)	mm	50	

		Project	Electrical High Temperature Sand Heater for Laboratory Test Rig	
		Equipment	Electrical High Flux Heating Rods	
		Vulcanic Ref	A670908B1	
		Date	28.01.2022	
		Revision	A	
1	Datasheet No.	UNIT	112331-92	
2	Inquiry Number / Customer Data sheet		Specification No. 2	
3	Product		High flux heating rod - Plain Tube Element	
4	Installation		Laboratory Rig	
5	Quantity		1	
56	Surface load on the sheath @ installed power	W/cm2	49,35	
57	Heating element features		80-20 Ni/Cr Resistive wire	
58	Electrical Insulator		High compacted BN	
59	Heating element Terminal sealing		Weather-proof epoxy seals	
60	Finned element		Yes	
61	Type		N/A	
62	Fin OD1	mm	N/A	
63	Fin ID	mm	19	
64	Fin Thickness	mm	N/A	
65	Pitch P	mm	N/A	
66	Fins Qty		N/A	
67	Exchange surface (Plain tube)	cm2	215	
68	Exchange surface (tube with fins)	cm2	N/A	
69	Surface load on the sheath @ installed power	W/cm2	49,4	
70	Surface load on the fins @ installed power	W/cm2	N/A	
71	OFFSET ASSEMBLY AND HEATER ENCLOSURE			
72	Junction box offset length (B)	mm	400	
73	Construction type		N/A	
74	Anti-radiation Shield		Not fitted	
75	Heater Enclosure Type		as per Manufacturer Standards	
76	Power Stage Quantity Per Flange Heater		1	
77	Design current	A	54	
78	IP rating		IP54	
79	Space heater	W	N/A	
80	Cable gland(s) for power connection		Fitted	
81	Size and type		To be defined	
83	Cable gland(s) for space heater		N/A	
84	Size and type		N/A	
81	Breather / Drain		Not fitted	
82	Notes		The area "B" between flange and terminal box can be hot in operating conditions. There is risk of burns in case of accidental contact. Precautions shall be taken by Client to protect the personal against accidental contact when the heating rod is in operation.	
83	INSTRUMENTATION			
84	Heating rod wire over temperature safety		1 Piece	
86	Location		in thermowell located in the center of the heating rod	
85	Measuring the temperature of		resistive wire(s)	
86	Distance of the sensing point from flange face		310	
87	Heating rod internal sheath over temperature safety		1 Piece	
88	Location		in thermowell located onto the internal wall of the of the heating rod sheath	
89	Measuring the temperature of		internal skin temperature	
90	Distance of the sensing point from flange face		310	
91	Sensors type		K-type metal sheathed mineral insulated cable	
92	Hot junction style		ungrounded - Simplex	
93	Standard		IEC 60584, Class 1	
93	Removable sensors		**Yes**	
94	Connection of the sensors		K-type therminals in the main terminal box of the heating rod	
95	Temperature transmitter		N/A	
97	MATERIAL			
98	Heating rod sheath		Inconel 600 - Seamless type	
99	Sheath thickness	mm	2,60	
100	Sheath tip		Inconel 600 (machined and welded to the rod sheath)	
101	Rod fitting / Flange		Inconel 600	
102	Fins		N/A	
106	Heater enclosure		Aluminium or painted carbon steel or Stainless steel (C1 type)	
107	Name plate		Aluminium or stainless steel	
108	Thermocouple Sheath		Inconel 600	
109	Thermowell for Thermocouple		Inconel 600	

		Project	Electrical High Temperature Sand Heater for Laboratory Test Rig	
		Equipment	Electrical High Flux Heating Rods	
		Vulcanic Ref	A670908B1	
		Date	28.01.2022	
		Revision	A	
1	Datasheet No.	UNIT	112331-92	
2	Inquiry Number / Customer Data sheet		Specification No. 2	
3	Product		High flux heating rod - Plain Tube Element	
4	Installation		Laboratory Rig	
5	Quantity		1	
111	Instrument Cable Glands		Polyamide	
112	Power Cable Glands		Polyamide	
111	Bolting and nuts		N/A	
112	Gasket		N/A	
113	SURFACE TREATMENT / COATING			
114	Heater enclosure		Painted as per Manufacturer standard (if not stainless steel)	
115	Offset between flange and terminal box		Unpainted	
116	Flange / Fittings		N/A	
116	Bolts and Nuts		N/A	
117	Rod sheath		Unpainted	
118	Thermal insulation cladding		N/A	
120	OTHERS			
121	Testing		• Dimensional and visual check • Insulation measurement at 500 VDC (in cold conditions) • ohm value (in cold conditions) • high voltage (2xU + 1000V) • 3.1 material certificated for heating rod sheath	
122	Approx. Bundle Weight (kg)		To be defined	
123	Others			
124				
125			Heating element power is controlled by a thyristor unit (recommended cycle time: 1 second)	
125			Maximum allowed temperarture of the resistive wire : 950°C	
127			Maximum allowed temperarture of the element tube : 800°C	
128				
129				
130				
131				
126				

Heating rod Preliminary GA Drawing:

Drawing not to scale

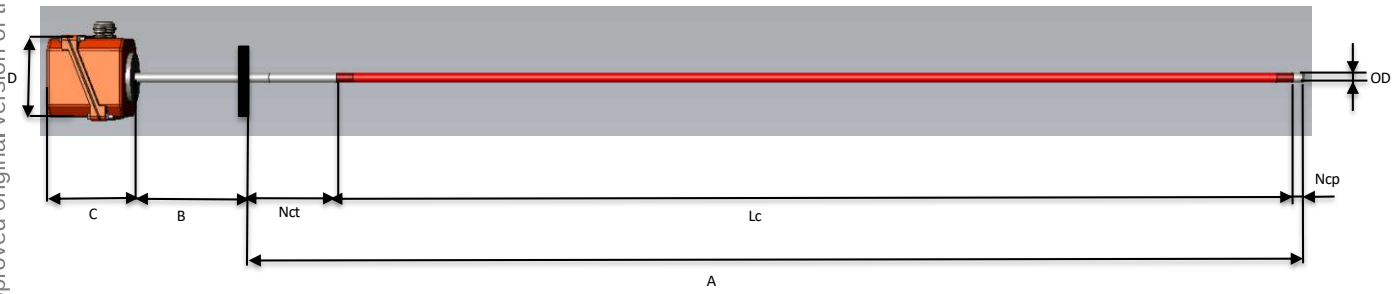

Preliminary dimensions (mm) To be confirmed at detailed engineering

A (immersed length)	560
B (offset length)	400
C	135
D	To be defined
Lc (Active length)	360
Nct (inactive length)	150
Ncp (inactive length)	50
OD	19
OD1	N/A
P (pitch)	N/A

All confirmed and validated dimensions are the ones indicated in the corresponding General Arrangement Drawing No. 112331-01

REV	AMENDMENTS	DATE	VISA	CHECK	REV	AMENDMENTS	DATE	VISA	CHECK
A	First issue	07/03/2022	MB	JLT					
B	Modif flange facing : 05B --> 05A	08/03/2022	MB	JLT					

Electrical specification :

Power = 10 600 W
Pow. Tol. = +5 / -5 %
Voltage = 230 VAC 1Ph+E
C / S = 49,4 W/cm²

Process specification :

Medium : Sand
Medium state : Solid
Min operating temperature : 400°C
Max operating temperature : 650°C
Maximum operating pressure : Atmospheric
Min allowable temperature TS : 10°C
Max allowable temperature TS : 800°C
Maximum allowable pressure PS : Atmospheric
Ambient temperature Mini / Maxi : 10°C / 30°C

Heating element specifications :

Ø = 19 mm (seamless type)
Material : Inconel 600
Treatment : Without
Sealing : WP+ 160

Safety device specification :

Device S1 : Thermocouple Type K Ø1 Inconel 600 simplex point hot insulated from the ground Class 1 according to IEC 60584
Mounting : At size "T", in thermowell, in center of the sheath
Function : Heating rod wire over temperature safety
Device S2 : Thermocouple Type K Ø1 Inconel 600 simplex point hot insulated from the ground Class 1 according to IEC 60584
Mounting : At size "T", in thermowell, onto internal wall of heating rod sheath
Function : Heating rod internal sheath over temperature safety

Fitting specification : B

Fitting piece : Flange ND25, NP6, 05A acc.to EN1092-1
Material : Inconel 600
Treatment : Without

Connections Features :

Power Connection: Terminal Block for 16mm² Maxi
Sensor S1 Connection: Terminal Block for Tc K 2,5 mm² Maxi
Sensor S2 Connection: Terminal Block for Tc K 2,5 mm² Maxi

Construction Code : Standard Vulcanic

NOTES:

- PARTICULARITIES:

- FLANGE DRILLING ACC. TO CUSTOMER REQUEST (SEE DETAIL A)
- HEATING ROD POWER IS CONTROLLED BY A THYRISTOR UNIT (RECOMMENDED CYCLE TIME = 1 SECOND)
- MAX ALLOWED TEMPERATURE OF RESISTIVE WIRE = 950°C
- MAX ALLOWED TEMPERATURE OF ELEMENT SHEATH = 800°C

- TESTING:

- DIMENSIONAL AND VISUAL CHECK
- ELECTRICAL TESTING (IN COLD CONDITIONS) :
  - INSULATION MEASUREMENT
  - OHM VALUE
  - DIELECTRIC RIGIDITY
- 3.1 MATERIAL CERTIFICATE FOR HEATING ROD SHEATH

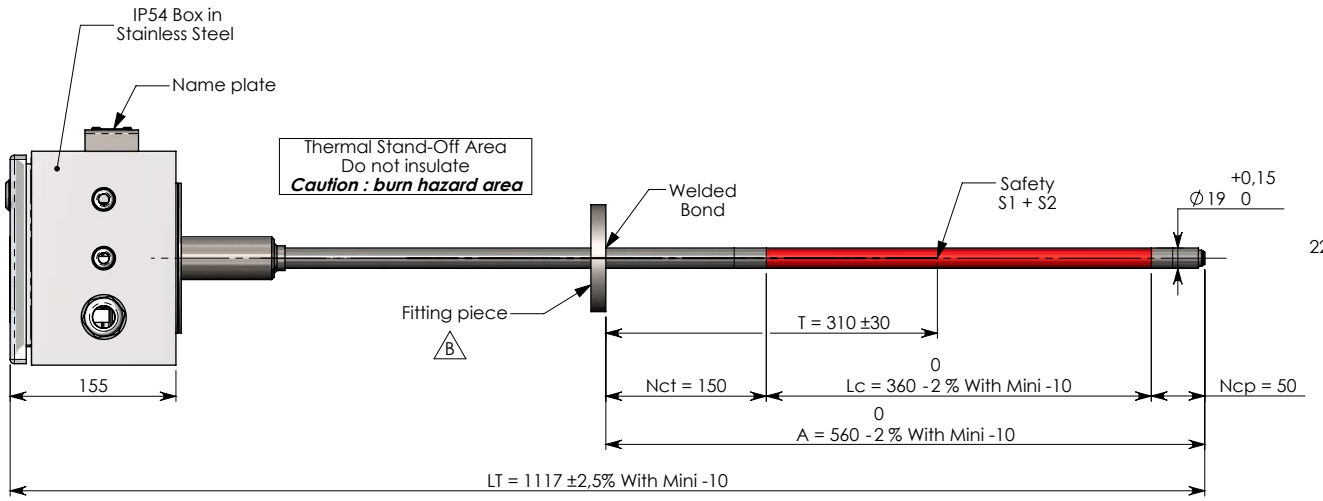

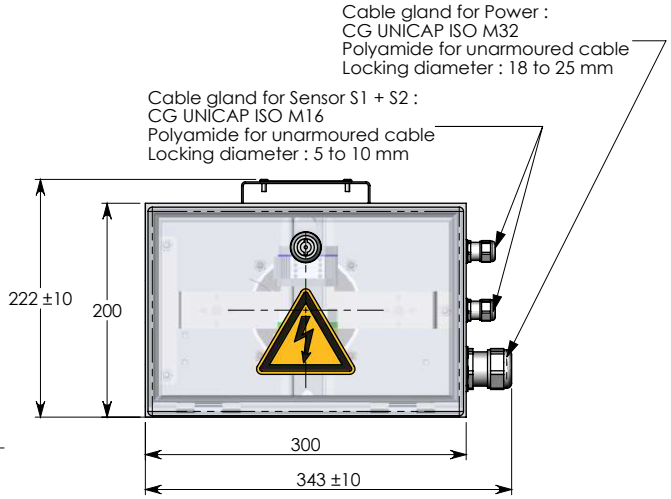

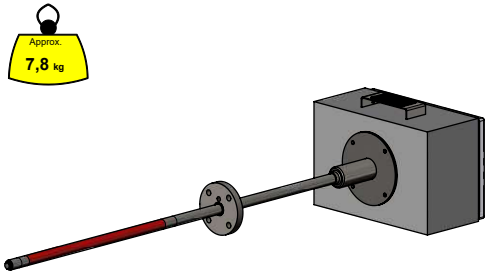

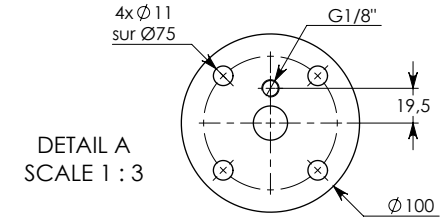

DETAIL A
SCALE 1 : 3

WIRING DIAGRAM OF THE HEATING ROD

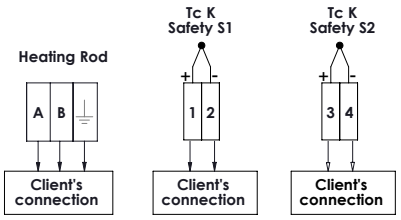

general tolerances	10 to 50 mm : + / - 0,2	>100 mm : + / -1	Angle : + / -30'	Sheet-iron maker : 0 to 50 mm : + / -0,5	> 1000 mm : + / -2	Sheathed element : + / -5% with mini + / -5 mm	
Mechanic : 0 to 10 mm : + / - 0,1	50 to 100 mm : + / - 0,5	ray : 0,1 to 0,3	Broken angle : 0,1 to 0,3	50 to 1000 mm : + / -1	Pyrometry : + / -1% with mini + / -2 mm	Boiler making : + / -1% with mini + / -5 mm	

Vulcanic

Draw	MB	on	07/03/2022	HIGH FLUX HEATING ROD - PLAIN TUBE ELEMENT	SCALE
Check	JLT	on	07/03/2022	GENERAL ARRANGEMENT DRAWING	N° 112331.02 / SHEET NUMBER 1/1 / REV B

PREPARATION BOTTOM PLAN N°BE 039 .REV A

REV	AMENDMENTS	DATE	VISA	CHECK
A	First issue	07/03/2022	MB	JLT
B	Modif flange facing : 05B --> 05A	08/03/2022	MB	JLT

Electrical specification :

Power = 10 600 W
Pow. Tol. = +5 / -5 %
Voltage = 230 VAC 1Ph+E
C / S = 49,4 W/cm²

Process specification :

Medium : Sand
Medium state : Solid
Min operating temperature : 400°C
Max operating temperature : 650°C
Maximum operating pressure : Atmospheric
Min allowable temperature TS : 10°C
Max allowable temperature TS : 800°C
Maximum allowable pressure PS : Atmospheric
Ambient temperature Mini / Maxi : 10°C / 30°C

Heating element specifications :

Ø = 19 mm (seamless type)
Material : Inconel 600
Treatment : Without
Sealing : WP+ 160

Safety device specification :

Device S1 : Thermocouple Type K Ø1 Inconel 600 simplex point hot insulated from the ground Class 1 according to IEC 60584
Mounting : At size "T", in thermowell, in center of the sheath
Function : Heating rod wire over temperature safety
Device S2 : Thermocouple Type K Ø1 Inconel 600 simplex point hot insulated from the ground Class 1 according to IEC 60584
Mounting : At size "T", in thermowell, onto internal wall of heating rod sheath
Function : Heating rod internal sheath over temperature safety

Fitting specification : B

Fitting piece : Flange ND25, NP6, 05A acc.to EN1092-1
Material : Inconel 600
Treatment : Without

Connections Features :

Power Connection: Terminal Block for 16mm² Maxi
Sensor S1 Connection: Terminal Block for Tc K 2,5 mm² Maxi
Sensor S2 Connection: Terminal Block for Tc K 2,5 mm² Maxi

Construction Code : Standard Vulcanic

NOTES:

- PARTICULARITIES:

- ROD EQUIPED WITH FINS IN INCONEL 600 (SEE DETAIL A) --> FINS ARE WASHER TYPE
- FLANGE DRILLING ACC. TO CUSTOMER REQUEST (SEE DETAIL B)
- HEATING ROD POWER IS CONTROLLED BY A THYRISTOR UNIT (RECOMMENDED CYCLE TIME = 1 SECOND)
- MAX ALLOWED TEMPERATURE OF RESISTIVE WIRE = 950°C
- MAX ALLOWED TEMPERATURE OF ELEMENT SHEATH = 800°C

- TESTING:

- DIMENSIONAL AND VISUAL CHECK
- ELECTRICAL TESTING (IN COLD CONDITIONS) :
  - INSULATION MEASUREMENT
  - OHM VALUE
  - DIELECTRIC RIGIDITY
- 3.1 MATERIAL CERTIFICATE FOR HEATING ROD SHEATH

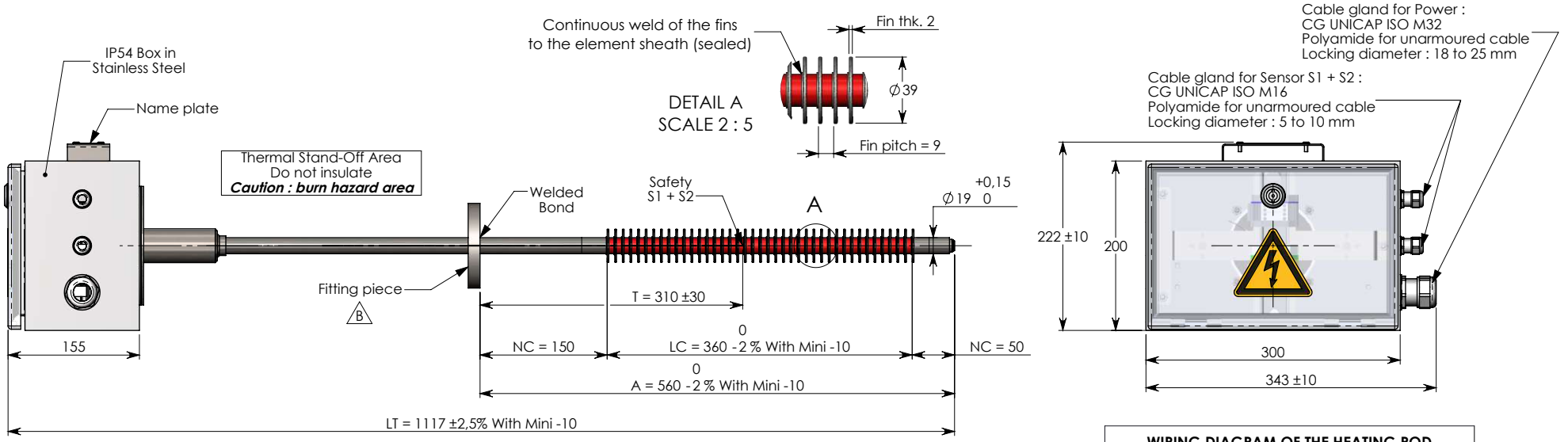

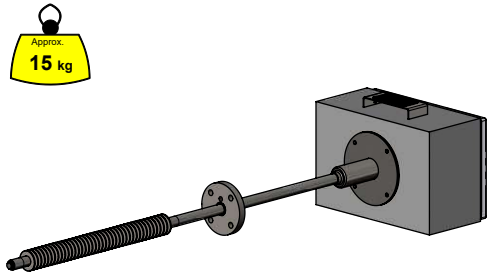

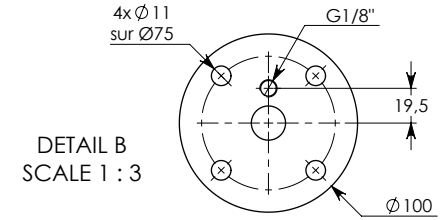

WIRING DIAGRAM OF THE HEATING ROD

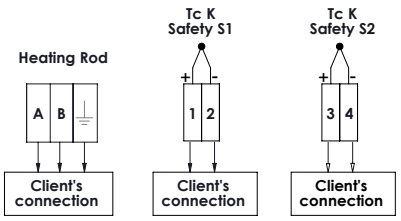

general tolerances	10 to 50 mm : + / - 0,2	>100 mm : + / -1	Angle : + / -30'	Sheet-iron maker : 0 to 50 mm : + / -0,5	> 1000 mm : + / -2	Sheathed element : + / -5% with mini + / -5 mm
Mechanic : 0 to 10 mm : + / - 0,1	50 to 100 mm : + / - 0,5	ray : 0,1 to 0,3	Broken angle : 0,1 to 0,3	50 to 1000 mm : + / -1	Pyrometry : + / -1% with mini + / -2 mm	Boiler making : + / -1% with mini + / -5 mm

Draw	MB	on	07/03/2022	HIGH FLUX HEATING ROD - FINNED ELEMENT	SCALE	N° 112331.01 / REV B
Check	JLT	on	07/03/2022	GENERAL ARRANGEMENT DRAWING		SHEET NUMBER 1/1

PREPARATION BOTTOM PLAN N°BE 039 .REV A

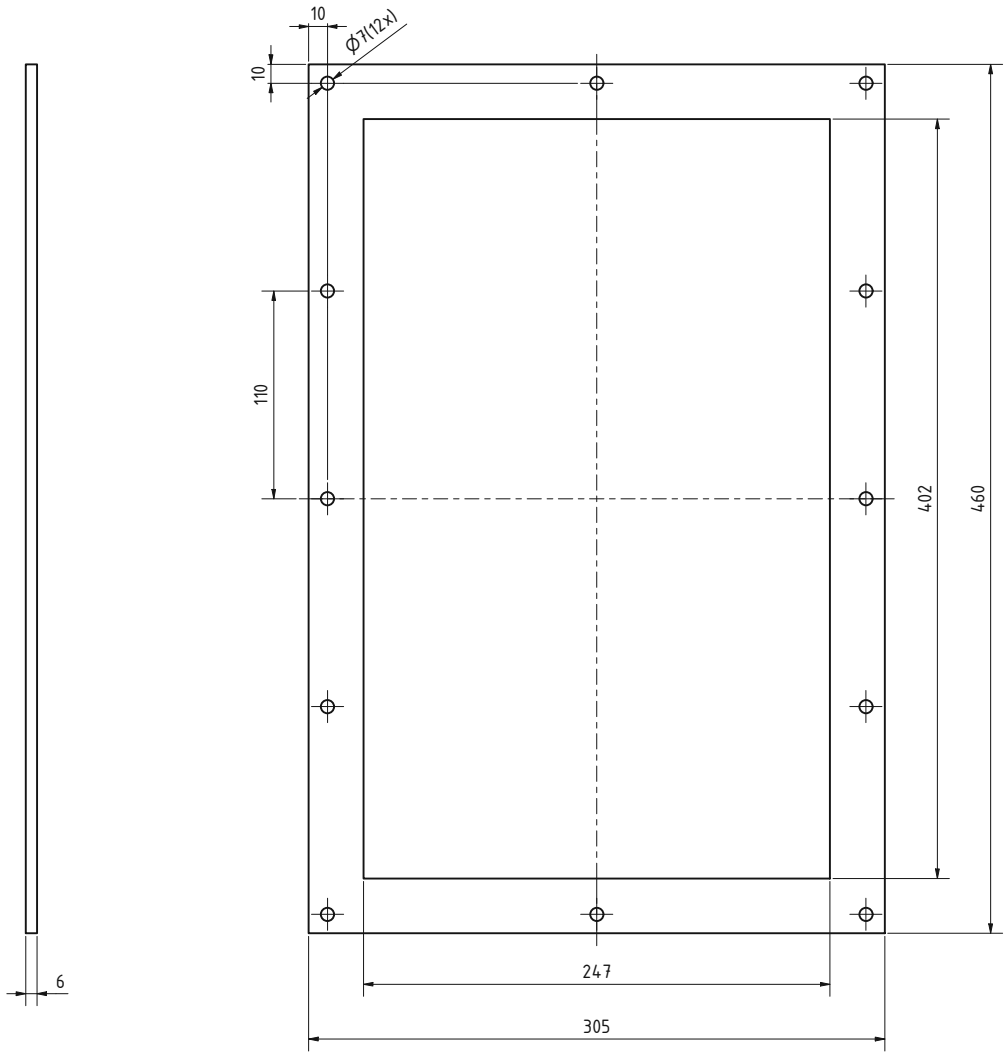

unbemaßte Werkstückkanten DIN ISO 13715	ISO 128	Allgemeintoleranz ISO2768 mK	Maßstab: 1 : 2	Masse: 1,922 kg	
			Oberflächenbehandlung:	Material: Edelstahl (1.4841)	
		Datum / Name	Benennung: Windkasten Flansch oben		
		Gezeichn. 10.01.2022 Philipp Mayer			
		Kontrolli.	Projekt: Micro Hot Prüfstand		
		Norm	INSTITUT FÜR ENERGIETECHNIK UND THERMODYNAMIK Institute for Energy Systems and Thermodynamics	Z-Nummer: MH001	Blatt 1/1 A2
Status	Änderungen	Datum / Name			

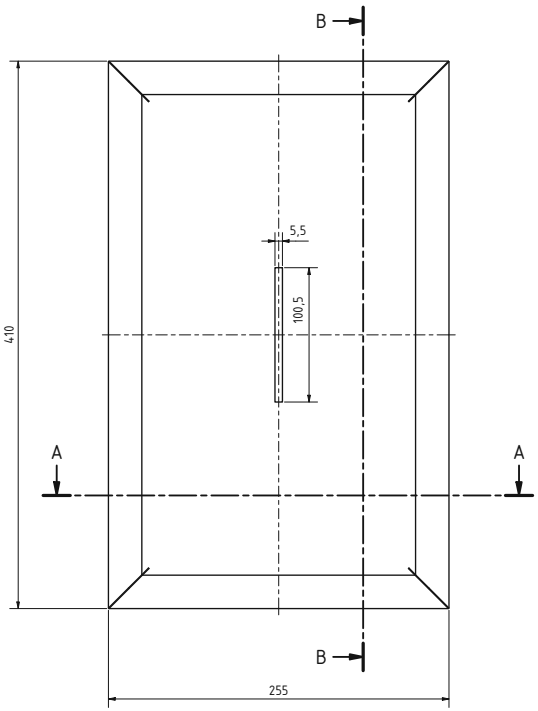

B-B (1 : 2)

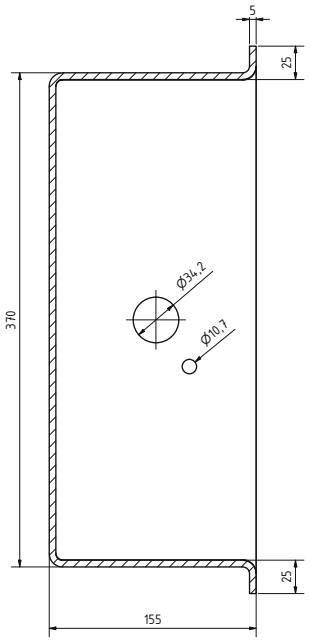

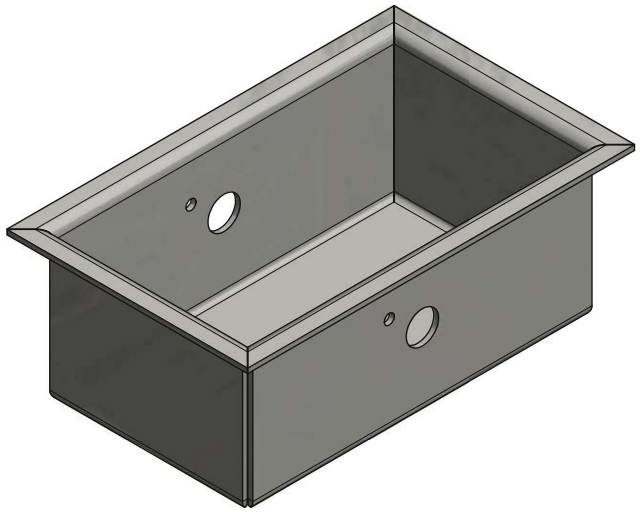

A-A (1 : 2)

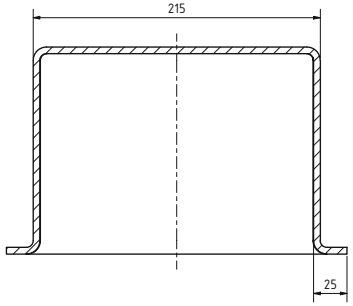

Abwicklung (1 : 5)

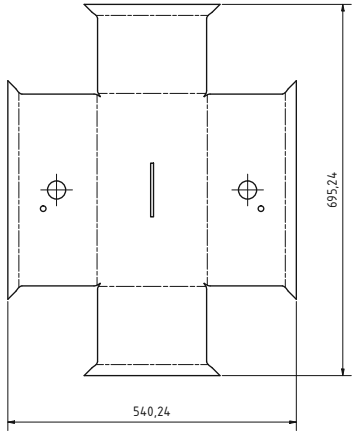

Fertigungshinweis: Ecken gasdicht verschweißen

unbemaßte Werkstückkanten DIN ISO 13715	ISO 128	Allgemeintoleranz ISO2768 mK	Maßstab: 1 : 2
			Masse: 10,412 kg
			Oberflächenbehandlung:
			Material: Edelstahl (1.4841)
	Datum	Name	Benennung: Windkasten Unterteil
	Gezeichn. 10.01.2022	Philipp Mayer	
	Kontrollt.		Projekt: Micro Hot Prüfstand
	Norm		
INSTITUT FÜR ENERGIETECHNIK UND THERMODYNAMIK			Z-Nummer: MH002
Index Änderungen Datum Name			Blatt 1/1 A1

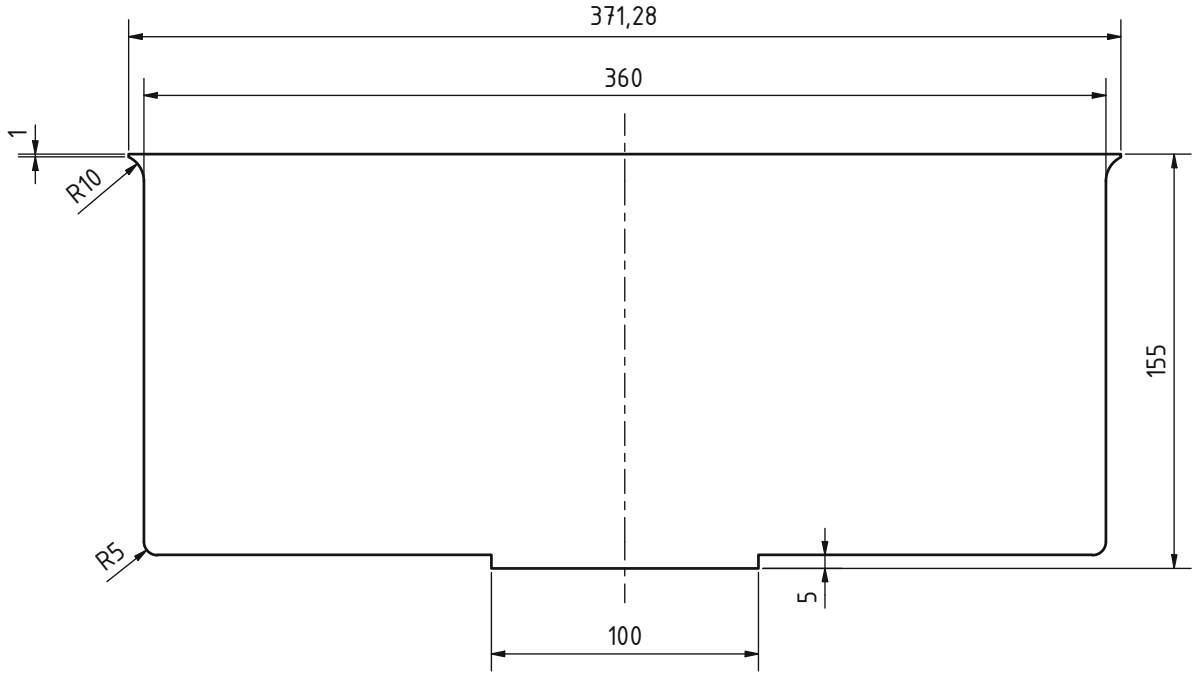

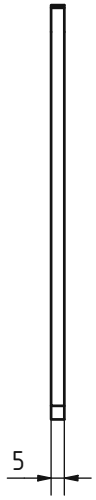

unbemaßte Werkstückkanten DIN ISO 13715	ISO 128	Allgemeintoleranz ISO2768 mK	Maßstab: 1 : 2
		Oberflächenbehandlung:	Masse: 2,154 kg
			Material: Edelstahl (1.4841)
	Datum	Name	Benennung: Windkasten Trennblech
	Gezeichn 10.01.2022	Philipp Mayer	
	Kontroll		Projekt: Micro Hot Prüfstand
	Norm		
Status Änderungen Datum Name	INSTITUT FÜR ENERGIETECHNIK UND THERMODYNAMIK Institute for Energy Systems and Thermodynamics		Z-Nummer: MH003
			Blatt 1/1 A3

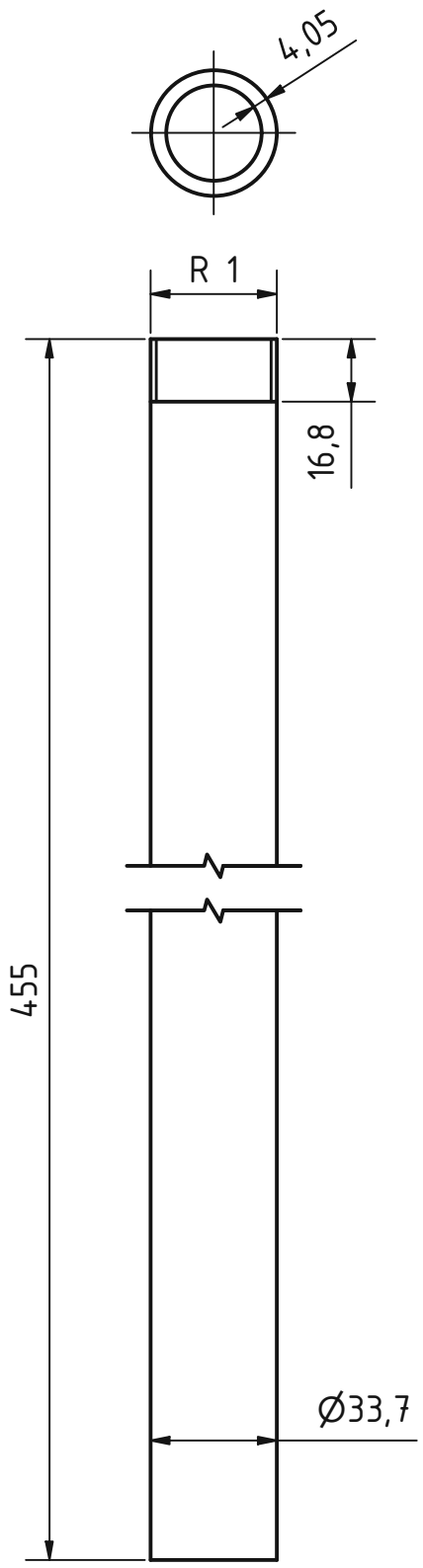

Fertigungshinweis:
Ausgangsmaterial Rohr EN 10216

unbemaßte Werkstückkanten DIN ISO 13715

0,3 0,3

ISO 128

Allgemeintoleranz
ISO2768
mK

Maßstab: 1 : 2

Masse: -

Oberflächenbehandlung:

Material:
Edelstahl (1.4841)

	Datum	Name
Gezeichn	10.01.2022	Philipp Mayer
Kontroll		
Norm		

Benennung:
Windkasten Zuluftrohrstutzen

Projekt: Micro Hot Prüfstand

INSTITUT FÜR ENERGIETECHNIK UND THERMODYNAMIK
Institute for Energy Systems and Thermodynamics

Z-Nummer: ER004

Blatt 1/1
A4

Status	Änderungen	Datum	Name

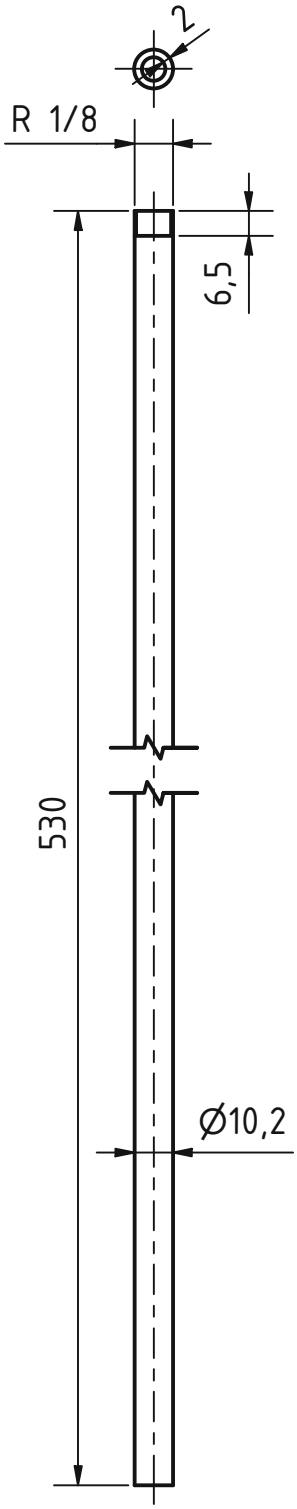

Fertigungshinweis:
Ausgangsmaterial Rohr EN 10216

unbemaßte Werkstückkanten DIN ISO 13715 ⌐0,3 ⌐0,3	ISO 128	Allgemeintoleranz ISO2768 mK	Maßstab: 1 : 2
			Masse: -
			Oberflächenbehandlung:
			Material: Edelstahl (1.4841)

	Datum	Name
Gezeichn	11.01.2022	Philipp Mayer
Kontroll		
Norm		

Benennung: Druckmessstutzen

Projekt: Micro Hot Prüfstand

INSTITUT FÜR ENERGIETECHNIK UND THERMODYNAMIK
Institute for Energy Systems and Thermodynamics

Z-Nummer: MH005

Blatt 1/1
A4

Status	Änderungen	Datum	Name

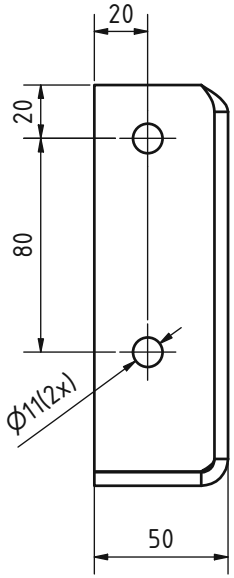

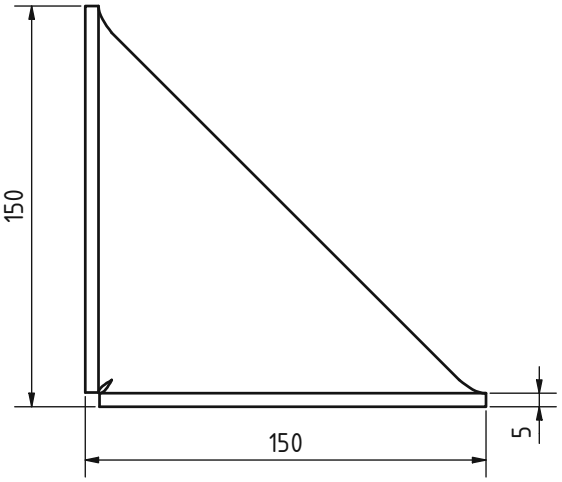

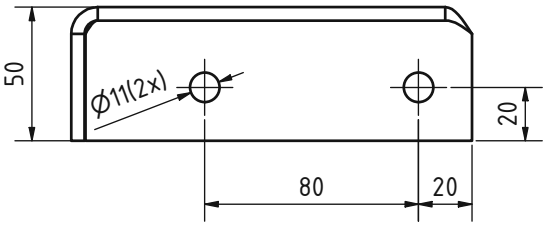

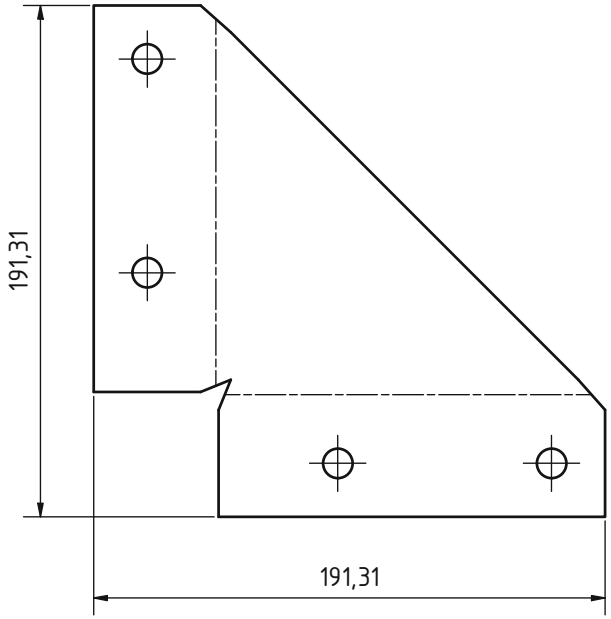

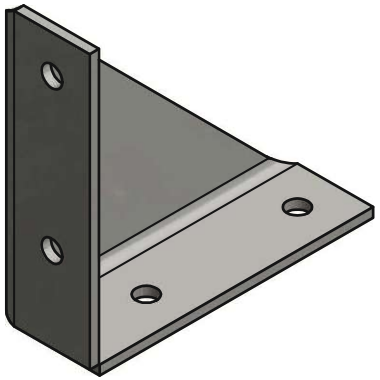

unbemaßte Werkstückkanten DIN ISO 13715 (0,3 / 0,3)	ISO 128	Allgemeintoleranz ISO2768 mK	Maßstab: 1 : 2
		Oberflächenbehandlung:	Masse: 0,904 kg
			Material: Edelstahl (1.4841)
	Datum	Name	Benennung: Aufstandsfuß
	Gezeichn 11.01.2022	Philipp Mayer	
	Kontroll		Projekt: Micro Hot Prüfstand
	Norm		
Status / Änderungen / Datum / Name	INSTITUT FÜR ENERGIETECHNIK UND THERMODYNAMIK, Institute for Energy Systems and Thermodynamics		Z-Nummer: MH006
			Blatt 1/1, A3

A–A (1 : 5)

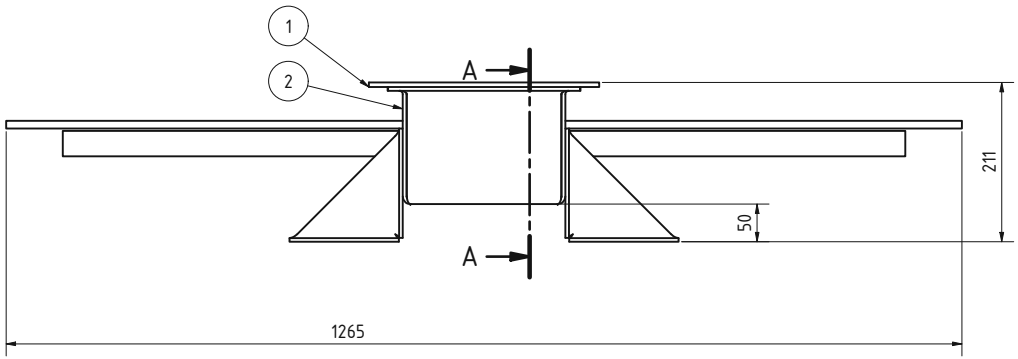

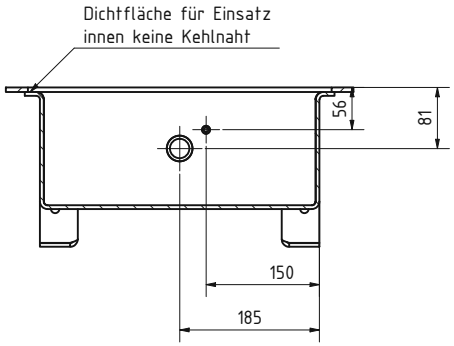

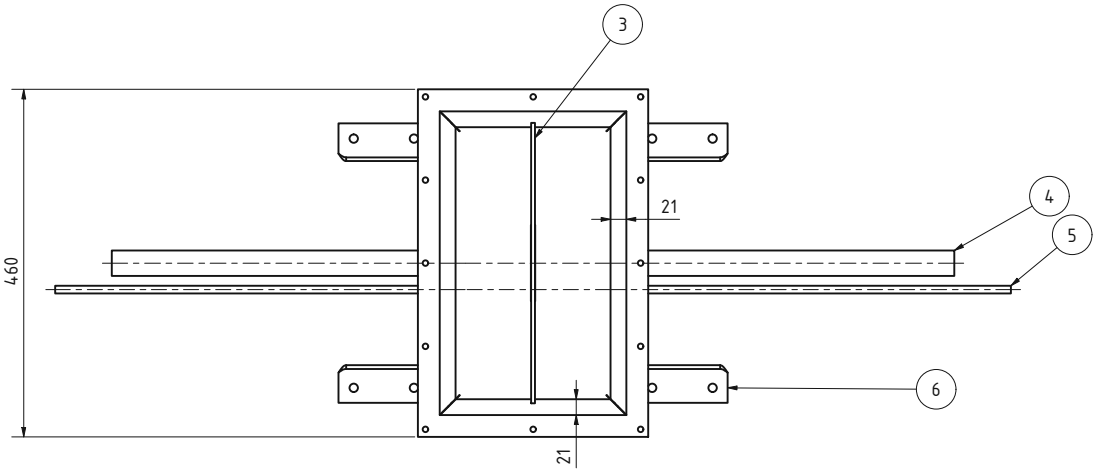

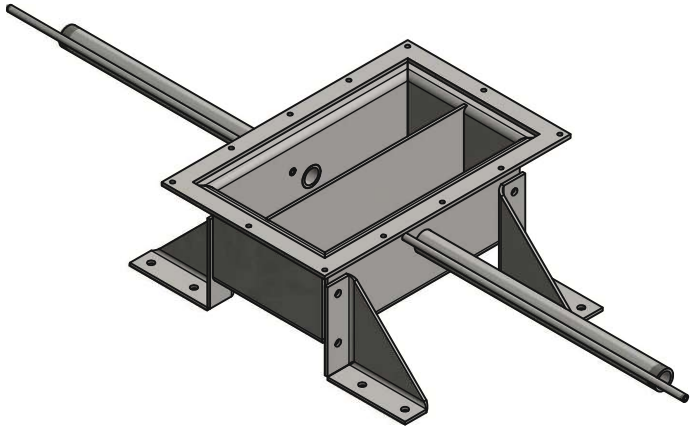

STÜCKLISTE				
OBJEKT	ANZAHL	BAUTEILNUMMER	Z-NUMMER	BESCHREIBUNG
1	1	Windkasten Flansch oben	MH001	
2	1	Windkasten Unterteil	MH002	
3	1	Windkasten Trennblech	MH003	
4	2	Windkasten Zuluftrohrstutzen	ER004	
5	2	Druckmessstutzen	MH005	
6	4	Aufstandsfuß	MH006	

unbemaßte Werkstückkanten DIN ISO 13715 | ISO 128 | Allgemeintoleranz ISO2768 mK | Maßstab: 1 : 5 | Masse: –

Oberflächenbehandlung: | Material:

	Datum	Name
Gezeichn.	11.01.2022	Philipp Mayer
Kontroll.		
Norm		

Benennung: Windkasten Schweißbaugruppe

Projekt:

INSTITUT FÜR ENERGIETECHNIK UND THERMODYNAMIK
Institute for Energy Systems and Thermodynamics

Z-Nummer: MH007

Blatt 1/1 A2

Status | Änderungen | Datum | Name

Fertigungshinweis:
Bauteile gasdicht verschweißen

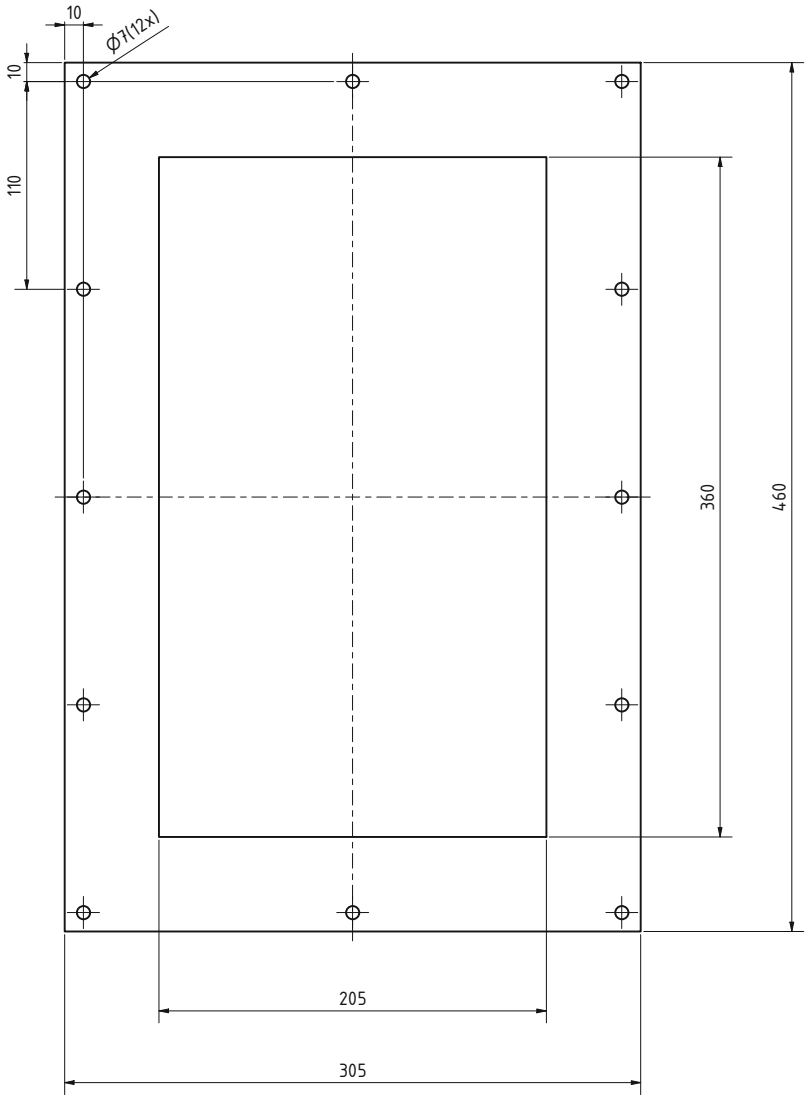

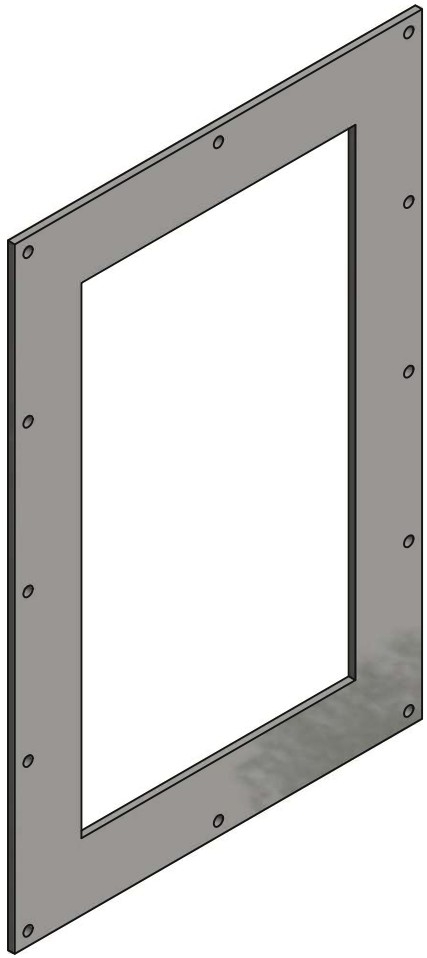

unbemaßte Werkstückkanten DIN ISO 13715	ISO 128	Allgemeintoleranz	Maßstab: 1 : 2	Masse: 2,609 kg	
		ISO2768 mK	Oberflächenbehandlung:	Material: Edelstahl (1.4841)	
	Datum	Name	Benennung: Wirbelschichtkammer Flansch unten		
	Gezeichn. 11.01.2022	Philipp Mayer	Projekt: Micro Hot Prüfstand		
	Kontroll				
	Norm		INSTITUT FÜR ENERGIETECHNIK UND THERMODYNAMIK	Z-Nummer: MH008	Blatt 1/1 A2
Status Änderungen	Datum	Name			

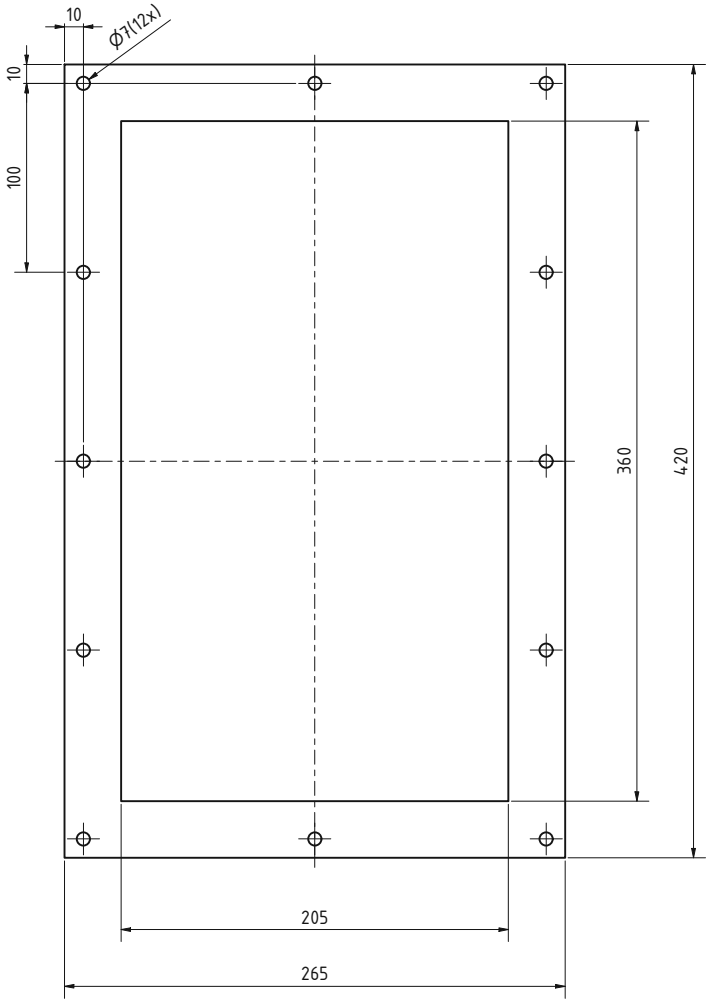

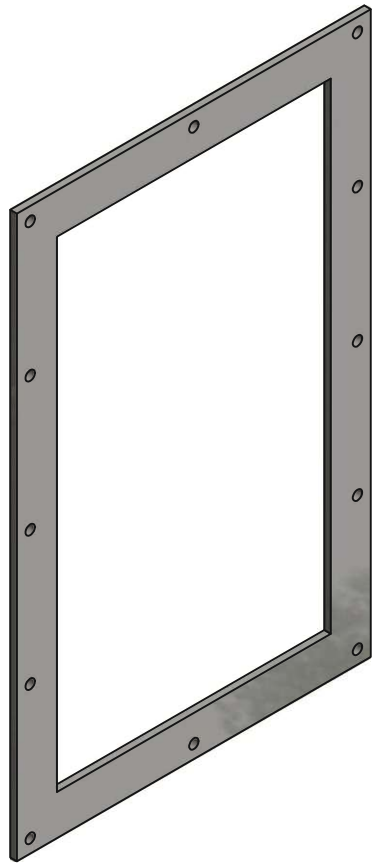

unbemaßte Werkstückkanten DIN ISO 13715	ISO 128	Allgemeintoleranz ISO2768 mK	Maßstab: 1 : 2	Masse: 1,463 kg	
			Oberflächenbehandlung:	Material: Edelstahl (1.4841)	
	Datum	Name	Benennung: Wirbelschichtkammer Flansch oben		
Gezeichn.	11.01.2022	Philipp Mayer	Projekt: Micro Hot Prüfstand		
Kontroll.					
Norm					
INSTITUT FÜR ENERGIETECHNIK UND THERMODYNAMIK Institute for Energy Systems and Thermodynamics			Z-Nummer: MH009	Blatt: 1/1 A2	
Status	Änderungen	Datum	Name		

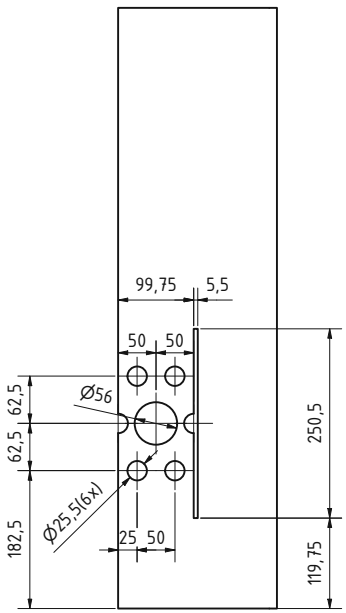

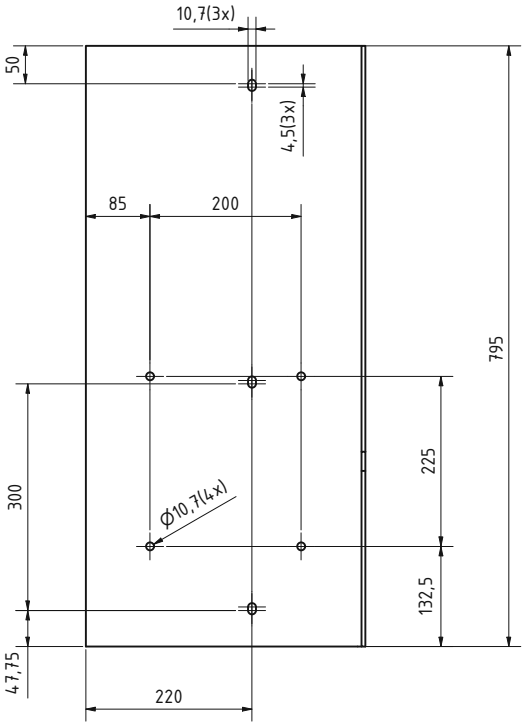

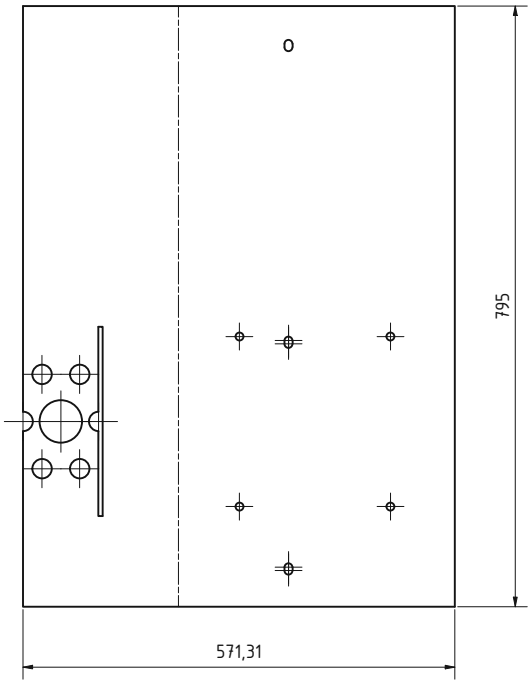

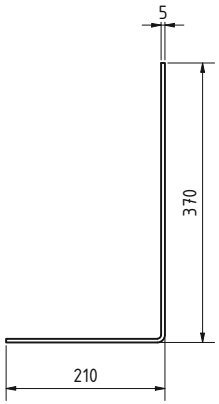

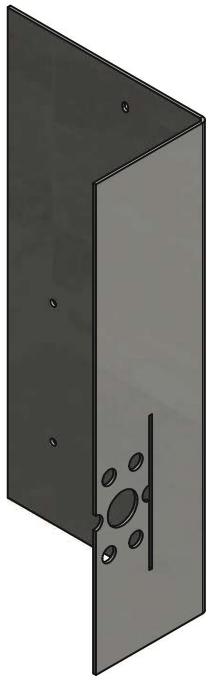

unbemaßte Werkstückkanten DIN ISO 13715	ISO 128	Allgemeintoleranz ISO2768 mK	Maßstab: 1 : 5	Masse: 17,672 kg	
			Oberflächenbehandlung:	Material: Edelstahl (1.4841)	
	Datum	Name	Benennung: Wirbelschichtkammer Blech vorne		
Gezeichn.	11.01.2022	Philipp Mayer	Projekt: Micro Hot Prüfstand		
Kontroll.					
Norm					
INSTITUT FÜR ENERGIETECHNIK UND THERMODYNAMIK Institute for Energy Systems and Thermodynamics			Z-Nummer: MH010	Blatt 1/1 A2	
Status	Änderungen	Datum	Name		

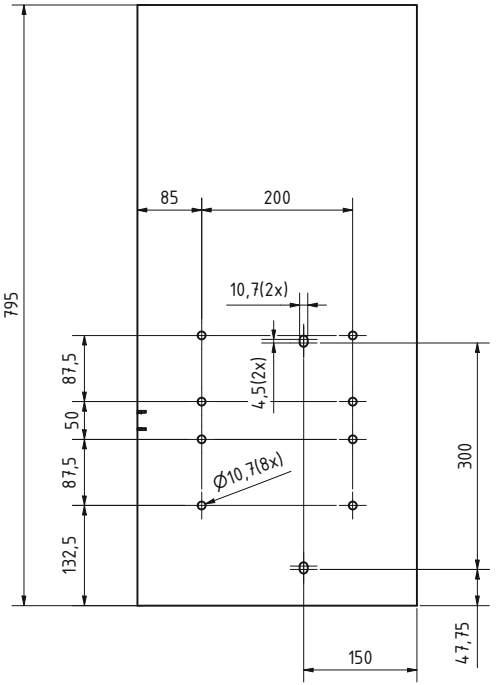

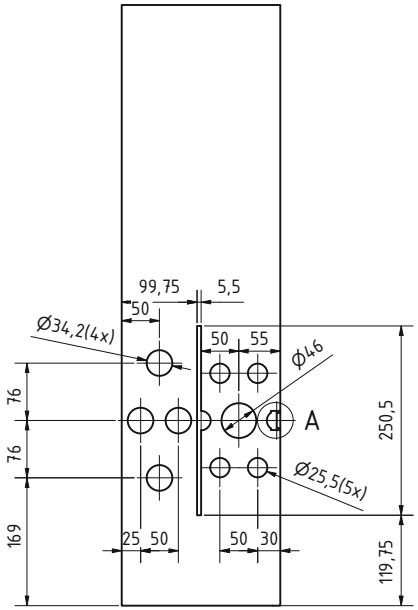

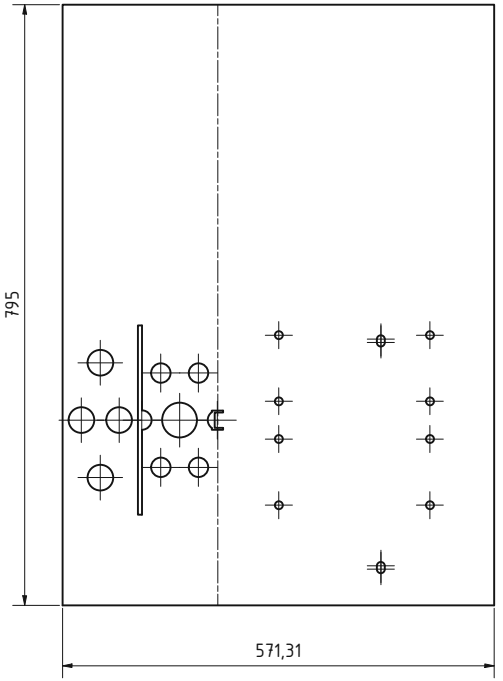

A (1 : 1)

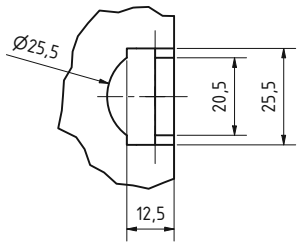

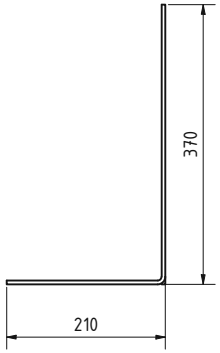

unbemaßte Werkstückkanten DIN ISO 13715	ISO 128	Allgemeintoleranz	Maßstab: 1 : 5	Masse: 17,551 kg	
		ISO2768 mK	Oberflächenbehandlung:	Material: Edelstahl (1.4841)	
	Datum	Name	Benennung: Wirbelschichtkammer Blech hinten		
	Gezeichn. 11.01.2022	Philipp Mayer	Projekt: Micro Hot Prüfstand		
	Kontroll				
	Norm				
Status Änderungen Datum Name	INSTITUT FÜR ENERGIETECHNIK UND THERMODYNAMIK Institute for Energy Systems and Thermodynamics		Z-Nummer: MH011	Blatt 1/1	A2

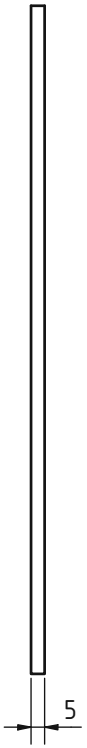

unbemaßte Werkstückkanten DIN ISO 13715

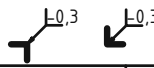

ISO 128

Allgemeintoleranz ISO2768 mK

Maßstab: 1 : 2

Masse: 3,604 kg

Oberflächenbehandlung:

Material: Edelstahl (1.4841)

	Datum	Name
Gezeichn	11.01.2022	Philipp Mayer
Kontroll		
Norm		

Benennung:

Wirbelschichtkammer Trennblech

Projekt: Micro Hot Prüfstand

INSTITUT FÜR ENERGIETECHNIK UND THERMODYNAMIK
Institute for Energy Systems and Thermodynamics

Z-Nummer: MH012

Blatt 1/1

A3

Status	Änderungen	Datum	Name

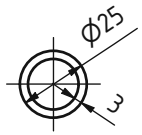

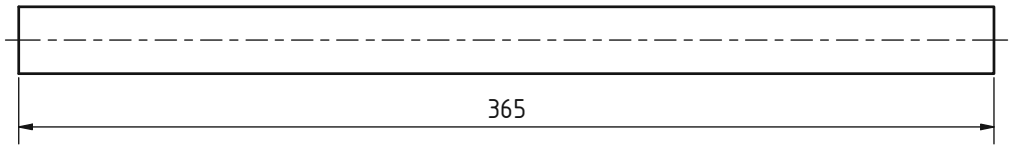

Fertigungshinweis:
Ausgangsmaterial Rohr EN 10216

unbemaßte Werkstückkanten DIN ISO 13715 — 0,3 — 0,3

ISO 128

Allgemeintoleranz ISO2768 mK

Maßstab: 1 : 2

Masse: 0,598 kg

Oberflächenbehandlung:

Material: Edelstahl (1.4841)

	Datum	Name
Gezeichn	11.01.2022	Philipp Mayer
Kontroll		
Norm		

Benennung:
Wirbelschichtkammer
Einsatzrohrdummy
Projekt: Micro Hot Prüfstand

INSTITUT FÜR ENERGIETECHNIK UND THERMODYNAMIK
Institute for Energy Systems and Thermodynamics

Z-Nummer: MH013

Blatt 1/1
A3

Status	Änderungen	Datum	Name

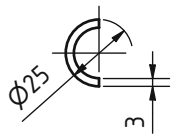

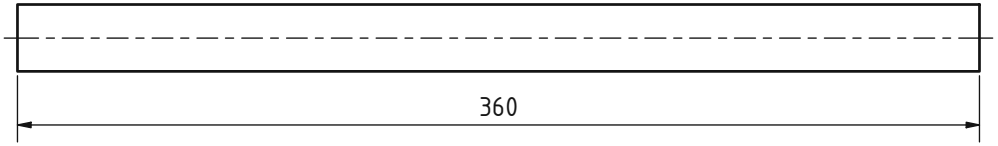

Fertigungshinweis:
Ausgangsmaterial Rohr EN 10216

unbemaßte Werkstückkanten DIN ISO 13715 (0,3 / 0,3)	ISO 128	Allgemeintoleranz ISO2768 mK	Maßstab: 1 : 2
		Oberflächenbehandlung:	Masse: 0,295 kg
			Material: Edelstahl (1.4841)

	Datum	Name
Gezeichn	11.01.2022	Philipp Mayer
Kontroll		
Norm		

Benennung:
Wirbelschichtkammer Einsatzrohrdummy Hälfte
Projekt: Micro Hot Prüfstand

INSTITUT FÜR ENERGIETECHNIK UND THERMODYNAMIK
Institute for Energy Systems and Thermodynamics

Z-Nummer: MH014

Blatt 1/1
A3

Status	Änderungen	Datum	Name

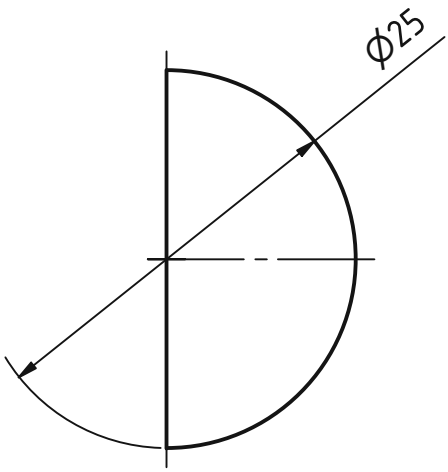

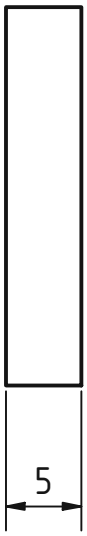

unbemaßte Werkstückkanten DIN ISO 13715

0,3 0,3

ISO 128

Allgemeintoleranz ISO2768 mK

Maßstab: 2 : 1

Masse: 0,010 kg

Oberflächenbehandlung:

Material: Edelstahl (1.4841)

	Datum	Name
Gezeichn	11.01.2022	Philipp Mayer
Kontroll		
Norm		

Benennung:

Verschlussblech Einsatzrohrdummy Hälfte

Projekt:

INSTITUT FÜR ENERGIETECHNIK UND THERMODYNAMIK
Institute for Energy Systems and Thermodynamics

Z-Nummer: MH015

Blatt 1/1

A4

Status	Änderungen	Datum	Name

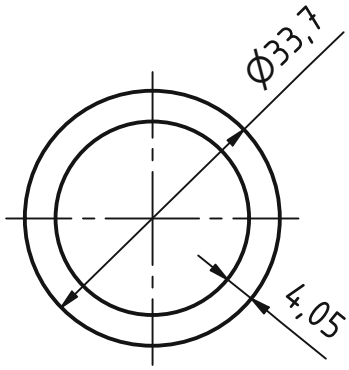

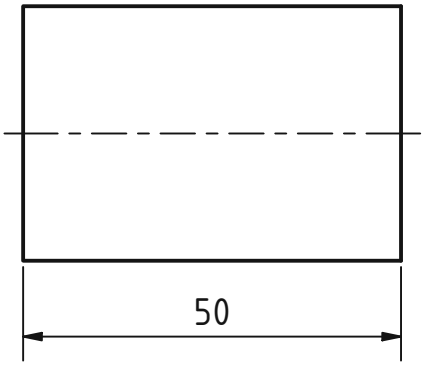

Fertigungshinweis:
Ausgangsmaterial Rohr EN 10216

unbemaßte Werkstückkanten DIN ISO 13715 ⌐0,3 ⌐0,3	ISO 128	Allgemeintoleranz ISO2768 mK	Maßstab: 1 : 1
			Masse: 0,149 kg
			Oberflächenbehandlung:
			Material: Edelstahl (1.4841)

	Datum	Name
Gezeichn	11.01.2022	Philipp Mayer
Kontroll		
Norm		

Benennung:
Wirbelschichtkammer Durchgangsmuffe
Projekt: Micro Hot Prüfstand

INSTITUT FÜR ENERGIETECHNIK UND THERMODYNAMIK
Institute for Energy Systems and Thermodynamics

Z-Nummer: MH016

Blatt 1/1
A4

Status	Änderungen	Datum	Name

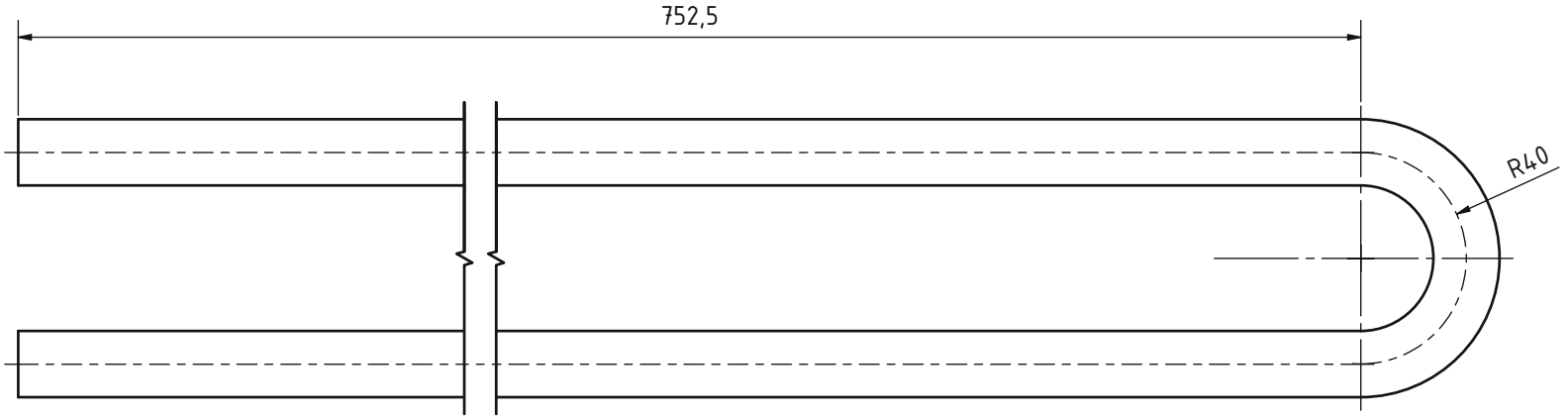

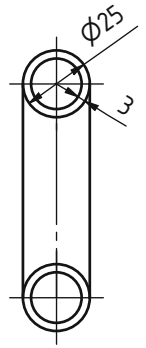

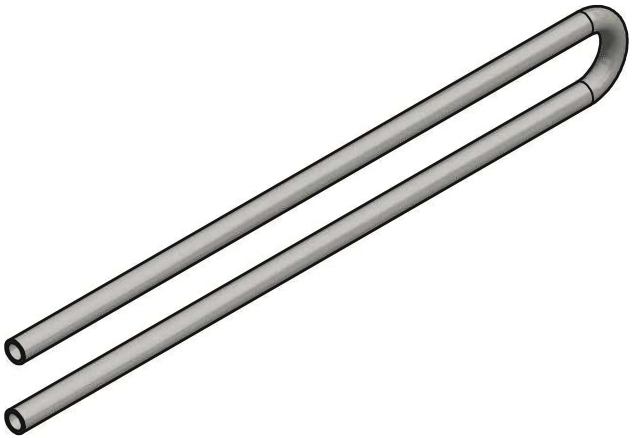

Fertigungshinweis:
Ausgangsmaterial Rohr EN 10216

unbemaßte Werkstückkanten DIN ISO 13715 (0,3 / 0,3)	ISO 128	Allgemeintoleranz ISO2768 mK	Maßstab: 1 : 2
			Masse: 2,671 kg
		Oberflächenbehandlung:	Material: Edelstahl (1.4841)
	Datum	Name	Benennung: Wirbelschichtkammer Kühlrohreinsatz
	Gezeichn 11.01.2022	Philipp Mayer	
	Kontroll		
	Norm		Projekt: Micro Hot Prüfstsnd
Status Änderungen Datum Name	INSTITUT FÜR ENERGIETECHNIK UND THERMODYNAMIK Institute for Energy Systems and Thermodynamics		Z-Nummer: MH017
			Blatt 1/1 A3

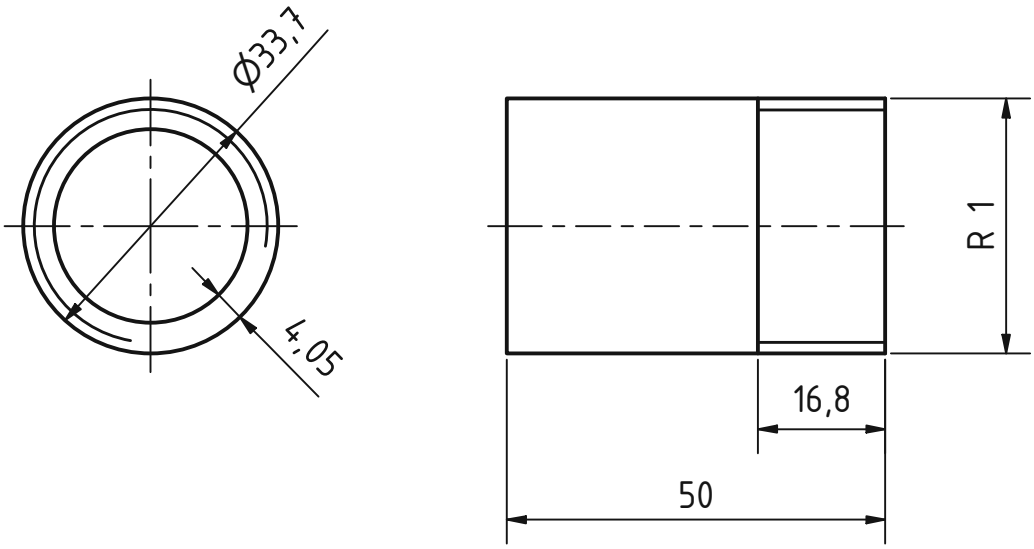

Fertigungshinweis:
Ausgangsmaterial Rohr EN 10216

unbemaßte Werkstückkanten DIN ISO 13715 | ISO 128 | Allgemeintoleranz ISO2768 mK

Maßstab: 1 : 1	Masse: 0,149 kg		
Oberflächenbehandlung:	Material: Edelstahl (1.4841)		

	Datum	Name
Gezeichn	11.01.2022	Philipp Mayer
Kontroll		
Norm		

Benennung:
Wirbelschichtkammer Gewindemuffe
Projekt: Micro Hot Prüfstand

INSTITUT FÜR ENERGIETECHNIK UND THERMODYNAMIK
Institute for Energy Systems and Thermodynamics

Z-Nummer: MH018

Blatt 1/1
A4

Status	Änderungen	Datum	Name

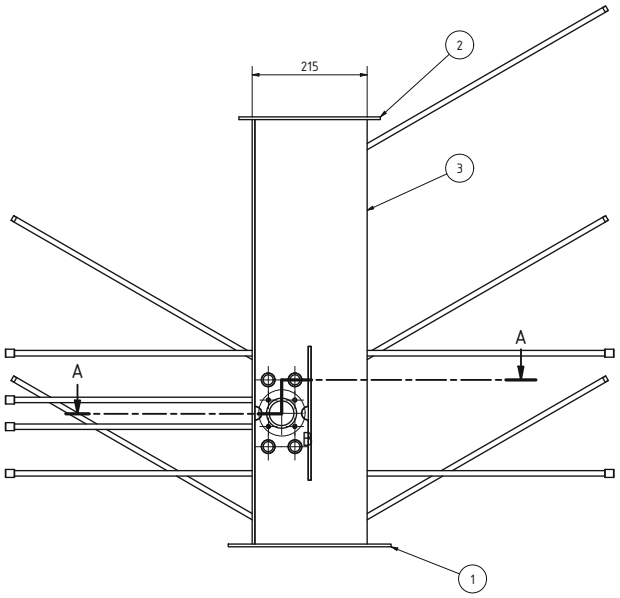

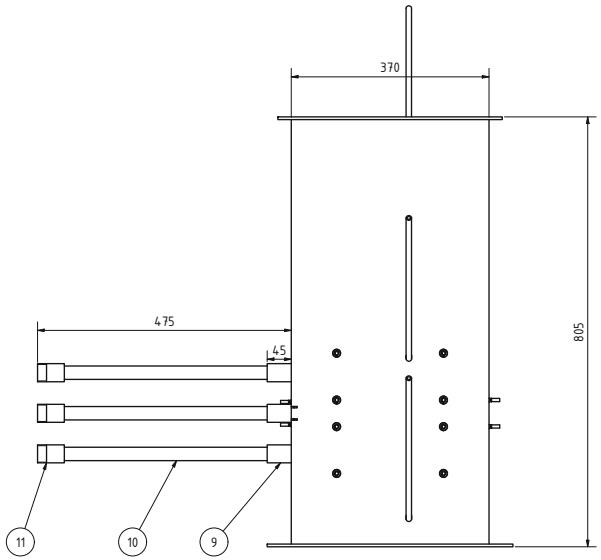

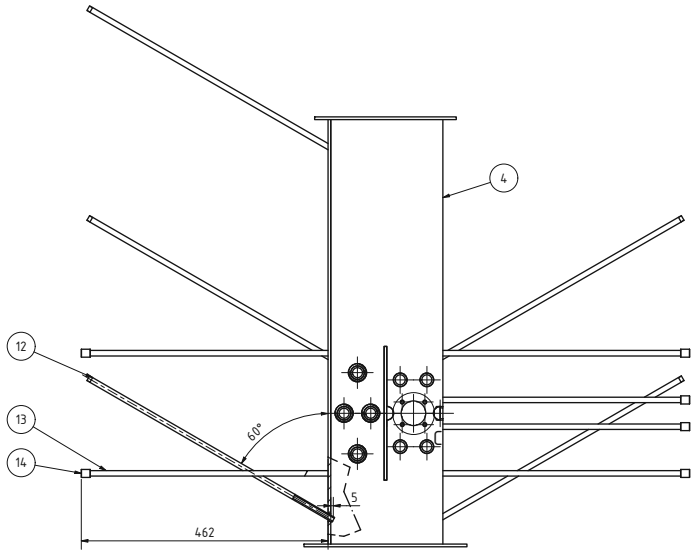

A-A (1 : 5)

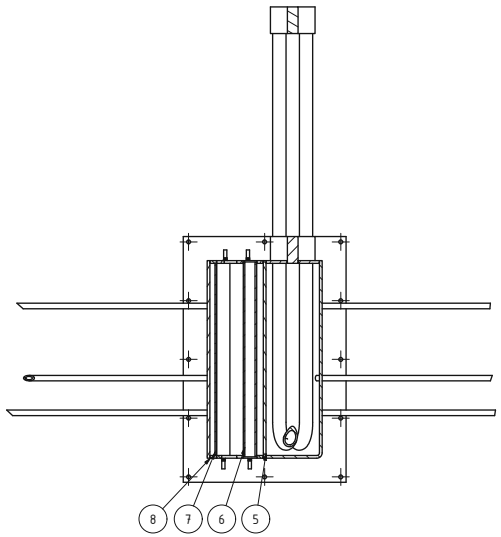

C (1 : 1)

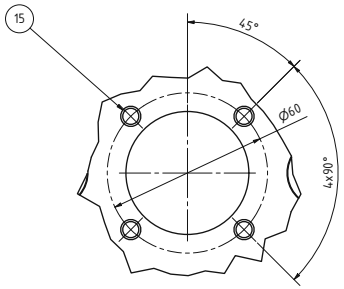

B (1 : 1)

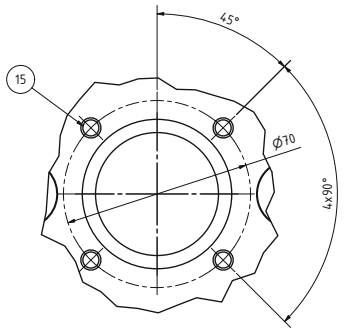

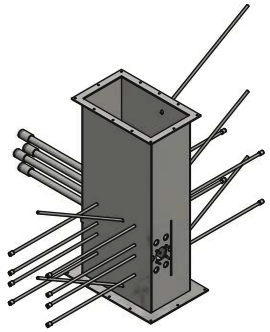

Fertigungshinweis:
Einsatzrohrdummys und Trennblech von außen gasdicht verschweißen und eben mit Blech verschleifen (Dichtfläche).
Kühlrohreinsatz und Muffen mit Kehlnähten dicht verschweißen.

STÜCKLISTE

OBJEKT	ANZAHL	BAUTEILNUMMER	Z-NUMMER	BESCHREIBUNG
1	1	Wirbelschichtkammer Flansch unten	MH008	
2	1	Wirbelschichtkammer Flansch oben	MH009	
3	1	Wirbelschichtkammer Blech vorne	MH010	
4	1	Wirbelschichtkammer Blech hinten	MH011	
5	1	Wirbelschichtkammer Trennblech	MH012	
6	4	Wirbelschichtkammer Einsatzrohrdummy	MH013	
7	2	Wirbelschichtkammer Einsatzrohrdummy Hälfte	MH014	
8	4	Wirbelschichtkammer Verschlussblech Einsatzrohrdummy Hälfte	MH015	
9	4	Wirbelschichtkammer Durchgangsmuffe	MH016	
10	2	Wirbelschichtkammer Kühlrohreinsatz	MH017	
11	4	Wirbelschichtkammer Gewindemuffe	MH018	
12	5	Druckmessstutzen	MH005	
13	12	Wirbelschichtkammer Rohr Temperaturmessung	MH033	
14	12	Gewindemuffe Rp1/8	MUR 18 AS ES	Landefeld, DIN EN 10241
15	8	Schweißbolzen ISO 13918 - PT M6x20 - Edelstahl A2		Würth, Art.-Nr.: 44776 20

unbemaßte Werkstückkanten DIN ISO 13715 | ISO 128 | Allgemeintoleranz ISO2768 mK | Maßstab: 1 : 5 | Masse: 55,790 kg

Oberflächenbehandlung | Material

	Datum	Name
Gezeichn.	12.01.2022	Philipp Mayer
Kontrollt.		
Norm		

INSTITUT FÜR ENERGIETECHNIK UND THERMODYNAMIK

Benennung: Wirbelschichtkammer Schweißbaugruppe

Projekt: Micro Hot Prüfstand

Z-Nummer: MH019

Blatt 1/1 A1

Index	Änderungen	Datum	Name

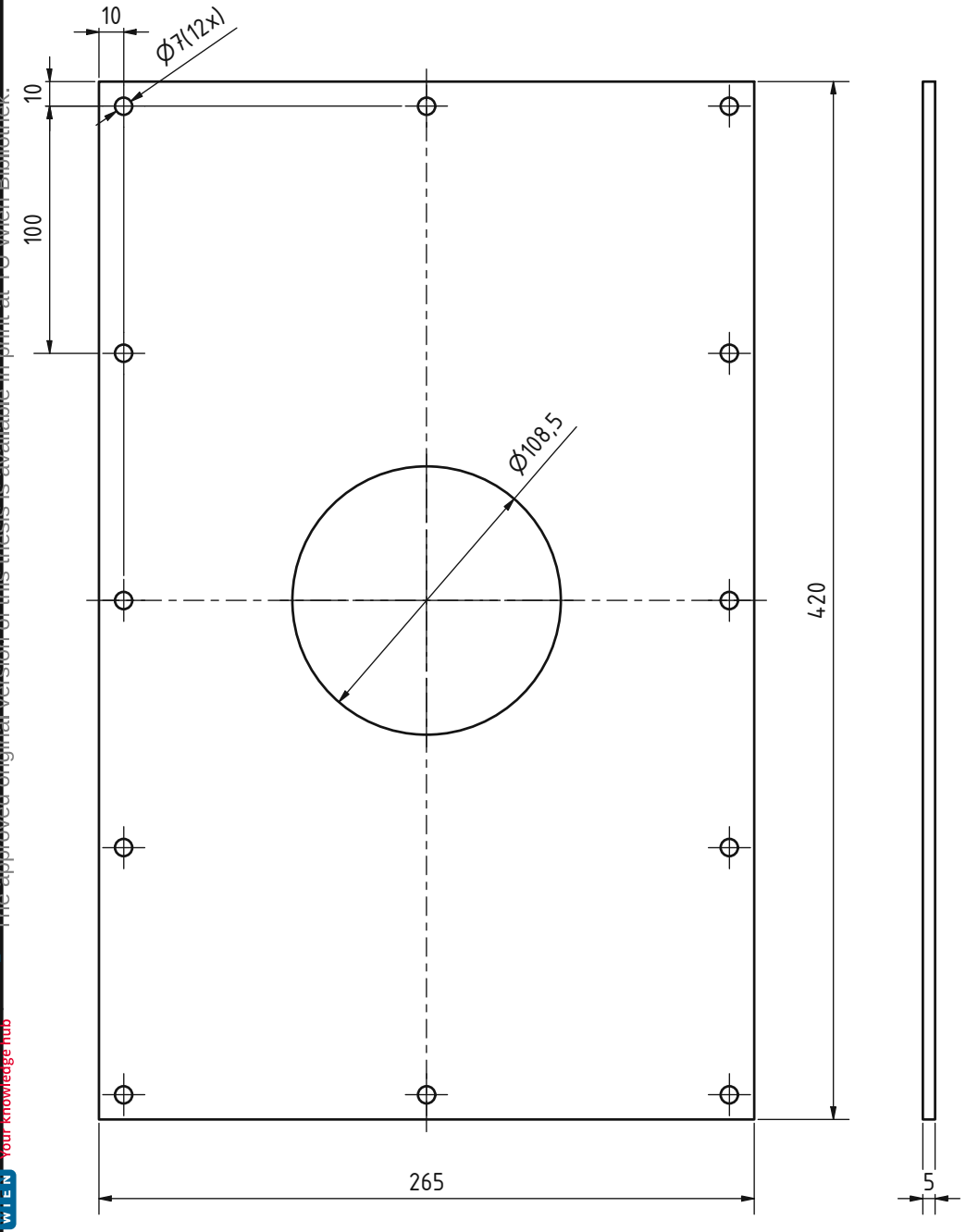

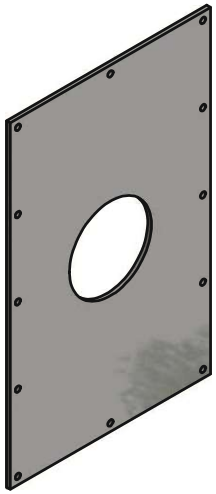

unbemaßte Werkstückkanten DIN ISO 13715	ISO 128	Allgemeintoleranz ISO2768 mK	Maßstab: 1 : 2
		Oberflächenbehandlung:	Masse: 4,013 kg
			Material: Edelstahl (1.4841)

	Datum	Name
Gezeichn	12.01.2022	Philipp Mayer
Kontroll		
Norm		

Benennung:
Deckel Wirbelschichtkammer Flansch
Projekt: Micro Hot Prüfstand

INSTITUT FÜR ENERGIETECHNIK UND THERMODYNAMIK
Institute for Energy Systems and Thermodynamics

Z-Nummer: MH020

Blatt 1/1
A3

Status	Änderungen	Datum	Name

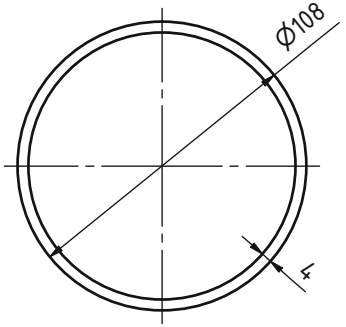

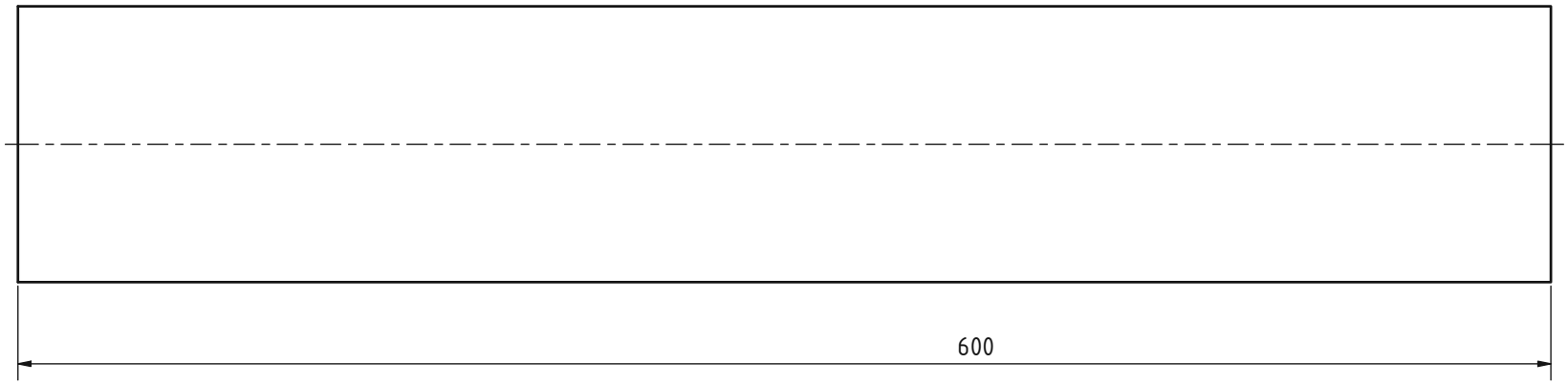

Fertigungshinweis:
Ausgangsmaterial Rohr EN 10216

unbemaßte Werkstückkanten DIN ISO 13715 (0,3 / 0,3)	ISO 128	Allgemeintoleranz ISO2768 mK	Maßstab: 1 : 2
Oberflächenbehandlung:			Masse: 6,195 kg
Material: Edelstahl (1.4841)			

	Datum	Name
Gezeichn	12.01.2022	Philipp Mayer
Kontroll		
Norm		

Benennung: Deckel Wirbelschichtkammer Rohr
Projekt: Micro Hot Prüfstand

INSTITUT FÜR ENERGIETECHNIK UND THERMODYNAMIK
Institute for Energy Systems and Thermodynamics

Z-Nummer: MH021

Blatt 1/1
A3

Status	Änderungen	Datum	Name

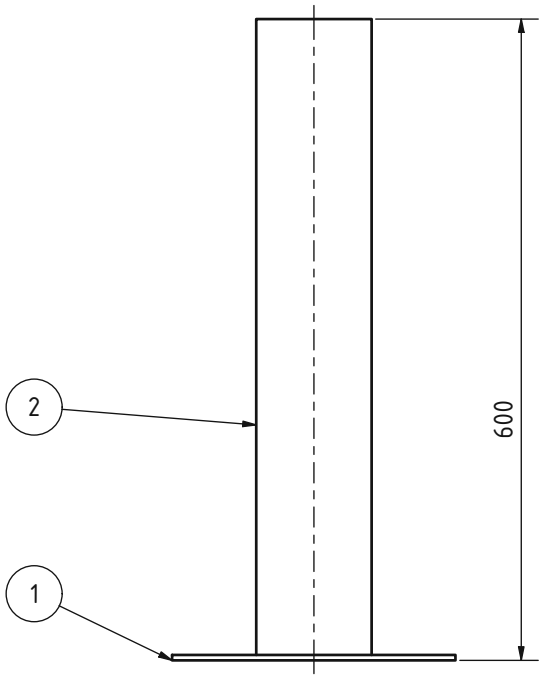

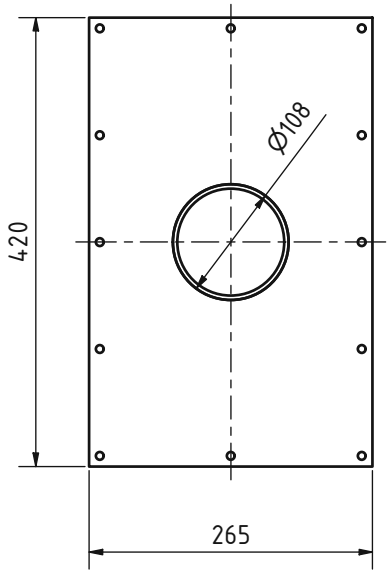

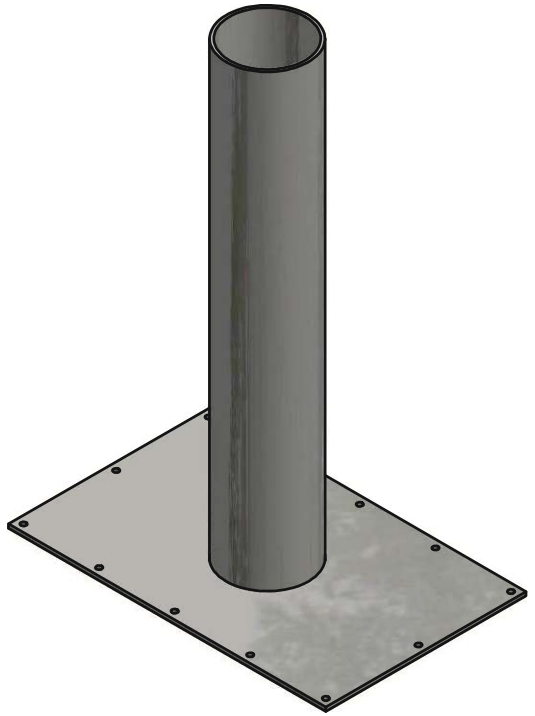

Fertigungshinweis:
Bauteile mit Kehlnaht verschweißen

STÜCKLISTE

OBJEKT	ANZAHL	BAUTEILNUMMER	Z-NUMMER	BESCHREIBUNG
1	1	Deckel Wirbelschichtkammer Flansch	MH020	
2	1	Deckel Wirbelschichtkammer Rohr	MH021	

unbemaßte Werkstückkanten DIN ISO 13715 — 0,3 — 0,3

ISO 128

Allgemeintoleranz ISO2768 mK

Maßstab: 1 : 5

Masse: 10,208 kg

Oberflächenbehandlung:

Material:

	Datum	Name
Gezeichn	12.01.2022	Philipp Mayer
Kontroll		
Norm		

Benennung:
Deckel Wirbelschichtkammer Schweißbaugruppe
Projekt: Micro Hot Prüfstand

INSTITUT FÜR ENERGIETECHNIK UND THERMODYNAMIK
Institute for Energy Systems and Thermodynamics

Z-Nummer: MH022

Blatt 1/1
A3

Status	Änderungen	Datum	Name

A-A (1 : 5)

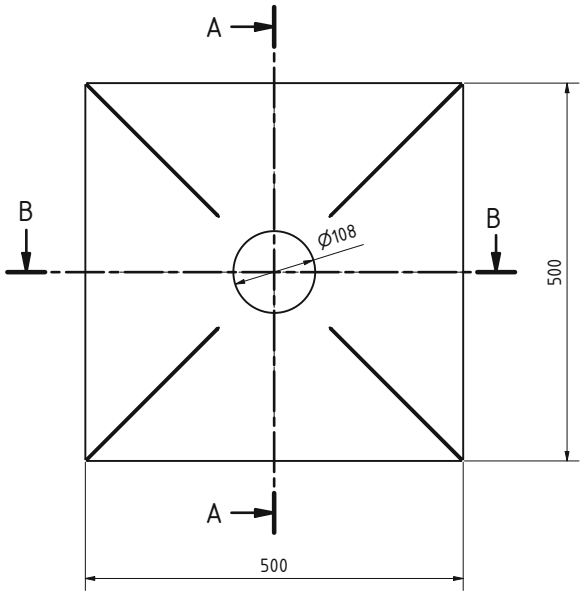

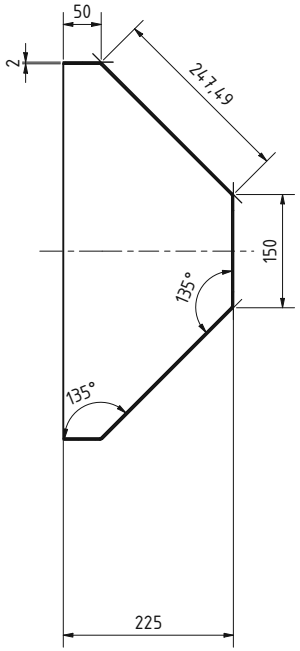

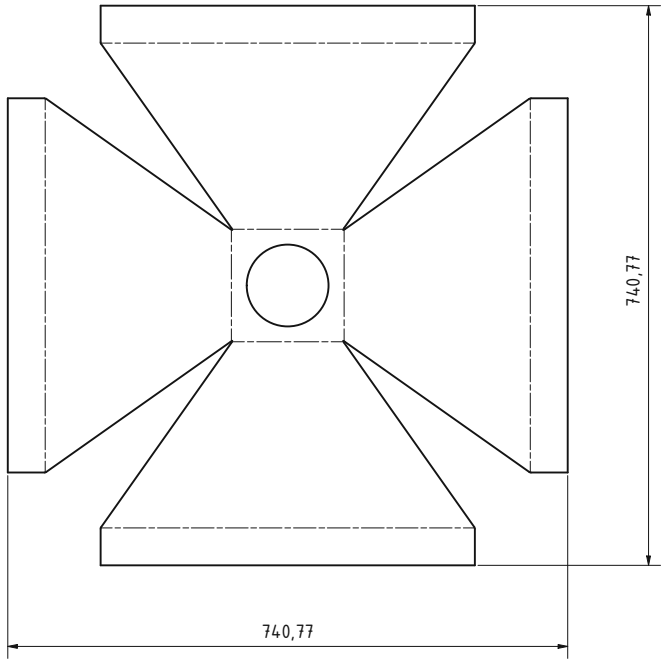

B-B (1 : 5)

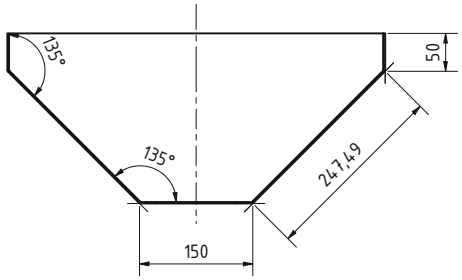

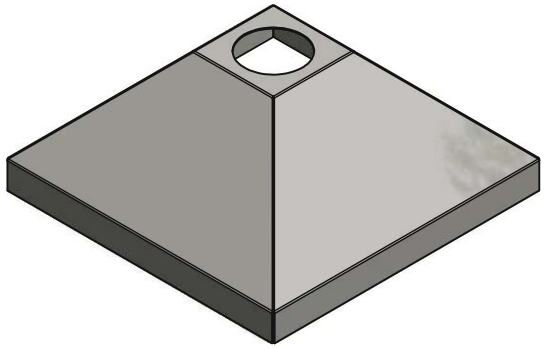

Fertigungshinweis:
Ecken gasdicht verschweißen

unbemaßte Werkstückkanten DIN ISO 13715	ISO 128	Allgemeintoleranz ISO2768 mK	Maßstab: 1 : 5	Masse: 6,722 kg	
			Oberflächenbehandlung:	Material: Stahl S235 JR	
	Datum	Name	Benennung: Abzugsbaube Blech		
	Gezeichn. 12.01.2022	Philipp Mayer			
	Kontroll		Projekt: Micro Hot Prüfstand		
	Norm		INSTITUT FÜR ENERGIETECHNIK UND THERMODYNAMIK	Z-Nummer: MH023	Blatt 1/1 A2
Status Änderungen	Datum	Name			

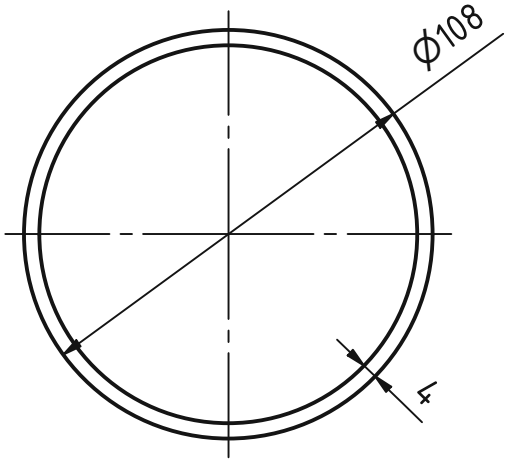

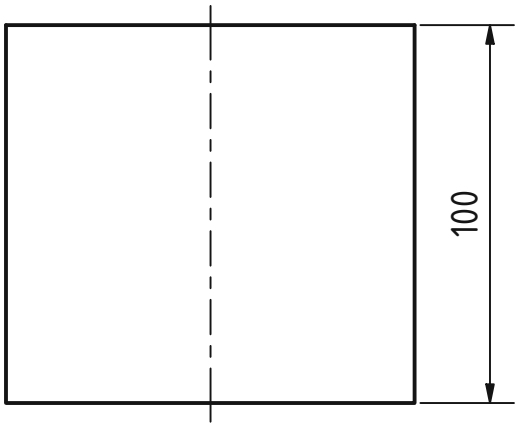

Fertigungshinweis:
Ausgangsmaterial Rohr EN 10216

unbemaßte Werkstückkanten DIN ISO 13715 | ISO 128 | Allgemeintoleranz ISO2768 mK

Maßstab: 1 : 2				Masse: 1,026 kg	
Oberflächenbehandlung:				Material: Stahl S235 JR	
			Datum	Name	Benennung: Abzugshaube Rohr
		Gezeichn	12.01.2022	Philipp Mayer	
		Kontroll			Projekt: Micro Hot Prüfstand
		Norm			
					Z-Nummer: MH024
					Blatt 1/1 A4
Status	Änderungen	Datum	Name		

INSTITUT FÜR ENERGIETECHNIK UND THERMODYNAMIK
Institute for Energy Systems and Thermodynamics

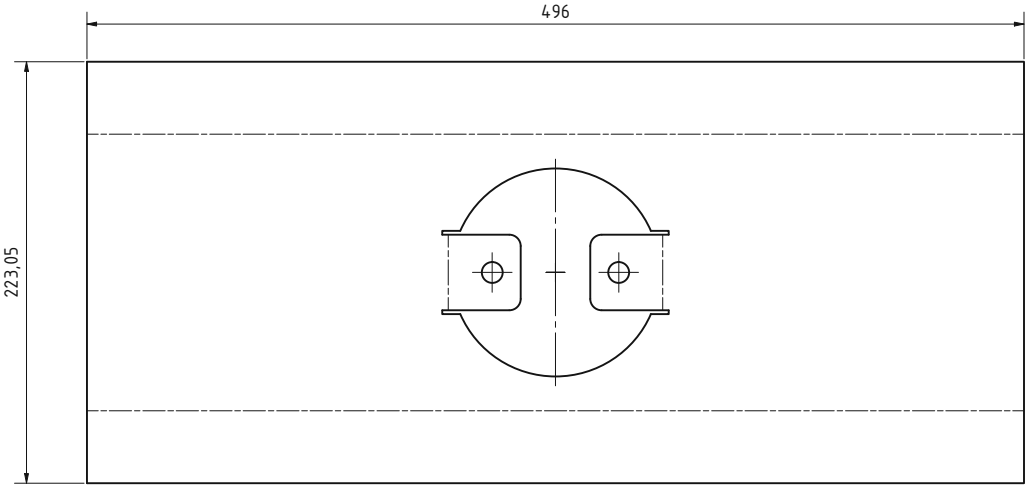

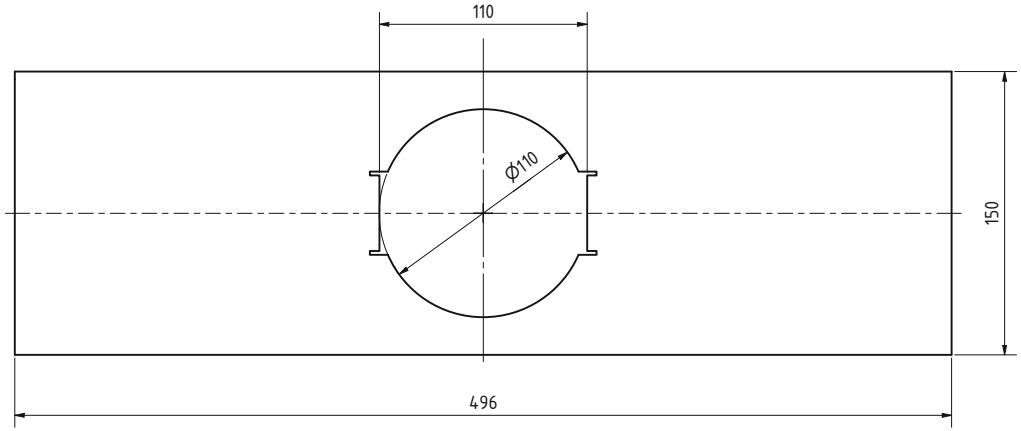

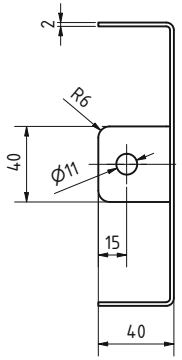

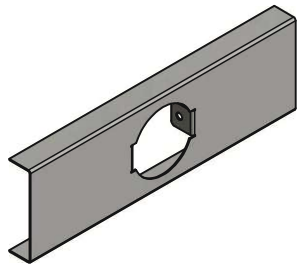

unbemaßte Werkstückkanten DIN ISO 13715	ISO 128	Allgemeintoleranz ISO2768 mK	Maßstab: 1 : 2	Masse: 1,631 kg	
			Oberflächenbehandlung:	Material: Stahl S235 JR	
	Datum	Name	Benennung: Abzugshaube Befestigungswinkel lange		
Gezeichn.	12.01.2022	Philipp Mayer			
Kontrolli.			Projekt: Micro Hot Prüfstand		
Norm			INSTITUT FÜR ENERGIETECHNIK UND THERMODYNAMIK Institute for Energy Systems and Thermodynamics	Z-Nummer: MH025	Blatt 1/1 A2
Status	Änderungen	Datum / Name			

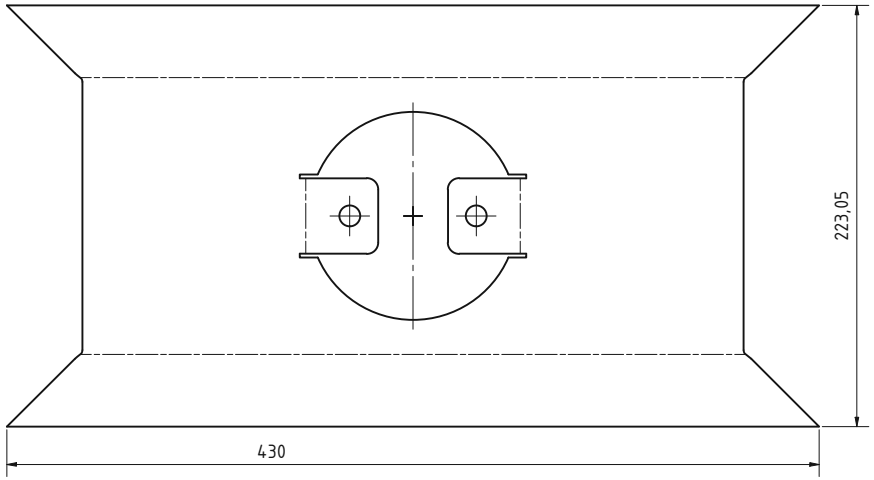

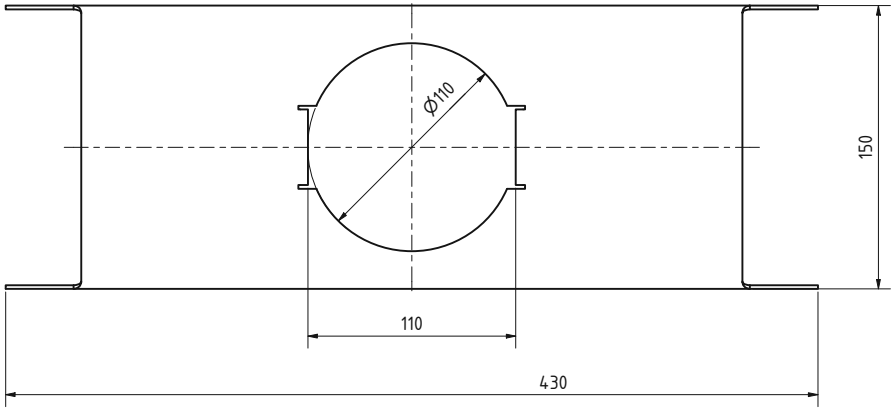

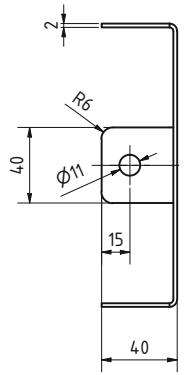

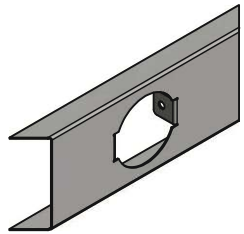

unbemaßte Werkstückkanten DIN ISO 13715	ISO 128	Allgemeintoleranz ISO2768 mK	Maßstab: 1 : 2
			Masse: 1,169 kg
		Oberflächenbehandlung:	Material: Stahl S235 JR
	Datum / Name		Benennung: Abzugshaube Befestigungswinkel kurz
Gezeichn.	12.01.2022 / Philipp Mayer		Projekt: Micro Hot Prüfstand
Kontroll.			
Norm			
INSTITUT FÜR ENERGIETECHNIK UND THERMODYNAMIK Institute for Energy Systems and Thermodynamics			Z-Nummer: MH026
Status / Änderungen / Datum / Name			Blatt 1/1 A2

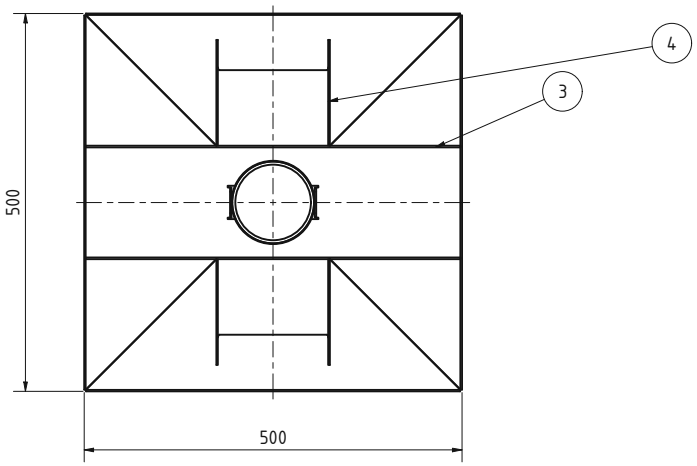

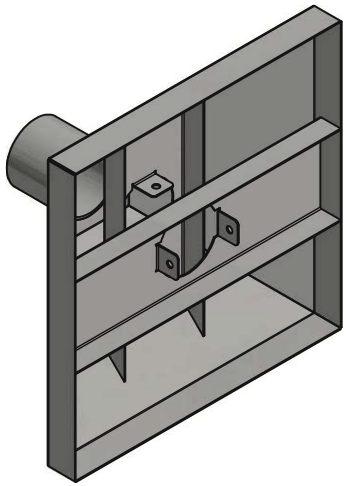

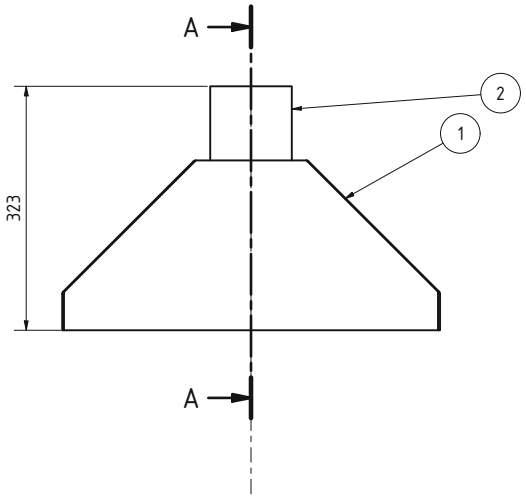

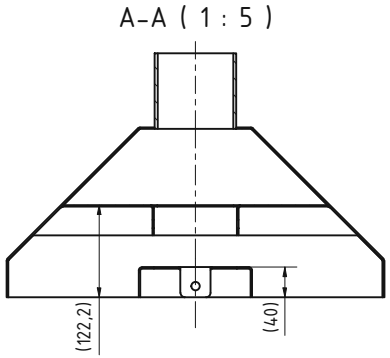

STÜCKLISTE				
OBJEKT	ANZAHL	BAUTEILNUMMER	Z-NUMMER	BESCHREIBUNG
1	1	Abzugsbaube Blech	MH023	
2	1	Abzugshaube Rohr	MH024	
3	1	Abzugshaube Befestigungswinkel lange	MH025	
4	1	Abzugshaube Befestigungswinkel kurz	MH026	

Fertigungshinweis:
Bauteile mit Kehlnähten verschweißen

unbemaßte Werkstückkanten DIN ISO 13715 | ISO 128 | Allgemeintoleranz ISO2768 mK | Maßstab: 1 : 5 | Masse: 10,547 kg

Oberflächenbehandlung: | Material:

	Datum	Name
Gezeichn.	12.01.2022	Philipp Mayer
Kontroll.		
Norm		

INSTITUT FÜR ENERGIETECHNIK UND THERMODYNAMIK
Institute for Energy Systems and Thermodynamics

Benennung:
Abzugshaube Schweißbaugruppe
Projekt: Micro Hot Prüfstand

Z-Nummer: MH027

Blatt 1/1 A2

Status | Änderungen | Datum | Name

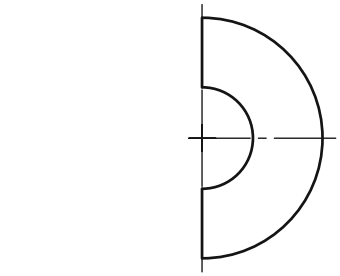

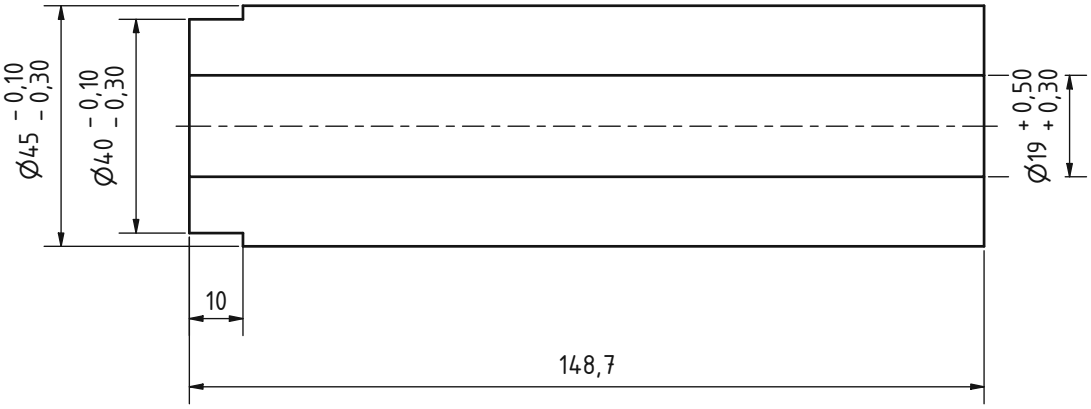

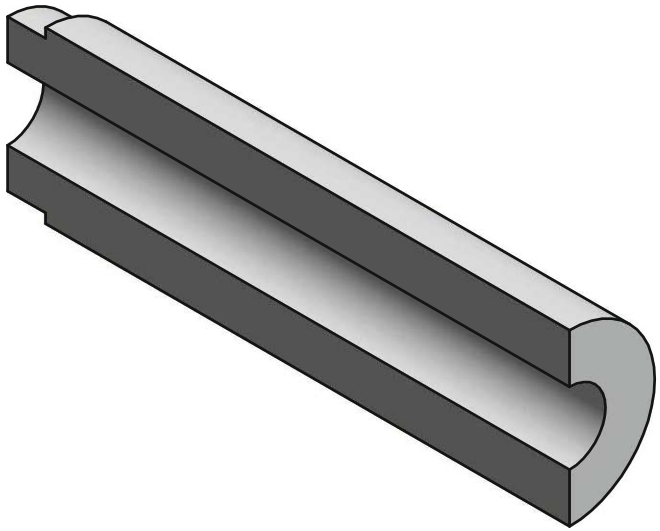

Bauteiloberfläche: Ra3,2

unbemaßte Werkstückkanten DIN ISO 13715 (0,3 / 0,3)	ISO 128	Allgemeintoleranz ISO2768 mK	Maßstab: 1 : 1
Oberflächenbehandlung:			Masse: 0,241 kg
Material: Keramik Macor			

	Datum	Name
Gezeichn	12.01.2022	Philipp Mayer
Kontroll		
Norm		

Benennung:
Heizelement Keramikhalbschale vorne
Projekt: Micro Hot Prüfstand

INSTITUT FÜR ENERGIETECHNIK UND THERMODYNAMIK
Institute for Energy Systems and Thermodynamics

Z-Nummer: MH028

Blatt 1/1 A3

Status	Änderungen	Datum	Name

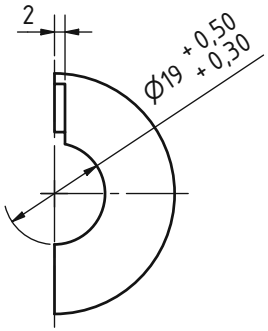

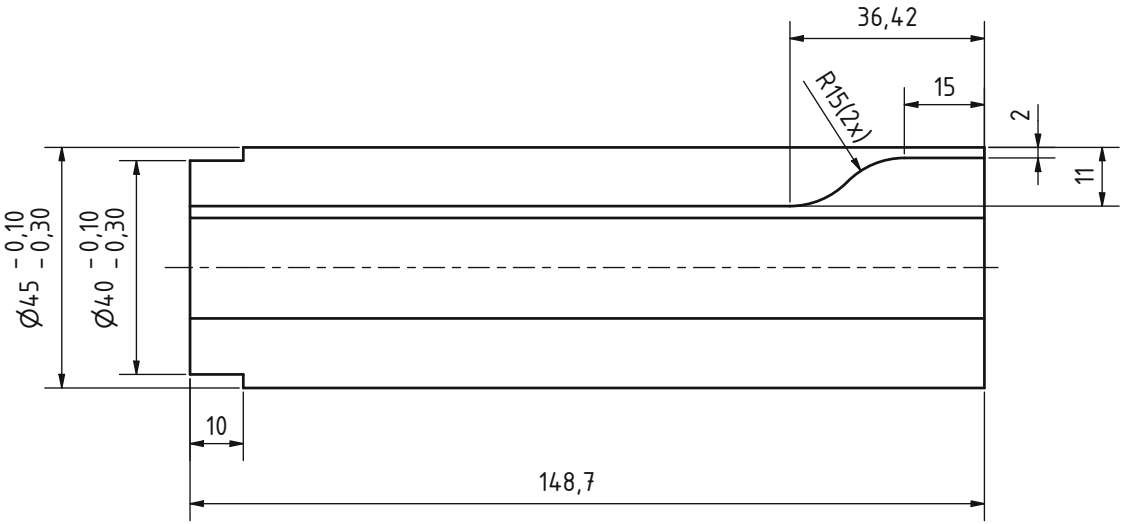

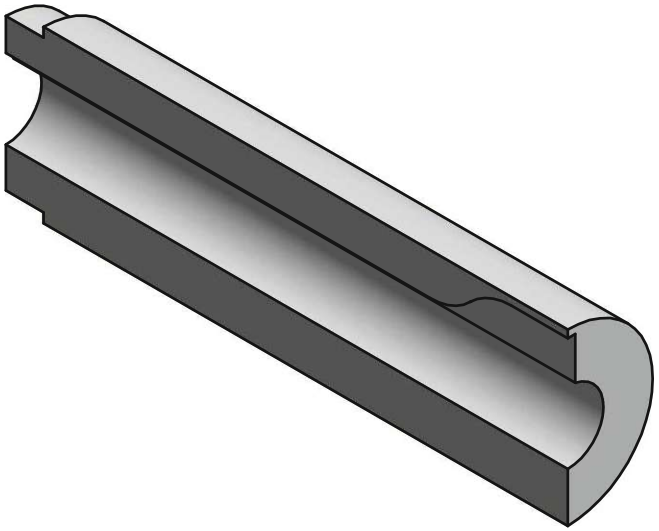

Bauteiloberfläche: Ra3,2

unbemaßte Werkstückkanten DIN ISO 13715 (0,3 / 0,3)	ISO 128	Allgemeintoleranz ISO2768 mK	Maßstab: 1 : 1
Oberflächenbehandlung:			Masse: 0,238 kg
Material: Keramik Macor			

	Datum	Name
Gezeichn	12.01.2022	Philipp Mayer
Kontroll		
Norm		

Benennung:
Heizelement Keramikhalbschale vorne Nut
Projekt: Micro Hot Prüfstand

INSTITUT FÜR ENERGIETECHNIK UND THERMODYNAMIK
Institute for Energy Systems and Thermodynamics

Z-Nummer: MH029

Blatt 1/1
A3

Status	Änderungen	Datum	Name

A-A (1 : 1)

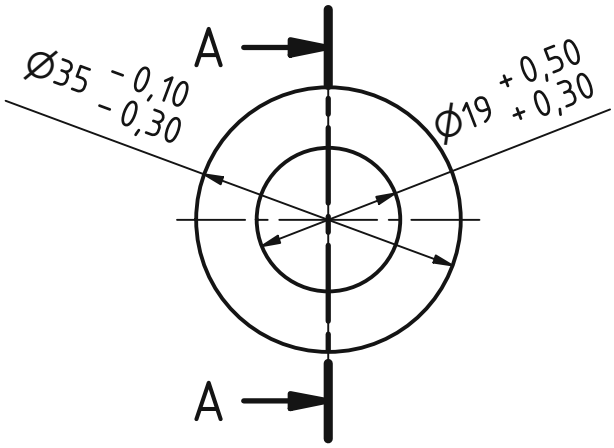

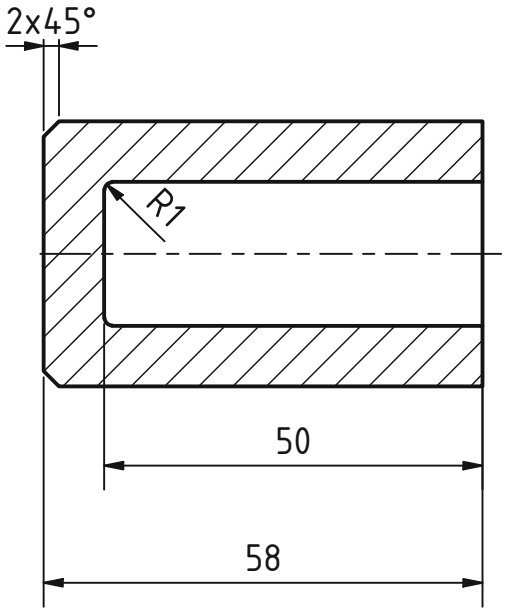

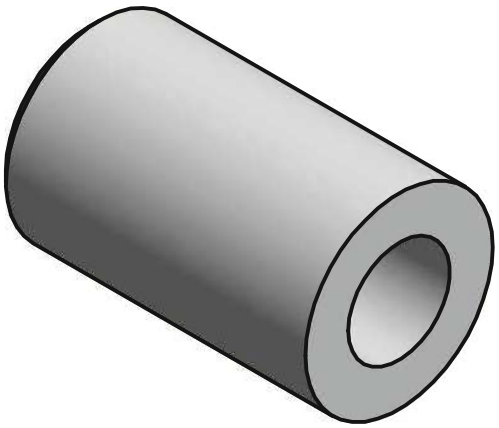

Bauteiloberfläche: Ra3,2

unbemaßte Werkstückkanten DIN ISO 13715 ⌊0,3 ⌊0,3	ISO 128	Allgemeintoleranz ISO2768 mK	Maßstab: 1 : 1 / Masse: 0,104 kg
			Oberflächenbehandlung: / Material: Keramik Macor
	Datum	Name	Benennung: Heizelement Keramikbuchse hinten
	Gezeichn 12.01.2022	Philipp Mayer	Projekt: Micro Hot Prüfstand
	Kontroll		
	Norm		
	INSTITUT FÜR ENERGIETECHNIK UND THERMODYNAMIK Institute for Energy Systems and Thermodynamics		Z-Nummer: MH030 / Blatt 1/1 / A4
Status Änderungen Datum Name			

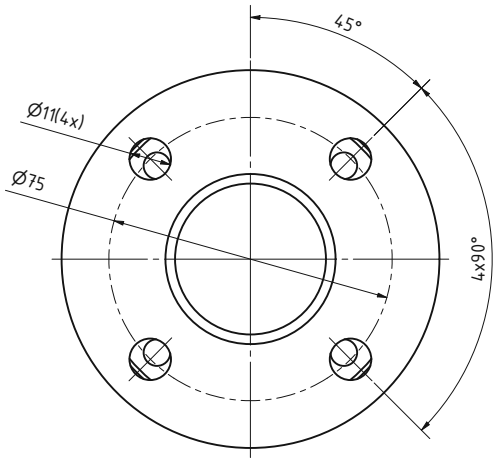

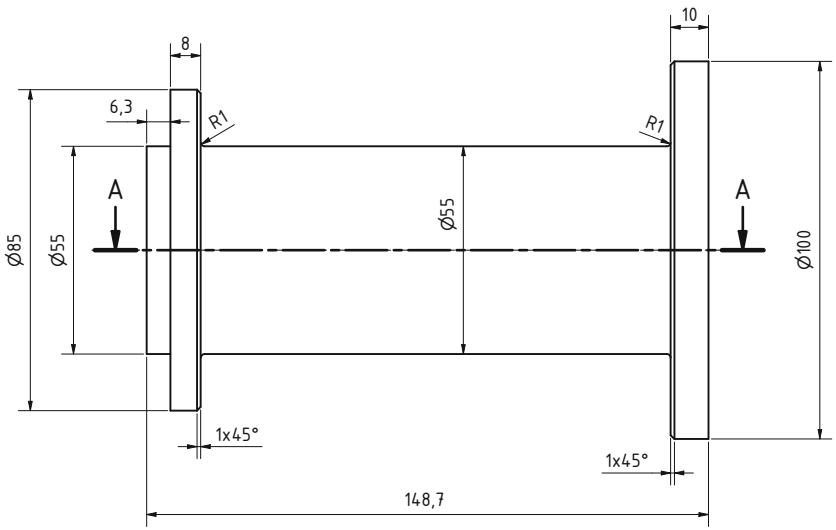

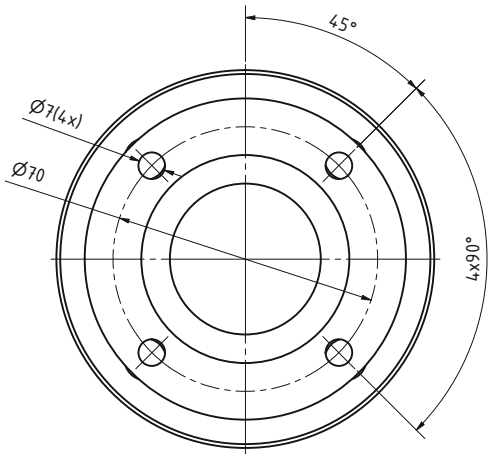

A-A (1 : 1)

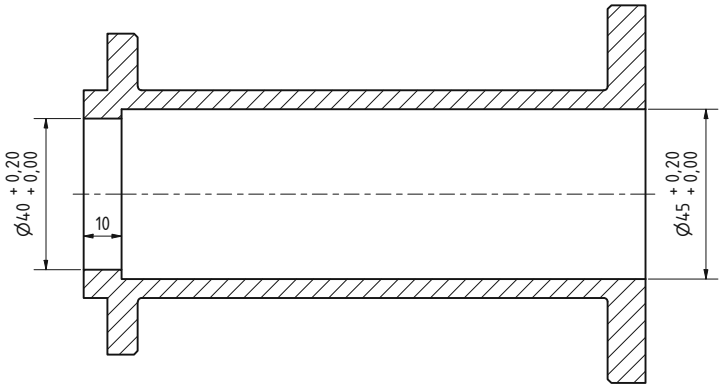

Bauteiloberfläche: Ra3,2

unbemaßte Werkstückkanten DIN ISO 13715	ISO 128	Allgemeintoleranz ISO2768 mK	Maßstab: 1 : 1	Masse: 1,549 kg	
			Oberflächenbehandlung:	Material: Edelstahl (1.4841)	
	Datum	Name	Benennung: Heizelement Montageflansch		
	Gezeichn. 12.01.2022	Philipp Mayer			
	Kontrolli		Projekt: Micro Hot Prüfstand		
	Norm		INSTITUT FÜR ENERGIETECHNIK UND THERMODYNAMIK Institute for Energy Systems and Thermodynamics	Z-Nummer: MH031	Blatt 1/1 A2
Status	Änderungen	Datum Name			

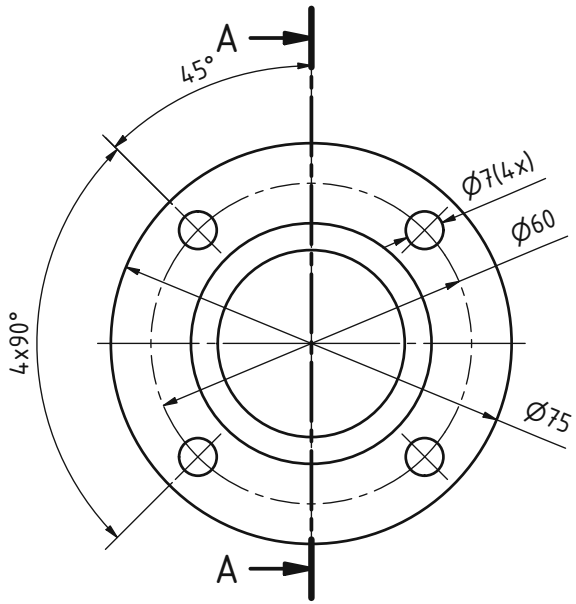

A-A (1 : 1)

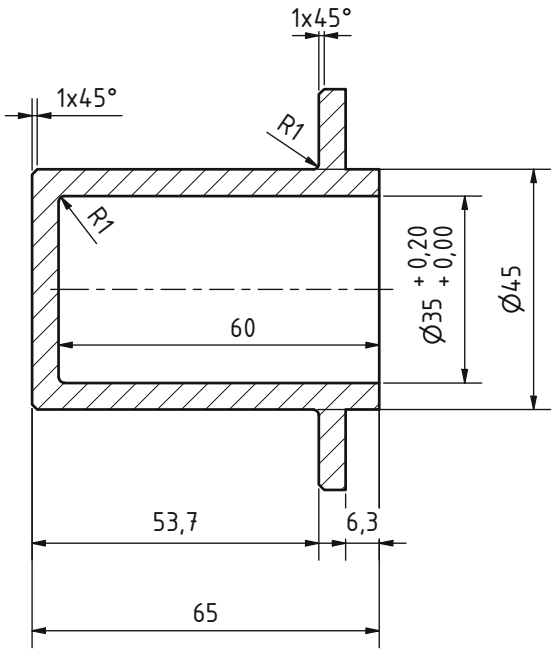

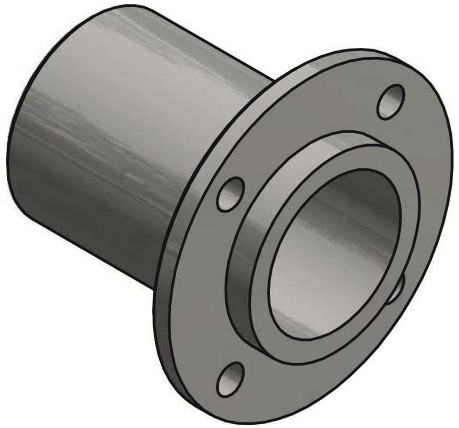

Bauteiloberfläche: Ra3,2

unbemaßte Werkstückkanten DIN ISO 13715 0,3 0,3	ISO 128	Allgemeintoleranz ISO2768 mK	Maßstab: 1 : 1
Oberflächenbehandlung:			Masse: 0,465 kg
Material: Edelstahl (1.4841)			
Benennung: Heizelement Aufnahmenflansch			
Projekt: Micro Hot Prüfstand			
Z-Nummer: MH032			Blatt 1/1 A3

	Datum	Name
Gezeichn	13.01.2022	Philipp Mayer
Kontroll		
Norm		

INSTITUT FÜR ENERGIETECHNIK UND THERMODYNAMIK
Institute for Energy Systems and Thermodynamics

Status	Änderungen	Datum	Name

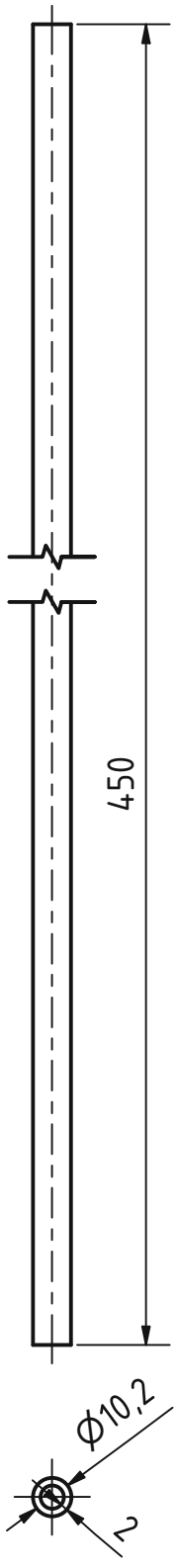

unbemaßte Werkstückkanten DIN ISO 13715

0,3 0,3

ISO 128

Allgemeintoleranz ISO2768 mK

Maßstab: 1 : 2

Masse: 0,183 kg

Oberflächenbehandlung:

Material: Edelstahl (1.4841)

	Datum	Name
Gezeichn	13.01.2022	Philipp Mayer
Kontroll		
Norm		

Benennung:

Wirbelschichtkammer Rohr Temperaturmessung

Projekt: Micro Hot Prüfstand

INSTITUT FÜR ENERGIETECHNIK UND THERMODYNAMIK
Institute for Energy Systems and Thermodynamics

Z-Nummer: MH033

Blatt 1/1

A4

Status	Änderungen	Datum	Name

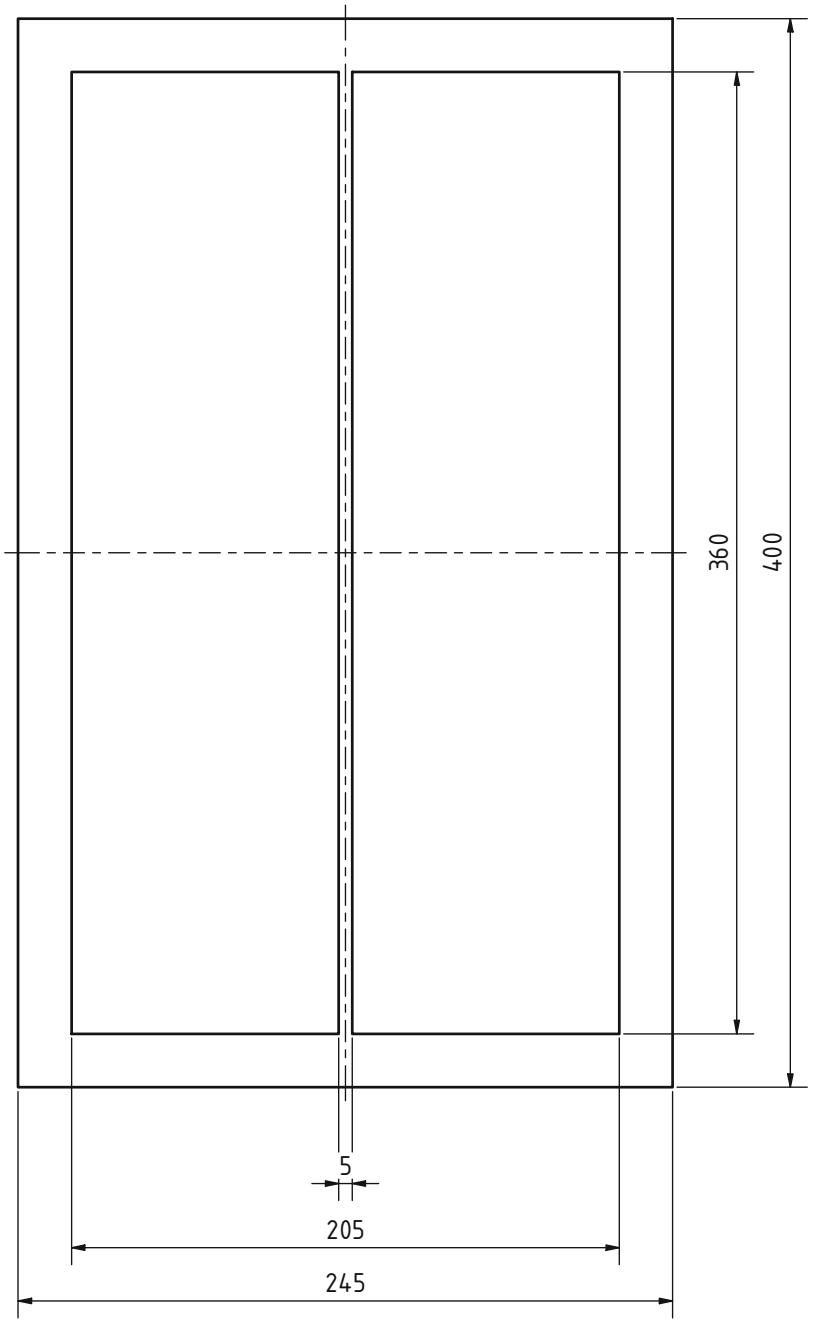

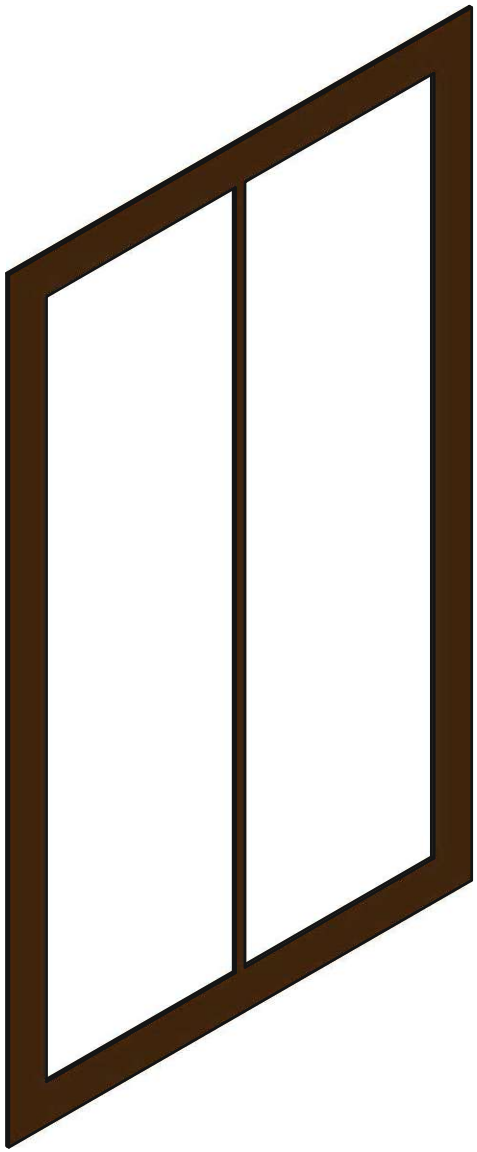

unbemaßte Werkstückkanten DIN ISO 13715	ISO 128	Allgemeintoleranz ISO2768 mK	Maßstab: 1 : 2
		Oberflächenbehandlung:	Masse: 0,041 kg
			Material: Klinger Milam PSS
	Datum	Name	Benennung: Dichtung Sinterplatte unten
	Gezeichn 17.01.2022	Philipp Mayer	
	Kontroll		
	Norm		Projekt: Micro Hot Prüfstand
INSTITUT FÜR ENERGIETECHNIK UND THERMODYNAMIK Institute for Energy Systems and Thermodynamics			Z-Nummer: MH034
Status Änderungen Datum Name			Blatt 1/1 A3

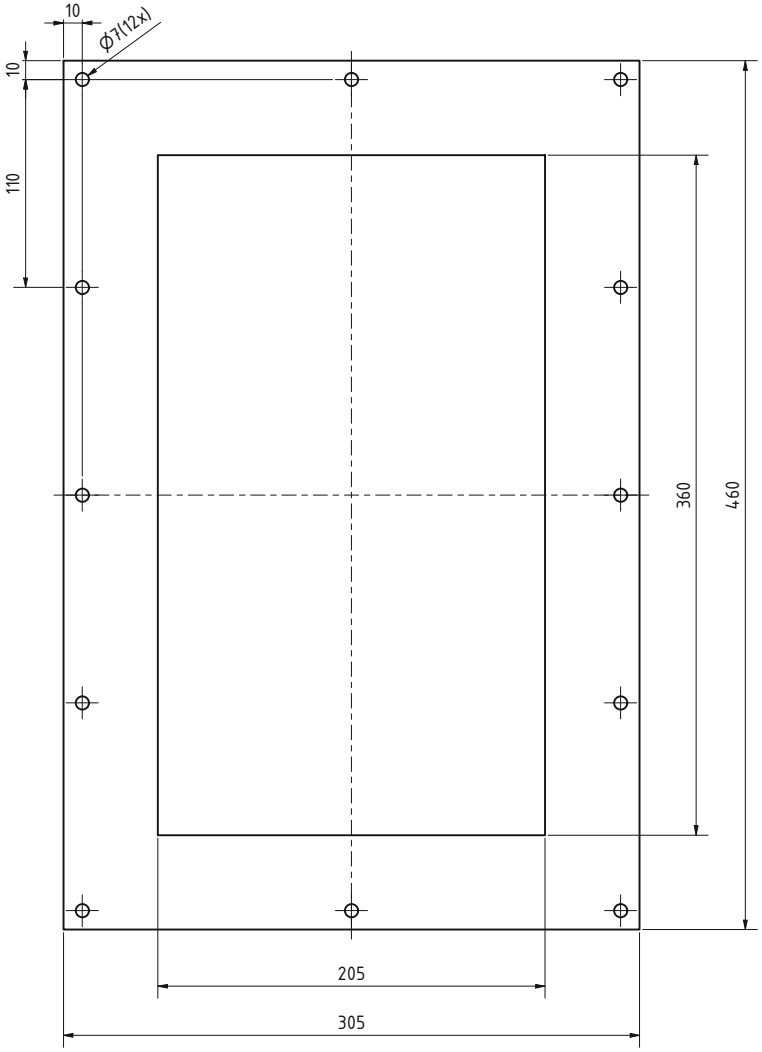

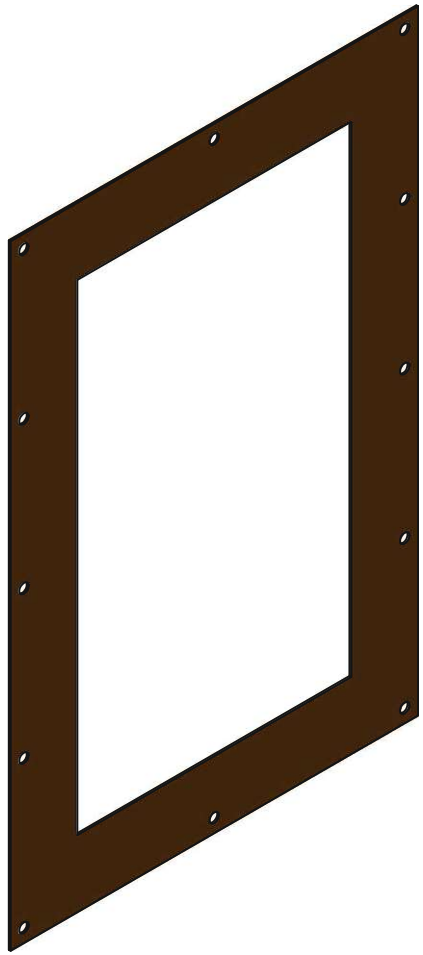

unbemaßte Werkstückkanten DIN ISO 13715	ISO 128	Allgemeintoleranz ISO2768 mK	Maßstab: 1 : 2
			Masse: 0,103 kg
		Oberflächenbehandlung:	Material: Klinger Milam PSS
	Datum / Name		Benennung: Dichtung Sinterplatte oben
Gezeichn.	17.01.2022	Philipp Mayer	
Kontroll.			Projekt: Micro Hot Prüfstand
Norm			
INSTITUT FÜR ENERGIETECHNIK UND THERMODYNAMIK Institute for Energy Systems and Thermodynamics			Z-Nummer: MH035
Status / Änderungen / Datum / Name			Blatt: 1/1 A2

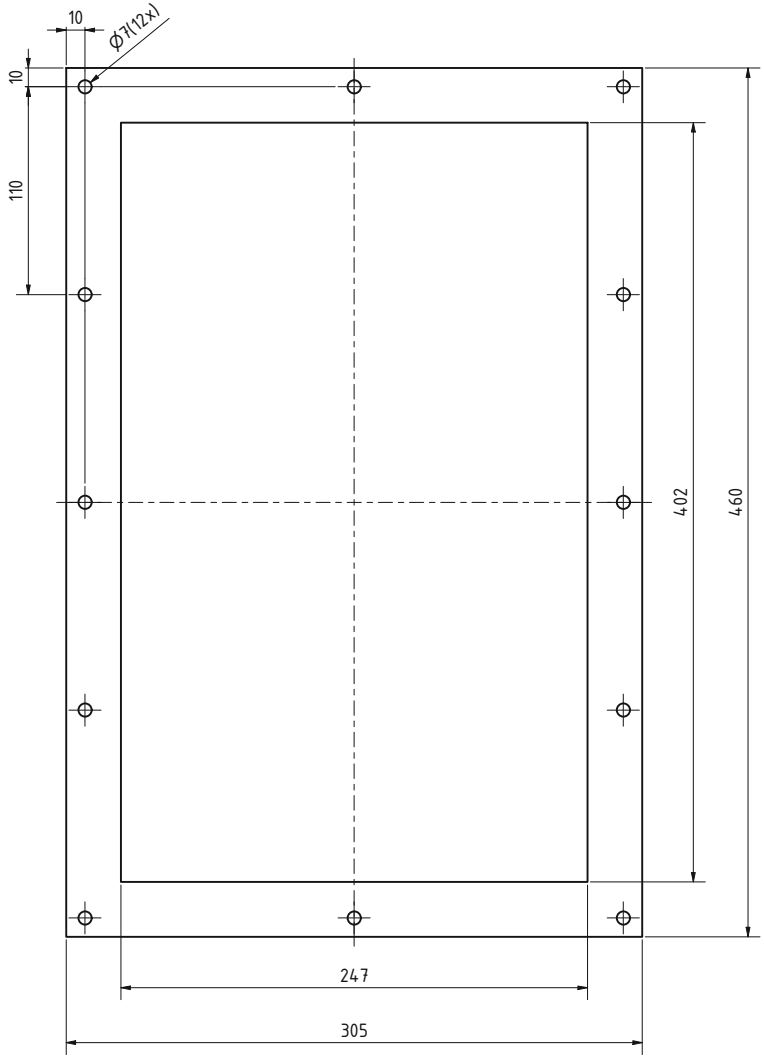

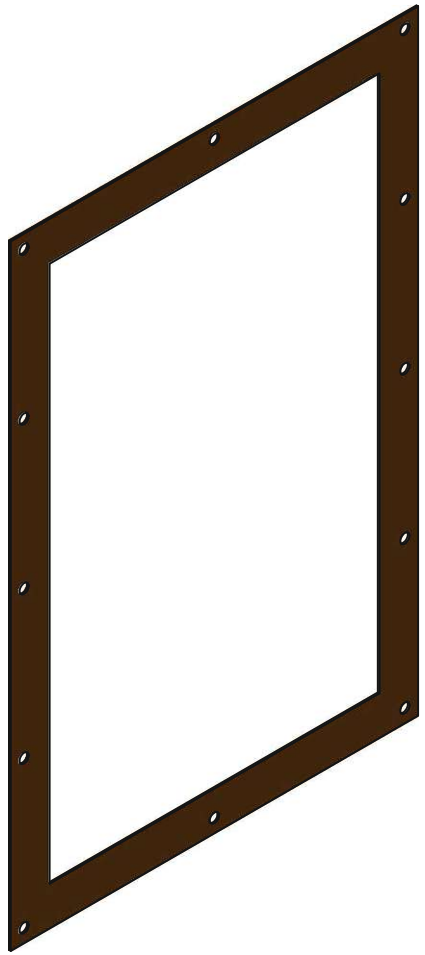

unbemaßte Werkstückkanten DIN ISO 13715	ISO 128	Allgemeintoleranz ISO2768 mK	Maßstab: 1 : 2	Masse: 0,063 kg	
			Oberflächenbehandlung:	Material: Klinger Milam PSS	
	Datum	Name	Benennung: Dichtung Wirbelschichtkammer Windkasten		
Gezeichn.	17.01.2022	Philipp Mayer	Projekt: Micro Hot Prüfstand		
Kontroll.					
Norm					
INSTITUT FÜR ENERGIETECHNIK UND THERMODYNAMIK Institute for Energy Systems and Thermodynamics			Z-Nummer: MH036	Blatt: 1/1 A2	
Status	Änderungen	Datum	Name		

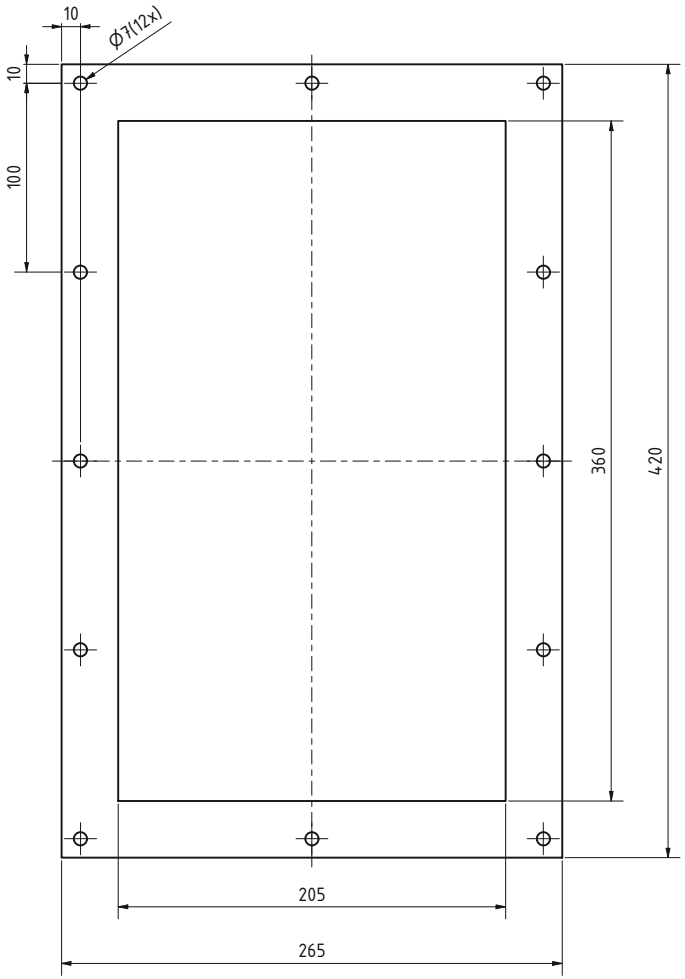

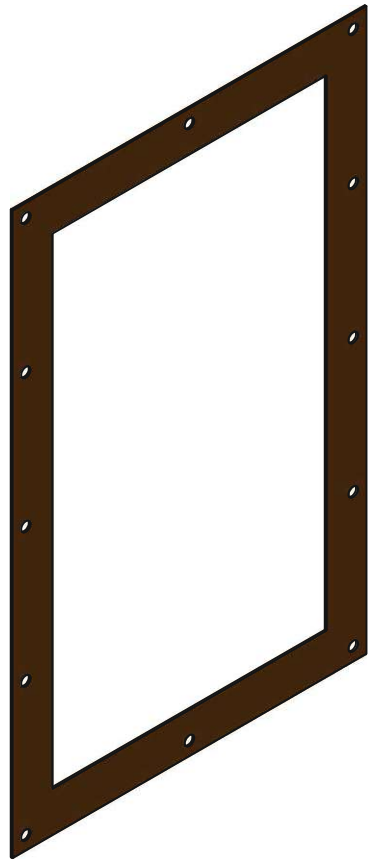

unbemaßte Werkstückkanten DIN ISO 13715	ISO 128	Allgemeintoleranz ISO2768 mK	Maßstab: 1 : 2
			Masse: 0,058 kg
		Oberflächenbehandlung:	Material: Klinger Milam PSS
	Datum / Name		Benennung: Dichtung Deckel Wirbelschichtkammer
Gezeichn.	17.01.2022	Philipp Mayer	Projekt: Micro Hot Prüfstand
Kontroll.			
Norm			
INSTITUT FÜR ENERGIETECHNIK UND THERMODYNAMIK			Z-Nummer: MH037
Status / Änderungen / Datum / Name			Blatt 1/1 A2

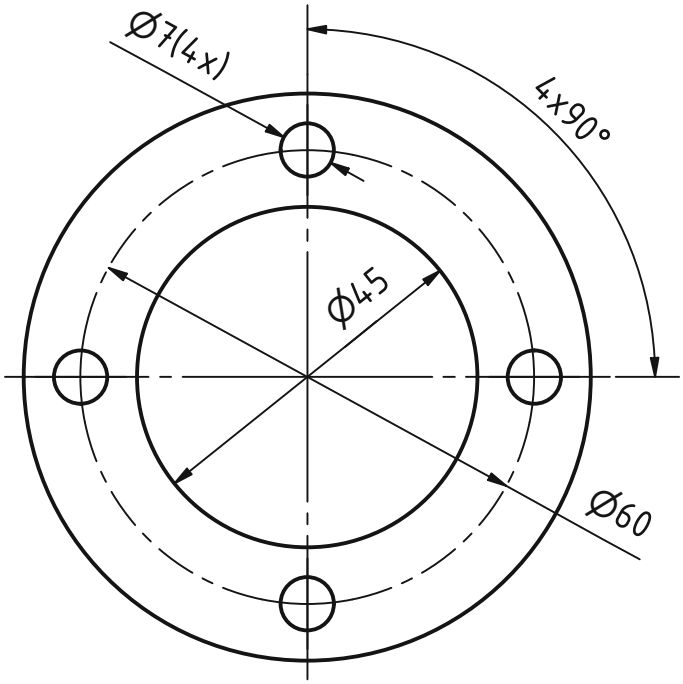

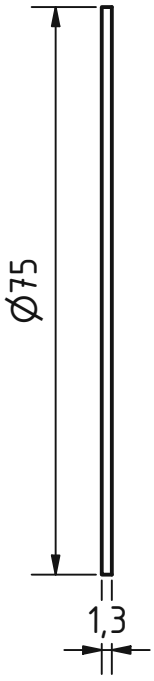

unbemaßte Werkstückkanten DIN ISO 13715 — 0,3 — 0,3

ISO 128

Allgemeintoleranz ISO2768 mK

Maßstab: 1 : 1

Masse: 0,004 kg

Oberflächenbehandlung:

Material: Klinger Milam PSS

	Datum	Name
Gezeichn	18.01.2022	Philipp Mayer
Kontroll		
Norm		

Benennung:

Dichtung Heizelement Aufnahmeflansch

Projekt: Micro Hot Prüfstand

INSTITUT FÜR ENERGIETECHNIK UND THERMODYNAMIK
Institute for Energy Systems and Thermodynamics

Z-Nummer: MH038

Blatt 1/1

A4

Status	Änderungen	Datum	Name

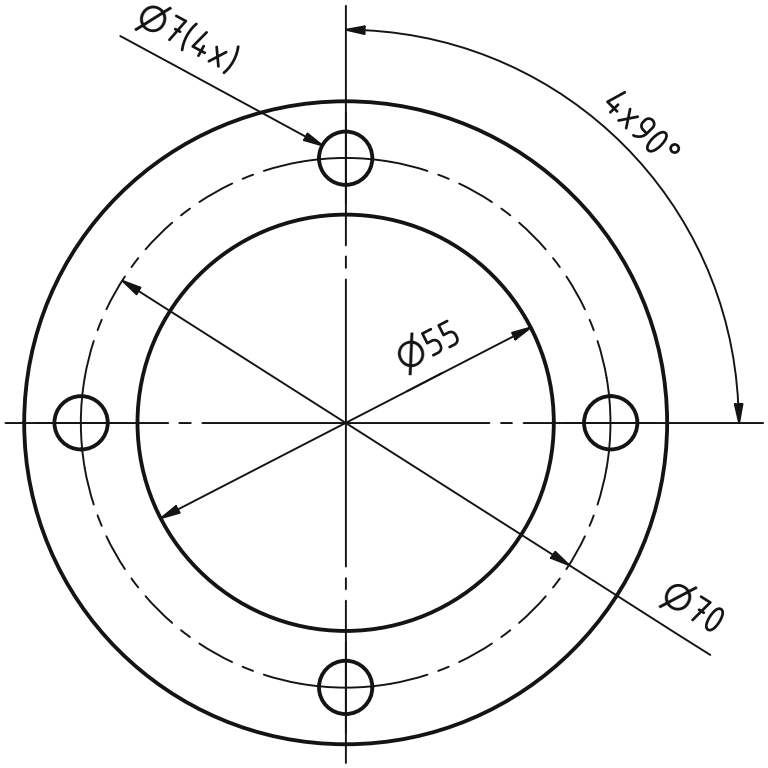

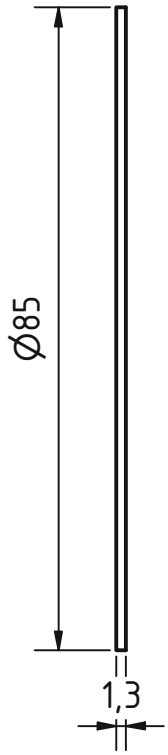

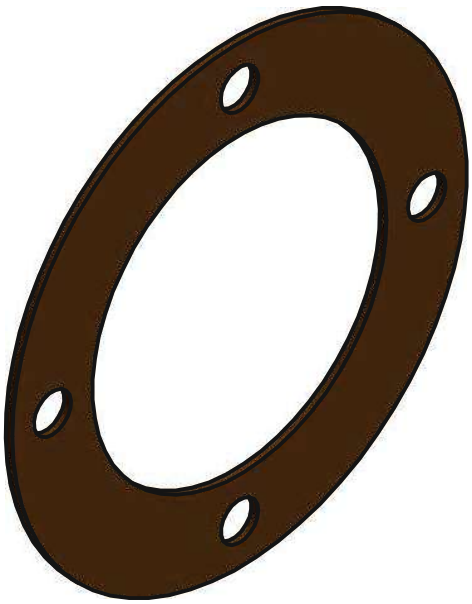

unbemaßte Werkstückkanten DIN ISO 13715 — 0,3 — 0,3

ISO 128

Allgemeintoleranz ISO2768 mK

Maßstab: 1 : 1

Masse: 0,005 kg

Oberflächenbehandlung:

Material: Klinger Milam PSS

	Datum	Name
Gezeichn	18.01.2022	Philipp Mayer
Kontroll		
Norm		

Benennung:

Dichtung Heizelement Montageflansch

Projekt: Micro Hot Prüfstand

INSTITUT FÜR ENERGIETECHNIK UND THERMODYNAMIK
Institute for Energy Systems and Thermodynamics

Z-Nummer: MH039

Blatt 1/1

A4

Status	Änderungen	Datum	Name

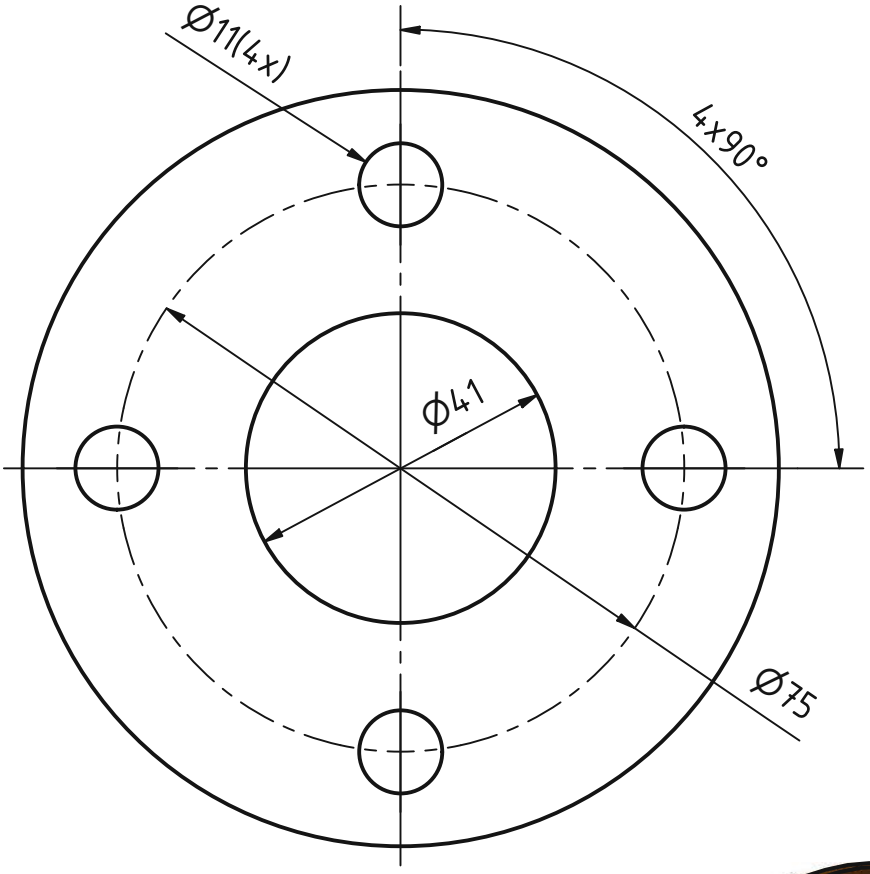

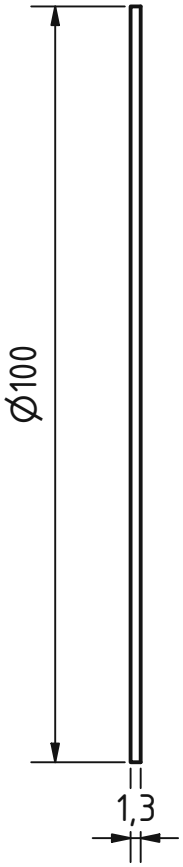

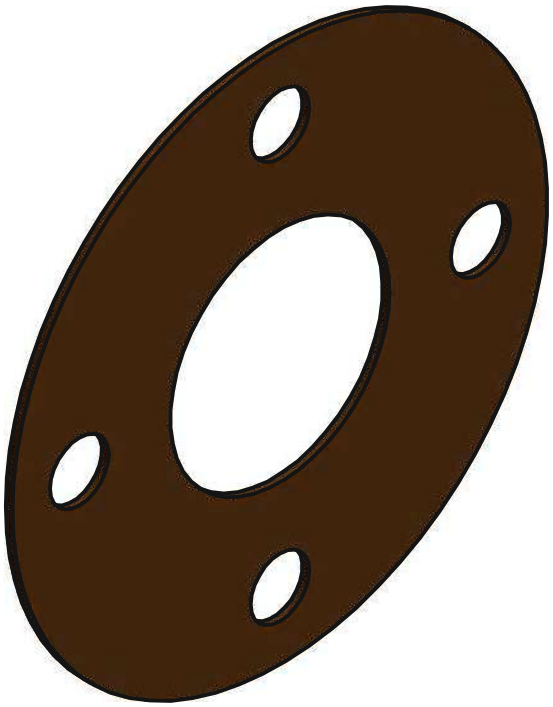

unbemaßte Werkstückkanten DIN ISO 13715 ⌐0,3 ⌐0,3

ISO 128

Allgemeintoleranz ISO2768 mK

Maßstab: 1 : 1

Masse: 0,010 kg

Oberflächenbehandlung:

Material: Klinger Milam PSS

	Datum	Name
Gezeichn	18.01.2022	Philipp Mayer
Kontroll		
Norm		

Benennung:

Dichtung Heizelement

Projekt: Micro Hot Prüfstand

INSTITUT FÜR ENERGIETECHNIK UND THERMODYNAMIK
Institute for Energy Systems and Thermodynamics

Z-Nummer: MH040

Blatt 1/1

A4

Status	Änderungen	Datum	Name

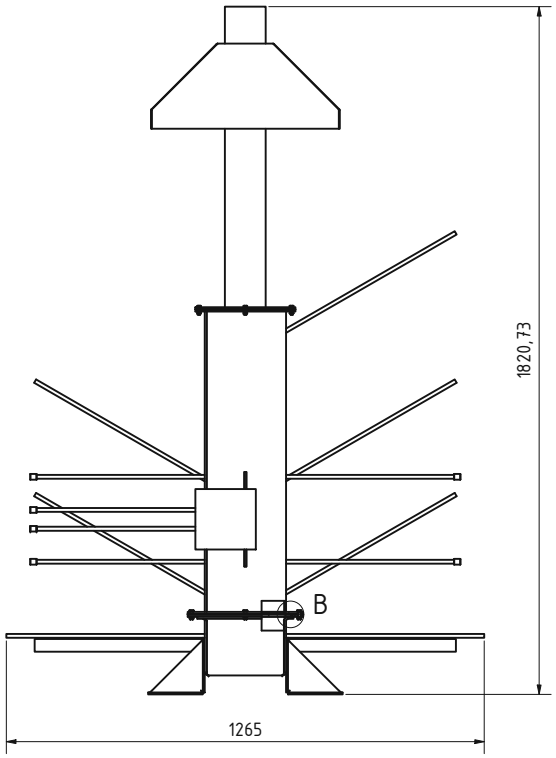

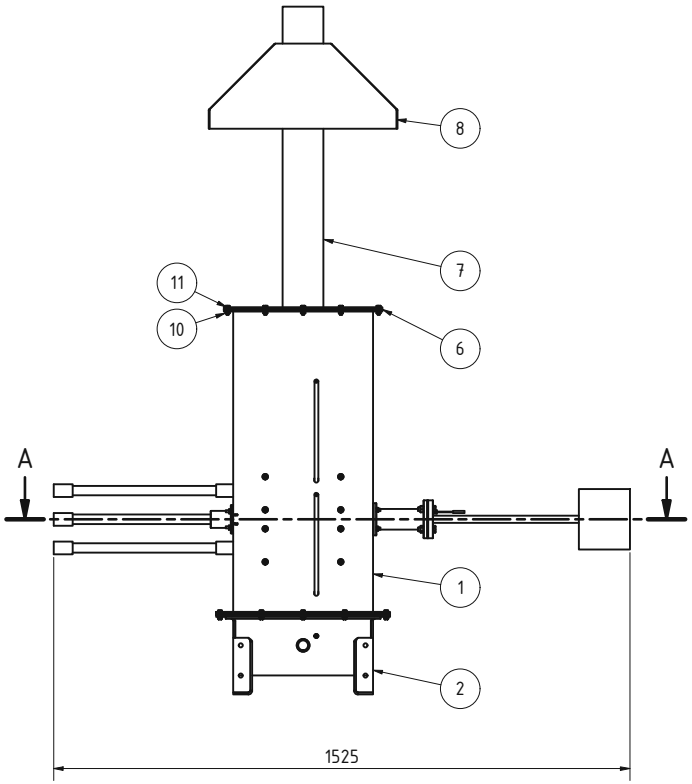

A-A (1 : 10)

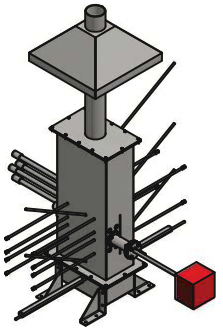

B (1 : 1)

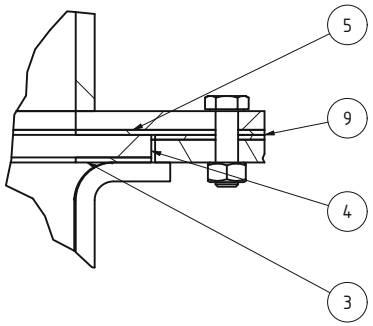

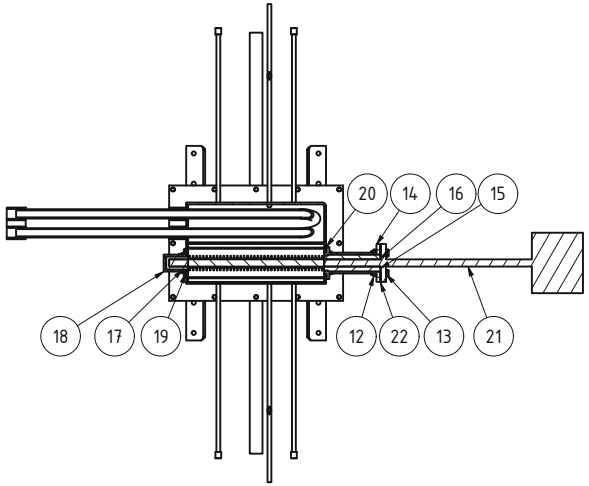

STÜCKLISTE

OBJEKT	ANZAHL	BAUTEILNUMMER	Z-NUMMER	BESCHREIBUNG
1	1	Wirbelschichtkammer Schweißbaugruppe	MH019	
2	1	Windkasten Schweißbaugruppe	MH007	
3	1	Dichtung Sinterplatte unten	MH034	
4	1	Sinterplatte Micro Hot Prüfstand		
5	1	Dichtung Sinterplatte oben	MH035	
6	1	Dichtung Deckel Wirbelschichtkammer	MH037	
7	1	Deckel Wirbelschichtkammer Schweißbaugruppe	MH022	
8	1	Abzugshaube Schweißbaugruppe	MH027	
9	1	Dichtung Wirbelschichtkammer Windkasten	MH036	
10	32	ISO 4032 - M6(4)		Sechskantmuttern
11	24	BS EN ISO 4017 - M6 x 20		Sechskantschrauben
12	4	ISO 4032 - M10(4)		Sechskantmuttern
13	4	ISO 4017 - M10 x 40(3)		Sechskantschrauben mit Ganzgewinde
14	1	Montageflansch Heizelement	MH031	
15	1	Keramikhalbschale vorne	MH028	
16	1	Keramikhalbschale vorne Nut	MH029	
17	1	Keramikbuchse hinten	MH030	
18	1	Heizelement Aufnahmenflansch	MH032	
19	1	Dichtung Heizelement Aufnahmeflansch	MH038	
20	1	Dichtung Heizelement Montageflansch	MH039	
21	1	Heizelement Vulcanic		
22	1	Dichtung Heizelement	MH040	

unbemaßte Werkstückkanten DIN ISO 13715 ↳0,3 ↳0,3

ISO 128

Allgemeintoleranz ISO2768 mK

Maßstab: 1 : 10

Masse: -

Oberflächenbehandlung:

Material:

	Datum	Name
Gezeichn.	11.11.2022	Philipp Mayer
Kontroll.		
Norm		

Benennung: Zusammstellungszeichnung Micro Hot Prüfstand

Projekt:

INSTITUT FÜR ENERGIETECHNIK UND THERMODYNAMIK
Institute for Energy Systems and Thermodynamics

Z-Nummer: MH043

Blatt 1/1 A2

Status | Änderungen | Datum | Name

KLINGER® milam PSS

KLINGER Switzerland

KLINGER®milam PSS engineered for highly demanding operating conditions.

Featuring a high-temperature Mica-based material with perforated stainless steel reinforcement, KLINGER® milam PSS gaskets are specifically designed for hot, dry gas applications at up to 900 °C and 5 bar. Their outstanding chemical resistance also makes them suitable for a wide range of other applications. This product is also available as Milam H, a high-quality homogeneous mica sheet.

Basis composition Mica-based sealing material with a perforated 0.1 mm thick stainless steel reinforcement.

Color Brown

Certificates German Lloyd

Sheet size 1000 x 1200 mm

Thickness PSS 130 = 1.3 mm, PSS 200 = 2.0 mm, PSS 300 = 3.2 mm

Tolerances

Thickness: ±10%
Length: ± 5 mm
Width: ± 5 mm

Industry

General industry / Chemical / Oil & Gas / Energy / Pulp & Paper / Marine / Automotive

TECHNICAL DATA - Typical values for different thicknesses

		PSS 130	PSS 200	PSS 300
Compressibility ASTM F 36 J	%	12 - 20	15 - 23	18 - 26
Recovery ASTM F 36 J	%	30 - 45	32 - 42	28 - 38
Stress relaxation DIN 52913, 50 MPa, 16 h/300°C	MPa	33	33	30
Ignition loss	%	<5	<5	<15
Sealability for nitrogen at 30 MPa and 6 bar, temperature within 100 to 400°C (Sample size 90 x 50 mm) max	ml/min	0.20	0.20	1.0
Thickness increase ASTM F 146, Oil IRM 903: 5 h/150°C	%	12	12	5
Weight increase ASTM F 146, Oil IRM 903: 5 h/150°C	%	26	26	28
Max. gasket load	MPa	100	80	80
Density	g/cm3	2.1	2.1	1.8
Max. temperature	°C	900	900	900
Thickness	mm	1.3	2.0	3.2
Number of stainless steel reinforcements		1	1	2
Material Tanged stainless steel		ASI 316 (L)		

P-T diagram - thickness 2.0 mm

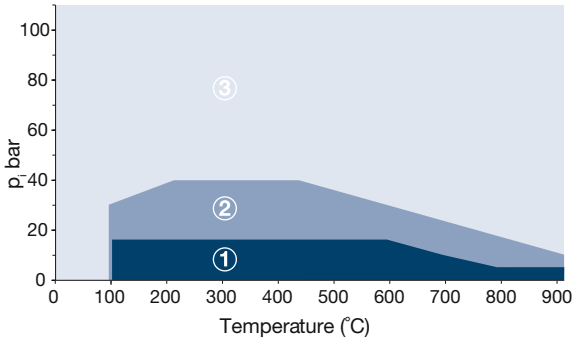

The area of the P-T diagram

① In area one, the gasket material is normally suitable subject to chemical compatibility.

② In area two, the gasket material may be suitable but a technical evaluation is recommended.

③ In area three, do not install the gasket without a technical evaluation.

Always refer to the chemical resistance of the gasket to the media.

Tightness performance

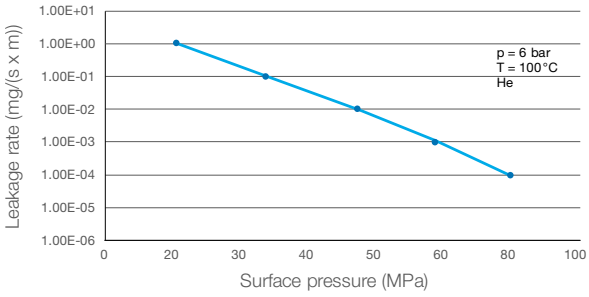

The tightness performance graph

The graph shows the required stress at assembling to seal a certain tightness class. The determination of the graph is based on EN13555 test procedure with Helium at 100 °C. The sloping curve indicates the ability of the gasket to increase tightness with raising gasket

Chemical resistance chart

Simplified overview of the chemical resistance depending on the most important groups of raw materials:

KLINGER® milam PSS — **A**: small or no attack — **B**: weak till moderate attack — **C**: strong attack

Paraffinic hydrocarbon	Motor fuel	Aromates	Chlorinated hydrocarbon fluids	Motor oil	Mineral lubricants	Alcohol	Ketone	Ester	Water	Acid (diluted)	Base (diluted)
A	**A**	**A**	**B**	**A**	**A**	**A**	**A**	**A**	**A**	**B**	**B**

For more information on chemical resistance please visit www.klinger-ag.ch.

Klinger AG Egliswil
Webereistrasse 1, CH–5704 Egliswil
Status: January 2020

www.klinger-ag.ch

A unique material

MACOR® Machinable Glass Ceramic

MACOR® machinable glass ceramic is recognized worldwide to be a major technological innovation, as well as a technical solution for a wide range of industrial applications.

Opening a wide range of possibilities MACOR® gives the performance of a technical ceramic with the versatility of a high performance polymer, while providing the machinability of a soft metal.

As a result, MACOR® is an outstanding engineering material which can quickly be designed into highly complex shapes, using conventional metalworking tools.

Unique composition

MACOR® can be considered unique as its composition comprises 55% fluorophlogopite mica and 45% borosilicate glass. Corning's unique production process results in Macor's microstructure that is a key to its versatile properties.

General properties

MACOR® offers a unique combination of properties, unlike any other technical material.

It is a white, nonwetting, odorless and non outgassing material that exhibits zero porosity.

Extremely machinable, MACOR® offers tight tolerances capabilities, allowing complicated shape design (optimal performances up to +/- 0.013 mm for dimensions, < 0.5 µm for finished surface and up to 0.013 µm for polished surface).

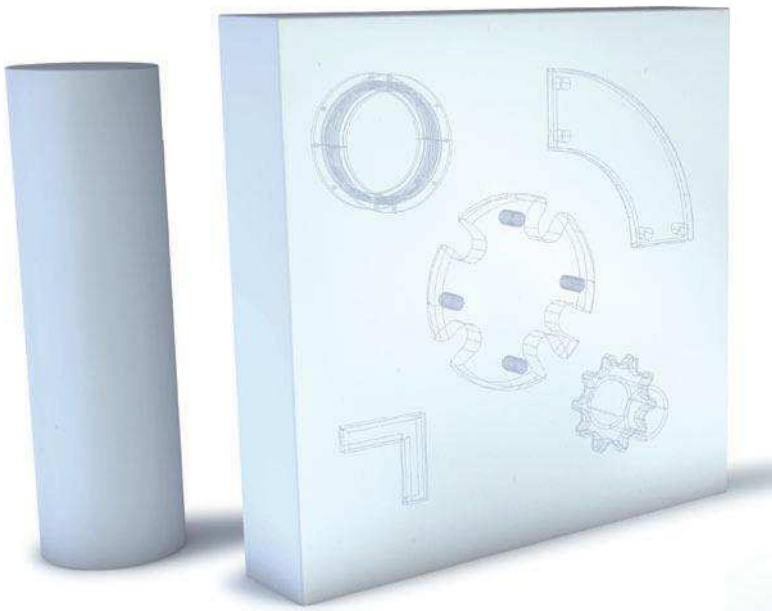

MACOR® remains continuously stable at 800 °C, with a maximum peak at 1000 °C under no load, and unlike ductile materials, doesn't creep or deform.

Its coefficient of thermal expansion readily matches most metals and sealing glasses.

As an electric insulator, particularly at high temperatures, it is excellent at high voltages and a broad spectrum of frequencies.

Material Forms

Corning supplies MACOR® as slab and rod.

High precision finished parts are manufactured by our specialist partners.

Properties

I. Thermal

	SI/Metric	Imperial
Coefficient of Expansion		
CTE -100°C → 25°C	81 x 10^{-7} /°C	45 x 10^{-7} /°F
CTE 25°C → 300°C	90 x 10^{-7} /°C	50 x 10^{-7} /°F
CTE 25°C → 600°C	112 x 10^{-7} /°C	62 x 10^{-7} /°F
CTE 25°C → 800°C	123 x 10^{-7} /°C	68 x 10^{-7} /°F
Specific Heat, 25°C	0,79 kJ/kg°C	0.19 Btu/lb°F
Thermal Conductivity, 25°C	1,46 W/m°C	10.16 Btu.in/hr.ft²°F
Thermal Diffusivity, 25°C	7,3 x 10^{-7} m²/s	0.028 ft²/hr
Continuous Operating Temperature	800°C	1472°F
Maximum No Load Temperature	1000°C	1832°F

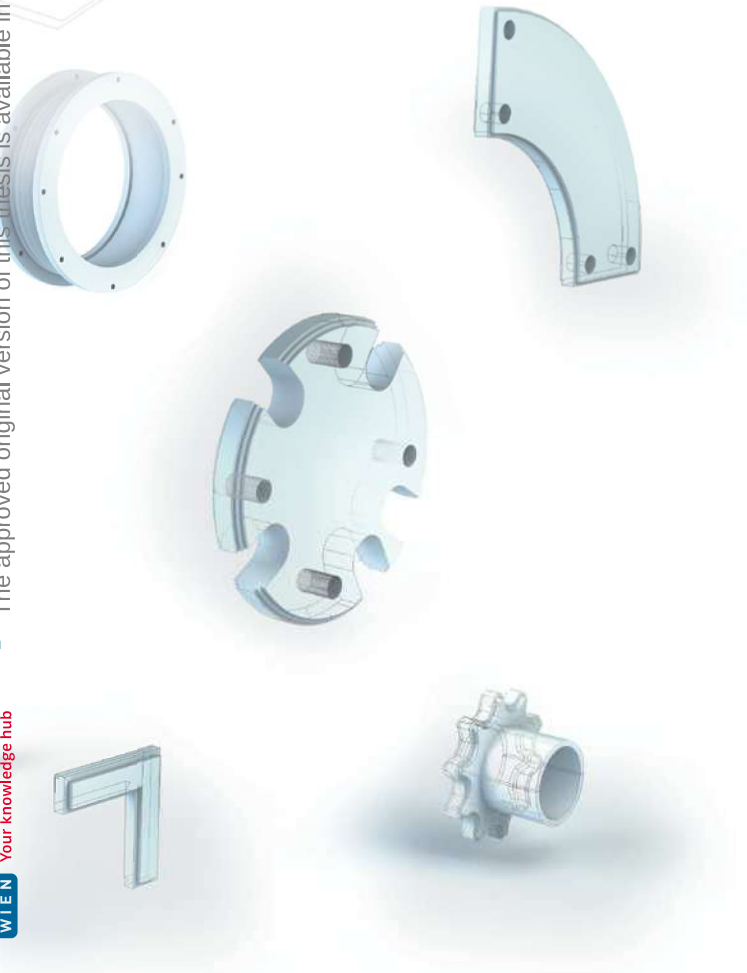

II. Mechanical

	SI/Metric	Imperial
Density	2,52 g/cm³	157 lbs/ft³
Porosity	0%	0%
Young's Modulus, 25°C (Modulus of Elasticity)	66,9 GPa	9.7 x 10^6 PSI
Poisson's Ratio	0,29	0.29
Shear Modulus, 25°C	25,5 GPa	3.7 x 10^6 PSI
Knoop Hardness, 100g	250 kg/mm²	
Modulus of Rupture, 25°C (Flexural Strength)	94 MPa (Minimum specified average value)	13 600 PSI
Compressive Strength (After polishing)	345 MPa up to 900 MPa	49 900 PSI 130 000 PSI

III. Electrical

	SI/Metric	Imperial
Dielectric Constant, 25°C		
1 kHz	6,01	6.01
8,5 GHz	5,64	5.64
Loss Tangent, 25°C		
1 kHz	0,0040	0.0040
8,5 GHz	0,0025	0.0025
Dielectric Strength (AC) avg. 25°C, under 0,3 mm thickness.	45 kV/mm	1143 V/mil
Dielectric Strength (DC) avg. 25°C, under 0,3 mm thickness	129 kV/mm	3277 V/mil
DC Volume Resistivity, 25°C	10^{17} Ohm.cm	10^{17} Ohm.cm

IV. Chemical

				Weight Loss (mg/cm²)
Solution	pH	Time	Temp.	Gravimetric
5% HCl (Hydrochloric Acid)	0,1	24 hrs	95°C	~100
0,002 N HNO_3 (Nitric Acid)	2,8	24 hrs	95°C	~0,6
0,1 N $NaHCO_3$ (Sodium Bicarbonate)	8,4	24 hrs	95°C	~0,3
0,02 N Na_2CO_3 (Sodium Carbonate)	10,9	6 hrs	95°C	~0,1
5% NaOH (Sodium Hydroxide)	13,2	6 hrs	95°C	~10

Chemical durability		Class
DIN 12111 / NF ISO 719	Water	HGB2
DIN 12116	Acid	4
DIN 52322 / ISO 695	Alkali	A3

Mineral Insulated Thermocouples - Type 12

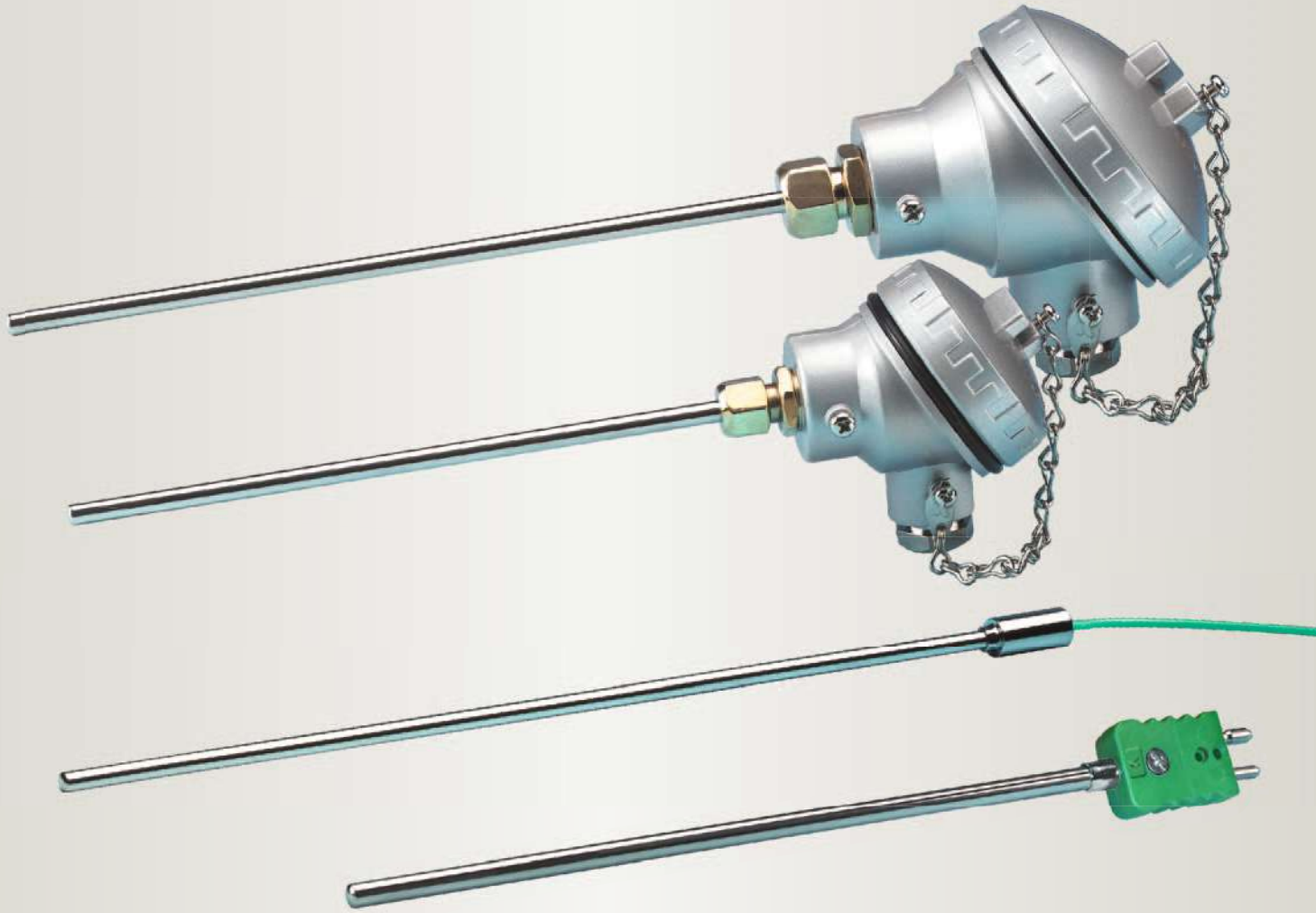

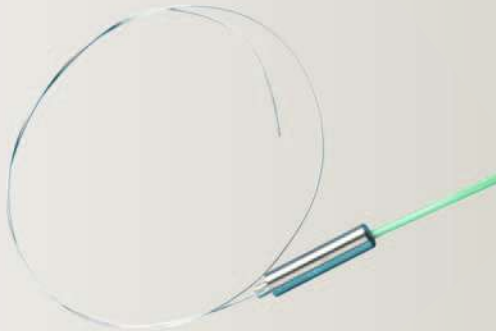

A range of semi flexible mineral insulated thermocouples, suited to a wide variety of industrial applications up to 1400°C.

Custom built to your specification and terminated in a large choice of end seal terminations and sheath materials from 0.25mm to 10.8mm diameter.

Type 12 Mineral Insulated Thermocouples

- **High integrity construction suited to arduous operating conditions at temperatures from -200°C to +1400°C**
- **High accuracy and stability maintained throughout operating life**
- **Fast response and high insulation resistance**
- **UKAS calibration is available for our range of Mineral Insulated thermocouple assemblies**
- **The cable used to manufacture these assemblies conforms to BS EN 61515: 2016 / IEC 61515: 2016 and BS EN 60584 class 2, other tolerances are available on request**
- **Available in K, T, J, N, E, R, S, & B with sheath diameters from 0.25mm to 10.8mm and lengths from a few millimetres to 200 metres or more dependent on the sheath diameter selected**
- **Sheaths can generally be bent, twisted and flattened to suit particular installations without impairing performance**
- **Swaged end assemblies are available where fast response high strength sheaths or low displacement are a necessity**

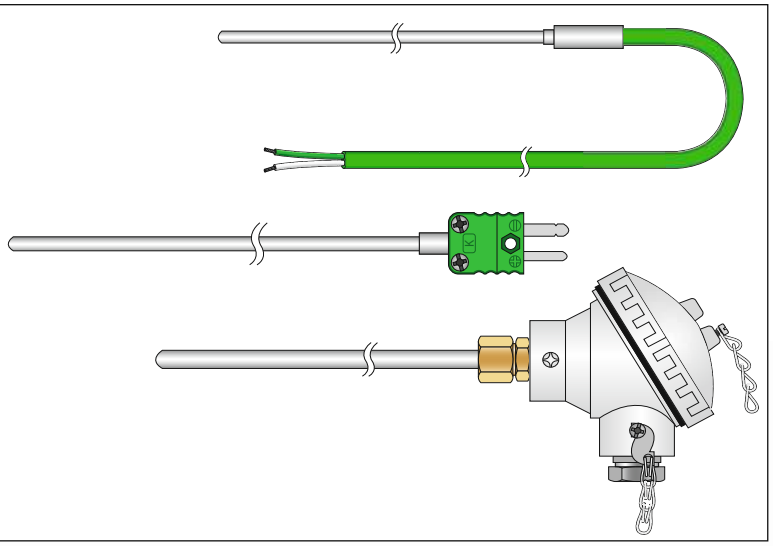

Typical Construction

The seamless metal sheath is available in a variety of materials with overall diameters from 0.25mm to 10.8mm. Sheath materials include: a range of stainless steels, Inconel 600*, Incoloy 800*, Chrome/Iron, Hastelloy X* , Nicrotherm D™ and other materials. Additionally these assemblies can be supplied with the sheaths bonded with a variety of fluoroplastic claddings to suit particular corrosive environments.

The complete assembly is a compact, self armoured, hermetically sealed, semi flexible probe providing the conductors with complete protection against oxidation and corrosion.

They are ideally suited for use in extreme environmental conditions of high vibration, high pressure/vacuum and over a wide operational temperature range of -200°C to +1400°C.

The length of the sheath of the finished assembly is to suit customer requirements (any length from a few millimetres to 200 metres or more dependent on the diameter).

A wide range of adjustable brass or stainless steel compression fittings screwed BSP or BSPT are available to suit the various sheath sizes for mounting Type 12 thermocouples. A selection of popular fittings is shown in section 7.

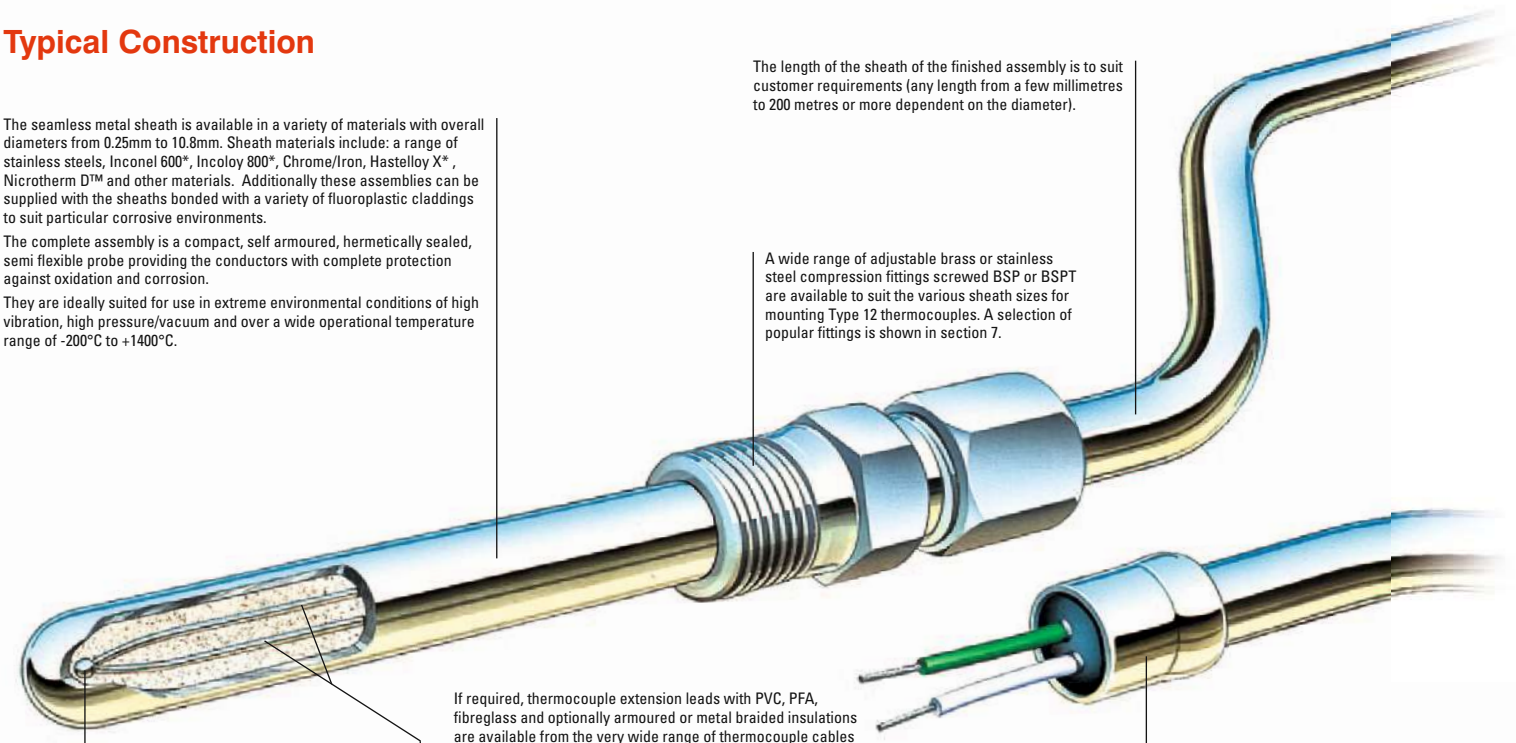

If required, thermocouple extension leads with PVC, PFA, fibreglass and optionally armoured or metal braided insulations are available from the very wide range of thermocouple cables offered by TC Ltd.

A wide range of end seal terminations are available within which the hermetic seal is effected.

The thermocouple junction is arc welded in an inert atmosphere. The junction may be insulated from the sheath, grounded to it or may be exposed from the sheath depending upon the application.

The conductors are insulated from one another and the sheath by very tightly compacted magnesium oxide powder. With an insulated junction, the insulation resistance between the conductors and sheath is in excess of 100 MΩ.

Quality Control. All materials and assemblies are subject to rigorous quality checks during manufacture through to final test and inspection in accordance with our approval to ISO 9001.

UKAS calibration is available as an additional service for our range of Mineral Insulated Thermocouple assemblies.

Swaged Reduced Tip

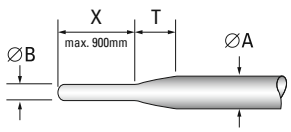

Swaged end reduced tip temperature sensors provide a unique fast response, high strength, low displacement, homogenous solution to many problematical temperature measurement applications. The technique combines the advantages of having a rugged large diameter metal sheath over most of its length with a low thermal mass, fast response, reduced diameter tip.

The length of the reduced tip (X) can be any length up to 900mm and virtually any diameter between 0.5mm and 5.2mm with the most popular sizes are shown in the table. Please contact us for other sizes.

	Approximate Transition Lengths ('T' mm) for given Ø 'A' mm						
ØB	**6.0mm**	**4.5mm**	**3.0mm**	**2.0mm**	**1.5mm**	**1.0mm**	**0.5mm**
6.0mm	–	–	–	–	–	–	–
4.5mm	6	–	–	–	–	–	–
3.0mm	12	6	–	–	–	–	–
2.0mm	16	10	4	–	–	–	–
1.5mm	18	12	6	2	–	–	–
1.0mm	20	14	8	4	2	–	–
0.5mm	–	–	–	6	4	2	–

Mineral Insulated Thermocouples Type 12

SECTION 1	Thermocouple Type	Temperature Range* (continuous)	(short term)
K	Nickel Chromium vs Nickel Aluminium	0 to +1100°C	-180 to +1350°C
T	Copper vs Constantan	-185 to +300°C	-250 to +400°C
J	Iron vs Constantan	+20 to +700°C	-180 to +750°C
N	Nicrosil vs Nisil	0 to +1100°C	-270 to +1300°C
E	Nickel Chromium vs Constantan	0 to +800°C	-40 to +900°C
R	Platinum - 13% Rhodium vs Platinum	0 to +1600°C	-50 to +1700°C
S	Platinum - 10% Rhodium vs Platinum	0 to +1550°C	-50 to +1750°C
B	Platinum - 30% Rhodium vs Platinum - 6% Rhodium	+100 to +1600°C	+100 to +1820°C

**Depending on sheath material.*

SECTION 3	Sheath Diameter (mm)	Sheath Diameter (inches)
Standard Sizes	0.25mm	0.010"
	0.5mm	0.020"
	0.75mm	0.030"
	1.0mm	0.039"
	1.5mm	0.059"
	1.6mm (1/16")	0.063"
	2.0mm	0.079"
	3.0mm	0.118"
	3.2mm (1/8")	0.125"
	4.5mm	0.177"
	5.5mm*	0.216"
	6.0mm	0.236"
	6.35mm (1/4")	0.250"
	8.0mm	0.315"
	9.5mm	0.374"
	10.8mm*	0.425"

For types R, S, B, C and D a more limited range of sheath diameters is available.
** 5.5mm and 10.8mm diameter are thick wall, heavy duty constructions.*

SECTION 4	Types of Sensing Junction	
2I	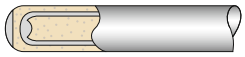	**Insulated** Hot junction insulated from sheath. Gives floating output with typical insulation resistance in excess of 100 megohms (or 2ID if Duplex element is required and 2IT if triplex element is required).
2G	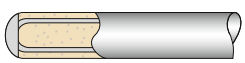	**Grounded** Hot junction welded to sheath tip giving earthed output and faster response to temperature changes (or 2GD if Duplex element is required and 2GT if triplex element is required).
2X	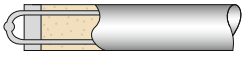	**Exposed** Fastest response mainly for the measurement of air temperature in ducts. Restricted to a maximum operating temperature of 600°C (or 2XD if Duplex element is required and 2XT if Triplex element is required).

To suit particular attachment requirements thermocouples with measuring junction configurations 2I or 2G can be supplied with an extended tip or welding pad. (Contact the company for details of standard welding pad and extension tip configurations.)
Other special measuring junction configuration requirements can be met upon request.

SECTION 2	Sheath Specifications	Operational Properties	Max. Temp.
Standard 321	**Grade 321 Stainless Steel** 18/8/1 Ni/Cr/Titanium Stabilised To BS EN 10088, Werkstoff No : 1.4541	Very good corrosion resistance throughout the operating temperature range. Suited to a wide range of industrial applications. Enjoys high ductility.	800°C
Standard 310	**Grade 310 Stainless Steel** 25/20 Nickel/Chromium To BS EN 10088, Werkstoff No : 1.4845	Good high temperature corrosion resistance and suitable for use in sulphur bearing atmospheres. 310 stainless steel has high oxidation resistance.	1100°C
Standard 600	**Inconel 600*** Nickel/Chromium/Iron alloy To BS EN 10095, Werkstoff No : 2.4816	Used in severely corrosive atmospheres to elevated temperatures. Has good resistance to oxidation. Not recommended for use above 800°C when used with Type R, S or B thermocouples. Do not use in sulphur bearing atmospheres above 550°C.	1100°C
Specialized 316L	**Grade 316L Stainless Steel** 18/8/1 Ni/Cr/Molybdenum Stabilised To BS EN 10088, Werkstoff No : 1.4404	Good high temperature corrosion resistance and suitable for use in sulphur bearing atmospheres. 316L stainless steel has high oxidation resistance.	800°C
Specialized 800	**Incoloy 800*** Iron/Nickel/Chromium alloy To BS EN 10095, Werkstoff No : 1.4876	Suitable for use in severely corrosive atmospheres to elevated temperatures. Enjoys a good resistance to oxidation and carburisation. Incoloy 800 is resistant to sulphur bearing atmospheres.	1100°C
Specialized 825	**Incoloy 825*** Iron/Nickel/Chromium alloy To BS EN 10204, Werkstoff No : 2.4858	Iron/Nickel/Chromium alloy with additions of molybdenum, copper, and titanium. Exceptional resistance to many corrosive environments. Resistant to chloride-ion stress-corrosion cracking.	1250°C
Specialized 446	**AISI 446** Chrome/Iron ASTM TP446, AISI 446, To BS EN 10095, DIN X18CrN28, Werkstoff No : 1.4762	Suitable for use in severely corrosive atmospheres to elevated temperatures. Particularly suited for use in high concentration sulphur bearing atmospheres at high temperature. Sensor should be mounted vertically at temperatures above 700°C.	1150°C
Specialized 156	**Hastelloy X*** Nickel/Chromium/Iron/Molybdenum 51/22/18/9 Werkstoff No : 2.4665	For use in reducing, neutral and inert atmospheres. Has improved high temperature resistance to oxidation and attack by sulphur. At high temperature it has excellent tensile strength and develops a tightly adherent oxide film which does not spall.	1220°C
Specialized 276	**Hastelloy C276*** Nickel/Chromium/Iron/Molybdenum To ASTM B574, Werkstoff No : 2.4819	Excellent corrosion resistance to both oxidizing and reducing media and excellent resistance to localized corrosion attack. Excellent resistance to sulphur compounds and chloride ions.	1250°C
Specialized 114	**Nicrotherm D™** Nickel/Chromium/Silicon/Molybdenum 73/22/1.4/3	For high temperature Type 'K' and almost all Type 'N' applications (optimum benefits with Type 'N'). Very good high temperature strength. Excellent in oxidising, carburising, reducing and vacuum atmospheres. Do not use in sulphur containing atmospheres.	1250°C
Specialized 160	**Haynes HR160** Solid solution strengthened Nickel/Cobalt/Chromium-Silicon alloy ASTM B626, Werkstoff No : 2.4880	Resistant to various forms of high temperature corrosion attack. Excellent resistance to sulphur and chloride attack. Resistant to oxidation, hot corrosion, carburization, metal dusting, nitridation, and corrosion attack by low melting point compounds.	1200°C
Specialized P10R	**Platinum 10% Rhodium**	Primarily for use with thermocouple types R, S and B. Suitable for high temperature oxidizing atmospheres and inert atmospheres.	1400°C

Other sheath materials are available upon request. * Trade Names

Typical Response Times			
Ømm	Time	Ømm	Time
0.25mm	0.015 seconds	3.2mm (1/8")	0.880 seconds
0.5mm	0.030 seconds	4.5mm	1.400 seconds
0.75mm	0.090 seconds	5.5mm*	4.000 seconds
1.0mm	0.150 seconds	6.0mm	3.000 seconds
1.5mm	0.300 seconds	6.35mm (1/4")	3.450 seconds
1.6mm (1/16")	0.320 seconds	8.0mm	5.500 seconds
2.0mm	0.400 seconds	9.5mm	6.750 seconds
3.0mm	0.800 seconds	10.8mm*	9.000 seconds

Response times for these assemblies are governed by and vary with the environmental conditions of particular applications. The information above refers to typical response times for assemblies with insulated Type 2I junctions being plunged into boiling water from air at 20°C. The figures refer to the times taken for the thermocouple junctions to achieve 63.2% of this instantaneous step change. For assemblies with grounded Type 2G junctions the response times are approximately 50% of those listed. ** thick wall*

Type 12 Mineral Insulated Thermocouples

SECTION 5

Types of End Seal Configuration

	Diagram	Specification
3P1		**Internal Seal with Bare Conductors** for all sheath diameters 3P1 Maximum end seal temperature **135**°C 3P1B Maximum end seal temperature **300**°C 3P1C Maximum end seal temperature **650**°C *Note: Only suitable as a temporary seal for applications adding an alternative seal later*
3P2L	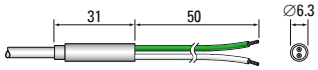	**Crimp on Stainless Steel Pot Seal** for sheath diameters up to 3.0mm 3P2L Pot Seal rated to **135**°C 3P2LA Pot Seal rated to **235**°C 3P2LB Pot Seal rated to **300**°C *see section 6 if extension leads are required*
3P2 TRL	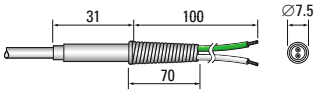 ** It is unlikely that any benefit would be derived from specifying this type of pot seal with the standard 100mm tails.*	**Stainless Steel Pot Seal with Anti Chafe Spring** for sheath diameters up to 3.0mm 3P2TRL Pot Seal rated to **135**°C 3P2TRLA Pot Seal rated to **235**°C 3P2TRLB Pot Seal rated to **300**°C *see section 6 if extension leads are required*
3P4CL	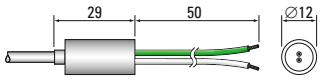	**Crimp on Stainless Steel Pot Seal** for sheath diameters between 3.0mm & 8.0mm 3P4CL Pot Seal rated to **135**°C 3P4CLA Pot Seal rated to **235**°C 3P4CLB Pot Seal rated to **300**°C *see section 6 if extension leads are required*
3P4 CTRL	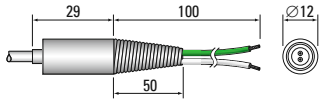 ** It is unlikely that any benefit would be derived from specifying this type of pot seal with the standard 100mm tails.*	**Stainless Steel Pot Seal with Anti Chafe Spring** for sheath diameters between 3.0mm & 8.0mm 3P4CTRL Pot Seal rated to **135**°C 3P4CTRLA Pot Seal rated to **235**°C 3P4CTRLB Pot Seal rated to **300**°C *see section 6 if extension leads are required*
3P3L	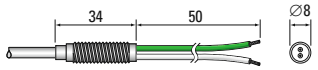 *Lock nuts are available in stainless steel to suit the 3P3L series and should be ordered separately as LN08S.*	**8mm ISO x 1mm Threaded Stainless Steel Pot Seal** for sheath diameters up to 3.0mm 3P3L Pot Seal rated to **135**°C 3P3LA Pot Seal rated to **235**°C 3P3LB Pot Seal rated to **300**°C *see section 6 if extension leads are required*
3P5	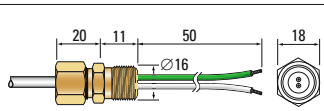	**16mm ISO x 1.5mm Brass Compression Gland Pot Seal** for sheath diameters 1.0mm to 8.0mm 3P5 Pot Seal rated to **135**°C 3P5A Pot Seal rated to **235**°C *see section 6 if extension leads are required*
3P5S	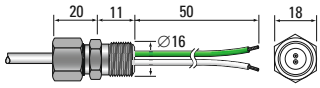	**16mm ISO x 1.5mm St. Steel Compression Gland Pot Seal** for sheath diameters 1.0mm to 8.0mm 3P5S Pot Seal rated to **135**°C 3P5SA Pot Seal rated to **235**°C 3P5SB Pot Seal rated to **300**°C *see section 6 if extension leads are required*
3P6	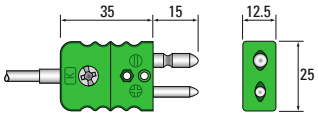 *3P6 illustrated*	**Standard 2-pin (round) Plug** for sheath diameters between 1.0mm & 8.0mm 3P6 Plug rated to **220**°C 3P6H Plug rated to **300**°C 3P6UH Plug rated to **425**°C 3P6C Plug rated to **600**°C
3P6M	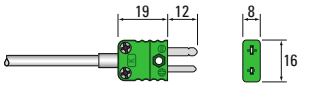 *3P6M illustrated*	**Miniature 2-pin (flat) Plug** for sheath diameters between 0.25mm & 3.2mm 3P6M Plug rated to **220**°C 3P6MH Plug rated to **300**°C 3P6MUH Plug rated to **425**°C 3P6MC Plug rated to **600**°C
3P7	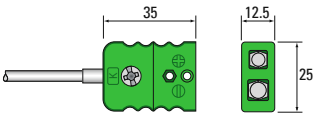 *3P7 illustrated*	**Standard 2-pin (round) Socket** for sheath diameters between 1.0mm & 8.0mm 3P7 Socket rated to **220**°C 3P7H Socket rated to **300**°C 3P7UH Socket rated to **425**°C 3P7C Socket rated to **600**°C
3P7M	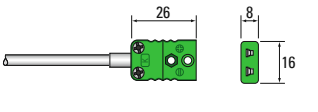 *3P7M illustrated*	**Miniature 2-pin (flat) Socket** for sheath diameters between 0.25mm & 3.2mm 3P7M Socket rated to **220**°C 3P7MH Socket rated to **300**°C 3P7MUH Socket rated to **425**°C 3P7MC Socket rated to **600**°C

	Diagram	Specification
MAA	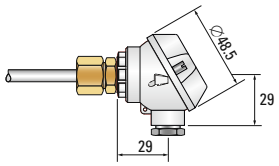	**Micro Die Cast Alloy Head** for diameters 3.0mm to 6.0mm Weatherproof die cast alloy, epoxy coated, screw down terminal head with tube entry and cable entry at a right angle to each other, with a ceramic terminal block. Suitable for simplex and duplex assemblies. Supplied with a 16mm x 1.5mm ISO metal pinch gland on the cable entry for cables from 4mm to 9.5mm diameter.
3P10	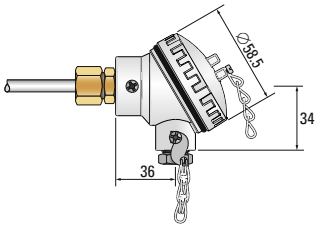	**Miniature Die Cast Alloy Head** for diameters 3.0mm to 8.0mm Weatherproof die cast alloy, epoxy coated, screw top terminal head with the tube entry and cable entry at a right angle to each other, with a ceramic terminal block. Suitable for simplex and duplex assemblies. Supplied with a 16mm x 1.5mm ISO metal pinch gland on the cable entry for cables from 3mm to 8mm diameter.
3P11	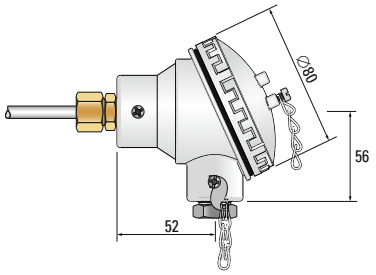	**Standard Die Cast Alloy Head** for diameters 4.5mm to 10.8mm Weatherproof die cast alloy, epoxy coated, screw top terminal head with the tube entry and cable entry at a right angle to each other, with a ceramic terminal block. Suitable for simplex, duplex and triplex assemblies. Supplied with a 20mm x 1.5mm ISO metal pinch gland on cable entry for cables from 6mm to 14mm diameter.
3P12	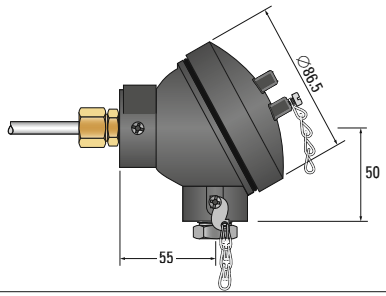	**Heavy Duty Cast Iron Head** for diameters 4.5mm to 10.8mm Weatherproof cast iron, screw top terminal head with the tube entry and cable entry at a right angle to each other, with ceramic terminal block. Suitable for simplex, duplex and triplex assemblies. Supplied with a 20mm x 1.5mm ISO metal pinch gland on cable entry for cables from 6mm to 14mm diameter.
3P16	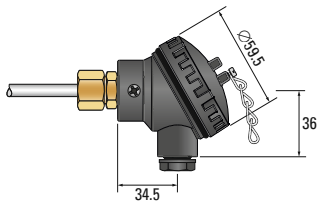	**Miniature Plastic Head** for diameters 3.0mm to 8.0mm Weatherproof plastic, screw top terminal head with the tube entry and cable entry at a right angle to each other, with a plastic terminal block. Suitable for simplex and duplex assemblies. Supplied with a 16mm x 1.5mm ISO plastic pinch gland on cable entry for cables from 3mm to 8mm diameter.
3P17	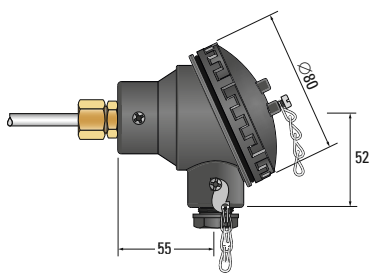	**Standard Plastic Head** for diameters 4.5mm to 10.8mm Weatherproof plastic, screw top terminal head with the tube entry and cable entry at a right angle to each other, with a plastic terminal block. Suitable for simplex, duplex and triplex assemblies. Supplied complete with a 20mm x 1.5mm ISO plastic pinch gland on the cable entry for cables from 6mm to 14mm diameter.

continued

Mineral Insulated Thermocouples Type 12

SECTION 5 — Types of End Seal Configuration (continued)

	Diagram	Specification
3P18	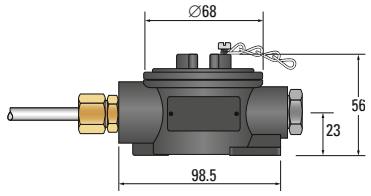	**Alloy Straight Through Head** for diameters 4.5mm to 10.8mm Die cast alloy straight through terminal head with a bakelite terminal block. Suitable for simplex or duplex assemblies. Supplied with a 20mm x 1.5mm pitch ISO pinch gland on the cable entry for cables from 6mm to 14mm diameter. **If supported at fixing holes, suitable for diameters of 1mm and above.*
3P19	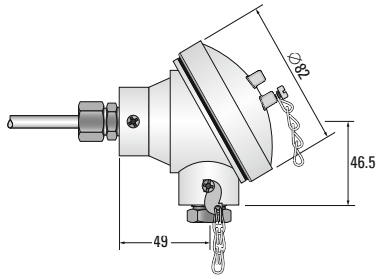	**Stainless Steel Head** for diameters 4.5mm to 10.8mm Weatherproof stainless steel, screw top terminal head with the tube entry and cable entry at a right angle to each other, with a ceramic terminal block. Suitable for simplex, duplex and triplex assemblies. Supplied with a 20mm x 1.5mm ISO metal pinch gland on cable entry for cables from 6mm to 14mm diameter.

	Diagram	Specification
3P20	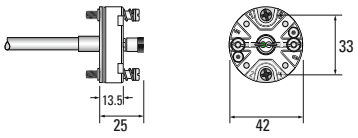	**Spring Loaded Terminal Block** for diameters 3.0mm to 8.0mm Spring loaded insert assemblies. The end seal is incorporated into a terminal block suitable for mounting into a 3P11, 3P12, 3P17 or any other standard terminal head. Suitable for use with 3mm, 4.5mm, 6mm and 8mm sheaths only. The ceramic terminal block has 2 x 33mm spaced mounting holes. Suitable for simplex, duplex and triplex assemblies.
3P20/ BP	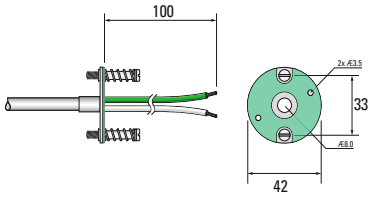	**DIN Mounting Plate** for diameters 3.0mm to 8.0mm Spring loaded mounting plate assemblies. The end seal is incorporated into a mounting plate suitable for mounting into a 3P11, 3P12, 3P17 or any other standard terminal head. Suitable for use with 3mm, 4.5mm, 6mm and 8mm sheaths only. 100mm tails allows for connection to a head mounting transmitter or other suitable terminal block.

SECTION 6 — Extension Cables

	Diagram	Specification
A30		**HR PVC Flat Twin (105°C)** One pair of 7/0.2mm stranded conductors HR PVC insulated. Pair laid flat and HR PVC sheathed overall.
A27	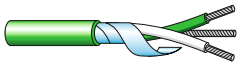	**HR PVC Twisted Pair with Screen (105°C)** One pair of 7/0.2mm stranded conductors HR PVC insulated. Pair twisted, screened with Mylar® aluminium tape and drain wire. HR PVC sheathed overall.
B50		**PFA Flat Twin (250°C)** One pair of 7/0.2mm stranded conductors PFA insulated. Pair laid flat. PFA sheathed overall.
BM 0702		**PFA 2-pair for duplex sensors (250°C)** Two pairs of 7/0.2mm dia stranded conductors PFA insulated. Pairs twisted and bunched and screened with Mylar® aluminium tape with a drainwire. PFA sheathed.
BM 0702/ SSB		**PFA 2-pair for duplex sensors with Stainless Steel braid (250°C)** Two pairs of 7/0.2mm stranded conductors PFA insulated. Pairs twisted and bunched and screened with Mylar® aluminium tape with a drainwire. PFA sheathed with overall stainless steel braid.

	Diagram	Specification
B80		**PFA Twisted Pair with Screen (250°C)** One pair of stranded conductors PFA insulated. Pair twisted, screened with Mylar® aluminium tape and drain wire. PFA sheathed overall.
B40		**PFA Twisted with Ni Plated Cu Braid (250°C)** One pair of 7/0.2mm stranded conductors PFA insulated. Pair twisted with overall nickel plated copper braid and PFA sheathed.
SR30		**Silicone Rubber, Twisted Pair (200°C)** One pair of 7/0.2mm stranded conductors PFA insulated. Silicone rubber sheathed.
C40		**Fibreglass Flat Twin (480°C)** One pair of 7/0.2mm stranded conductors double glass fibre lapped, braided and varnished. Pair laid flat, glass fibre braided and varnished.
C60		**Fibreglass Flat Twin with Steel Braid (480°C)** One pair of 7/0.2mm stranded conductors double glass fibre lapped, braided and varnished. Pair laid flat, glass fibre braided and varnished. Stainless steel wire braided overall.

If no cable is required, leave this section of the order code blank and the sensor will be supplied with PFA tails. Other cables are available on request.

'HR' = Heat Resistant

SECTION 7 — Optional Stainless Steel Compression Fittings

Dia.	1/8" BSPT	1/4" BSPT	1/2" BSPT	Dia.	1/8" BSPT	1/4" BSPT	1/2" BSPT
0.5mm	SFS18T05	–	–	3.0mm	SFS18T30	SFS14T30	SFS12T30
0.75mm	SFS18T75	–	–	4.5mm	SFS18T45	SFS14T45	SFS12T45
1.0mm	SFS18T10	SFS14T10	SFS12T10	6.0mm	SFS18T60	SFS14T60	SFS12T60
1.5mm	SFS18T15	SFS14T15	SFS12T15	8.0mm	–	SFS14T80	SFS12T80

Other sizes and materials are available, please contact us for details.

SECTION 8 — Optional 4 to 20mA Head Mounted Transmitter (please specify range in °C)

TXLTC

Fully Linearised

Suitable for use with the following terminal heads: **3P11, 3P12, 3P17, 3P18** and **3P19** and other standard heads with 33mm fixing.

Typical Order Code: **TXLTC (0/200°C)**

Order Code - Example

Style No.	Thermocouple Type (see section 1)	Sheath Length	Sheath Material (see section 2)	Sheath Diameter (see section 3)	Sensing Junction (see section 4)	End Seal Termination (see section 5)	Extension Cable (see section 6)	Optional Compression Fitting (see section 7)	Reduced Tip Dimensions (if required)	Optional Transmitter (see section 8)
12	K	450	310	6.0	2I	3P4CL	2 MTRS A30KX	SFS18T30	REDUCED TIP: 3.0mm x 50mm LONG	